UNIVERSITAT DE BARCELONA

Investigating Glial Contributions During Parkinson's Disease Pathogenesis Using Patient-Specific iPSC-Derived Cells

Angelique di Domenico

UNIVERSITAT DE BARCELONA

Investigating Glial Contributions During Parkinson's Disease Pathogenesis Using Patient-Specific iPSC-Derived Cells

By:

Angelique di Domenico, BS.c., MS.c.

December 18, 2017
Barcelona, Spain

FACULTAT DE FARMÀCIA I CIÈNCIES DE L'ALIMENTACIÓ

Programa de Doctorat en Biomedicina

Investigating Glial Contributions During Parkinson's Disease Pathogenesis Using Patient-Specific iPSC-Derived Cells

Memòria presentada per Angelique di Domenico per optar al títol de doctor per la Universitat de Barcelona

_____

Antonella Consiglio, Ph.D
(Directora de la Tesis)

_____

Angelique di Domenico, MS.c
(Doctoranda)

_____

Marta Giralt, Ph.D
(Tutora Academica)

I dedicate this thesis to

Wally Gilbert

for his invaluable mentoring

Trust yourself. Create the kind of self that you will be happy to live with all your life. Make the most of yourself by fanning the tiny, inner sparks of possibility into flames of achievement.

– Golda Meir

DECLARATION

This dissertation is the result of my own work and includes nothing, which is the outcome of work done in collaboration except where specifically indicated in the text. It has not been previously submitted, in part or whole, to any university or institution for any degree, diploma, or other qualification, unless indicated in the text.

This thesis is in accordance with the Department of Biomedicine of the University of Barcelona (Barcelona, Spain) guidelines.

_____

Angelique di Domenico, MSc. BSc. (Doctoral Student)

_____

Dated, Barcelona

ABSTRACT

Parkinson's disease (PD) is associated with the degeneration of ventral midbrain dopaminergic (vmDA) neurons and the accumulation of cytoplasmic inclusions, known as Lewy Bodies, composed mainly of aggregated α-synuclein in the surviving vmDA neurons. This process, along with the underlying cell-autonomous pathogenic mechanisms, has been successfully modeled using patient-specific induced pluripotent stem cell (iPSC) technology. Non-cell autonomous neurodegeneration during PD has been suggested by past observational studies, but remains to be experimentally tested. Here, we generated astrocytes from iPSC lines derived from familial Parkinson's disease patients with the G2019S mutation on the Leucine rich repeat kinase 2 (LRRK2) gene, and astrocytes from Sporadic PD patients, as well as healthy age-matched individuals (to whom we will refer as wild type (WT)). To assess the possible non-cell autonomous role during PD pathogenesis, a co-culture system was devised between iPSC-derived astrocytes and vmDAn to assess the potential pathogenic neuron-glia crosstalk. WT vmDAn displayed morphological signs of neurodegeneration (such as few and short neurites, as well as beaded-like necklace neurites) and abnormal, astrocyte-derived, α-synuclein accumulation when co-cultured on top of LRRK2-PD astrocytes. Upon further investigation, PD astrocytes alone displayed phenotypes reminiscent of those observed in PD-iPSC-derived vmDAn, those including alterations in autophagy and mitochondrial dynamics, as well as a progressive accumulation of α-synuclein, when compared with WT astrocytes. A CMA activator drug, QX77.1, successfully rescued CMA dysfunction and as a consequence cleared the previously accumulated α-synucein in PD astrocytes. Conversely, the co-culture of

LRRK2-PD vmDA neurons with WT astrocytes partially prevented the appearance of disease-related neurodegeneration. This neuroprotective role appears to be managed via the activation of glia to a reactive state, and suggests LRRK2-PD astrocytes have an impaired relation between neuroprotection and reactivity, which results in neurodamaging effects. Our findings unveil a crucial non-cell autonomous contribution of astrocytes during PD pathogenesis, and open the path to exploring novel therapeutic strategies aimed at blocking the pathogenic cross-talk between neurons and glial cells.

ACKNOWLEDGEMENTS

Thank you to my Ph.D supervisor, Dr. Antonella Consiglio, for giving me the opportunity to work on this project, my academic tutor Prof. Marta Giralt, and to the European Research Council (2012-StG-311736-PD-HUMMODEL) for fully funding my studies. Thank you Barcelona for being so good to me. Thank you to all of my lab mates for making the lab a real *home away from home* for the last four years, those being Armida Faella, Carles Calatayud Aristoy, Irene Fernandez, Roger Torrent, Neus Bayo Puxan, Francesca DeAngelis, Isabel Fernandez, Marta Cañizares, Chrysanthi Blithikioti, Monika Matusiak Brueckner, Helena Xicory, Marco Valtorta, Alba Tristan Noguero, and Andreu Matamoros Angles. Thank you Yvonne Richaud Patin for teaching me all of your secrets in iPSC technology. An *extra* special thank you to Giulia Carola, with whom I worked very closely throughout my entire Ph.D journey, a true lab sister. More recently, thank you to Meritxell Pons Espinal for guiding me through one of the toughest stages of my career – the review process for publication. Thank you to my collaborators, Jordi Soriano, Ana Maria Cuervo, José Antonio del Río, Juan Pablo Muñoz, and Carlos Matute who provided me with valuable tools, knowledge, and expertise in order to thoroughly investigate cellular mechanisms. Last, but not least, thank you to my *family* Martine, Luca, Philip, Nava, Mila, Grandma & Grandpa, Papou et Mamie, and *friends*, especially Laura Bryson, Alex Perez Castells, Anna Cigarini, Alisha Gori, Luis Miguel Tepedino Pittaluga, Clara Pretus Gomez, Angelina Colao, and Jennyfer Choukroun for their constant support, and without whom this incredible journey would never have been possible.

Moltes Gràcies!

CONTENTS

List of Tables

List of Figures

LIST OF ABBREVIATIONS AND ACRONYMS

AD	Alzheimer’s disease
ALS	Amyotrophic Lateral Sclerosis
AQP4	Aquaporin-4
CCCP	Carbonyl cyanide m-chlorophenyl hydrazone
CD44	Astrocyte-restricted precursor cells
CMA	Chaperone mediated autophagy
CNTF	Ciliary neurotrophic factor
DAPI	4',6-diamidino-2-phenylindole
DMSO	Dimethyl sulfoxide
DRP1	Dynamin-related protein 1
EB	Embryoid body
EGF	Epidermal growth factor
FBS	Fetal bovine serum
FGF2	Basic fibroblast growth factor
FOXA2	Forkhead box A2
GFAP	Glial fibrillary acidic protein
GIRK2	G protein-activated inward rectifier potassium channel
GLT1	Excitatory amino acid transporter 2
HD	Huntington’s disease
HFF	Human foreskin fibroblasts
ICC	Immunocytochemistry
IFN	Interferon
IL	Interleukin
iNOS	Induced nitric oxide synthesis
iPSC	Induced pluripotent stem cells
LAMP1	Lysosome-associated membrane protein 1

LAMP2A	Lysosome-associated membrane protein 2 receptor
LC3	Microtubule-associated protein 1A/1B-light chain 3
LIF	Leukemia inhibitory factor
LRRK2	Leucine rich repeat kinase 2
$LRRK2^{G2019S}$	G2019S mutation on the LRRK2 gene
MAP2	Microtubule-associated protein 2
MFN1	Mitofusion-1
MFN2	Mitofusion-2
NEAA	Non-essential amino acids
NDS	Normal donkey serum
NG2	Oligodendrocyte precursor cells (OPCs)
NO	Nitric oxide
p62	Nucleoporin p62
PBS	Phosphate-buffered saline
PD	Parkinson’s disease
PFA	Paraformaldehyde
PVA:DABCO	Polyvinyl alcohol mounting medium with DABCO®
ROS	Reactive oxygen species
qRT-PCR	Quantitative real time polymerase chain reaction
RT	Room temperature
s.e.m	Standard error of the mean
shRNA	Short hairpin Ribonucleic acid
SNCA	α-synuclein
SNM	Spherical neural masses
SNpc	Substantia nigra pars compacta
TBS	Tris-buffered saline
TH	Tyrosine Hydroxylase
TIM44	Translocase of inner membrane 44
TBK1	TANK binding kinase

TNF-α	Tumor necrosis factor alpha
TOM20	Translocase of outer membrane 20
TUJ1	Neuron-specific Class III β-tubulin
WB	Western Blot
WT	Wild type/control
vmDAn	Ventral midbrain dopaminergic neurons

List of Appendices

1 INTRODUCTION

1.1 Parkinson's Disease

1.1.1 Prevalence and Etiology

Parkinson's disease (PD) is the most prevalent movement disorder and second most chronic neurodegenerative disease after Alzheimer´s disease, affecting seven to ten million people worldwide (Collaborators, 2015). The exact cause of sporadic PD is unknown, however fifteen percent of patients with Parkinson's disease have a family history. Familial causes of PD can be caused by mutations in the *LRRK2*, *PARK7*, *PINK1*, *SNCA*, or *PARKIN* genes, or by genes that have not yet been identified (Bonifati et al., 2003; Fonzo et al., 2009; Kitada et al., 1998; Nichols et al., 2005; Paisán-Ruíz et al., 2004; Polymeropoulos et al., 1997; Ramirez et al., 2006; Schapira, 2006; Shojaee et al., 2008; Singleton et al., 2003; Valente et al., 2004; Vilarino-Guell et al., 2011; Zimprich et al., 2004). Several risk factors also exist, such as mutations in the GBA and UCHL1 genes, which do not directly cause PD, but which increase the possibility in contracting the disease (Cloud Lee & Danny Hsu, 2016). In addition, environmental factors such as exposure to pesticides have been described to play a crucial role (Sanders et al., 2017).

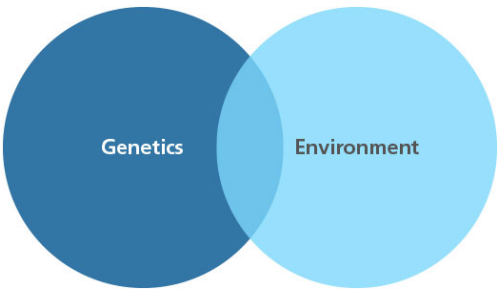

1.1.2 Symptoms

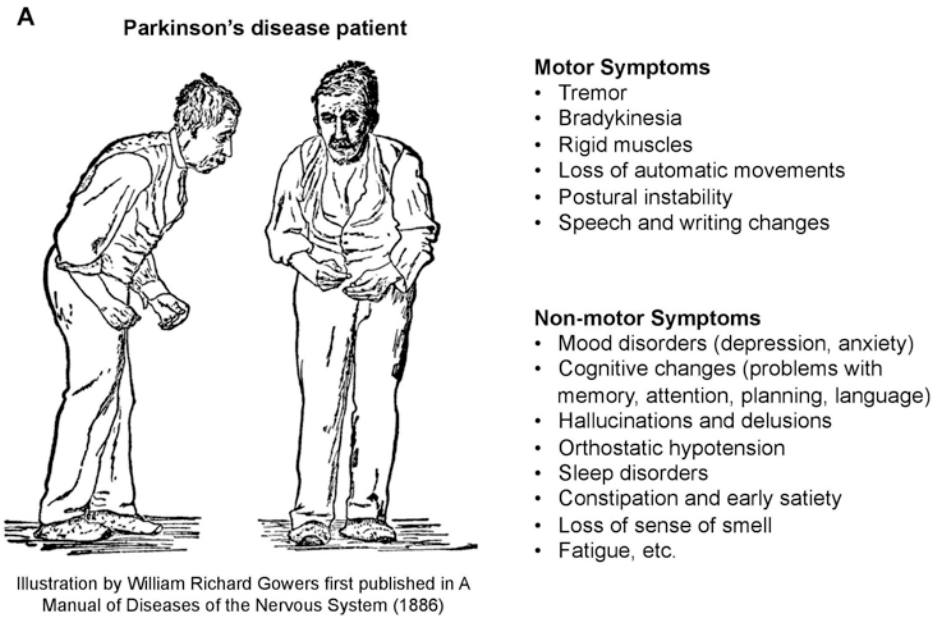

Figure 1. Motor and Non-Motor Symptoms of Parkinson's Disease.

The main motor symptoms observed in patients with PD include resting tremor, bradykinesia, postural instability, and severe muscle rigidity (**Fig. 1**). PD is characterized by a significant loss of ventral midbrain dopaminergic (vmDA) neurons in the substantia nigra pars compacta (SNpc) (Zis, Erro, Walton, Sauerbier, & Chaudhuri, 2015).

During PD pathogenesis, the cogent loss of vmDA neurons in the SNpc results in the subsequent loss of striatal dopamine. This dopamine deficiency causes motor symptoms in PD patients as well as non-motor symptoms at later stages, such as depression, sleep disorders, olfactory dysfunction, and

autonomic deficits (Zis et al., 2015). Another pathological hallmark of PD is an aggregation and accumulation of toxic oligomeric α-synuclein in the surviving vmDA neurons, making PD a proteinopathy (Sánchez-Danés et al., 2012). These α-synuclein aggregates form Lewy bodies and Lewy neurites in both the central and sympathetic nervous systems, which is proposed to be a consequence of the disease, however the exact process is still unclear (Braak, Ghebremedhin, Rüb, Bratzke, & Del Tredici, 2004).

Several dysfunctions occurring in the affected vmDA neurons already have been unveiled, including problems in protein degradation pathways (Ebrahimi-Fakhari, Wahlster, & McLean, 2012), mitochondrial alterations (Dryanovski et al., 2013; Perfeito, Lázaro, Outeiro, & Rego, 2014; Sanders et al., 2014; Zuo & Motherwell, 2013), an increase in ROS production (Perfeito et al., 2014; Zuo & Motherwell, 2013), defective electrical activity patterns (Dragicevic, Schiemann, & Liss, 2015; Dryanovski et al., 2013), Lewy body and Lewy neurite formation, and, as was previously mentioned, the accumulation and aggregation of α-synuclein (Bir et al., 2015; Li et al., 2014; Mbefo et al., 2015; Nash et al., 2014; Perfeito et al., 2014; Reyes et al., 2015; Rothaug et al., 2014; Wilson et al., 2014). Exactly how these dysfunctions occur and whether they are the cause or a consequence of disease pathogenesis, however, is still yet to be uncovered.

1.1.3 Alpha-Synuclein

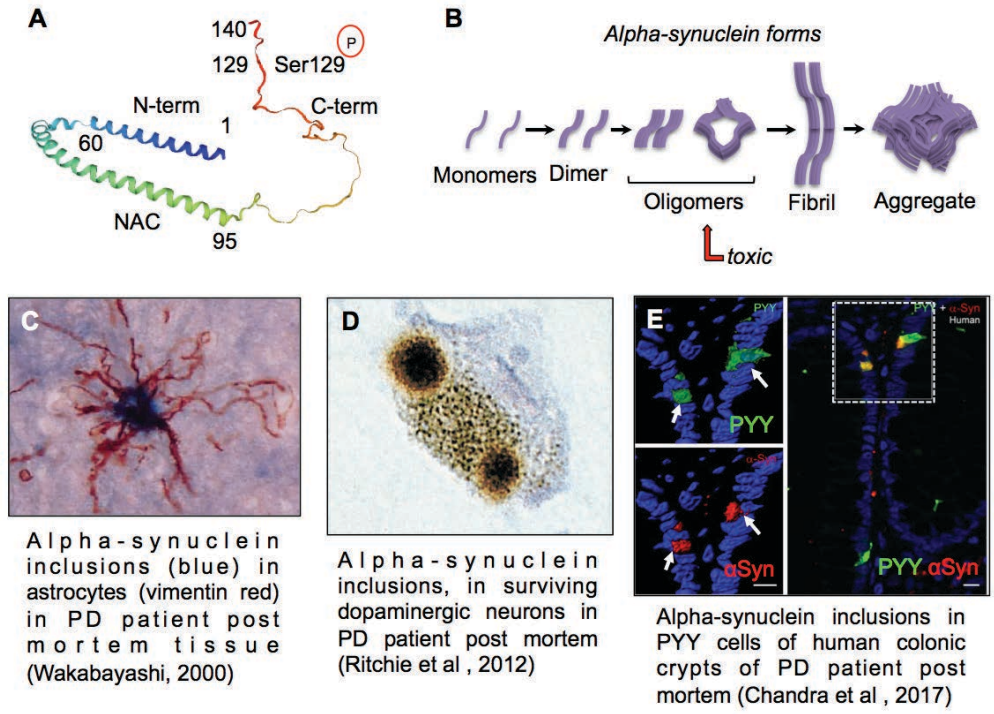

Figure 2. Toxic Alpha-Synuclein Found in Neurons, Glia and the Gut of PD Patients.

(**a**) α-Synuclein protein structure. (**b**) Different forms of α-synuclein that are adopted during pathogenesis. (**c**) α-Synuclein containing astrocyte in PD post-mortem tissue. (**d**) Neurons in PD post-mortem tissue containing Lewy bodies filled with alpha-synuclein. (**e**) α-Synuclein found in the colonic crypts in post-mortem tissue of PD patients.

The presence of intracellular protein aggregates of the toxic insoluble oligomeric form of α-synuclein (encoded by the *SNCA* gene) forming part of large structures, otherwise known as Lewy Bodies (Greenamyre & Hastings, 2004), in the surviving vmDAn, as well as in both astrocytic and

oligodendroglial cells, has been reported to occur during PD (**Fig. 2c,d**) (Ritchie & Thomas, 2012; Wakabayashi, Hayashi, Yoshimoto, Kudo, & Takahashi, 2000). Although the exact function of α-synuclein is not yet fully understood, it is a small protein (14kDa) known to have a role in vesicle trafficking in pre-synaptic terminals (**Fig. 2a**) (Ritchie & Thomas, 2012).

The monomeric form of α-synuclein can be misfolded and start to form dimers and tetramers, eventually forming toxic oligomers, fibrils, and aggregates toxic to neurons (**Fig. 2b**) (Jang et al., 2010; Neupane, Solanki, Sosova, Belov, & Woodside, 2014; Urrea et al., 2017). Recently, there have been reports of α-synuclein present in the gut of PD patients (**Fig. 2e**) that is able to spread as if adopting some characteristics of a prion protein (Chandra, Hiniker, Kuo, Nussbaum, & Liddle, 2017; Kuo et al., 2010; Urrea et al., 2017).

α-Synuclein has also been reported to interact with inflammatory pathways during PD through the activation of microglia and astrocytes leading to cytokine release, inducible Nitric Oxid synthesis (iNOS), ROS and Nitric oxide (NO) production, the enhancement of microglial phagocytosis and inducing lymphocyte infiltration (Hoenen et al., 2016; H. J. Lee et al., 2010; Q. S. Zhang, Heng, Yuan, & Chen, 2017; W. Zhang, 2005). Microglial activation and α-synuclein accumulation can potentiate each other furthering the pathogenic mechanisms of PD. The toxic misfolded protein α-synuclein also has been found to alter the expression of Toll like receptors (TLR), a family of scavenger receptors found on both microglia and astrocytes (Béraud & Maguire-Zeiss, 2012). These studies reinforce the notion that PD pathogenesis is not just a cell autonomous process.

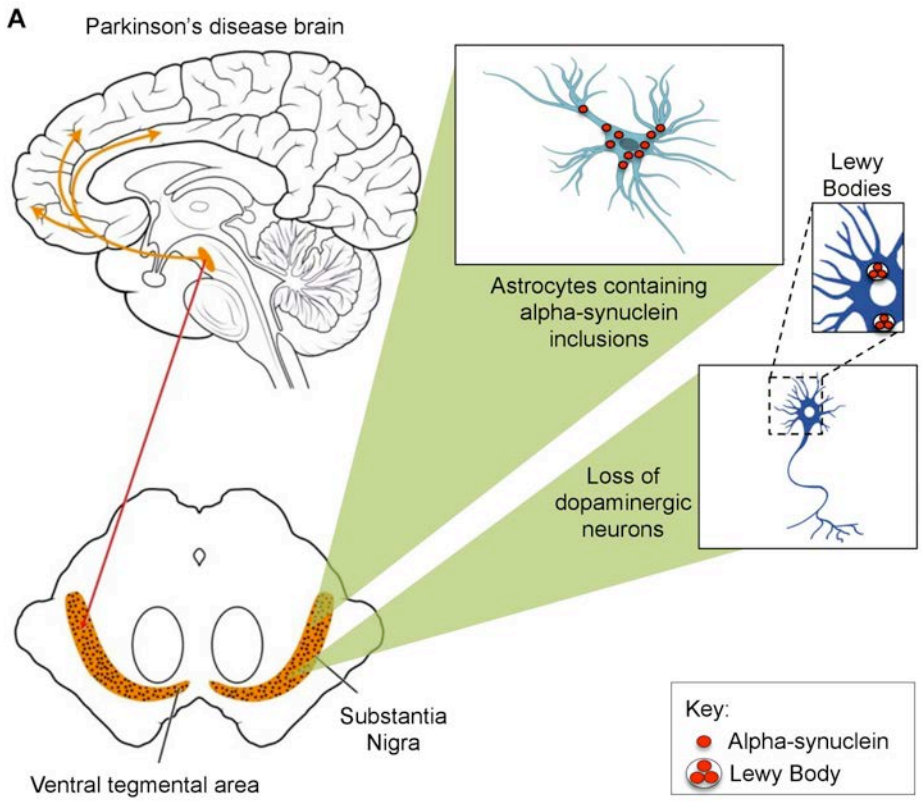

Figure 3. A Closer Look Into the PD Brain.

Post-mortem tissue has revealed a loss of dopaminergic neurons in the substantia nigra pars compacta of PD patients, resulting in consequent loss of dopamine, as well as α-synuclein accumulation in surviving dopaminergic neurons and astrocytes.

The number of inclusions in glial cells usually correlates with the severity of nigral neuronal loss (**Fig. 3**), thus indicating that abnormal accumulation of α-synuclein in glial cells is a pathological feature of PD related to its progression (Wakabayashi et al., 2000).

It was reported that α-synuclein is involved in vesicle trafficking and is normally located in the presynaptic terminals of neurons (L. Wang et al., 2014). This highly mobile 14kDa protein plays a role in the release of dopamine, and, during PD, misfolds into toxic oligomers which then aggregate, forming the main constituent of Lewy bodies (Braak & Del Tredici, 2008). Primary culture cells that were treated with medium containing α-synuclein were able to uptake the protein (H. J. Lee et al., 2010). Astrocytes are able to uptake this "prion-like" α-synuclein and degrade it through the lysosomal degradation pathway elucidating a neuroprotective role. Therapeutics developed to enhance astrocytic-mediated clearance of α-synuclein may therefore be useful for future therapeutic targets.

1.1.4 Genetics

Despite significant advances in the identification of genes and proteins involved in PD, there are still appreciable gaps in our understanding of the mechanisms underlying the chronic neurodegenerative process in this disease (Dawson, Ko, & Dawson, 2010; Melrose, Lincoln, Tyndall, & Farrer, 2006). Most PD cases are sporadic (85%), but familial mutations are accountable for PD in fifteen percent of patients (Lill, 2016). Transcriptomic data has become available showing the expression levels of genes known to be causative in PD in astrocytes and neurons from humans and mice (**Fig. 4**). Some PD related genes, such as *PINK1*, *PARK7*, *FBXO7*, and *GBA*, are more expressed in human astrocytes than in human neurons, further pointing to the possibility of non-cell autonomy during PD pathogenesis (Booth, Hirst, & Wade-Martins, 2017).

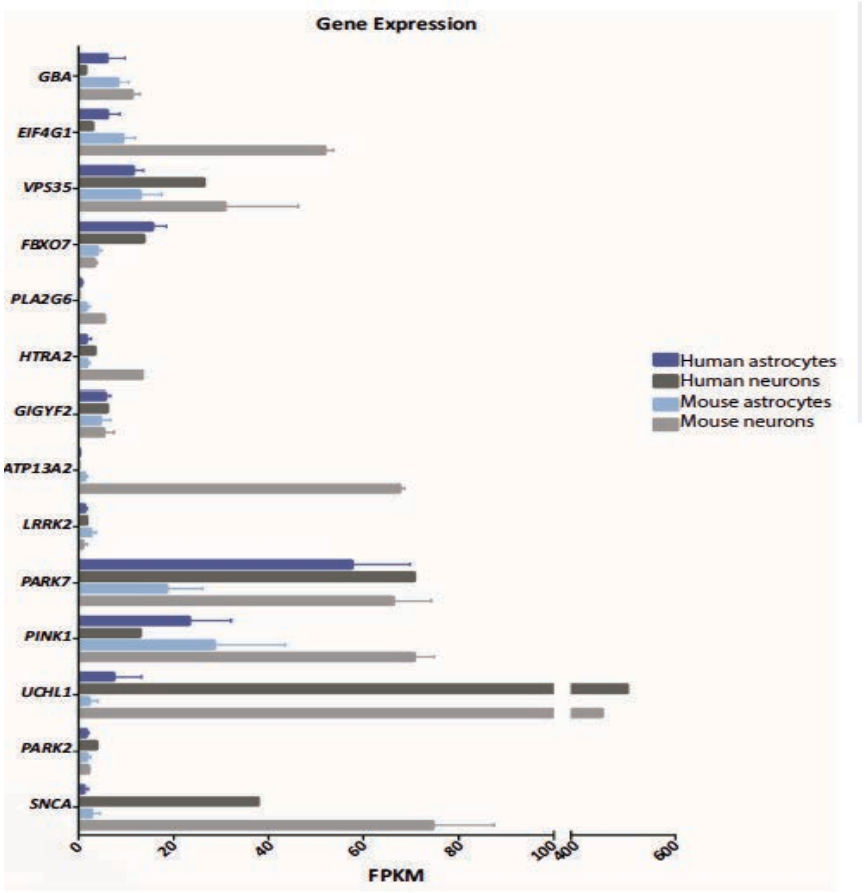

Figure 4. Expression Levels of Key PD Genes in Astrocytes and Neurons.

Transcriptome data showing the expression levels of genes known to be causative in PD in astrocytes and neurons from humans and mice. Human astrocytes N = 12 subjects; human neurons N = 1 subject; mouse astrocytes N = 6 animals; mouse neurons N = 2 animals. Image courtesy of Booth and colleagues (Booth et al., 2017).

Mutations in the gene encoding leucine-rich repeat kinase 2 (*LRRK2*), causing an autosomal dominant form of PD, account for 5% of familial cases and 2% of sporadic cases (Gilks et al., 2005; Nichols et al., 2005). LRRK2 is a highly complex protein with both GTPase and kinase functions with multiple enzymatic domains. It has been reported to be involved in

mitochondrial function, vesicle trafficking together with endocytosis, retromer complex modulation, and autophagy (Cherra, Steer, Gusdon, Kiselyov, & Chu, 2013; Orenstein et al., 2013; Su, Guo, & Qi, 2015). With LRRK2's main roles still elusive, mutations affecting the protein kinase domain of LRRK2 (such as the most prevalent LRRK2^{G2019S} mutation) have been reported to increase kinase activity (Covy & Giasson, 2009).

Correlation between mutant LRRK2 and several pathogenic mechanisms linked to PD progression have been reported, including alterations in autophagy and accumulation of α-synuclein. During PD pathogenesis, mutant LRRK2 was found to directly bind LAMP2A, the receptor responsible for chaperone-mediated autophagy (CMA) normally used by both LRRK2 and α-synuclein for degradation (Orenstein et al., 2013). This binding blocks the proper functioning of the CMA translocation complex, resulting in defective CMA leading to the accumulation of α-synuclein and cell death. When the CMA translocation complex is blocked, the cell responds in producing more reactive lysosomal receptors, in an attempt to compensate for the dysfunction. This lysosomal hyperactivity was also reported to affect macroautophagic functioning. When LRRK2 kinase activity was inhibited in human neuroglioma cells, macroautophagy was stimulated (Manzoni et al., 2013).

1.1.5 Treatments

There currently is no cure for Parkinson's disease. One drug is on the market, Levodopa, however, it alleviates the symptoms of PD for a period of approximately five years. Levodopa is a chemical building block that replaces the depleted dopamine in PD brains; directly administrated

dopamine does not cross the blood brain barrier (Huang et al., 2017). After five years, Levodopa causes side effects which can be worse than the actual symptoms of PD (Cerri, Siani, & Blandini, 2017).

There exist nondopaminergic systems treatments for the symptoms of PD such as adenosine, glutamatergic, adrenergic, serotoninergic, histaminic, and iron chelator pathways, which could include potential therapeutic targets for motor symptoms (Du & Chen, 2017). However, although targeting nondopaminergic systems could have an ameliorative effect on the symptoms of PD as an adjunct therapy to Levodopa, further investigation is required in order to validate its potential success (Du & Chen, 2017). Currently, Levodopa is used in conjunction with MAO-B inhibitors, COMT inhibitors, dopamine agonists, glutamate antagonists, and anticholinergics, the choice of which is determined according to the particular symptoms experienced by the patient.

1.2 Astrocytes' Role in the Brain

Astrocytes are a star-shaped sub-type of glial cells found in both the brain and spinal cord which participate in all essential CNS functions, including adult neurogenesis (Song, Stevens, & Gage, 2002), neurotransmission (Nedergaard, Takano, & Hansen, 2002), synapse formation and maturation (Christopherson et al., 2005; Molofsky et al., 2014; Ullian, 2001; Ullian, Christopherson, & Barres, 2004), synaptic plasticity (Tyzack et al., 2014), nutrient transfer from blood vessels (Broux, Gowing, & Prat, 2015), and immunity (Farina, Aloisi, & Meinl, 2007). The astrocytic population within the brain is widely heterogeneous, not only in shape, but also in function, and it plays several crucial roles involved in maintaining a homeostatic

microenvironment to ensure neuronal survival. Depending upon which molecules they secrete or uptake, astrocytes can play both neuroprotective and neurodegenerative roles.

Under physiological conditions, astrocytes ensure the termination of neuronal transmission by mopping up any extracellular glutamate and recycling it into glutamine for further neuronal usage in the synapse (Uwechue, Marx, Chevy, & Billups, 2012). This neuroprotective role is crucial, as a defect in this glutamate clearance capability can cause excitotoxicity and neuronal death. On the other hand, when astrocytes become reactive, not only do they actively proliferate, or release toxic molecules, they also can release pro-inflammatory cytokines resulting in the recruitment of microglia furthering the neurodegeneration process. This dual role of neuroprotection and neurodegeneration elicits the importance of investigating the mechanisms behind non-neuronal cell function during PD.

Gene	Protein	Astrocyte function
PARK7	DJ-1	Glutamate uptake
		Inflammatory response
		Mitochondrial function
		Neurotrophic capacity
		Oxidative stress
SNCA	α-synuclein	Endocytosis
		Fatty acid metabolism
		Glutamate uptake
		Inflammatory response
		Neurotrophic capacity
		Water transport
PLA2G6	Group VI Ca^{2+}-independent phospholipase A_2 ($iPLA_2$)	Calcium signalling
		Fatty acid metabolism
		Inflammatory response
ATP13A2	Lysosomal type 5 ATPase (ATP13A2)	Inflammatory response
		Lysosome function
		Neurotrophic capacity
LRRK2	Leucine-rich repeat kinase 2 (LRRK2)	Autophagy
		Lysosome function
GBA	β-Glucocerebrosidase (GCase)	Autophagy
		Lysosome function
		Mitochondrial function
PINK1	PTEN-induced putative kinase 1 (PINK1)	Embryonic development
		Mitochondrial function
		Proliferation
PARK2	Parkin	Inflammatory response
		Mitochondrial function
		Neuroprotection
		Proliferation
		Unfolded protein response

Figure 5. Genes That Are Causative in the Development of PD Relative to Function in Astrocyte Biology.

Image courtesy of Booth and Colleagues (Booth et al., 2017).

Past studies have proposed a role for astrocytes during PD pathogenesis, however the same has yet to be experimentally validated (Wakabayashi et al., 2000). There are several genes related to the function of astrocyte

biology, which are known to be causative of the development of PD (**Fig. 5**). For example, *PARK7* (protein DJ-1), has been shown to have an effect in glutamate uptake, mitochondrial function, inflammatory response, oxidative stress, and neurotrophic support, many functions that astrocytes adopt (Booth et al., 2017).

Astrocytes play crucial roles to support neuronal homeostasis, including metabolic and physical support for neurons (Khakh & Sofroniew, 2015; A. Lee & Pow, 2010), absorption and clearance of molecules released by neurons in the synaptic cleft (Panatier et al., 2011), guidance during neuronal migration, regulation of energy metabolism through the release of lactate and glutamine (Suzuki et al., 2011), and transport of blood-born nutrients via astrocytic end-feet from blood capillaries to neuron (Gordon, Mulligan, & MacVicar, 2007). In addition, astrocytes react to injury (formation of glial scar, gliosis) (Ye et al., 2015; Yi & Hazell, 2006) and play a role in the body's inflammatory response (reactive astrocytes activated by microglia) (Ben Haim, Carrillo-de Sauvage, Ceyzériat, & Escartin, 2015; Liddelow et al., 2017; Liddelow & Barres, 2017). If any one of these pathways is altered during disease pathogenesis, neuronal homeostasis will be compromised.

1.2.1 Neuronal Homeostasis (Axon Guidance and Synaptic Support)

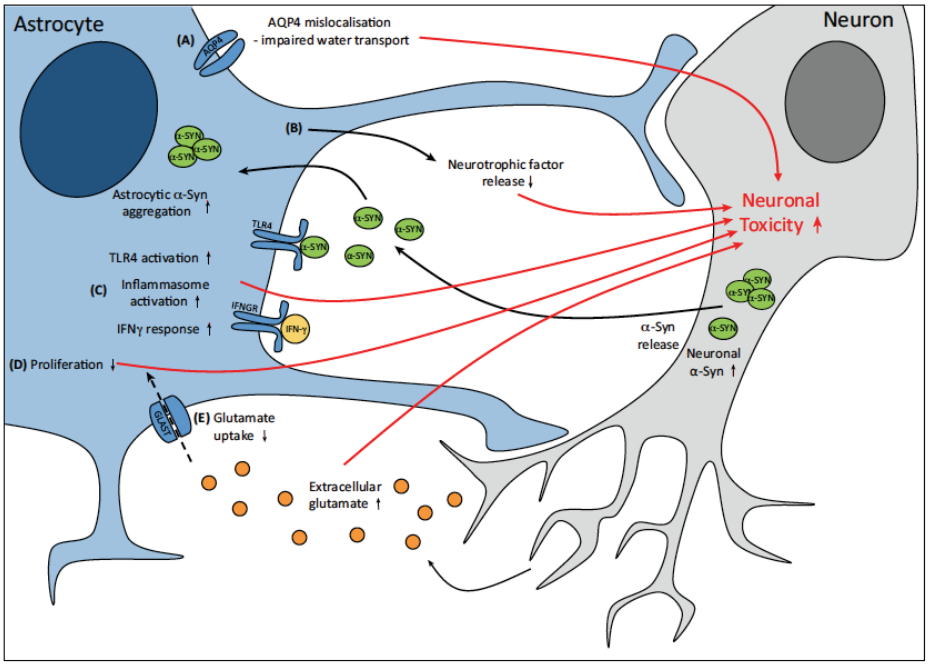

Figure 6. Astrocyte Dysfunction Elicits Neuronal Toxicity via Five Main Mechanisms.

(**a**) Aquaporin-4 (AQP4) water channels are mislocalized away from the astrocyte end-feet, resulting in impaired water transport. (**b**) The neuroprotective capacity of astrocytes is reduced because of decreased neurotrophic factor release. (**c**) Inflammatory signaling via the TLR4, IFN-g, and NLPR3 inflammasome pathways is increased. (**d**) Astrocyte proliferation is impaired, reducing the capacity of the cells to respond to an insult. (**e**) Glutamate uptake is reduced, potentially resulting in increased extracellular glutamate and, therefore, neuronal excitotoxicity. Image courtesy of Booth and Colleagues(Booth et al., 2017).

Neuronal homeostasis relies on a functional astrocyte network, especially at the synapse. Neurons communicate with each other through the release of neurotransmitters into the synaptic cleft. This area usually is immediately cleared out by astrocytes following an action potential relieving the neurons

from potential neuronal excitotoxicity (Hubbard, Szu, Yonan, & Binder, 2016).

During disease, astrocyte dysfunction has been reported to elicit neuronal toxicity (**Fig. 6**). Astrocyte processes have end-feet, which can wrap around capillaries to absorb nutrients from the blood to supply neurons. Water channels, known as Aquaporins, in particular Aquaporin-4 (AQP4), have been reported during PD to be displaced from the end-feet causing impairment in water transport in the cell (Booth et al., 2017; Gu et al., 2010; Hubbard et al., 2016). A reduction in glutamate uptake has been reported during astrocyte dysfunction, which could result in an increased extracellular level of glutamate, thus resulting in neuronal excitotoxicity (Hubbard et al., 2016). Overall neuroprotective capacity of astrocytes can be reduced if a dysfunction impairs neurotrophic factor release (Solano et al., 2008). In addition, a reduced astrocyte proliferation capacity after insult could take effect and inflammatory signaling via the inflammasome pathways increased (Khasnavis & Pahan, 2014).

1.2.2 Detoxification and Oxidative Stress

Astrocytes play a pivotal role in the regulation of reactive oxygen species (ROS) toxicity through a process of detoxification (Dringen, Brandmann, Hohnholt, & Blumrich, 2015). Under physiological conditions, astrocytes contain high levels of antioxidant molecules, which help in the clearance of accumulated toxic ROS levels. The brain’s high metabolic rate makes it highly vulnerable to oxidative stress. The mitochondrion is responsible for reducing oxygen to water within its respiratory chain, however there is still approximately 1-2% of consumed oxygen that is converted to ROS (Dias et

al., 2013). During PD, this rate is increased by the leakage of electrons from the electron transport chain, further propagating the presence of ROS and damaging the surrounding cells, including neurons (Riederer et al., 1989). Endogenous antioxidants in the brain such as antioxidant gluthione (GSH) tend to inhibit excessive ROS damage. Levels of GSH are found to be elevated in the astrocyte compared to neurons under normal conditions (Riederer et al., 1989). During PD, however, the levels of this antioxidant are dramatically reduced, impeding it from protecting the neurons from ROS damage (Rappold & Tieu, 2011). Re-establishing this depleted antioxidant through the astrocyte could be an option for future PD therapeutics.

1.2.3 Control of the Blood Brian Barrier (BBB)

Astrocytes play an important role at the Blood Brain Barrier (BBB) by interacting with endothelial cells which are lining cerebral micro-vessels (Abbott, Rönnbäck, & Hansson, 2006). Proper maintenance of the BBB is crucial for a reliable neuronal signaling network. Astrocyte perivascular end-feet wrap around a basal lamina surrounding endothelial cells, which are wrapped around capillaries via tight junctions. Astrocytes provide the cellular link to the neurons. Endothelial cells also express a number of transporters and receptors, which interact with astrocytes. This bidirectional interaction reinforces BBB function and maintenance. Disruption in this BBB maintenance crosstalk can have pathological repercussions, which have been observed during stroke (Lo, Dalkara, & Moskowitz, 2003), trauma (Schwaninger et al., 1999), Multiple Sclerosis (Spencer, Bell, & DeLuca, 2017), HIV (Berger M., 2004), Alzheimer’s disease (G. Lee & Bendayan, 2004), brain tumors (Davies, 2002), pain (Huber et al., 2001), epilepsy

(Marroni et al., 2003), as well as Parkinson's disease (Kortekaas et al., 2005).

1.3 Glial Contribution During Neurodegenerative Diseases

In recent years, studies have shifted the focus from the dying neuron to a possible glial contribution during neurodegeneration. Astrocytes have been described to play a very critical role during Amyotrophic Lateral Sclerosis (ALS) pathogenesis, which is extremely toxic to motor neurons. Several murine studies (Chen et al., 2004; Henkel et al., 2009; Liu et al., 2012; McCrate & Kaspar, 2008; Subramanian et al., 2008; Winton et al., 2008)have described a toxic effect of astrocytes on motor neurons during ALS, however it was not until recently that this effect could be recapitulated by isolating human astrocytes from post-mortem ALS patient tissue in a living system (*i.e.*, mouse model) (Haidet-Phillips et al., 2011). Astrocytes from both familial and sporadic ALS patients were found to be toxic to motor neurons (Haidet-Phillips et al., 2011). Several subsequent *in vitro* studies have also recapitulated this glia-derived toxic effect (Colombrita et al., 2012; Ferraiuolo, 2014; Johnson et al., 2009; Richard & Maragakis, 2014; Serio et al., 2013). Astrocytes also have been reported as playing a role during Alzheimer's disease (AD) in several mouse models (Beauquis et al., 2013, 2014; Olabarria, Noristani, Verkhratsky, & Rodríguez, 2010), and also, more recently, in iPSC-derived astrocytes from familial and sporadic AD patients (Jones, Atkinson-Dell, Verkhratsky, & Mohamet, 2017). Astrocytes from AD patients were described to harbor a pronounced pathological phenotype, such as atrophic processes and abnormal localization of important astroglial markers (Jones et al., 2017).

In addition to astrocytes, microglia, the second glial type in the brain, have been found to play a crucial role during Huntington's disease (HD) (Crotti et al., 2014). Reactive microglia and elevated cytokine levels have been found during analysis of post-mortem brain tissue of HD patients. Through the use of genome-wide approaches, it was revealed that expression of mutant Huntingtin in microglia results in a pro-inflammatory transcriptional activation of the myeloid lineage-determining factors PU.1 and C/EBPs (Crotti et al., 2014). Microglia have also been described to play a role during ALS pathogenesis. C9orf72 loss-of-function model did not produce signs of motor neuron degeneration, however it led to an accumulation of lysosomes and altered immune response in microglia (O'Rourke et al., 2016). Furthermore, a gene that has recently been described as an ALS-susceptibility gene, TANK binding kinase (*TBK1*), has been found to play a role in autophagy and innate immunity signaling, resulting in the regulation of interferon α (IFN-α) and IFN-β (Ahmad, Zhang, Casanova, & Sancho-Shimizu, 2016). These studies promote the notion that impaired autophagy is linked to pro-inflammatory responses and pathogen clearance by immune cells during disease (Geloso et al., 2017; Plaza-Zabala, Sierra-Torre, & Sierra, 2017). Finally, microglia and astrocytes have also been implicated in inflammation-mediated PD pathogenesis in response to toxic α-synuclein (Q. S. Zhang et al., 2017). Toxic α-synuclein has been reported to directly activate TLR on both astrocytes and microglia resulting in pro-inflammatory cytokine activation, harming dopaminergic neurons (Hoenen et al., 2016).

1.3.1 Astrocytes in Parkinson's Disease

Studies investigating PD pathogenesis have been focused mostly on the mechanisms underlying vmDA neuron degeneration and death. Evidence has

been obtained through post-mortem analysis, however, of astrocytes up-taking and accumulating α-synuclein during PD (Braak, Sastre, & Del Tredici, 2007; Wakabayashi et al., 2000). Altered α-synuclein released by axon terminals in the surrounding synapses was taken up by astrocytes, supporting the hypothesis of the spread of α-synuclein through neuron-astrocyte interactions (Braak et al., 2007; H. J. Lee et al., 2010). Overexpression of mutant *SNCA* in primary astrocytes altered their normal functioning and impaired proper blood-brain-barrier control and glutamate homeostasis, and eventually resulted in a significant loss of vmDA neurons (Gu et al., 2010). In a different study overexpressing mutant α-synuclein in PD mice, astrocytes were found to have altered mitochondria and to have reduced the secretion of factors fundamental to neuronal survival (Schmidt et al., 2011). Furthermore, uptake of neuronal-derived or recombinant α-synuclein by both primary and human astrocytes were observed to result in impaired mitochondrial function (Braidy et al., 2013; H. J. Lee et al., 2010). These findings suggest that α-synuclein accumulation in astrocytes may be of great importance to the initiation of PD (Brück, Wenning, Stefanova, & Fellner, 2016). Nevertheless, the main roles of astrocytes during the progression and development of PD pathogenesis remain elusive.

1.4 Astrocytes and Inflammation

1.4.1 Reaction to Injury

Astrocytes have been described to react to injury. During injury, astrocytes migrate to the injury site and cause the formation of a glial scar contributing to neuronal repair, and they also begin to proliferate, which is known as reactive gliosis (Anderson et al., 2016; Cabezas et al., 2013; Sadelli et al.,

2017; Ye et al., 2015; Yuan et al., 2017; Zhu et al., 2017). The presence of astrocytes during injury is necessary and crucial for axonal repair (Anderson et al., 2016), thus suggesting an important role of astrocyte reactivity during neuroprotection.

1.4.2 The Immune System and PD

Astrocytes can release pro-inflammatory cytokines during disease in response to microglia and the immune system. A classic example of an astrocytic-mediated neuroprotective role switching to being neurodegenerative is when there is an excess of extracellular α-synuclein uptaken by the astrocyte causing α-synuclein accumulation inside the astrocyte (H. J. Lee et al., 2010). As this occurs, the astrocyte not only secretes TNF-α and IL-6, but transcriptional upregulation in inflammatory genes IL-1α, IL-1β, and IL-6 is also observed (H. J. Lee et al., 2010). The increase in the presence of pro-inflammatory cytokines is correlated with an increase of DA neuronal death in PD. This neuroprotective role played by astrocytes is a tightly regulated system which has been found to be partly mediated by the immune system, therefore any dysfunction can be pathogenic (Glass, Saijo, Winner, Marchetto, & Gage, 2010; Saijo et al., 2009).

1.4.3 Microglial Activation

Astrocytes not only release pro-inflammatory cytokines, but also have been found to become activated by the cytokines released by microglia during disease such as tumor necrosis factor-α (TNF-α) and interleukin-1β (IL-1β),

leading to ROS and NO production (Liddelow et al., 2017; Saijo et al., 2009). In the same study, Gage and colleagues also found that microglial inflammatory response could be enhanced by astrocytes through the NF-kβ pathway, increasing DA neuronal death. In addition, a different study described astrocyte activation by microglia through the release of a cytokine cocktail containing TNF-α, IL-1β, and complement system protein complex, C1q, as well as high expression of inflammatory marker complement 3 (C3) in astrocytes during PD pathogenesis (Liddelow et al., 2017). Therefore, crosstalk between both microglia and astrocytes can severely impact DA neuronal survival during PD.

1.5 iPSC Disease Modeling

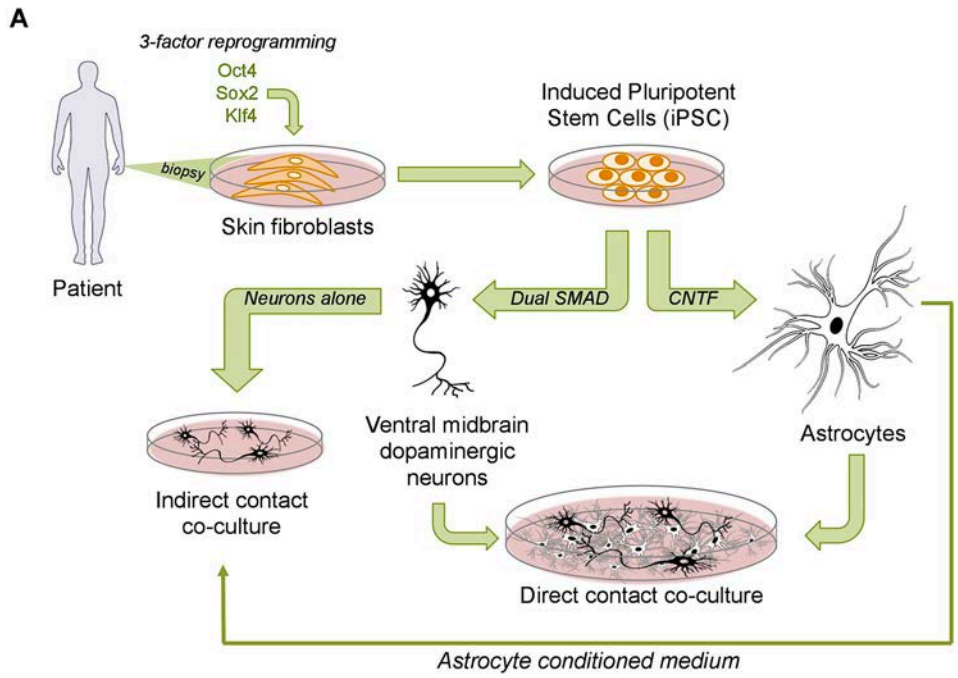

Figure 7. Modeling PD Through the Use of iPSC Technology.

After a skin biopsy is collected from either a healthy patient or a patient with PD, 3-factors (Oct4, Sox2, Klf4) are LV-inserted into the genome to produce iPSC. Patient-specific iPSC can then be directed into a neural or astrocitic fate to later perform direct and in-direct co-cultures.

Induced pluripotent stem cells (iPSC), when generated from patients with genetic conditions, can be exploited to create genuinely human experimental models of diseases (Zeltner & Studer, 2015). In the case of PD, previous studies by our group and others have generated iPSC from patients with PD associated to *LRRK2* mutations, and have described the appearance of disease-specific phenotypes in iPSC-derived neurons, including impaired axonal outgrowth and deficient autophagic vacuoles clearance (Nguyen et al., 2011; Reinhardt et al., 2013; Sánchez-Danés et al., 2012). Moreover,

DAn from LRRK2-mutant patient-specific iPSC displayed alterations in CMA that were, at least in part, responsible for the abnormal accumulation of α-synuclein observed in these cells, which predated any morphological signs of neurodegeneration (Orenstein et al., 2013).

2 PROJECT AIMS

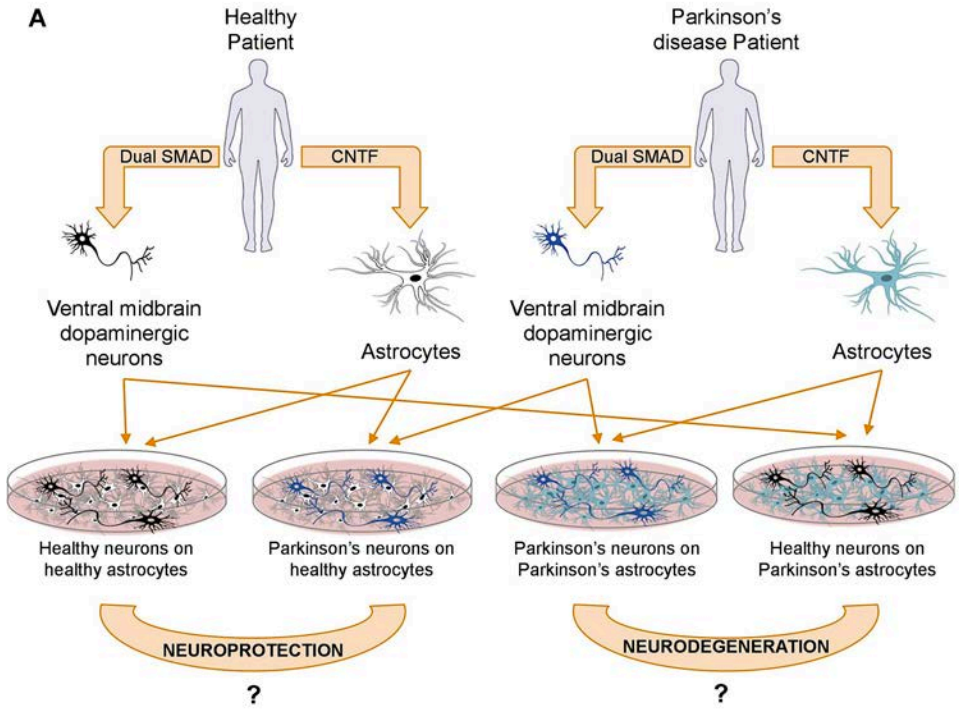

Figure 8. Scheme Depicting Project Aims.

Once iPSC-derived A9 ventral midbrain dopaminergic neurons and astrocytes had been produced, a series of different co-culture combinations were created to evaluate the possible role astrocytes play during PD pathogenesis.

The aims of this project were the following:

1. Generate patient-specific iPSC-derived astrocytes from two controls, two LRRK2-PD patients and two Sporadic-PD patients.
2. Fully characterize the newly generated patient-specific iPSC-derived astrocytes and check for known PD related phenotypes.
3. Investigate the possible pathological crosstalk between astrocyte and neuron in a newly devised co-culture system.

In the present studies, we generated patient-specific iPSC-derived astrocytes and vmDA neurons from PD patients with *LRRK2*^{G2019S} mutation and Sporadic-PD patients, as well as from healthy age-matched individuals. We consistently generated a population of human vmDA neurons in vitro that expressed post-mitotic dopaminergic markers and fired action potentials. Subsequently, we co-cultured healthy iPSC-derived vmDA neurons with iPSC-derived astrocytes expressing the mutated form of LRRK2 associated to PD. In our co-cultures, we detected a specific decrease in the number of vmDA neurons in the presence of LRRK2-mutated astrocytes, which correlated well with the abnormal accumulation of α-synuclein. Conversely, WT astrocytes were able to partially rescue disease-related phenotypes in LRRK2-PD neurons when co-cultured together, suggesting that LRRK2-PD astrocytes are lacking neuroprotective functions found in the WT astrocytes. A more in-depth investigation revealed PD-related phenotypes, such as impaired autophagic components, as well as a progressive accumulation of α-synuclein in both LRRK2-PD (100%) and Sporadic-PD astrocytes (20-40%), compared to healthy controls (0%). Moreover, by treating the cells with an activator of CMA, we were able to prevent the α-synuclein accumulation in LRRK2-PD astrocytes. Together, this data represents a first direct indication that astrocytes play a role during PD pathogenesis and may have broad implications for future intervention in early stages of PD.

3 MATERIALS AND METHODS

3.1 Cell Culture

3.1.1 iPSC to Astrocytes

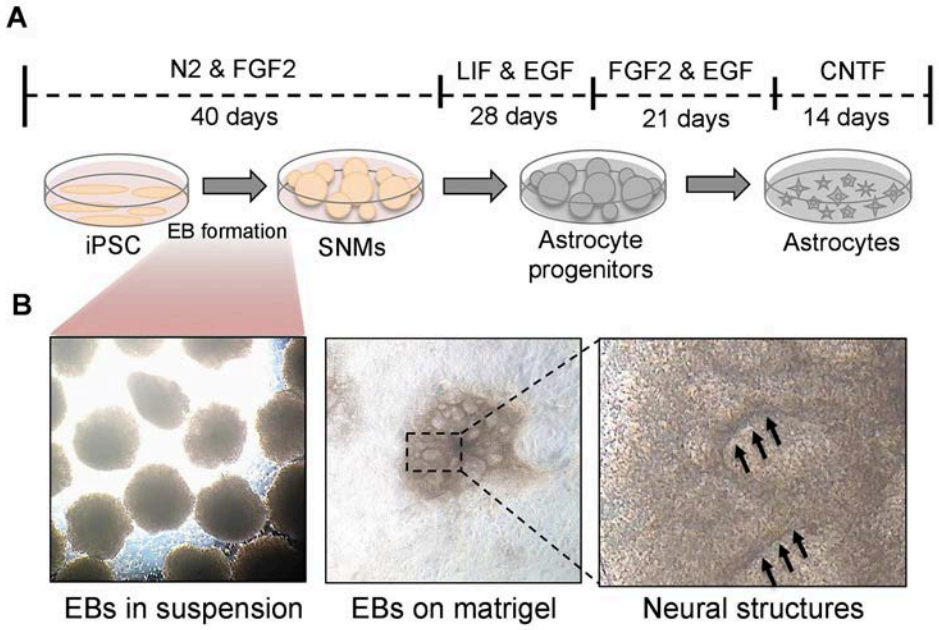

Figure 9. Scheme of Astrocyte Generation Protocol: Formation of EBs and Selection of Neural Structures.

(**a**) Scheme of step in astrocyte generation protocol. (**b**) Brightfield microscopy depicting the different stages of the protocol from EB formation to the manual selection of neural structures to form SNMs.

As previously described (Sánchez-Danés et al., 2012), fibroblasts were collected from two patients harboring the GS2019S mutation on the LRRK2 gene (SP13 and SP12), two from sporadic PD patients (SP04 & SP16) and two healthy age-matched controls (SP17 and SP09) and converted into four clones for each donor to induced pluripotent stem cell (iPSC) stocks (**Tables 1 & 2**). One iPSC clone from each donor was used to generate patient-specific astrocytes (in duplicates). Embryoid Bodies (EBs) were created from

each iPSC line and then plated on matrigel for 14 days with medium supplemented with N2 and FGF2. Once neural structures started to form (neural rosettes and neural tubes), these structures were mechanically selected and placed in suspension in non-adherent plates, thus becoming SNMs (**Fig. 9b**). After approximately 30 days of mechanical passaging (cutting), the SNMs adopted a homogenous rounded spherical shape and were ready to be characterized (**Fig. 10b**). Some SNMs were fixed *in toto* and immunocytochemical analysis was performed, staining for pluripotency markers, namely Ki67, Sox2, Nestin, and Pax6 (**Fig. 11b**).

Table 1. Summary of iPSC used

Summary of iPSC Lines Used

Patient			Disease				iPSC		Astrocytes	
Code	Status	Sex	Age at Biopsy	Age of Onset	Family history	Mutation	# of iPSC lines generated	# of iPSC lines used	# of astrocyte generations	# of n per assay
SP09	Control	M	66	N/A	No	No	4	1	2	3
SP17	Control	M	52	N/A	No	No	4	1	2	3
SP11	Control - SNCA Flag	F	48	N/A	No	No	4	1	2	3
SP13	PD LRRK2 Mutant	F	68	57	Yes	LRRK2G2019S	4	1	2	3
SP12	PD LRRK2 Mutant PD LRRK2 Mutant - SNCA Flag	F	63	49	Yes	LRRK2G2019S	4	1	2 2	3 3
SP08	PD Sporadic	F	66	60	No	No	4	1	1	0
SP04	PD Sporadic	M	46	40	No	No	4	1	1	2
SP16	PD Sporadic	F	51	48	No	No	4	1	1	2

Table 2. Summary of Astrocyte Lines Generated From iPSC

Summary of Astrocyte Lines Generated from iPSC

Patient			iPSC		Astrocytes	
Code	Status	Sex	# of iPSC lines generated	# of iPSC lines used	# of astrocyte generations	# of n per assay
SP09	Control	M	4	1	2	3
SP17	Control	M	4	1	2	3
SP11	Control - SNCA Flag	F	4	1	2	3
SP13	PD LRRK2 Mutant	F	4	1	2	3
SP12	PD LRRK2 Mutant PD LRRK2 Mutant - SNCA Flag	F	4	1	2 2	3 3
SP08	PD Sporadic	F	4	1	1	0
SP04	PD Sporadic	M	4	1	1	2
SP16	PD Sporadic	F	4	1	1	2

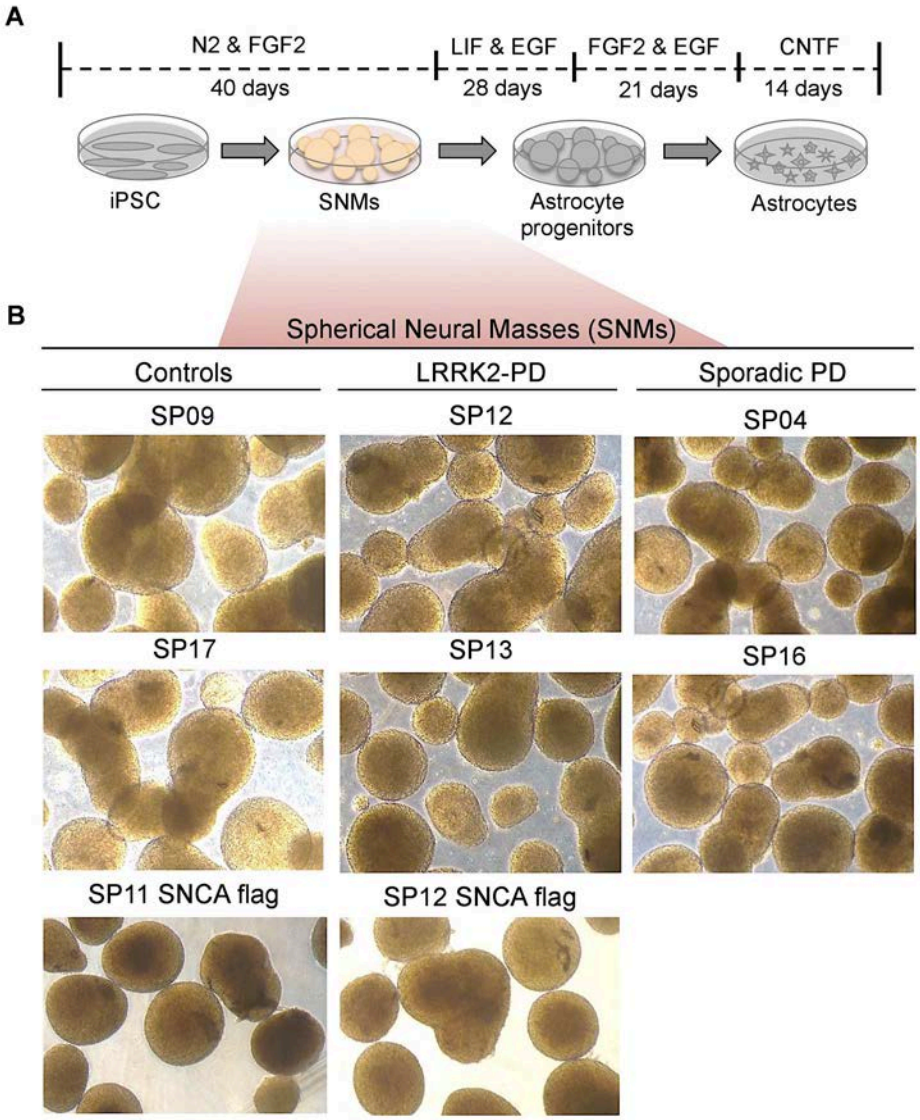

Figure 10. Scheme of Astrocyte Generation Protocol: Formation SNMs.

(**a**) Scheme of step in astrocyte generation protocol. (**b**) Brightfield microscopy images of all SNM lines newly generated.

SNMs were pushed towards an astrocytic lineage following a previously published protocol (Serio et al., 2013). Other SNMs were used for the neural differentiation part of the characterization to see if they are able to produce both neurons and glia cells (**Fig. 11b**). To do this, SNMs were seeded on matrigel-coated plates and left to differentiate for 3 weeks with medium supplemented with N2 and B27. Cells were fixed after the 3-week time-point and immunocytochemical analysis was performed using marker TUJ1 and GFAP.

First, the SNMs were grown in suspension for 28 days with medium supplemented with LIF and EGF, and then for a further 21 days with medium containing FG2 and EGF. Finally, SNMs were left with accutase (LabClinics) for 15 minutes at 37ºC and mechanically desegregated and plated on matrigel-coated plates (let set for 1 hour at RT) as a monolayer. The monolayer of neural progenitors was cultured for 14 more days in CNTF (Prospec Cyt-272) medium (Neurobasal, Glutamax, PenStrep, NEAA, CNTF) resulting in the formation of astrocyte progenitors ready for characterization. These astrocyte progenitors were successfully frozen in Astrocyte Freezing Medium (90% CNTF medium and 10% DMSO) and stored in liquid nitrogen for future use. When needed for an experiment, vials were thawed in medium containing FBS and resuspended in CNTF medium and plated on matrigel-coated plates. Cells were passaged four times before considered mature and then further characterized. Plastic cover slides were coated with matrigel in 24-well plates to conduct experiments.

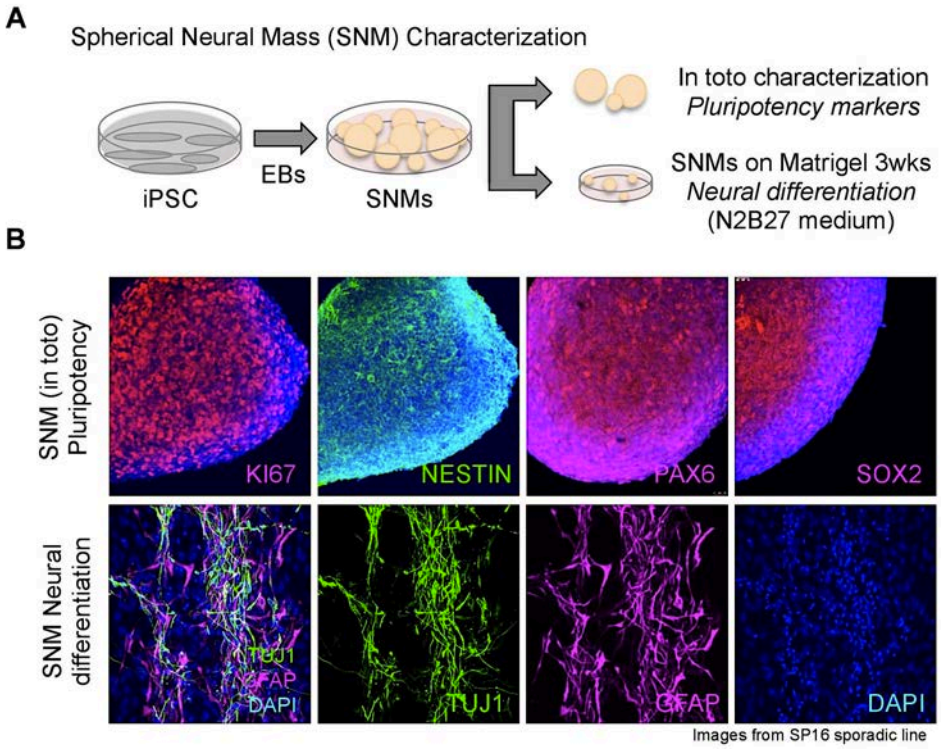

Figure 11. Scheme of Astrocyte Generation Protocol: Characterization of SNMs.

(**a**) Scheme of astrocyte generation protocol step being described. (**b**) Immunofluorescence images of SNMs in *toto* marked for pluripotency markers (Ki67, Nestin, Pax6, and Sox2) and SNMs on matrigel for 3 weeks marked neuronal differentiation markers (TUJ1 and GFAP).

3.1.2 iPSC to Ventral Midbrain Dopaminergic Neurons

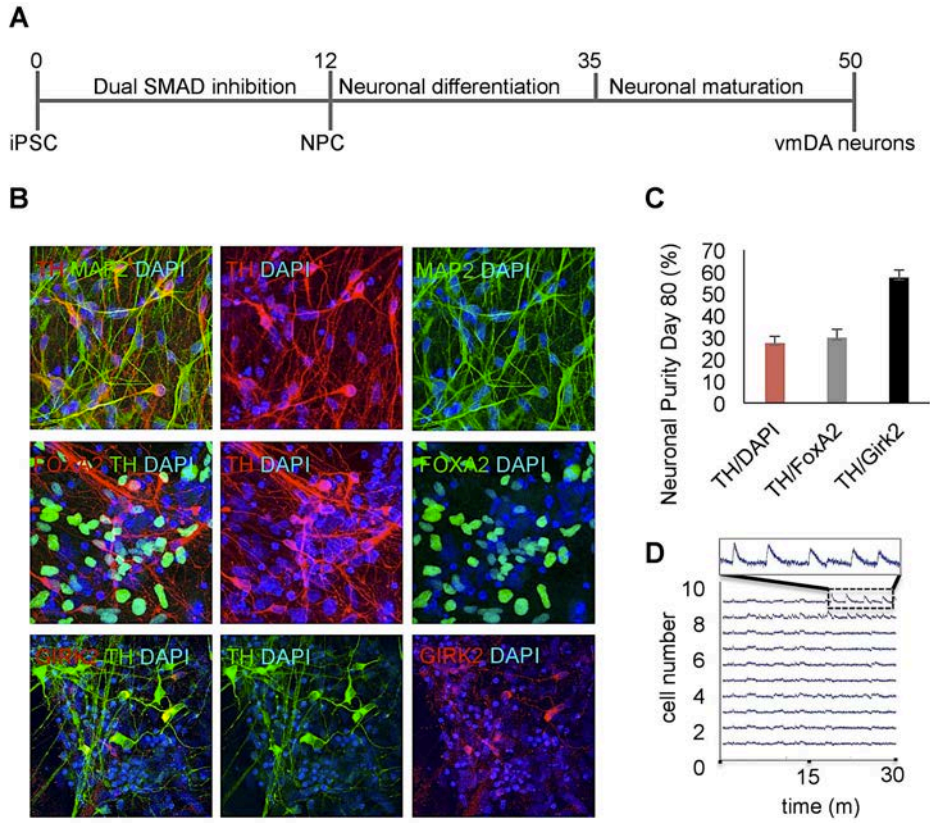

Figure 12. Generation of A9 Ventral Midbrain Dopaminergic Neurons.

(**a**) Scheme of dual SMAD inhibition protocol. (**b**) Representative immunofluorescence images of vmDAn after neuronal differentiation (80 days). iPSC-derived neural cultures express markers specific for neurons (MAP2), mature DA neurons (TH), and midbrain-type DA neurons (FoxA2 and Girk2), scale bar 20µm. (**c**) Percentage of vmDAn staining positive for Tyrosine hydroxylase (TH)/DAPI, double positive for TH and FOXA2 (transcriptional activator for vmDAn differentiation) and TH and GIRK (G-protein in vmDAn). (**d**) Graph representing day 35 vmDA neurons calcium wave flux recording over 30 minutes with calcium marker Fluo4-AM (n = 3).

Using a combination of two previously published protocols (Chambers et al., 2009; Kriks et al., 2011), vmDA neurons were obtained after 35 days after which they were co-cultured with LRRK2-PD and healthy astrocytes.* The vmDAn were fully characterized and displayed functional viability with calcium imaging techniques. After 35 days of differentiation, 20% of overall cells stained positive for TH, a number that increased with time reaching 45% after 50 days – a point at which the protocol named the neurons mature.

3.1.3 Set-up of Neuron-Astrocyte Co-Culture System

3.1.3.1 Direct Contact

The co-culture system was intended to house immature/young neurons and to continue the differentiation process on the top of the astrocytes; hence why day 35 neurons were used. Astrocytes were plated one week before the neurons were plated to ensure the development of a mature astrocyte feeder layer and to provide sufficient co-culturing time before the cells would be affected by stressed caused by prolonged culture conditions. vmDAn from both a control (SP11) and LRRK2-PD (SP12) lines were generated and $5x10^4$ cells/well were plated on the top of one-week-old astrocytes ($2x10^4$ cells/well) which were plated on the top of matrigel coated plastic cover slides in 24-well plates for two and four weeks. The medium used was basic and contained Neurobasal, B27, NEAA, PenStrep, and Glutamax. Cells were

*Data courtesey of Giulia Carola who generated neurons at the Institute of Biomedicine at the University of Barcelona (IBUB).

fixed with 4% PFA for 15 minutes and washed three times with PBS for 5 minutes before performing immunocytochemistry. TH positive cells and DAPI were counted for a series of 600 cells per condition using FIJI is Just ImageJ™ cell counter plugin and Microsoft excel for data plotting.

3.1.3.2 Indirect Contact

Following the previously published protocol, at day 20, neurons were split and plated on glass coverslips coated with poly-l-ornithine laminin and fibronectin. In the meantime, astrocytes (both PD and WT) were thawed and cultured for 14 days at passage 4 in wells of a 6-well plate with only one milliliter of medium in each well. After one week, 1 more milliliter of medium was added to the astrocytes. After 14 days, this medium was collected and placed directly on top of the day 35 neurons. The astrocyte-conditioned medium was added to the neurons 3 times for 7 days. Cells were then fixed for 15 minutes with 4% PFA and followed by the necessary immunocytochemistry, GFAP, TH, and SNCA.

3.2 Biochemistry Techniques

3.2.1 Protein Extraction

Live cells were washed twice with PBS and incubated for six minutes at 37ºC with accutase (Sigma). Cells were lifted and collected in washing medium containing FBS and centrifuged at 800rpm for five minutes. After centrifugation, cells were resuspended in cold PBS and placed in 1.5mL eppendorfs and centrifuged for five minutes at 4ºC at 600x*g*. After

discarding the supernatant, pellets were immediately stored at -80ºC for future use. Alternatively, the protein extraction could immediately take place after pellet collection at 4ºC. Pellets were homogenized in 50 mM Tris-HCl, pH 7.4/150 mM NaCl/0.5% Triton X-100/0.5% Nonidet P-40 and a mixture of proteinase inhibitors (Sigma, Roche tablet). Samples were then centrifuged at 15,000x*g* for 20 minutes at 4ºC. The resulting supernatant was normalized for protein using BCA kit (Pierce).

Protein extraction for oligomeric α-synuclein: Mila lysis buffer (0.5M Tris at pH 7.4 containing 0.5 methylenediaminetetraacetic acid at pH 8.0, 5M NaCl, 0.5% Na doxicholic, 0.5% Nonidet P-40, 1mM phenylmethylsulfonyl fluoride, bi-distilled water, protease and phosphatase inhibitor cocktails) (Roche Molecular Systems, Pleasanton, CA, USA), and then centrifuged for 15 min at 13,000rpm at 4°C (Ultracentrifuge Beckman with 70Ti rotor, CA, USA).

3.2.2 Immunoblotting

Cell extracts were then boiled at 100ºC for 5 minutes, followed by 7-15% electrophoresis in Running buffer, then electrotransferred in Transfer buffer at 100v to PVDF membranes for 1.5 hours at 4ºC. Buffers and reagents were prepared (**Table 3**). After treating the membranes with Ponceau S solution (Sigma) in order to cut separately the protein of interest and the loading control protein for separated antibody incubations, the membranes were then blocked in blocking solution for 1 hour and incubated overnight in containing primary antibodies (**Table 4**). After incubation with peroxidase-tagged secondary antibodies (**Table 5**), membranes were revealed with ECL-plus chemiluminescence Western blot kit (Amershan-Pharmacia Biotech).

Table 3: Buffers and Reagents for Immunoblot

Buffer	Recipe
Running Buffer	30.0g Tris base, 144.0g glycine, 10.0g SDS in 1000 ml of H_2O, pH 8.3
Transfer Buffer	25 mM Tris-HCl (pH 7.6), 192 mM glycine, 20% methanol, 0.03% sodium dodecyl sulfate (SDS)
Blocking solution	TBS 1x/BSA 3%/TWEEN 0.1%

Table 4: Primary Antibodies for Immunoblot

Antibody	Species	Product code	Dilution
Oligomeric α-synuclein	anti-Mouse	Agisera AS13 2718	1:500
Monomeric α-synuclein	anti-Mouse	BD, 610787	1:1000
MFN1	anti-Rabbit	Santa Cruz sc-50330	1:1000
MFN2	anti-Mouse	Abcam ab56889	1:1000
pDRP1	anti-Rabbit	Cell Signaling (3455)	1:1000
DRP1	anti-Mouse	BD 611112	1:1000
OPA1	anti-Mouse	BD 612606,	1:1000
TIM44	anti-Mouse	BD T14720	1:1000
TOM20	anti-Rabbit	Sant Cruz, sc-11415	1:1000
LC3B	anti-Rabbit	Cell Signaling, 2775	1:1000
Actin	Anti-Rabbit	Sigma (A2066)	1:10,000
Tubulin	Rabbit (serum)	Sigma (T3526)	1:10,000

Table 5: Secondary Antibodies for Immunoblot

Antibody	Product code	Dilution
Goat Anti-Rabbit IgG H&L (HRP)	ab205718	1:10,000
Goat Anti-Mouse IgG H&L (HRP)	ab205719	1:10,000

3.2.3 Immunocytochemistry

After medium removal, samples were fixed using 4% PFA for 15 minutes and then washed three times for 15 minutes with PBS. Solutions for immunocytochemistry were prepared (**Table 6**). Samples were blocked with TBS++ with low triton for two hours and 48-hour incubation with primary

antibodies at 4ºC. After 48-hour incubation with the primary antibody (**Table 7**), samples were then washed with TBS 1x for 15 minutes three times, before being blocked again for one hour at room temperature. Samples were incubated with their rightful secondary antibody (**Table 8**) for two hours at room temperature. Samples were then further washed with TBS 1x for 15 minutes three times and then incubated with nuclear staining DAPI (Invitrogen, dilution 1:5000) for 10 minutes. After having washed the samples twice with TBS 1x for 10 minutes, samples were mounted with PVA:DABCO and stored at 4ºC until imaged. Samples were imaged using an SP5 confocal microscope (Leica) and analyzed with FIJI is Just ImageJ™.

Table 6: Solutions for Immunocytochemistry

Solution	Recipe
TBS1x	6.05g Tris, 8.76g NaCl, 800 mL of H_2O, pH 7.6 with 1M HCl
TBS++	TBS1x, NDS 3%, Triton 0.01%

Table 7: Primary Antibodies for Immunocytochemistry

Antibody	Species	Reference	Dilution
CD44	anti-Mouse	Abcam ab6124	1:100
GFAP	anti-Guinea pig	Synaptic Systems, 173 004	1:1000
S100β	anti-Rabbit	Dako, 311	1:250
Vimentin	anti-Mouse IgM	Iowa, 3CB2	1:100
TUJ1	anti-Mouse	Covance 435P	1:500
MAP2	anti-Rabbit	Santa Cruz sc-20172	1:1000
NG2	anti-Rabbit	Millipore, AB5320	1:250
GLT1	anti-Guinea pig	Millipore, AB1783	1:500
GIRK2	anti-Rabbit	Sigma P8122	1:40
FOXA2	anti-Mouse	Santa Cruz sc-101060	1:250
Synapsin 1	anti-Mouse	Calbiochem 574777	1:1000
TOM20	anti-Rabbit	Sant Cruz, sc-11415	1:250
TOM20	anti-Mouse	BD, 612278	1:1000
LC3B	anti-Rabbit	Cell Signaling, 2775	1:100
LAMP-2A	anti-Rabbit	Abcam, 18528	1:100
α-synuclein	anti-Mouse	BD, 610787	1:500
TH	anti-Sheep	Pel-Freez, P60101-0	1:500
TH	anti-Rabbit	Santa Cruz, sc-14007	1:250
LAMP1	anti-Mouse	Iowa, H4A3	1:100
MAP2	anti-Rabbit	Sant Cruz sc-20172	1:500

Table 8: Secondary Antibodies for Immunocytochemistry

Antibody	Species	Product code
Alexa Fluor 488	anti-Mouse IgG	Jackson 715-545-150
Cy3	anti-Rabbit IgG	Jackson 711-165-152
DyLight 649	anti-Guinea pig IgG	Jackson 706-495-148
Alexa Fluor 647	anti-Sheep	Jackson 713-605-147
Cy™2 AffiniPure Donkey	Anti-Rabbit IgG (H+L)	Jackson 711-225-152
Cy™3 AffiniPure Donkey	Anti-Mouse IgG (H+L)	Jackson 715-165-151

3.2.4 Real-Time Quantitative Polymerase Chain Reaction

The isolation of total mRNA was performed by guanidinium thiocyanate–phenol–chloroform extraction (TRIzol, Invitrogen) and treated with DNase I. One microgram was used to synthesize cDNA with the SuperScript III Reverse Transcriptase Synthesis Kit (Invitrogen). Quantitative RT-PCR analyses were done in triplicate on 50ng with Platinum Syber Green qPCR Super Mix (Invitrogen) in an ABI Prism 7000 thermocycler (Applied Biosystems). All results were normalized to GAPDH. Primers listed in **Table 9**.

Table 9: Primers Used for qRT-PCR

Gene	Forward primer	Reverse primer
Aquaporin 4	AGATCAGCATCGCCAAGTCT	AACCAGGAGACCATGACCAG
p62	CCCTGAGGAACAGATGGA	GACTGGAGTTCACCTGTAGA
GapDH	GCACCGTCAAGGCTGAGAAC	AGGGATCTCGCTCCTGGAA
TFEB	CATGCATTACATGCAGCAG	GTAGGACTGCACCTTCAAC
Alpha-synuclein	GAAGTGGCCATTCGACGAC	CCTGCTGCTTCTGCCACAC

3.2.5 Fluo-4 Calcium Imaging*

Live cells were incubated with Fluro4-AM flurofore for 30 minutes slowly shaking at room temperature. Cells were then imaged for 20-minute recordings using the Hokawo program and when finished data was converted from video to images. The data was then put through the NeuroImage

*Done in collaboration with Professor Jordi Soriano, Department of Physics, University of Barcelona.

program where Calcium Activity Map and individual Calcium Graphswere generated. Data is further analyzed in a Matlab code made by Jordi Soriano.

3.2.6 CRISPR guideRNA (gRNA) and Donor Plasmid Design*

CRISPR/Cas9 gRNAs against the last exon-3'UTR junction of the human *SNCA* gene were designed so that the spacer sequence overlapped the STOP codon. Complementary oligos encoding for the desired spacer sequences were annealed into the BbsI site of the gRNA scaffold of the Cas9-T2A-EGFP/gRNA co-expression plasmid px458 (Addgene, #48138). For increased expression of the Cas9 protein in hPSC, Cbh promoter was replaced by a full-length version of the CAGGS promoter. The cleavage efficiency of two gRNAs was tested by T7EI assay. Both gRNAs displayed a similar cutting efficiency but gRNA2-OL was selected for the editing process. Donor plasmid for knocking-in a FLAG tag fused C-terminal to the α-synuclein open reading frame (ORF) was engineered using two homology arms (HAs) spanning approximately 800 bp from both sides of the STOP codon. The sequence encoding for the FLAG tag was placed immediately after the last codon of the SNCA ORF and before the STOP codon. A selection cassette (pRex1-NeoR) surrounded by loxP sites was cloned between the STOP codon and the 3'HA. The sequence of the cloning primers and gRNA oligonucleotides can be found in **Table 10**.

*CRISPR/CASP9 gene editing techniques were all performed by Dr. Carles Calatayud Aristoy and Giulia Carola of the Institute of Biomedicine of the University of Barcelona (IBUB), Spain.

Table 10: Sequence of Cloning Primers and gRNA Oligonucleotides

Purpose	Oligo name	Sequence
Annealed oligo cloning of gRNAs	SNCA_gRNA1_OL-F	AAAGATATTTCTTAGGCTTC
	SNCA_gRNA1_OL-R	GAAGCCTAAGAAATATCTTT
	SNCA_gRNA2_OL-F	TGGGAGCAAAGATATTTCTT
	SNCA_gRNA2_OL-R	AAGAAATATCTTTGCTCCCA
Primers for generating the donor plasmid	SNCA_5-F_XhoI	AACTCGAGACTCAAGCTTAGGAACAAGGA
	SNCA_5Flag-R_SalI	AAGTCGACTTACTTGTCGTCATCGTCTTTGTAGTCGGCTTCAGGTTCGTAGTCTT
	Rex1_F-loxP-SalI	AAGTCGACATAACTTCGTATAGCATACATTATACGAAGTTATGACCGATTCCTCCCGATAAG
	Neo_R-loxP-BamHI	AAGGATCCATAACTTCGTATAGCATACATTATACGAAGTTATTAAGATACATTGATGAGTTTGGA
	SNCA_3-F_BamHI	AAGGATCCGAAATATCTTTGCTCCCAGT
	SNCA_3-R_NotI	AAGCGGCCGCTTAAGGAACCAGTGCATAC
Primers for screening PCR	SNCA_5Out_R	
	Check_Rex1Neo_5HA_R	CTTATCGGGAGGAATCGGTC
	Check_Rex1Neo_3HA_F	CCCGTCTGTTGTGTGACTC
	SNCA_3Out_R	ACGTAAAGCAAACATTGACAGG

3.2.7 CRISPR-Mediated SNCA Locus Edition in hiPSC [*]

The day before transfection, 800.000 hiPSC were seeded in a 10cm plate coated with matrigel. The following day, hiPSC were co-transfected with a mix of 6 μg of Cas9-T2A-EGFP/gRNA, 9 μg of the donor plasmid, 45 μL of FuGENE HD (Promega) transfection reagent, and KO-DMEM up to 750 μL. The transfection mixture was incubated for 15 minutes at room temperature and subsequently added dropwise to the cells. Geneticin (G-418; 50 μg/mL) selection was initiated 72h post-transfection and was maintained until the emerging colonies were transferred to another plate. Between 10 and 14 days after the initiation of the selection, colonies were large enough to be screened. Half of the colony was sampled in order to check site-specific integration by means of PCR. The colonies that were positive for the targeted recombination were transferred to a different well in order to be transfected with a CRE-recombinase expressing plasmid. After CRE transfection, cells were singularized and seeded at a low density on top of irradiated human fibroblast feeder layer in the presence of ROCK inhibitor (Miltenyi). Once the colonies attained a certain size, they were isolated and screened for selection cassette-excision. Those clones whose both SNCA alleles were tagged with the FLAG epitope were expanded and characterized in terms of pluripotency and genome stability.

[*]CRISPR/CASP9 gene editing techniques were all performed by Dr. Carles Calatayud Aristoy and Giulia Carola of the Institute of Biomedicine of the University of Barcelona (IBUB), Spain.

3.2.8 Cell Viability Assay for Flow Cytometry*

Calcein Green AM (Thermofisher ref. C3100MP) (1µM final concentration) was added to the cells in 0,5ml suspension medium (not exceeding 1M cells) containing PBS. In addition, 2µL of Propidium iodide (Sigma ref. P4170) (1mg/mL) was also added to the cells and incubated 5 min in the same conditions as above. Flow cytometry analysis was performed with excitation at 488 nm and emission collected at ~520 nm (FITC channel) for Calcein Green AM, and at ~585nm (Phycoerythrin channel) for the PI. Cells were run on a Gallios flow cytometer analyzer and file analysis was done using Kaluza Software, both from Beckman Coulter Inc. (Brea, CA).

3.3 Techniques to Evaluate Protein Degradation Pathways

3.3.1 Chaperone Mediated Autophagy Reporter Assay†

CMA activity was measured using a photoactivatable CMA fluorescent reporter with a CMA targeting motif added to the PS-dendra protein (KFERQ-PS-dendra) developed and updated by Dr. Ana Maria Cuervo and Colleagues (Koga, Martinez-Vicente, Macian, Verkhusha, & Cuervo, 2011; Park, Suh, & Cuervo, 2015). Cells transduced with the lentivirus carrying the

*Done in collaboration with José Miguel Andrés Vaquero of the Center of Regenerative Medicine of Barcelona (CMRB), Spain.

†CMA Reporter KFERQ-DENDRA was kindly provided by Dr. Ana Maria Cuervo of Albert Einstein College of Medicine, Bronx, NY, USA.

reporter were photoactivated with a UV light for 3 minutes and then imaged after 52 hours to monitor CMA activity.

3.3.2 Knock-Down of LAMP2A Gene (shLAMP2A)*

After 14 days in culture, cells were transduced with a lentivirus containing shLAMP-2A (Ashish C Massey, Follenzi, Kiffin, Zhang, & Cuervo, 2008). Half of the medium was added the following day, and the virus was left to take effect for 72 hours. Cells were then fixed with 4% PFA for 15 mins and stained with anti-GFAP and anti-α-synuclein in ICC, in accordance with the protocol previously described in the ICC section. α-Synuclein puncta were counted using a macro developed in FIJI is for ImageJ™ measuring α-synuclein area within the cell. 100 cells per condition were measured. The shLAMP-2A plasmid was kindly supplied by AMC.

3.3.3 LC3-Flux Assay

After 14 days of culture, cells were either not treated with a drug (control), or were treated with lysosomal inhibitors (**Table 11**), Leupeptin (100µg, Sigma L2884) and NH4Cl (20µg, Sigma A9434) for 2 hours. The assay was terminated by washing the cells twice in PBS. The pellets were collected as previously described under the 'protein extraction' section. Western blots were performed using 13% gels, and as previously described in WB section.

*Plasmid of shLAMP2A was kindly provided by Dr. Ana Maria Cuervo of Albert Einstein College of Medicine, Bronx, NY, USA.

Ratio of 2-hour drug treatment versus no drug was performed per line to determine speed of fusion.

Table 11: Lysosomal Inhibitors

Inhibitor	Stock solution	Final concentration
NH_4Cl	2M	20mM
Leupeptin	10mM	100µM

3.3.4 Alpha-Synuclein Flux Assay

After 14 days of culture, cells were either not treated with a drug (control), or were treated with inhibitors (**Table 12**), Lactacystin (5mM, Enzo BML-PI104) for 2 hours, or with Leupeptin (100µg, Sigma L2884) for 12 hours. The assay was terminated by washing the cells twice in cold PBS. The pellets were collected as previously described under the 'protein extraction' section. WB was performed using 12.5% gels, and as previously described in WB section.

Table 12: Lysosomal and Proteosomal Inhibitors

Inhibitor	Stock solution	Final concentration
Leupeptin	10mM	100µM
Lactacystin	5mM	5µM

3.4 Data Analysis

3.4.1 Mitochondria Counting

Individual mitochondria were counted manually using the FIJI is Just ImageJ™ software and separated by eye between elongated (>0.5μm) and fragmented (<0.5μm) groups. Mitochondria staining positive with TOM20 were counted for 100 cells.

3.4.2 Densitometry

After having been developed at several different times (1 second, 30 seconds, 1 minute, 3 minutes, 5 minutes, 10 minutes, and 20 minutes to burn) films were scanned at 2,400 x 2,400 dpi (i800 MICROTEK high quality film scanner), and the densitometric analysis was performed using FIJI is Just ImageJ™. Other membranes were imaged using the ChemiTouch machine under the 'Optimal exposure' setting and digitally saved.

3.4.3 Sholl Analysis

Individual neurites were traced per neuron using the plug-in NeuronJ in FIJI for ImageJ™. Once all primary, secondary, and tertiary neurites were traced, the appropriate Sholl analysis plug-in was run. Each data set per individual neuron was plotted in an excel document. Once 20 neurons per condition were analyzed, the average neurite intersections per 10 microns were calculated and plotted on a line graph along with the standard error of the mean.

3.4.4 Confocal Imaging

Images were acquired with an Leica TCS SP5 II Confocal microscope with 40x and 63x objectives. For colocalization analysis of α-synuclein and LAMP2A or LAMP1 and LC3, the 63x objective was used with a zoom factor 4. Laser power for all lasers (visible 488, 561, 633; invisible 405) was set to 30% with a gain of 800.

3.4.5 Statistics

Statistical analyses of the obtained data was performed using two-tailed unequal variance Student *t*-tests of the average of 3 independent repeats (* $p<0.05$, ** $p<0.01$, *** $p<0.001$) and the mean and standard error of the mean were plotted using Microsoft Excel (MacOsx).

4 RESULTS

4.1 Generation and Characterization of Functional iPSC-Derived Astrocytes

Using a previously published protocol (Serio et al., 2013), astrocyte-like cells were successfully differentiated from iPSC lines representing six independent individuals: two from PD patients carrying the LRRK2^{G2019S} mutation (SP12 and SP13), two from patients with Sporadic PD (SP04 and SP16), and two healthy age-matched controls (SP17 and SP09).

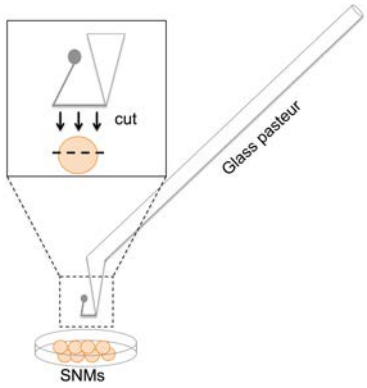

Figure 13. SNM Cutting Tool.

The first step of the protocol required the generation of Embryoid Bodies (EBs), followed by plating those EBs on matrigel for 14 days, and then allowing for neural structures to form and to be mechanically picked and kept in suspension (**Fig. 9 in Materials and Methods section**). Once neural structures were in suspension, they were considered to be spherical neural masses (SNMs). SNMs were passaged by mechanically cutting them with a handmade cutting tool from a glass Pasteur (**Fig. 13**). The protocol required the SNMs to be passaged once per week and then were considered to be ready for full SNM characterization after 30 days in culture (after 4 passages), mechanical selection of neural structure in suspension being day 1 (**Fig. 10 in Materials and Methods section**).

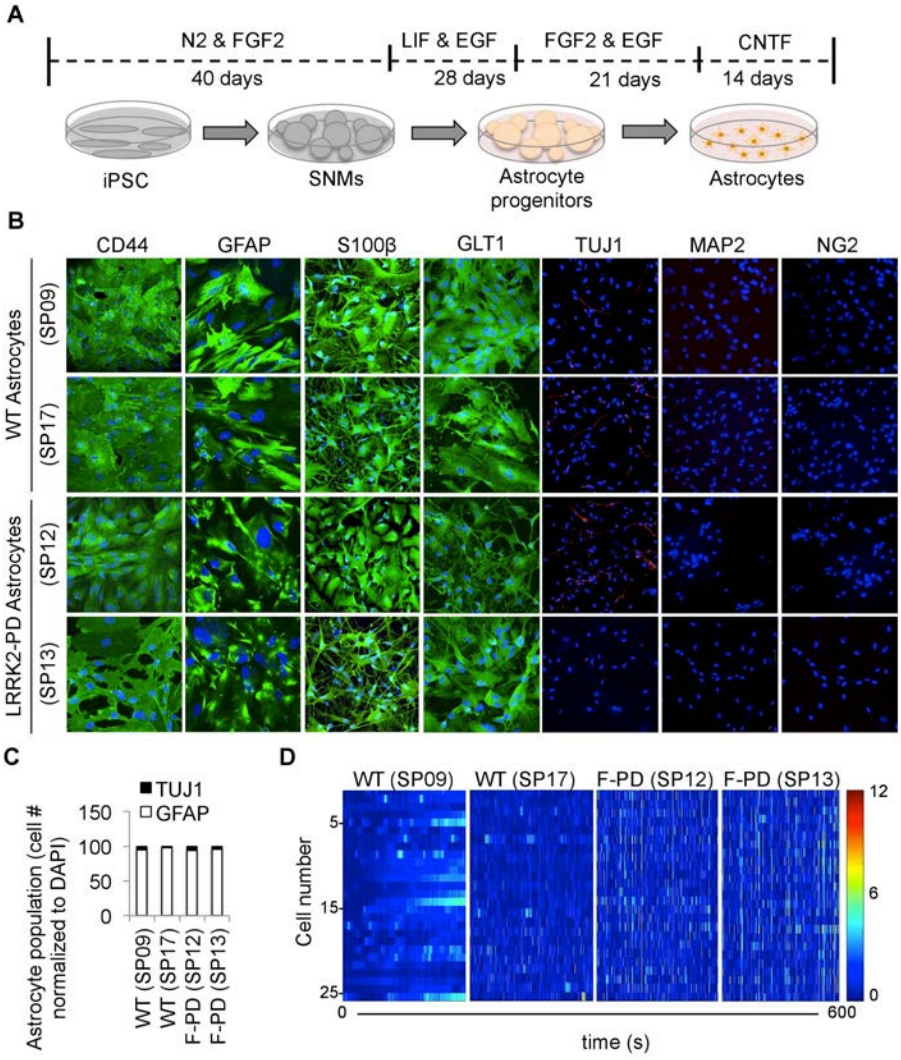

Figure 14. Characterization of LRRK2-PD and WT iPSC-Derived Astrocytes.

(**a**) Scheme of astrocyte generation protocol step. (**b**) Representative images of two control lines and two LRRK2-PD lines staining positive for astrocytic markers CD44 (precursor), GFAP (general astrocytes), and S100β (mature astrocytes), GLT1 (excitatory amino acid transporter 2) and negative or low expression for TUJ1 (immature neuron), no MAP2 (mature neuron) nor NG2 (oligodendrocytes) expression (n = 3). Scale bar, 100 µm. (**c**) Astrocyte population is highly pure amongst all lines. (**d**) Heatmap representing calcium fluctuation recording using Fluo4-AM (n = 2).

Once SNMs reached 30 days, some were plated on matrigel with medium supplemented with N2 and B27 for a 3-week neural differentiation and others were fixed *in toto* for immunocytochemical analysis of pluripotency markers (**Fig. 11 in Materials and Methods section**). After having been fully characterized, SNMs underwent the astrocyte generation protocol. SNMs were placed in suspension with medium supplemented with LIF and EGF for three weeks, FGF2 and EGF for another three weeks, mechanically desegregated and plated as a monolayer with FGF2 and EGF for two weeks, and finally cultured with medium supplemented with CNTF for two more weeks where they were deemed as astrocyte progenitors (passage 0). For this project, astrocytes were passaged up to four passages to reach full astrocyte identity.

All six iPSC-derived astrocyte lines were fully characterized through immunocytochemistry (ICC) using the appropriate markers (**Fig. 14b, 15b**). Cells positively stained for astrocyte progenitor markers CD44 when at the progenitor level. Astrocytes were further characterized, once reaching complete astrocyte identity and maturity at passage 4, by positively staining for astrocyte maturity marker S100 calcium-binding protein β (S100β), as well as excitatory amino acid transporter 2 (EAAT2, also known as GLT1). Additional markers including general neuronal marker TUJ1, neuronal maturity marker MAP2, and oligodendrocyte marker NG2 were negatively stained. The vast majority (95%) of the cells expressed astrocytic marker glial fibrillary acidic protein (GFAP), indicating a highly pure population of iPSC-derived astrocytes (**Fig. 14c, 15c**).

In addition to qualitative characterization, we performed functional quantitative analysis to determine if these cells reflected the functional qualities of astrocytes found in the brain. Calcium (Ca^{2+}) recordings from PD

and non-PD astrocytes showed a heterogeneous pattern of calcium fluctuations under basal conditions, revealing functionality (**Fig. 14d, 15d**). As this technique measured whole cell Ca^{2+} fluctuations, differences between PD and WT astrocytes were not evident. In addition to Ca^{2+}, we measured ATP production, which resulted in similar levels (**Fig. 16a**), further supporting the successful generation of functionally equivalent astrocyte-like cells from both groups.

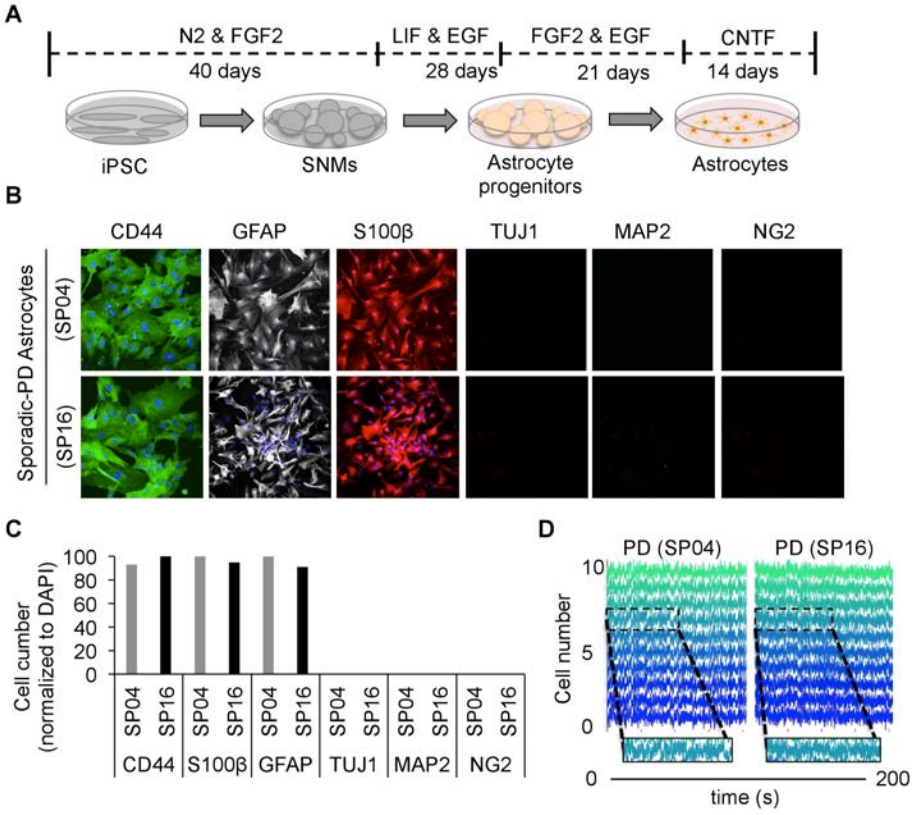

Figure 15. Characterization of Sporadic-PD iPSC-Derived Astrocytes.

(**a**) Scheme of astrocyte generation protocol step. (**b**) Immunofluorescence staining of astrocyte markers CD44, GFAP, S100β, and negative for TUJ1, MAP2 and NG2. (**c**) Astrocyte population is highly pure amongst all lines. (**d**) Calcium recording using Fluo4-AM.

Quantitative Real Time PCR (qRT-PCR) was performed in parallel revealing mRNA expression of astrocyte end-feet marker Aquaporin-4 (AQP4) in both control and PD astrocytes (**Fig. 16b**). These results were consistent for all PD and WT astrocytes.

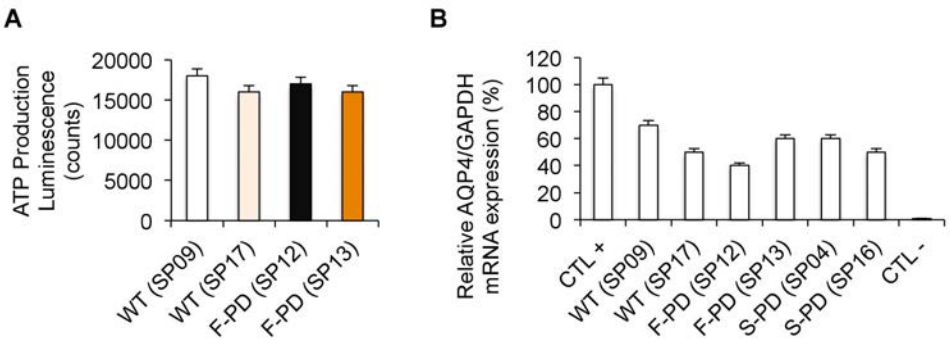

Figure 16. iPSC-Derived Astrocytes Are Functional.

(**a**) Astrocytes produce similar levels of ATP. (**b**) Relative AQP-4 mRNA expression in all astrocyte lines. All graphs plot mean ± s.e.m, unpaired two-tailed Student's *t*-test, *p<0.05, **p<0.01, ***p<0.001.

4.2 Astrocytes Can Support Neuronal Homeostasis in Newly Established Co-Culture System.

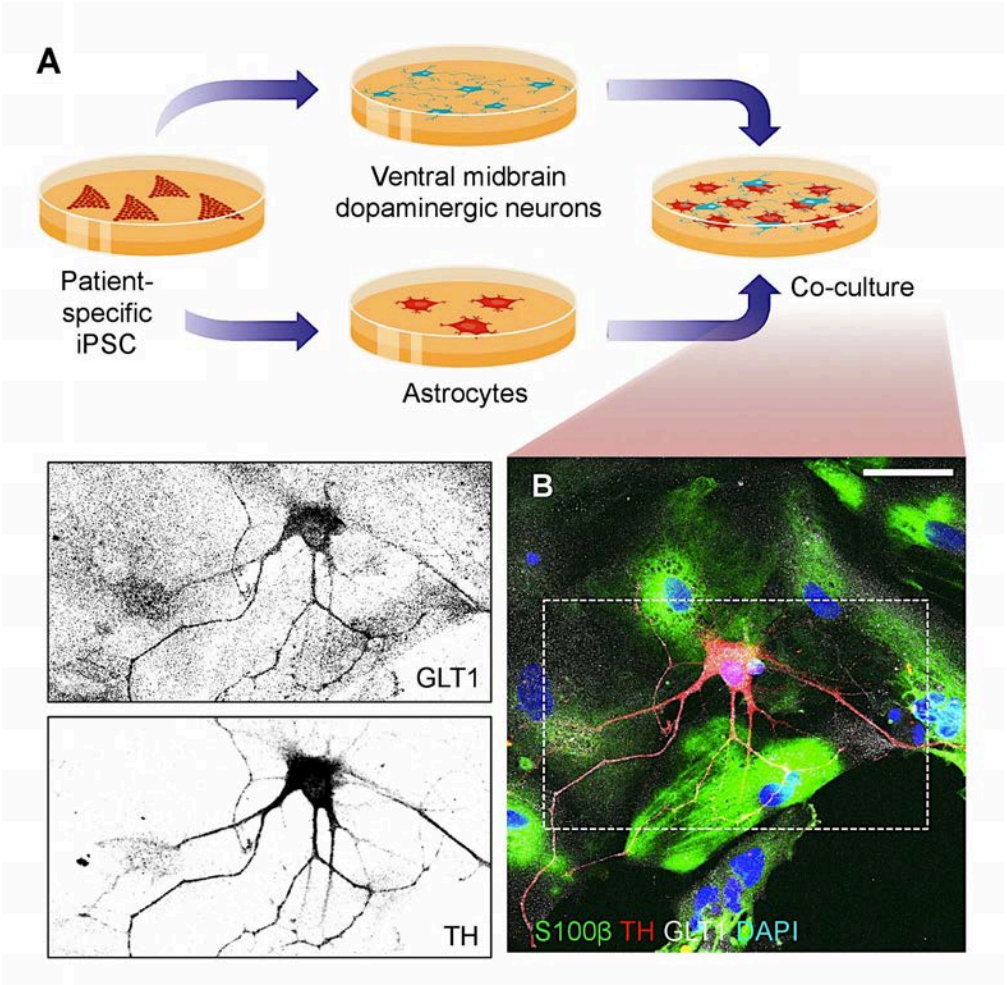

Figure 17. Set-Up of Neuron-Astrocyte Co-Culture System.

(**a**) Diagram of newly devised co-culture system. (**b**) Representative images of 4-week co-culture staining positive for WT vmDA neurons (TH), WT astrcoytes (GFAP), Excitatory Amino Acid Transporter 2 (GLT1), and nuclear DAPI. Scale bar 20 µm.

To evaluate glial contribution during PD, a newly devised co-culture system was created (**Fig. 17a**) either by directly placing neurons on the top of astrocytes (direct contact) or by culturing neurons alone with astrocyte conditioned medium (indirect contact). To do this, A9 ventral midbrain dopaminergic (vmDA) neurons were generated[*] and fully characterized using a combination of two previously published protocols (Chambers et al., 2009; Kriks et al., 2011) (**Fig. 12a**). After 80 days under differentiation conditions, the cells expressed neuronal markers such as MAP2, and vmDAn lineage markers tyrosine hydroxylase (TH), FOXA2, and G protein-activated K+ channel (GIRK2). Neuronal cultures were typically comprised of approximately 30% TH positive neurons, and, within that population, 30% were TH/FOXA2 and 60% were TH/GIRK double positive cells (**Fig. 12c**).

[*]Neurons were generated by Giulia Carola of the Institute of Biomedicine of the University of Barcelona (IBUB).

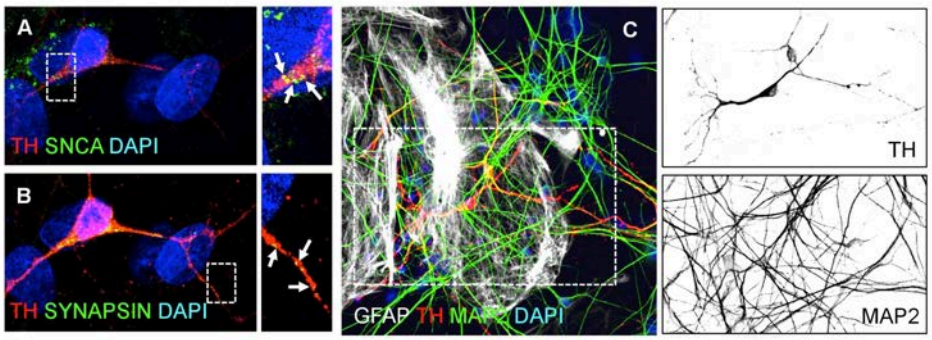

Figure 18. Neurons are Functional and Create a Connected Network During a Co-Culture.

(**a**) Neurons expressing α-synuclein in the pre-synaptic terminals. (**b**) Neurons expressing synapsin 1 in the pre-synaptic terminals. (**c**) TH neurons form a connected network with other MAP2 positive cells.

These neurons were determined functional through successful generation of Ca^{2+} fluctuation waves (**Fig. 12d**). The neuronal differentiation protocol calls for the addition of several factors to maintain a nutritious environment for the neurons to live in. During the co-culture, however, all factors were removed since the astrocytes were expected to provide trophic support. The co-culture system was efficacious and WT astrocytes were able to allow for the proper maturation of WT vmDA neurons and glutamate exchange through GLT1 expression (**Fig. 17b**), as well as to promote neuronal synapse formation (**Fig. 18a,b**) and an overall healthy neuronal network comprised of many MAP2 positive cells (**Fig. 18c**). Once the co-culture system was successfully created, we combined neurons and astrocytes from LRRK2-PD patients with neurons and astrocytes of WT controls in order to determine if glia cells play a role during PD.

4.3 Non-Cell Autonomy in Parkinson's Disease Pathogenesis

4.3.1 Parkinson's Disease Astrocytes Cause Neurodegeneration in Healthy Dopaminergic Neurons in a Direct Contact Co-Culture.

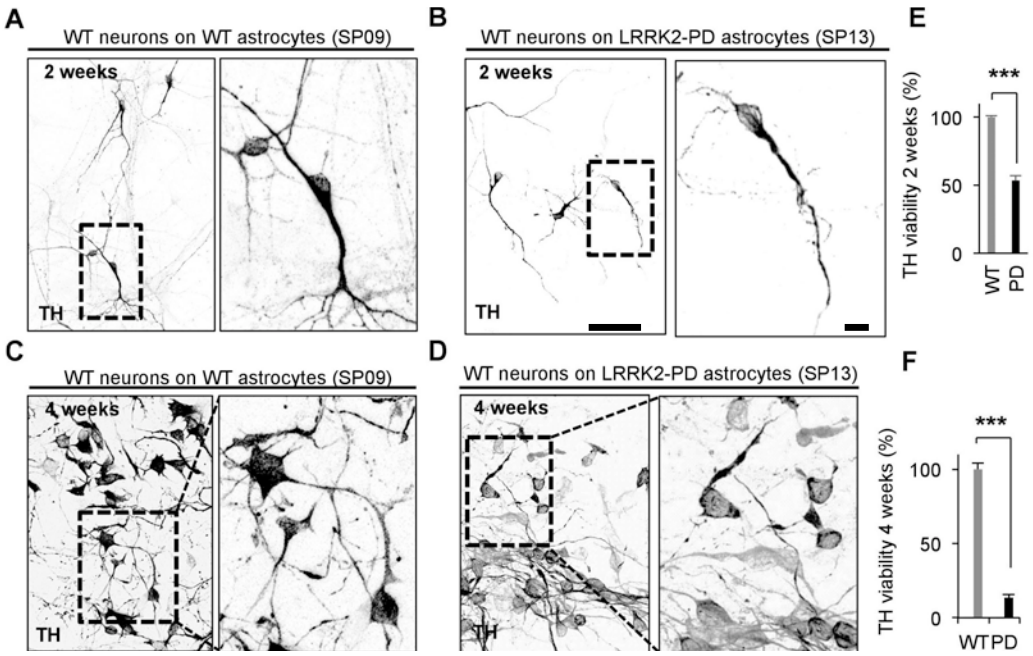

Figure 19. WT vmDA Neurons Show Morpholigical Signs of Neurodegeneration when Co-Cultured with LRRK2-PD Astrocytes.

(**a**) Representative images staining WT vmDAn (TH) on the top of WT astrocytes during a 2-week co-culture, scale bar 20µm and 0.2µm zoom. (**b**) WT vmDAn (TH) on the top of LRRK2-PD astrocytes during a 2-week co-culture, scale bar 20µm and 0.2µm zoom. (**c**) WT vmDAn (TH) on the top of WT astrocytes during a 4-week co-culture, scale bar 20µm and 0.2µm zoom. (**d**) WT vmDAn (TH) on the top of LRRK2-PD astrocytes during a 4-week co-culture, scale bar 20µm and 0.2µm zoom. (**e**) Graph representing TH/DAPI WT neuron count when co-cultured with WT or LRRK2-PD astrocytes at 2 weeks, (n = 3, total neurons counted = 1245). (**f**) 4 weeks (n = 3, total neurons counted = 1160). All graphs plot mean ± s.e.m, unpaired two-tailed Student's t-test, *p<0.05, **p<0.01, ***p<0.001.

We examined the effects of astrocytes expressing mutated LRRK2^{G2019S} on the survival of WT iPSC-derived vmDA neurons upon co-culture. After two weeks of culture with PD astrocytes, WT vmDA neurons started to show some signs of aberrant morphology (**Fig. 19b**). We detected a decrease of 50% of TH positive cells (**Fig. 19e**) compared to those cultured with WT astrocytes (**Fig. 19a**). After four weeks in co-culture, WT vmDAn on the top of WT astrocytes developed many arborizations comprised of several long smooth neurites forming complex networks (**Fig. 19c**). In contrast, WT neurons placed on LRRK2-PD astrocytes for four weeks rarely formed more than two neurites, some displaying overt signs of neurodegeneration (short/few arborizations and beaded-necklace neurites) (**Fig. 19d**), and were overall lower in number (TH/DAPI) compared to those on healthy astrocytes (**Fig. 19f**). WT vmDAn when co-cultured on LRRK2-PD astrocytes were comprised of 35 fold more TH neurons with neurodegenerative phenotypes compared to when on WT astrocytes (**Fig. 19e**). Sholl analysis revealed WT neurons on the top of WT astrocytes reaching a maximum of approximately 10 neurite intersections per neuron reaching lengths of 300 microns (**Fig. 20b,d**). On the contrary, WT neurons cultured on the top of LRRK2-PD astrocytes never surpassed more than two neurite intersections during Sholl analysis with neurite length reaching barely 100 microns (**Fig. 20c,d**).

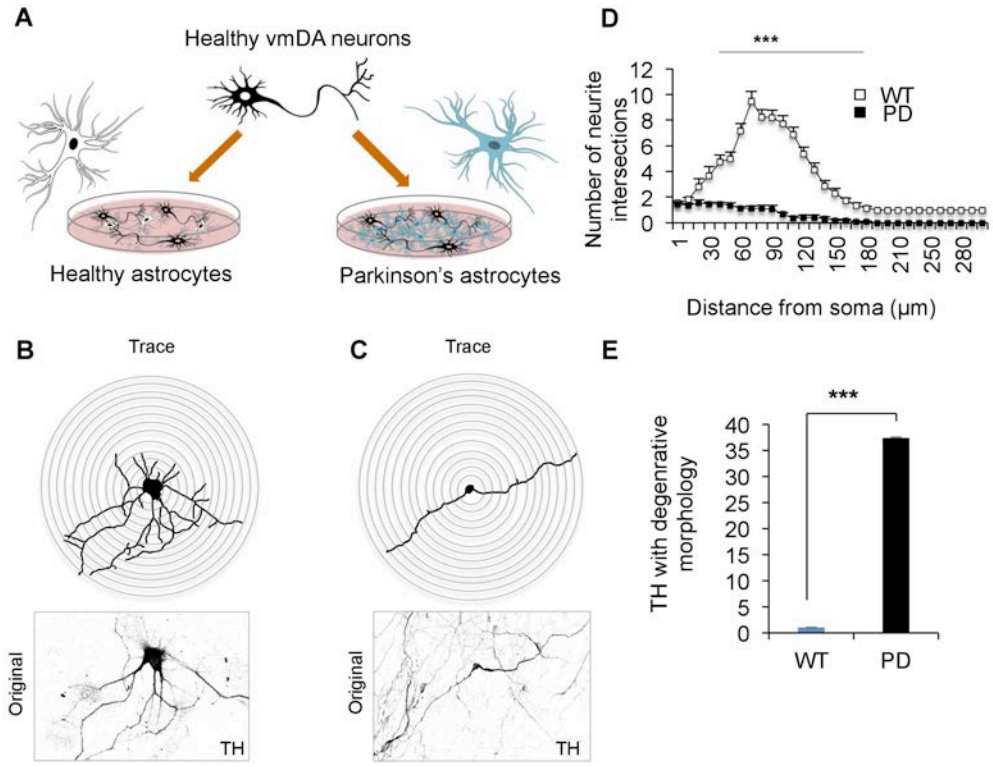

Figure 20. WT vmDA Neurons Have Shorter Neurites and Fewer Neurite Intersections When Co-Cultured with LRRK2-PD Astrocytes.

(**a**) Scheme representing co-culture system of WT neurons on the top of both WT and PD astrocytes for 4-weeks. (**b and c**) Scholl analysis image of neurite traces of WT neurons in both co-culture conditions. (**d**) Graph representing Scholl analysis of number of neurite intersections in WT neurons when co-cultured on WT astrocytes or PD astrocytes for 4 weeks (n = 3, total neurons counted = 40). (**e**) Graph plotting fold increase of TH with degenerative morphology during a 4-week co-culture on either WT or LRRK2-PD astrocytes normalized to total TH (fold change normalized to WT condition, n = 3, total neurons counted = 1160). All graphs plot mean ± s.e.m, unpaired two-tailed Student's t-test, *p<0.05, **p<0.01, ***p<0.001.

Interestingly, this neurodegeneration was TH specific as MAP2/DAPI positive cell numbers were maintained at similar levels (**Fig. 21c**) in both conditions – WT neurons on WT astrocytes (**Fig. 21a**) and WT neurons on PD astrocytes (**Fig. 21b**).

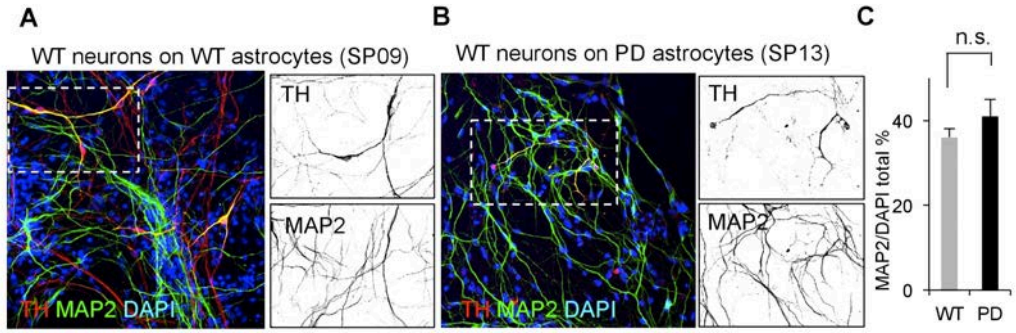

Figure 21. LRRK2-PD Astrocyte Induced Neurodegeneration is Dopaminergic Specific.

(**a**) WT vmDAn (TH) and mature neuron marker (MAP2) on the top of WT astrocytes (GFAP) during a 4-week co-culture, scale bar 20µm. (**b**) WT vmDAn (TH) and mature neuron marker (MAP2) on the top of LRRK2-PD astrocytes (GFAP) during a 4-week co-culture, scale bar 20µm. (**c**) MAP2/DAPI count in co-cultures on WT and LRRK2-PD astrocytes (n = 2, total neurons counted = 3583). All graphs plot mean ± s.e.m, unpaired two-tailed Student's t-test, *p<0.05, **p<0.01, ***p<0.001.

Viability tests of both WT and LRRK2-PD astrocytes at 2- and 4-week time-points were performed revealing highly similar values (differences non-significant), indicating that neurodegenerative signs displayed by WT vmDAn were not caused by the death of the PD astrocytes (**Fig. 22a,b**).

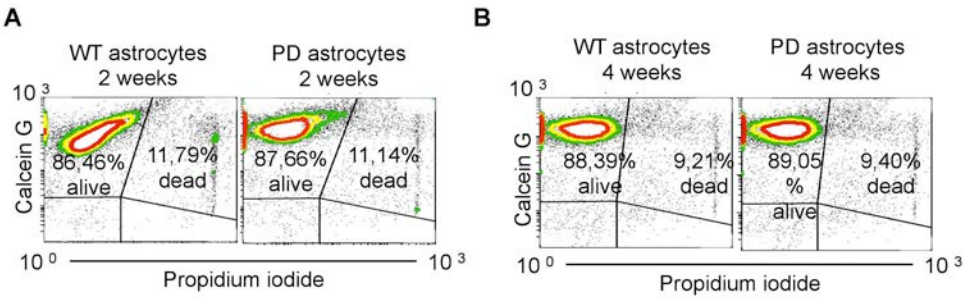

Figure 22. LRRK2-PD Astrocytes Are As Viable As WT Astrocytes.

(**a**) Contour plot of astrocyte viability using Calcein G and Propidium iodide (PI) at 2 weeks. (**b**) Contour plot of astrocyte viability using Calcein G and Propidium iodide (PI) at 4 weeks.

4.3.2 Parkinson's Disease Astrocytes Transfer Alpha-Synuclein to Healthy Dopaminergic Neurons During Direct Contact Co-Culture.

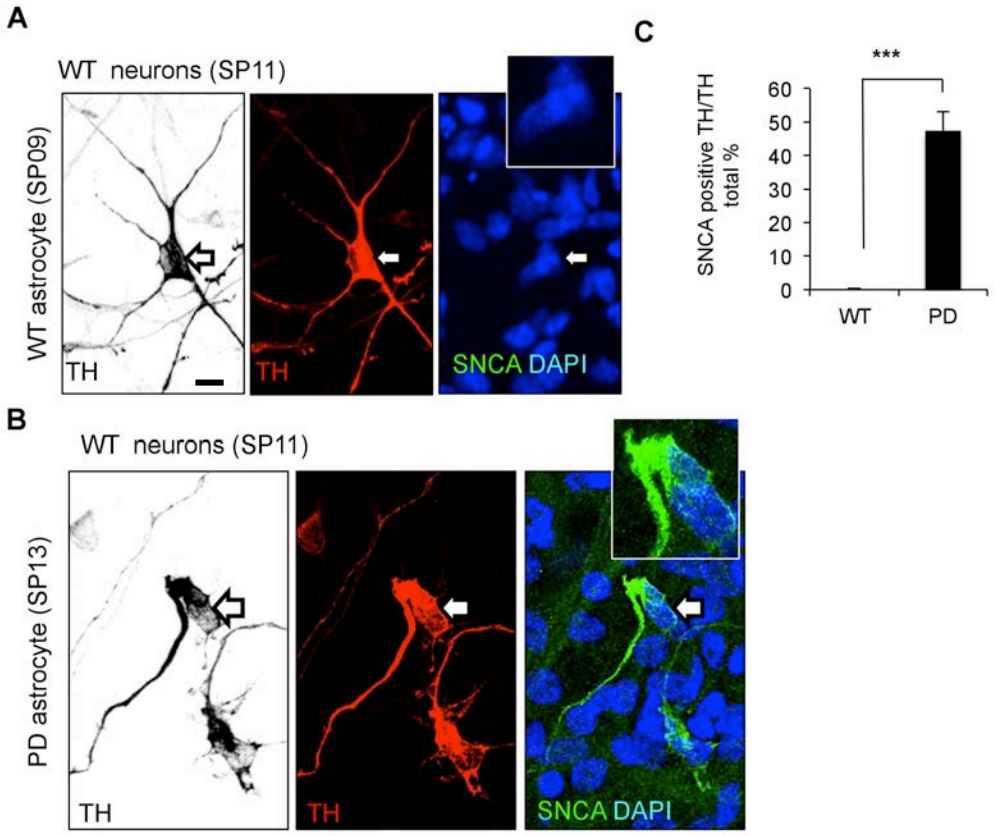

Figure 23. vmDAn Derived from Healthy Patients Accumulate Alpha-Synuclein when Co-Cultured with LRRK2-PD Astrocytes After 4 Weeks.

Representative images of WT vmDAn (TH) and α-synuclein (SNCA) when co-cultured with both WT (**a**) and LRRK2-PD (**b**) astrocytes after 4 weeks in culture, scale bar 0.2µm. (**c**) Graph representing SNCA positive TH/TH total count when WT vmDAn are co-cultured with WT or LRRK2-PD astrocytes after 4 weeks (n = 3, total neurons counted = 299). All graphs plot mean ± s.e.m, unpaired two-tailed Student's t-test, *p<0.05, **p<0.01, ***p<0.001.

Since α-synuclein accumulation is a hallmark of PD pathogenesis, we examined α-synuclein levels in our co-cultures. Apart from displaying morphological neurodegenerative phenotypes and a lack of complex neuronal networks, approximately 40% of TH positive WT vmDA neurons were found to accumulate α-synuclein when co-cultured with LRRK2-PD astrocytes (**Fig. 23b,c**). Conversely, α-synuclein was barely detectable in the cytoplasm of WT vmDAn when co-cultured with WT astrocytes (**Fig. 23a**).

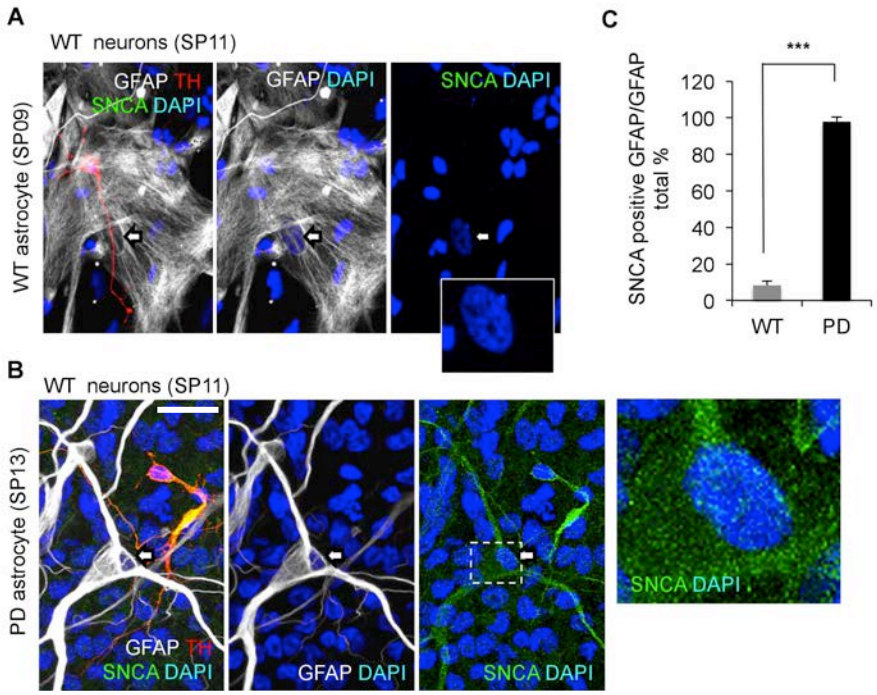

Figure 24. Overall Increase of Alpha-Synuclein Levels in Co-Cultures with LRRK2-PD Astrocytes

Representative images of GFAP either for WT astrocytes (**a**) or LRRK2-PD astrocytes (**b**) and α-synuclein (SNCA) when co-cultured with WT vmDAn after 4 weeks in culture, scale bar 20µm. (**c**) Graph representing SNCA positive GFAP/GFAP total count when WT vmDAn are co-cultured with WT or LRRK2-PD astrocytes after 4 weeks (n = 3, total astrocytes counted = 736). All graphs plot mean ± s.e.m, unpaired two-tailed Student's t-test, *p<0.05, **p<0.01, ***p<0.001.

Notably, while WT astrocytes had no or low levels of α-synuclein during the co-culture with WT neurons (**Fig. 24a**), PD astrocytes displayed high levels of α-synuclein when co-cultured with WT neurons (**Fig. 24b**). Upon counting, 98% of LRRK2-PD astrocytes had high levels of α-synuclein when co-cultured with WT vmDA neurons (**Fig. 24c**), which was a starting indicator that the accumulated α-synuclein in the WT vmDA neurons could originate from the LRRK2-PD astrocyte.

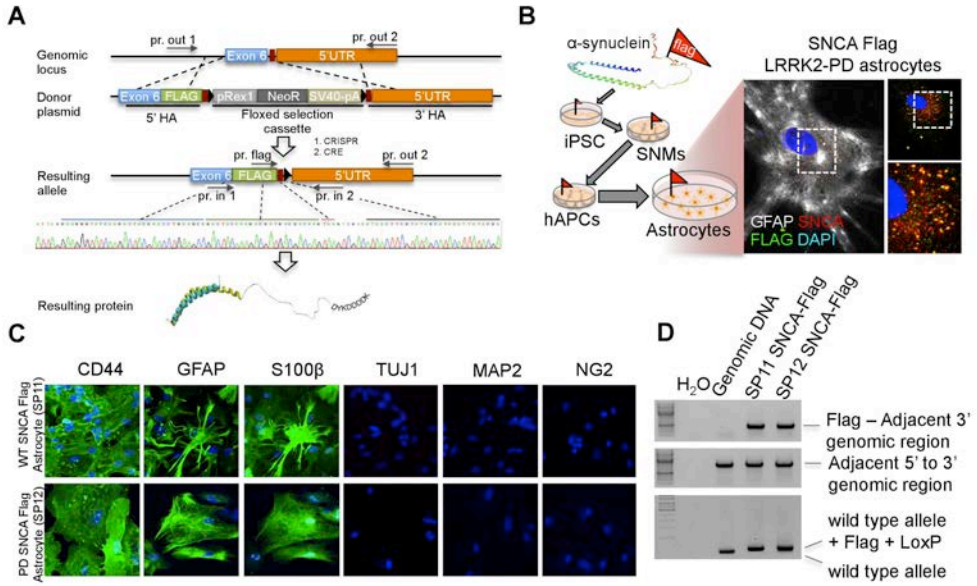

Figure 25. Generation and Characterization of Alpha-Synuclein Flag Tagged Line (SNCA-Flag).

(**a**) Scheme of flag tagged α-synuclein using CRISPR/CASP9 gene editing technology. (**b**) Scheme of astrocyte generation protocol and immunofluorescent colocalization analysis of flag and α-synuclein in LRRK2-PD astrocytes (GFAP) after 14 days in culture. (**c**) Representative images of both edited WT and LRRK2-PD astrocyte lines characterized with astrocyte markers CD44, GFAP, S100β, and negative for TUJ1, MAP2 and NG2. (**d**) Gel of flag tagged SNCA insertion.

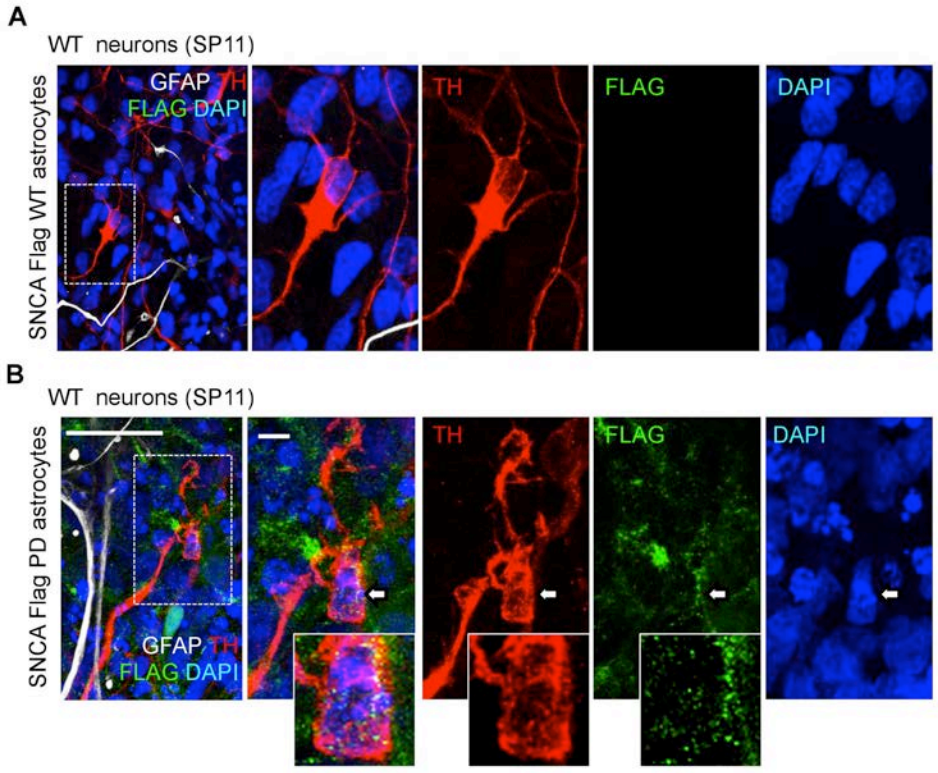

Figure 26. LRRK2-PD Astrocytes Transfer Flag Tagged Alpha-Synuclein to WT Neurons.

(**a**) Representative images of WT vmDAn (TH) on the top of WT SNCA Flag astrocytes during a 4-week co-culture, scale bar 20µm and 0.2µm zoom. (**b**) Representative images of WT vmDAn (TH) on the top of LRRK2-PD SNCA Flag astrocytes during a 4-week co-culture, scale bar 20µm and 0.2µm zoom.

In order to directly visualize whether or not α-synuclein was passed from the PD astrocyte to the WT neuron, α-synuclein-flag tagged astrocyte lines were

newly generated* and fully characterized (**Fig. 25**). Indeed, the tagged α-synuclein in the PD astrocytes was directly transferred to the WT neurons and accumulated (**Fig. 26b**), which was not present when WT vmDAn were co-cultured with WT astrocytes (**Fig. 26a; 27a**). The presence of α-synuclein in WT vmDAn cell body and major processes were confirmed by z-section of confocal imaging (**Fig. 27b,c**).

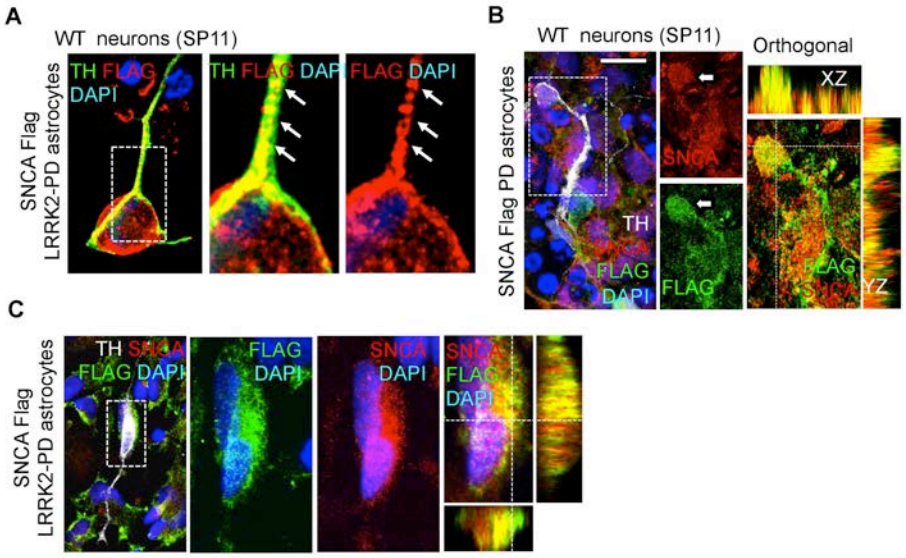

Figure 27. LRRK2-PD Astrocyte-Derived Alpha-Synuclein is Found in WT Neurons During Co-Culture.

(**a**) WT neurons on the top of LRRK2-PD SNCA flag astrocytes reveal direct transfer of flag tagged SNCA from the astrocyte to the neuron, scale bar 0.2µm. (**b**) Colocalization analysis of SNCA and Flag in a 4-week co-culture of WT vmDAn (TH) on the top of LRRK2-PD SNCA Flag astrocytes, scale bar 20µm. (**c**) Colocalization analysis of SNCA and Flag in a 4-week co-culture of WT vmDAn (TH) on the top of LRRK2-PD SNCA Flag astrocytes.

*SNCA-flag tagged iPSC derived lines generated by Dr. Carles Calatayud Aristoy and Giulia Carola of the Institute of Biomedicine of the University of Barcelona (IBUB), Spain.

4.3.3 Healthy Dopaminergic Neurons Show Signs of Neurodegeneration and Accumulate Alpha-Synuclein When Indirectly Co-Cultured with Conditioned Medium from Parkinson's Disease Astrocytes.

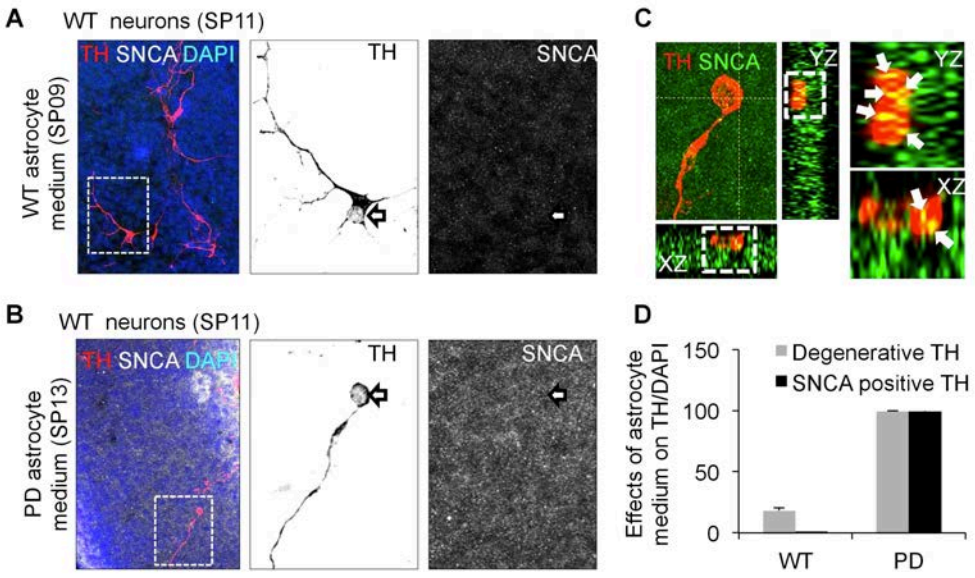

Figure 28. WT Neurons Show Signs of Neurodegeneration and Higher Levels of Alpha-Synuclein When Co-cultured with Medium Conditioned by LRRK2-PD Astrocytes.

(**a**) Representative images of WT vmDAn (TH) and α-synuclein (SNCA) when co-cultured with medium from both WT and (**b**) LRRK2-PD astrocytes after 4 weeks in culture, scale bar 50µm, zoom 0.2µm. (**c**) Orthogonal view confirming colocalization of SNCA with TH in WT neurons cultured with LRRK2-PD astrocyte medium. (**d**) Graph representing the effects of astrocyte medium on WT neurons in terms of neurons positive for SNCA inclusions as well as harboring a degenerated morphology (fewer than 2 neurites or beaded like neurites). All graphs plot mean ± s.e.m.

In addition to co-culturing cells with direct glia-neuron contact, we also tested the effect of supplying WT neurons with medium conditioned by WT

or PD astrocytes (**Fig. 28**). WT vmDA neurons showed morphological signs of neurodegeneration and α-synuclein accumulation when cultured with LRRK2-PD astrocyte-conditioned medium (**Fig. 28b**) compared to when co-cutured with medium conditioned by WT astrocytes (**Fig. 28a**). The α-synuclein accumulation in the WT neurons that were cultured with medium conditioned by LRRK2-PD astrocytes was confirmed through orthogonal view confocal microscopy analysis (**Fig. 28c**). Cell counting analysis revealed that almost all TH positive neurons, when conditioned with medium from LRRK2-PD astrocytes, had higher levels of α-synuclein and a degenerative morphology (2 or less neurites, or beaded-like necklace neurites) compared to when conditioned with medium from WT astrocytes (**Fig. 28d**). It is necessary to note that the indirect co-culture condition was not as successful in terms of supporting neuronal homeostasis as was the direct co-culture, since the TH number is lower during an indirect co-culture condition compared to the direct co-culture condition. Nevertheless, the effect of LRRK2-PD astrocytes compared to WT astrocytes on WT neurons was evident in both co-culture conditions.

4.3.4 Parkinson's Disease DA Neurons Recover Neurodegeneration and Alpha-Synuclein Accumulation when Co-Cultured with WT Astrocytes.

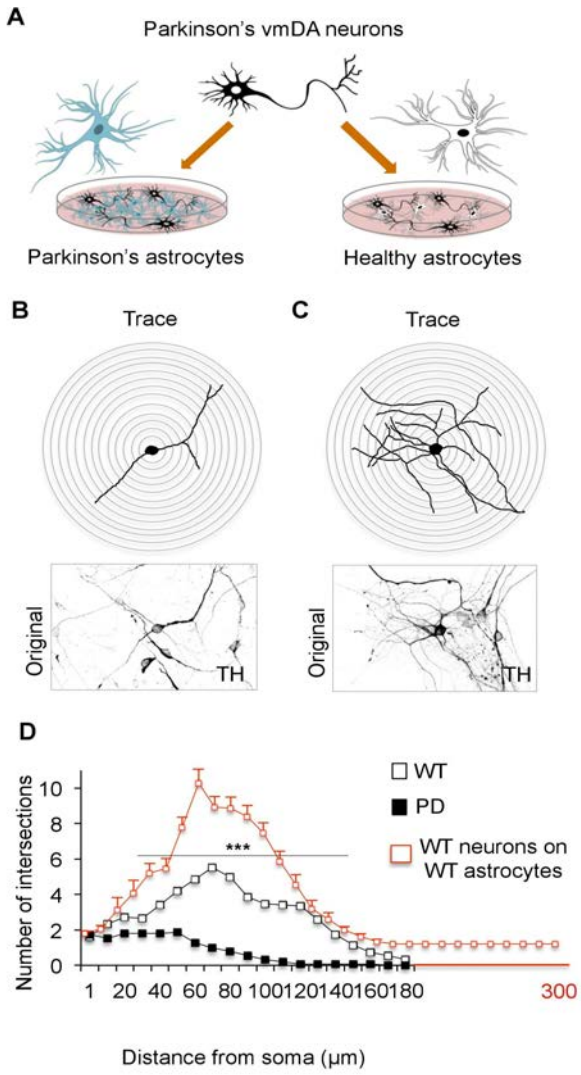

Figure 29. LRRK2-PD Neurons Have Partially Restored Arborized Neurite Morphology When Co-Cultured with WT Astrocytes.

(**a**) Scheme representing co-culture system of PD neurons on the top of both WT and PD astrocytes for 4 weeks. (**b and c**) Scholl analysis image of neurite traces of PD neurons in both co-culture conditions. (**d**) Graph representing Scholl analysis of number of neurite intersections in PD neurons when co-cultured on WT astrocytes or PD astrocytes for 4 weeks (n = 3, total neurons counted = 40). All graphs plot mean ± s.e.m, unpaired two-tailed Student's t-test, *p<0.05, **p<0.01, ***p<0.001.

In order to determine if the neurodegeneration could be rescued or prevented by healthy astrocytes, we co-cultured vmDA neurons derived from patients carrying the G2019S mutation on the LRRK2 gene with both WT and LRRK2-PD astrocytes (**Fig. 29a**). LRRK2-PD neurons alone (data not shown) show signs of neurodegeneration as early as 50 days of differentiation and accumulate α-synuclein in the soma when cultured with medium without factors. These LRRK2-PD neurons alone barely reach the 80-day time-point when cultured without factors, however, in order to visualize a phenotype, the factors had to be removed.

After a 4-week co-culture, LRRK2-PD neurons showed a partially recovered neurite number and complex neurite arborization when co-cultured on WT astrocytes (**Fig. 29c**) as opposed to when cultured with LRRK2-PD astrocytes (**Fig. 29b**). Sholl analysis revealed the average LRRK2-PD neuron while on WT astrocyte to harbor a maximum of five neurite intersections per neuron with a neurite length reaching 180 microns (**Fig. 29d**), whereas LRRK2-PD neurons when co-cultured with LRRK2-PD astrocytes never reached more than two neurite intersections per neuron with a maximum neurite length of 100 microns (**Fig. 29d**).

When comparing neurite intersection number of the rescued LRRK2-PD neuron on WT astrocyte co-culture (average of five neurite intersections per neuron) with the condition of WT neuron on WT astrocyte (average of ten neurite intersections per neuron), the rescue is partial. However, when comparing the LRRK2-PD neuron on WT astrocyte (average of five neurite intersections per neuron) to LRRK2-PD neuron on LRRK2-PD astrocyte (average of two neurite intersections per neuron) the rescue was statistically significant.

Levels of α-synuclein also were diminished in LRRK2-PD neurons when co-cultured with WT astrocytes compared to when co-cultured with LRRK2-PD astrocytes after 4 weeks (**Fig. 30a,b**). LRRK2-PD neurons on the top of WT astrocytes reached 25% TH/DAPI after two weeks in culture compared to when on LRRK2-PD astrocytes at 12% (**Fig. 30c**). After 4 weeks in culture LRRK2-PD neurons on the top of WT astrocytes increased to 45% TH/DAPI compared to when on LRRK2-PD astrocytes there was a decrease to 6% (**Fig. 30c**). Overall MAP2 positive cells (normalized to DAPI) were similar in number when LRRK2-PD neurons were co-cultured with WT and LRRK2-PD astrocytes, revealing that the fluctuation in cell number was TH specific (**Fig. 30d**).

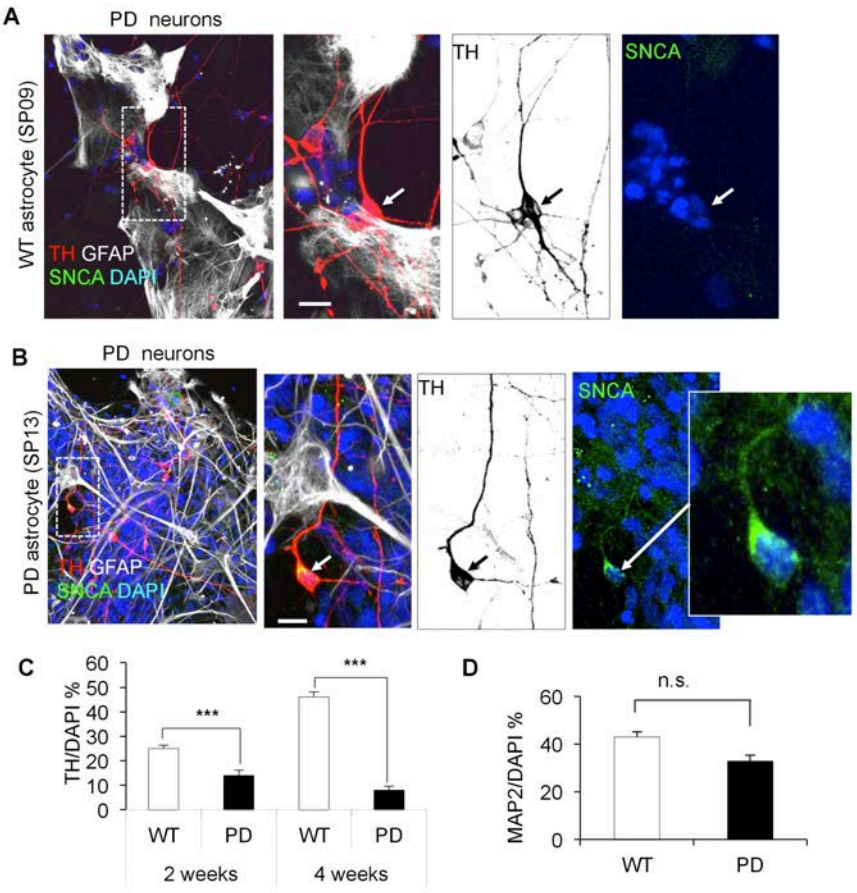

Figure 30. PD Neurons Restore Arborized Morphology and Have Less Accumulated Alpha-Synuclein When Co-Cultured with WT Astrocytes.

(**a**) Immunofluorescence representations of α-synuclein (SNCA) levels during a 4-week co-culture with PD neurons (TH) on the top of WT astrocytes (GFAP) (**b**) and PD neurons on the top of PD astrocytes. (**c**) Graph plotting TH/DAPI in co-cultures with PD neurons on the top of WT and PD astrocytes at 2 and 4 weeks (n = 2, total neurons counted = 6301). (**d**) Graph plotting MAP2 (normalized to DAPI) positive neurons in co-cultures with both WT and PD astrocytes (n = 2, total neurons counted = 4219). All graphs plot mean ± s.e.m, unpaired two-tailed Student's t-test, *p<0.05, **p<0.01, ***p<0.001).

4.4 Astrocytes and Inflammation: A Double-Edged Sword

4.4.1 Adverse Parkinson's Disease Astrocytes Harbor a Hypertrophic Morphology and Produce Super Oxide.

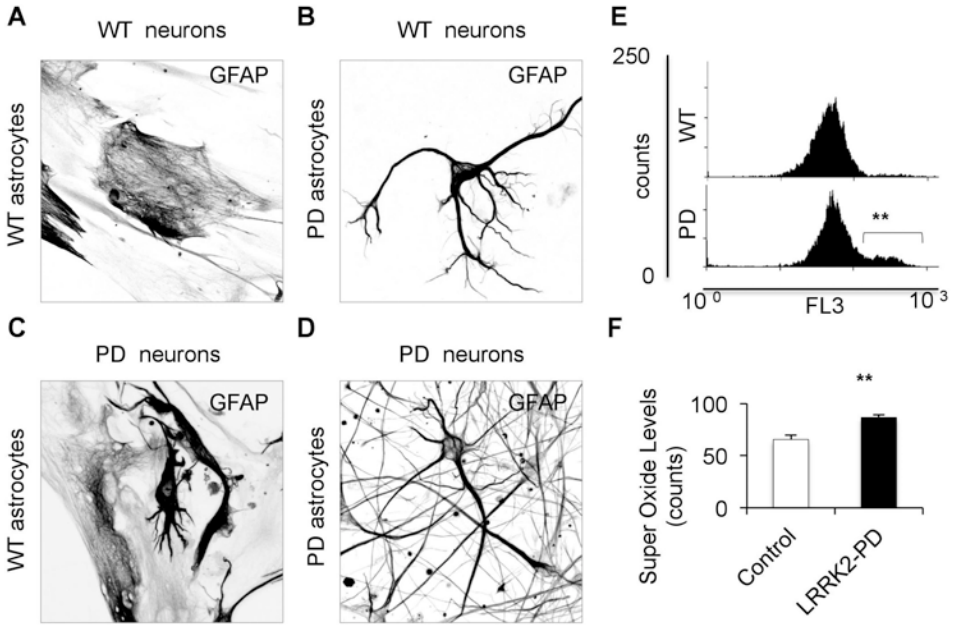

Figure 31. PD Astrocytes Adopt a Hypertrophic Morphology, As Do WT Astrocytes When Co-Cultured with PD Neurons.

(**a**) Representative images of WT astrocytes marked with GFAP when co-cultured with WT neurons for 4 weeks. (**b**) GFAP staining PD astrocytes when co-cultured with WT neurons. (**c**) GFAP staining WT astrocytes when co-cultured with PD neurons. (**d**) GFAP staining PD astrocytes when co-cultured with PD neurons. (**e**) Flow cytometry analysis of basal ROS levels in both WT and PD astrocytes. (**f**) Super Oxide levels in WT and PD astrocytes. All graphs plot mean ± s.e.m, unpaired two-tailed Student's t-test, *$p<0.05$, **$p<0.01$, ***$p<0.001$.

Astrocytes can adopt a myriad of morphologies depending on their function. We took a closer look at astrocyte morphology and GFAP signal in the co-cultures. When WT neurons were co-cultured with WT astrocytes, the WT astrocytes adopted a very flat and large morphology with lower GFAP signal (**Fig. 31a**). Interestingly, when LRRK2-PD neurons were co-cultured with those same WT astrocytes, most astrocytes maintained a large and flat morphology with low GFAP signal, however a select few (10%) adopted a hypertrophic morphology with retracted processes and high GFAP signal (**Fig. 31c**). LRRK2-PD astrocytes, whether they were co-cultured with WT or LRRK2-PD neurons, adopted a hypertrophic morphology with retracted processes and high GFAP signal (**Fig. 31b,d**). In order to determine if the retracted morphology of LRRK2-PD astrocytes reflects a pathogenic function, Super Oxide levels were measured. LRRK2-PD astrocytes produced significantly more Super Oxide levels than WT astrocytes (**Fig. 31e,f**).

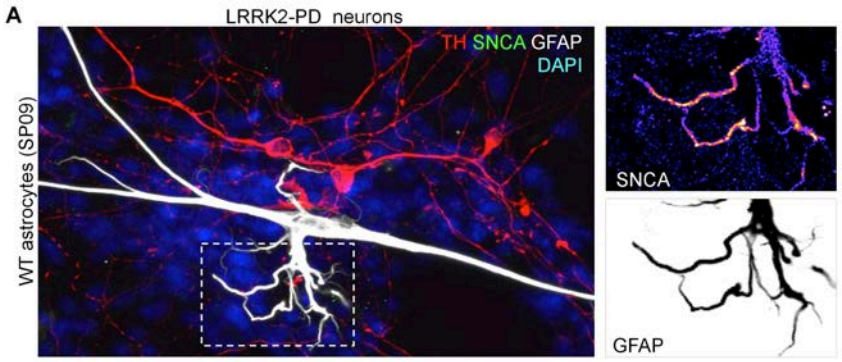

Figure 32. WT Astrocytes Are Neuroprotective When They Become Activated to Clear Alpha-Synuclein

(**a**) Immunofluorescence representing PD neurons (TH) on the top of WT astrocytes (GFAP) with a focus on α-synuclein (SNCA).

Table 13. Summary of Co-cultures

Summary of Phenotypes During Co-cultures

Co-culture			Phenotypes**							
Line		**Duration**	**Cell viability** (fold change*)		**SNCA acc.** (%/DAPI)		**Cell Morphology**			
Neuron	Astrocyte	weeks	Neuron	Astrocyte	Neuron	Astrocyte	Neuron	Average neurite intersection #/neuron	Average neurite length/neuron	Astrocyte
SP11	SP09	2	1	1	0	0	immature	N/A	N/A	flat, resting
	SP09	4	1	1	0	10%	normal	10	300 microns	flat, resting
	SP11 SNCA Flag	4	1	1	0	10%	normal	10	300 microns	flat, resting
	SP13	2	0.5	1.2	0	50%	immature	N/A	N/A	retracted, reactive
	SP13	4	0.2	1.5	45%	100%	degenerated	2	100 microns	retracted, reactive
	SP12 SNCA Flag	4	0.2	1.5	45%	100%	degenerated	2	100 microns	retracted, reactive
SP12	SP09	2	1	1	0	0	immature	N/A	N/A	flat, resting
	SP09	4	1.5	1	0	10%	normal	5	180 microns	flat, resting
	SP11 SNCA Flag	4	1.5	1	0	10%	normal	5	180 microns	flat, resting
	SP13	2	0.5	1.2	100%	100%	immature	N/A	N/A	retracted, reactive
	SP13	4	0.2	1.5	100%	100%	degenerated	2	100 microns	retracted, reactive
	SP12 SNCA Flag	4	0.2	1.5	100%	100%	degenerated	2	100 microns	retracted, reactive

* cell number normalized to WT astrocyte (SP09) per condition

** average of all independent tripicates

Wild type (control)

LRRK2-PD (mutant)

4.4.2 Activated Healthy Astrocytes Can Ignite Neuroprotective Pathways and Mop Up Alpha-Synuclein

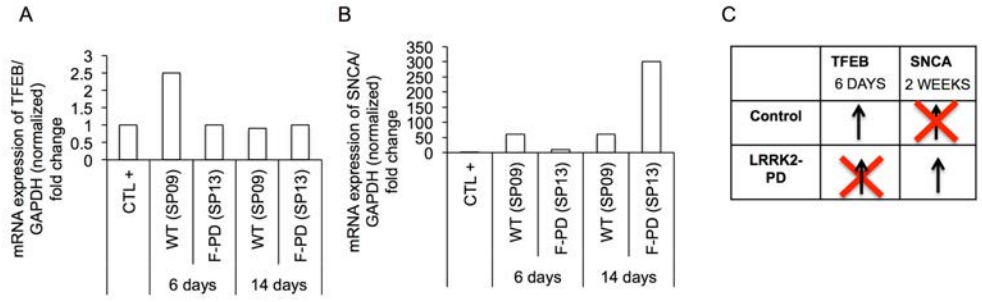

Figure 33. Lack of Neuroprotective TFEB Gene Expression Has Inverse SNCA Expression in LRRK2-PD Astrocytes.

(**a**) qRT-PCR graph depicting TFEB mRNA expression levels in human fibroblasts, WT and LRRK2-PD astrocytes at 6 and 14 days. (**b**) qRT-PCR graph depicting α-synuclein mRNA expression levels in human fibroblasts, WT and LRRK2-PD astrocytes at 6 and 14 days. (**c**) Scheme depicting possible correlation between TFEB and SNCA mRNA expression levels between astrocyte lines.

Astrocytes derived from healthy patients show to adopt a neuroprotective role when co-cultured with LRRK2-PD neurons. Co-culturing LRRK2-PD neurons with WT astrocytes resulted in preventing morphological phenotypes of neurodegeneration and the accumulation of α-synuclein (**Fig. 31**). Although the majority of WT astrocytes had a lower level of GFAP protein expression and a flat large morphology, approximately 10% of WT astrocytes in co-cultures with LRRK2-PD neurons adopted a hypertrophic morphology with extremely retracted processes and accumulated α-synuclein (**Fig. 32a**). This suggests that the WT astrocytes secrete neuroprotective factors to help in neuronal survival and maturation.

Upon qRT-PCR analysis, WT astrocytes expressed higher mRNA expression levels of transcription factor EB (TFEB), a gene involved in autophagy. Interestingly, when WT astrocytes expressed TFEB at 6 days, α-synuclein levels at 14 days were very low, whereas the LRRK2-PD astrocytes lacked in expression of TFEB at both 6 and 14 days, and expressed high levels of α-synuclein at 14 days (**Fig. 33**). This convers expression of TFEB with SNCA could have some neuroprotective effect on how SNCA is being degraded.

4.5 Parkinson's Disease Astrocytes Harbor Phenotypes Previously Described in Dopaminergic Neurons of Parkinson's Disease Patients.

4.5.1 Parkinson's Disease Astrocytes Display Calcium Sensitivity When Exposed to Ca^{2+} Agonists

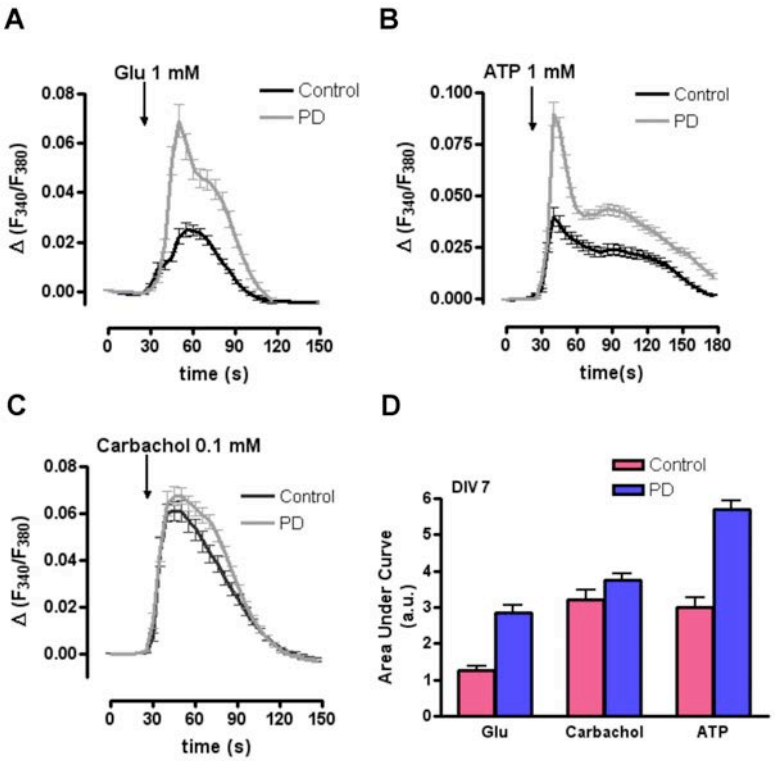

Figure 34. LRRK2-PD Astrocytes Have a Higher Calcium Sensitivity When Treated with Ca^{2+} Agonists Compared to WT Astrocytes After 7 Days in Culture.

Cells were treated with calcium agonists (**a**) 1mM of glutamate (**b**) 1mM ATP and (**c**) 0.1mm of carbachol after 7 days of culture and calcium levels were recorded.

We analyzed the effects of glutamate 1mM, carbachol 0.1mM, and ATP 1mM on intracellular calcium levels $[Ca^{2+}]_i$ in iPSC-derived astrocytes from control and PD patients at DIV7 (**Fig. 34**) and DIV14 (**Fig 35**). First, we observed that immediately after application of agonists, fluorescent calcium imaging with fura-2 showed increased $[Ca^{2+}]_i$ in the astrocytes.

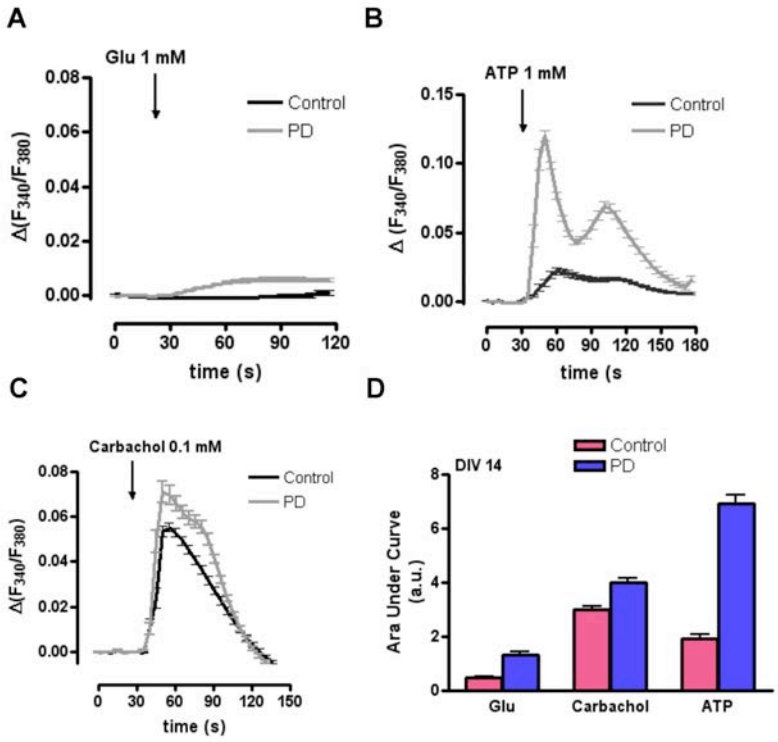

Figure 35. LRRK2-PD Astrocytes Have Higher Calcium Sensitivity When Treated with Ca^{2+} Agonists Compared to WT Astrocytes After 14 Days in Culture.

Cells were treated with calcium agonists (**a**) 1mM of glutamate (**b**) 1mM ATP and (**c**) 0.1mm of carbachol after 7 days of culture and calcium levels were recorded.

At both DIVs, increases of $[Ca^{2+}]_i$ to glutamate and ATP agonists were higher in LRRK2-PD than WT-derived cells, whereas increases of $[Ca^{2+}]_i$ to carbachol were similar in both types of cells (**Fig. 34; 35**)[*]. At DIV14, we observed lower responses to glutamate in control and PD cells and to ATP in control cells as compared to those that were obtained at DIV7. However, PD cells showed higher Ca^{2+} levels in ATP response at DIV14 than at DIV7. These preliminary results indicate that iPSC-derived astrocytes express functional receptors to glutamate, ATP, and carbachol agonists. In these cell lines, PD cells show higher responses to glutamate and ATP than to WT cells. Long-term cultured cells show smaller calcium responses to glutamate and ATP in control and PD-derived cells, with the exception of PD-derived cell response to ATP.

[*] Data courtesey of Elena Alberdi from Achucarro - Basque Center for Neuroscience, Bilbao, Spain.

4.5.2 Degradation Pathways in Parkinson's Disease Astrocytes Are Dysfunctional.

4.5.2.1 Parkinson's Disease Astrocytes Display Disrupted Chaperone Mediated Autophagy Machinery and Accumulate Alpha-Synuclein.

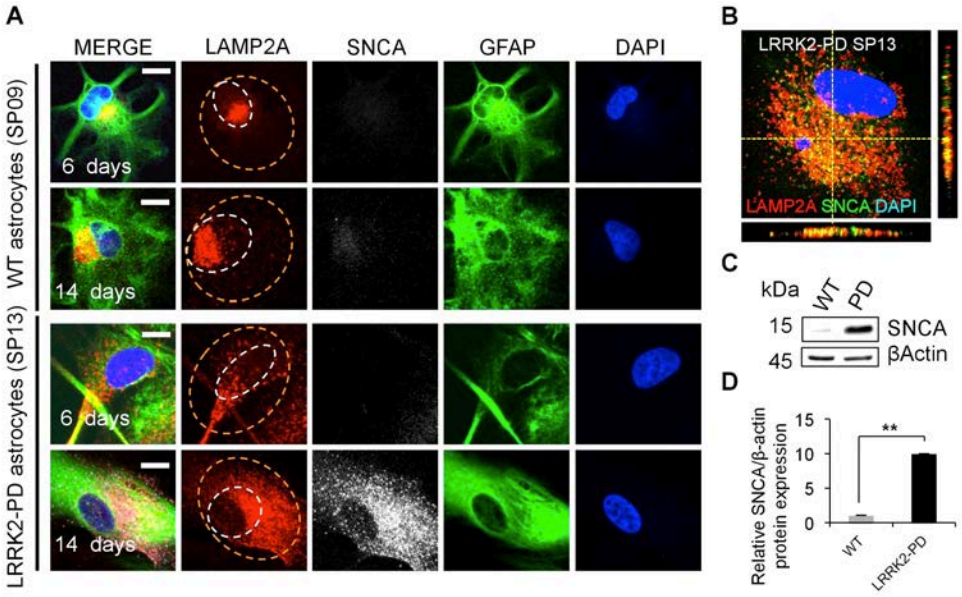

Figure 36. Altered CMA and SNCA Accumulation in LRRK2-PD (SP13) Astrocytes.

(**a**) Representative images of the receptor for CMA (LAMP2A), astrocyte marker GFAP, SNCA and nuclear marker DAPI in control and LRRK2-PD astrocytes at 6 and 14 days, scale bar 10μm. Smaller white circles represent perinuclear area, whereas larger green circles represent non-perinuclear area. Scale bar 20μm. (**b**) Positive co-localization between LAMP2A and SNCA in LRRK2-PD astrocytes. (**c**) Western blot of SNCA protein levels in control and LRRK2-PD astrocytes after 14 days, acting as a loading control, quantification in graph (n = 3) (**d**). All graphs plot mean ± s.e.m, unpaired two-tailed Student's t-test, *p<0.05, **p<0.01, ***p<0.001.

Degradation of α-synuclein in lysosomes occurs to a large extent through chaperone-mediated autophagy (CMA) (Cuervo, Stefanis, Fredenburg, Lansbury, & Sulzer, 2004; Martinez-Vicente et al., 2008). To investigate possible changes in CMA in LRRK2-PD astrocytes, we first stained at 6 and 14 days for both α-synuclein and LAMP2A, the receptor for CMA (**Fig. 36a**).

The control astrocytes showed LAMP2A in the perinuclear area (perinuclear lysosomal positioning occurs during CMA activation (Kiffin, 2004)) and low basal levels of α-synuclein at both 6 and 14 days. In contrast, LRRK2-PD astrocytes displayed LAMP2A positive vesicles completely dispersed all over the cell body as early as 6 days, and which continued to be present after 14 days. Moreover, higher α-synuclein levels were confirmed in LRRK2-PD iPSC-derived astrocytes after 14 days of culture, compared to control (**Fig. 36a; 37a**). Astrocytes derived from Sporadic-PD patients also showed an increase in α-synuclein accumulation and a mislocalization of lysosomes from the perinuclear area, however the phenotypes were not as strong as the familial LRRK2-PD astrocytes (**Fig. 39a**). Interestingly, this accumulation was not present after 6 days of culture, suggesting progressive α-synuclein accumulation over the 14-day time-point.

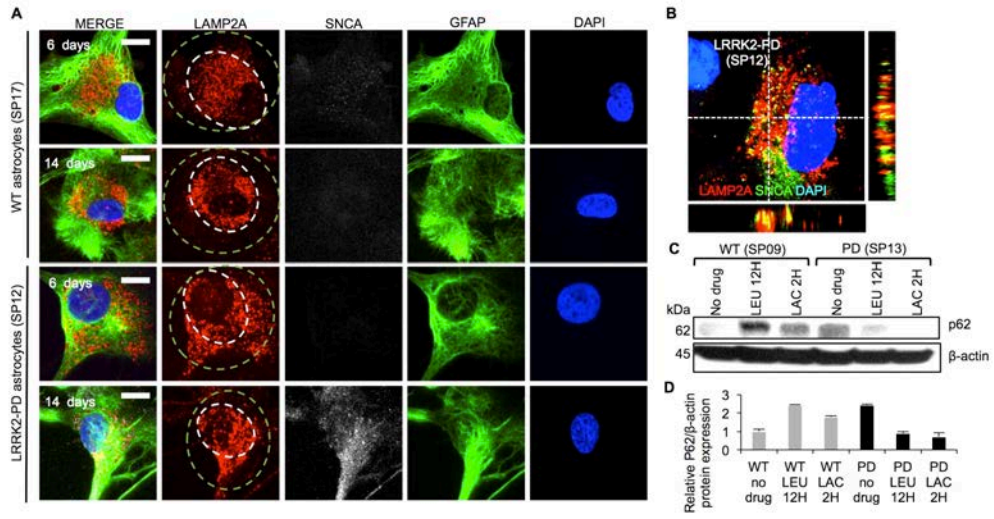

Figure 37. Altered CMA and SNCA Accumulation in LRRK2-PD (SP12) Astrocytes

(**a**) Representative images of the receptor for CMA (LAMP2A), astrocyte marker GFAP, SNCA and nuclear marker DAPI in second WT and second LRRK2-PD astrocyte lines at 6 and 14 days, scale bar 10μm. Smaller white circles represent perinuclear area, whereas larger green circles represent non-perinuclear area. (**b**) Positive co-localization between LAMP2A and SNCA in second LRRK2-PD astrocyte line. (**c**) Western blot of P62 after treatment with inhibitors of autophagy and the proteosomal system, mean ± s.e.m, plotted in graph (**d**).

Co-localization analyses of α-synuclein with the LAMP2A receptor revealed a positive co-localization that was higher in LRRK2-PD iPSC-derived astrocytes (**Fig. 36b; 37b**) as well as Sporadic-PD astrocytes (**Fig. 39b,c**). CMA substrates usually are rapidly internalized and degraded inside lysosomes, but we have previously described a similar persistent association of α-synuclein with LAMP2A positive lysosomes in PD models due to blockage in α-synuclein translocation inside lysosomes (Orenstein et al., 2013). These findings thus suggest a similar CMA blockage in the LRRK2-

PD astrocytes at the receptor level. Also supportive of reduced α-synuclein degradation, Western blot analysis confirmed a higher monomeric protein level of α-synuclein in the LRRK2-PD mutant compared to controls ($p<0.01$, **Fig. 36c,d**). Through Western blot analysis, we detected specifically different forms of α-synuclein, such as dimers and tetramers, in the LRRK2-PD astrocytes (**Fig. 38a,b**).

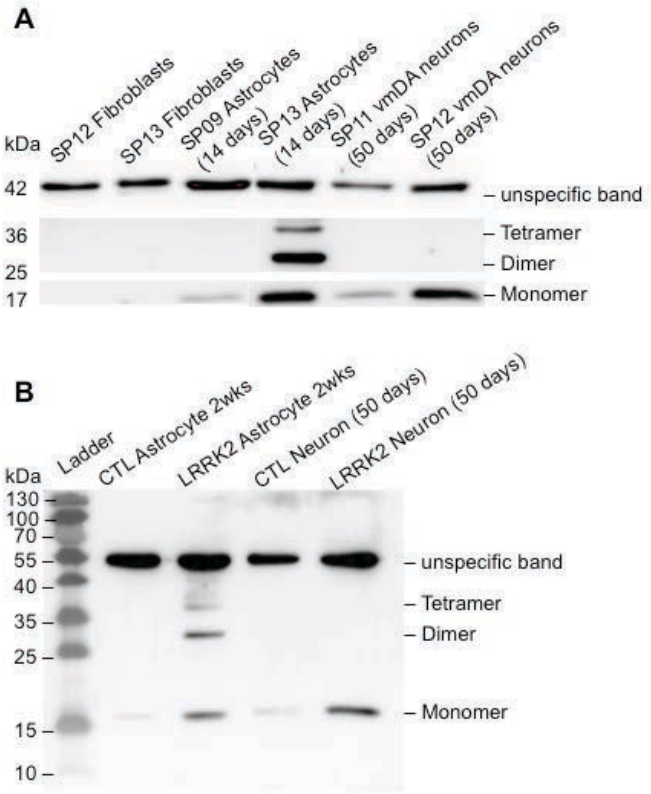

Figure 38. Western Blot Analysis Reveals Several SNCA Forms in LRRK2-PD Astrocytes

(**a**) Western blot of α-synuclein antibody in patient fibroblasts, astrocytes and neurons. (**b**) Confirmation of Western blot results.

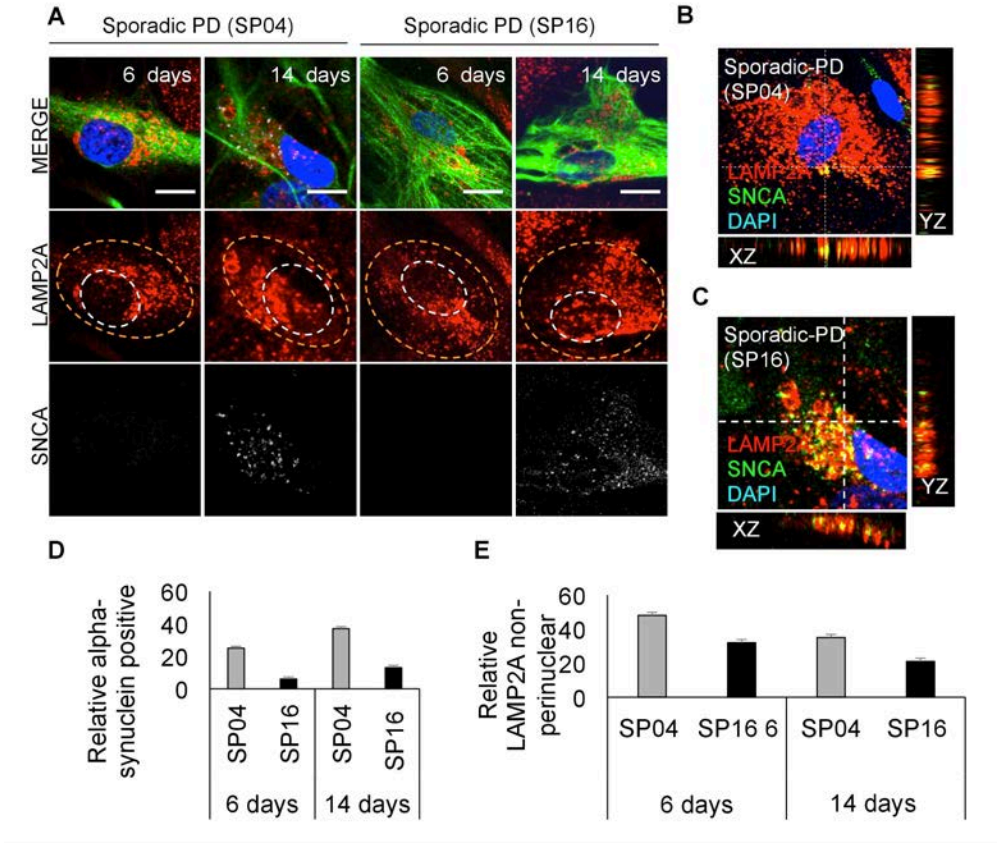

Figure 39. Sporadic Astrocytes Partly Accumulate Alpha-Synuclein*

(**a**) Immunofluorescence revealing both Sporadic-PD astrocyte lines accumulating α-synuclein after 14 days in culture. (**b and c**) Co-localization analysis of LAMP2A and SNCA in Sporadic-PD lines. (**d**) Graph displaying percentage of GFAP/DAPI cells which express high levels of SNCA or (**e**) have LAMP2A localized outside of the perinuclear area.

*Done in collaboration with Isabel Fernandez Lopez of the Institute of Biomedicine at the University of Barcelona (IBUB).

Since LRRK2-PD astrocytes displayed higher levels of α-synuclein compared to controls, we next investigated possible differences in α-synuclein turnover in these cells. α-Synuclein has previously shown to undergo degradation both by the ubiquitin/proteasome system and by autophagy(Cuervo et al., 2004; Webb, Ravikumar, Atkins, Skepper, & Rubinsztein, 2003), therefore α-synuclein flux in the presence of lysosomal and proteasome inhibitors (Leupeptin 100μM and Lactacystin 5μM, respectively) was evaluated in control and LRRK2-PD astrocytes at 14 days (**Fig. 40a**).

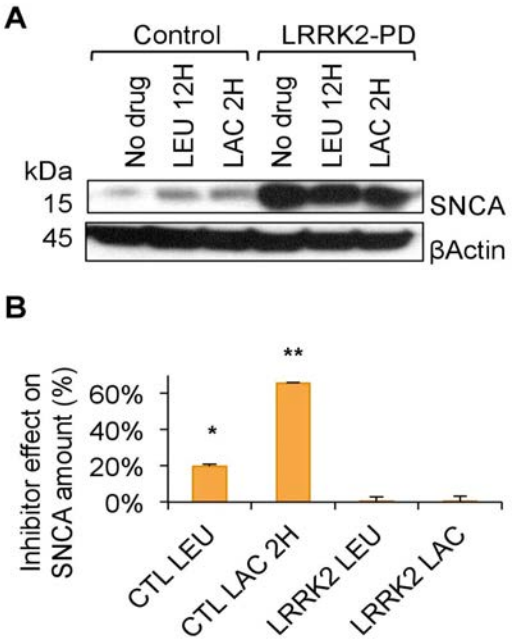

Figure 40 Lowered or No Alpha-Synuclein Flux in LRRK2-PD Astrocytes Compared to WT Astrocytes.

(**a**) Western blot of SNCA protein levels after the addition of inhibitors of autophagy and proteasomal degradation. (**b**) Effects of inhibitors of α-synuclein accumulation (n = 2). All graphs plot mean ± s.e.m, unpaired two-tailed Student's t-test, *p<0.05, **p<0.01, ***p<0.001.

Treatment with the inhibitors revealed a 20% increase of α-synuclein after a 12-hour Leupeptin treatment ($p<0.05$), and 65% after a 2-hour Lactacystin treatment ($p<0.01$) in WT cells, whereas α-synuclein levels remained unchanged upon the addition of both inhibitors in the LRRK2-PD astrocytes (**Fig. 40a,b**). These findings suggest major alterations in α-synuclein proteostasis due to poor degradation by both the proteasome and lysosomal systems, resulting in p62 protein levels increasing in controls after inhibitor treatment whereas in the LRRK2-PD it decreased (**Fig. 37c,d**).

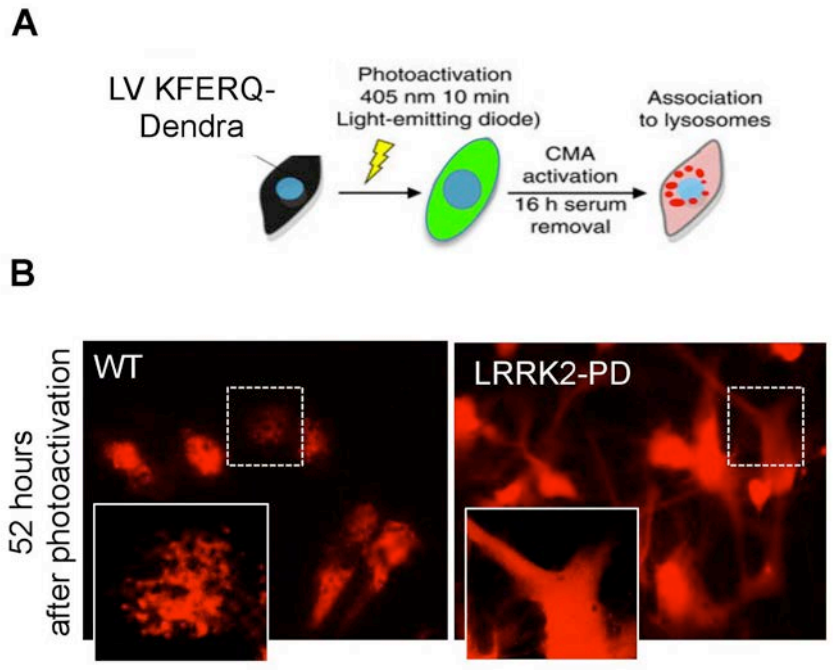

Figure 41. LRRK2-PD Astrocytes Have Inactive Chaperone Mediated Autophagic Machinery.

(**a**) Scheme of photoactivable KFERQ-DENDRA Chaperone Mediated Autophagy reporter (CMA reporter). (**b**) CMA reporter in control and LRRK2-PD astrocytes 52 hours after photo-activation with UV light.

CMA activity was monitored using a photoactivatable CMA reporter KFREQ-Dendra (Koga et al., 2011) in both control and LRRK2-PD astrocytes for 52 hours after photoactivation (**Fig. 41a**). KFREQ-Dendra was present in the cytosol (diffuse fluorescent pattern) but as it is delivered to lysosomes via CMA it changed to a fluorescent punctate pattern. The WT astrocytes displayed this puncta indicative of functional CMA, whereas the signal in the LRRK2-PD astrocytes remained diffused in the cytosol, suggestive of an inactive CMA (**Fig. 41b**).

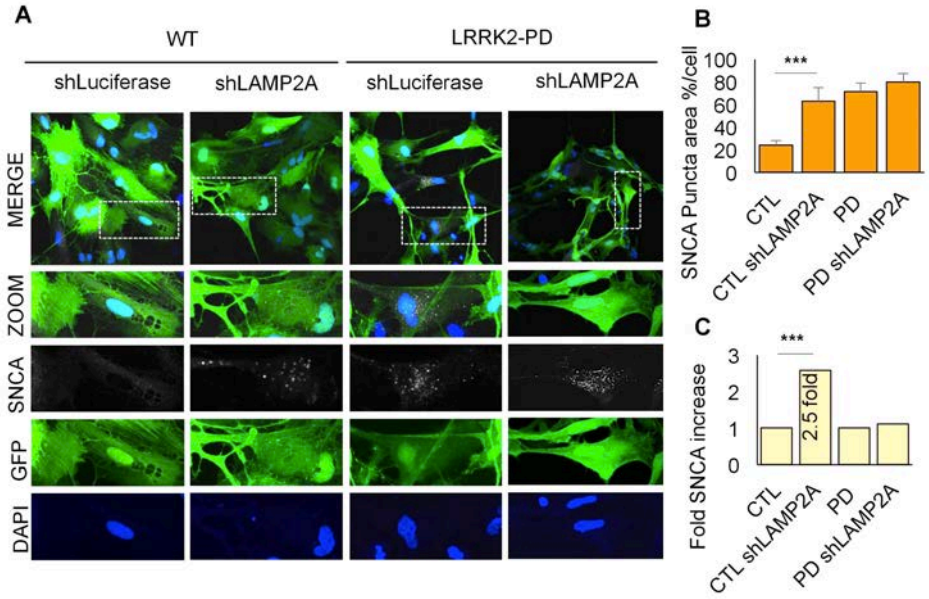

Figure 42. Knock-Down of CMA Receptor in WT and LRRK2-PD Astrocytes

(**a**) Knockdown shLAMP2A and shLuciferase (as a control) in control and LRRK2-PD astrocytes after 14 days. (**b**) SNCA puncta area percentage per cell in control and LRRK2-PD astrocytes with shLuciferase or shLAMP2A (n = 2). (**c**) SNCA puncta increase ratio in control and LRRK2-PD astrocytes with shLuciferase or CMA knockdown shLAMP2A (n = 2). All graphs plot mean ± s.e.m, unpaired two-tailed Student's t-test, *p<0.05, **p<0.01, ***p<0.001.

To investigate the contribution of the defect in CMA to the progressive accumulation of α-synuclein in the LRRK2-PD astrocytes, we next performed a knockdown of LAMP-2A using lentiviral-mediated shRNA targeting and silencing the LAMP-2A gene (shLAMP-2A) and in parallel an shRNA targeting the Luciferase gene (shLuc) as a control (**Fig. 42a**). The shLuc control astrocytes displayed an expected low level of α-synuclein, whereas after shLAMP-2A transduction, there was a highly significant 2.5-fold increase comparable to the levels observed in LRRK2-PD astrocytes ($p<0.001$) in α-synuclein puncta (**Fig. 42b,c**). Knockdown of LAMP-2A did not change α-synuclein puncta levels in the LRRK2-PD astrocytes further suggesting defective CMA for α-synuclein in these cells.

4.5.2.2 Parkinson's Disease Astrocytes Have Defective Macroautophagy and Accumulate Autophagosomes.

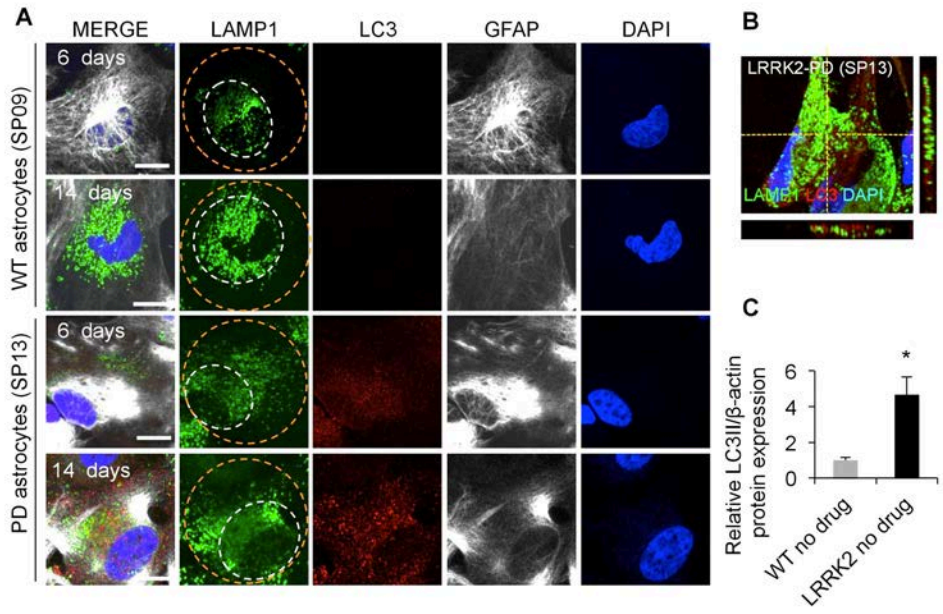

Figure 43. Dysfunctional Macroautophagy in LRRK2-PD (SP13) Astrocytes.

(**a**) Representative images of lysosomal protein marker LAMP1 and autophagosome marker LC3 in control and LRRK2-PD astrocytes at 6 and 14 days. Smaller white circles represent perinuclear area, whereas larger orange circles represent non-perinuclear area. Scale bar 50μm. (**b**) Orthogonal view representing a lack of co-localization between LAMP1 and LC3 in LRRK2-PD astrocytes. (**c**) Western blot of LC3 II protein levels with corresponding quantification (n = 2). All graphs plot mean ± s.e.m, unpaired two-tailed Student's t-test, *p<0.05, **p<0.01, ***p<0.001.

Cells often respond to blockage in CMA by upregulating other autophagic pathways such as macroautophagy (A. C. Massey, Kaushik, Sovak, Kiffin, & Cuervo, 2006; Schneider et al., 2015), however, altered macroautophagy has also been reported in the context of PD (Sánchez-Danés et al., 2012; Winslow et al., 2010). To investigate the status of macroautophagy,

lysosomal marker LAMP1, autophagosome marker LC3, astrocyte marker GFAP, and nuclear DAPI were used during ICC on WT and LRRK2-PD astrocytes at both 6 and 14 days. In the controls, there was lysosomal LAMP1 staining in the perinuclear area and very few visible autophagosomes both at 6 and 14 days.

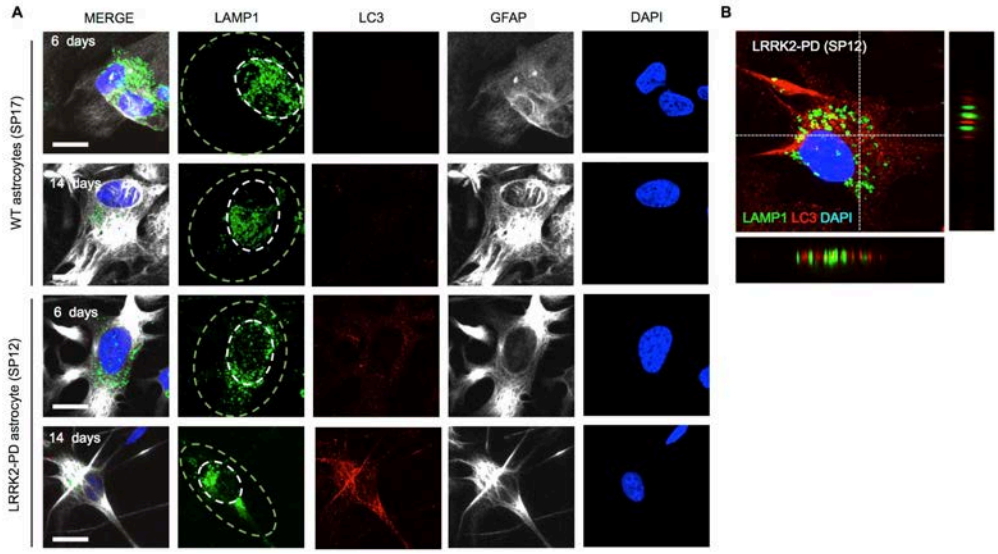

Figure 44. Dysfunctional Macroautophagy in LRRK2-PD (SP12) Astrocytes.

(**a**) Representative images of lysosomal protein marker LAMP1 and autophagosome marker LC3 in control and LRRK2-PD astrocytes at 6 and 14 days. Smaller white circles represent perinuclear area, whereas larger green circles represent non-perinuclear area. Scale bar 50µm. (**b**) Orthogonal view representing a lack of co-localization between LAMP1 and LC3 in LRRK2-PD astrocytes.

In the LRRK2-PD astrocytes, as for LAMP2A, LAMP1 positive vesicles lost the preferable perinuclear distribution and were found throughout the entire cell (**Fig. 43a; 44a**), as well as in Sporadic-PD astrocytes (**Fig. 45a**). In addition, there was a marked increase in autophagosome number (LC3

positive vesicles) starting as early as 6 days that continued increasing throughout the 14-day time-point. Most of the accumulated autophagosomes in the LRRK2-PD astrocytes did not co-localize with the LAMP1 lysosomes (**Fig. 43b; 44b; 45b,c**), suggesting that persistence of autophagosomes in these cells was due to their poor clearance by lysosomes.

In agreement with the fluorescence studies, basal LC3 II levels were found to be higher in LRRK2-PD astrocytes compared to wild type (mean ± s.e.m, *t* test, * $p<0.05$) through WB analysis (**Fig. 43c**). LC3 flux measured as the increase in LC3-II levels upon blockage of lysosomal proteolysis with Leupeptin (100μM) and NH_4Cl (20mM), was significantly reduced in the LRRK2-PD astrocytes compared to wild type ($p<0.001$, **Fig. 46a,b**). Lastly, basal p62 levels were higher in the LRRK2-PD astrocytes compared to wild type ($p<0.05$, **Fig. 46c,d**), and degradation of this macroautophagy receptor was also severely impaired in these cells.

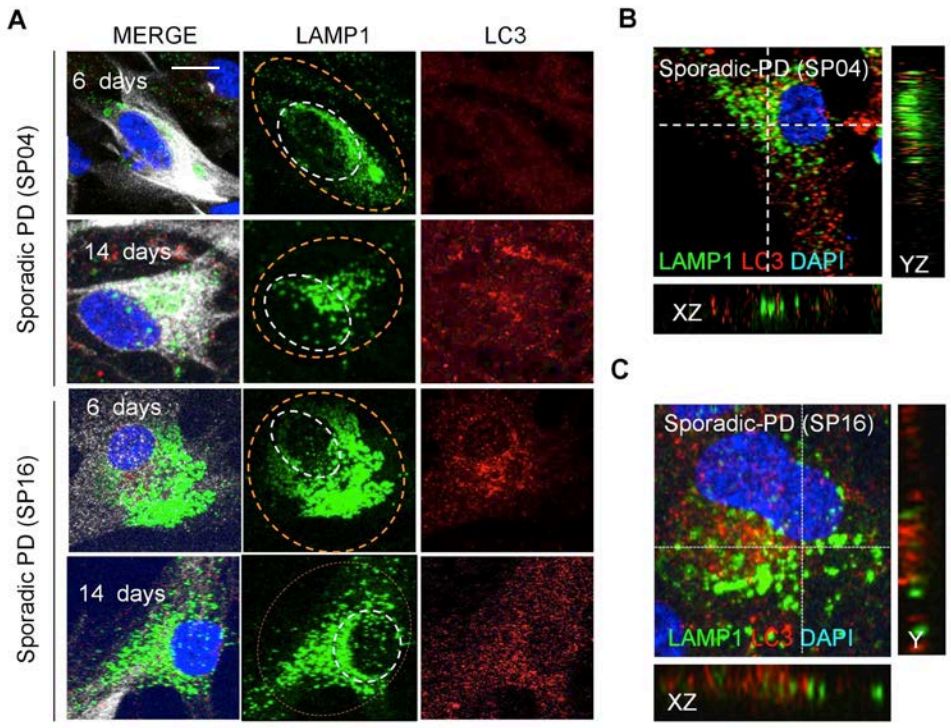

Figure 45. Dysfunctional Macroautophagy in Sporadic-PD Astrocytes.[*]

(**a**) Representative images of lysosomal protein marker LAMP1 and autophagosome marker LC3 in Sporadic-PD astrocytes at 6 and 14 days. Smaller white circles represent perinuclear area, whereas larger orange circles represent non-perinuclear area. Scale bar 50µm. (**b and c**) Orthogonal view representing a lack of co-localization between LAMP1 and LC3 in Sporadic-PD astrocytes.

[*]Done in collaboration with Isabel Fernandez Lopez of the Institute of Biomedicine at the University of Barcelona (IBUB).

Overall, these findings suggest that severe alterations in both autophagic pathways, CMA, and macroautophagy, contribute to the altered α-synuclein proteostasis observed in LRRK2-PD astrocytes.

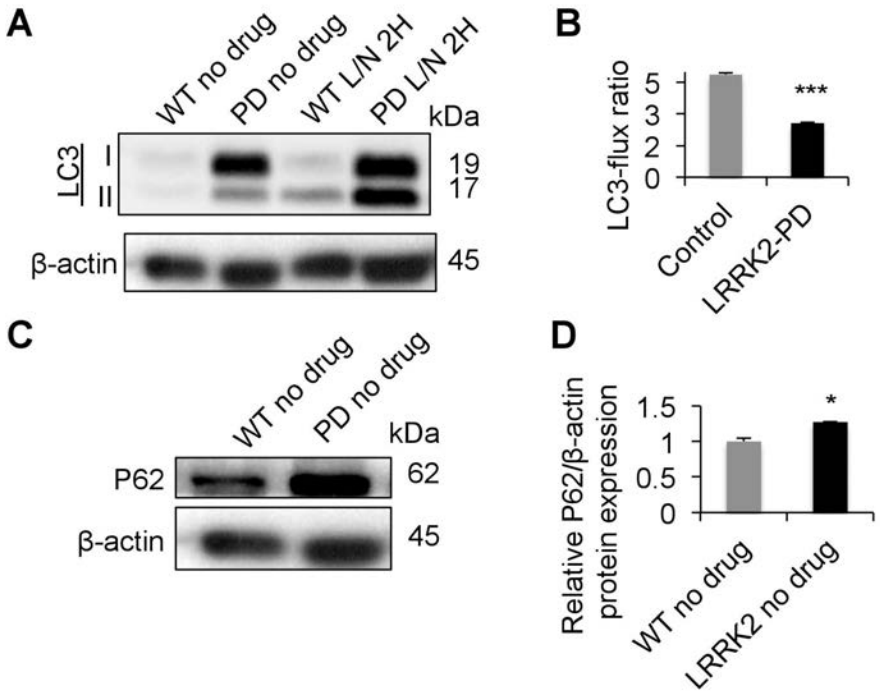

Figure 46. LRRK2-PD Astrocytes Have Impaired Autophagic Flux

(**a**) Western blot of LC3-flux analysis after inhibiting macroautophagy with Leupeptin and NH_4Cl. (**b**) LC3-flux ratio (2-hr drug treatment/no drug) representing the speed of fusion (n = 2). (**c**) Western blot of p62 protein levels with quantification (mean ± s.e.m) in graph (n = 2) (**d**). All graphs plot mean ± s.e.m, unpaired two-tailed Student's t-test, *p<0.05, **p<0.01, ***p<0.001.

4.5.3 Astrocytes from Parkinson's Disease Patients Have a Disrupted Mitochondrial Network

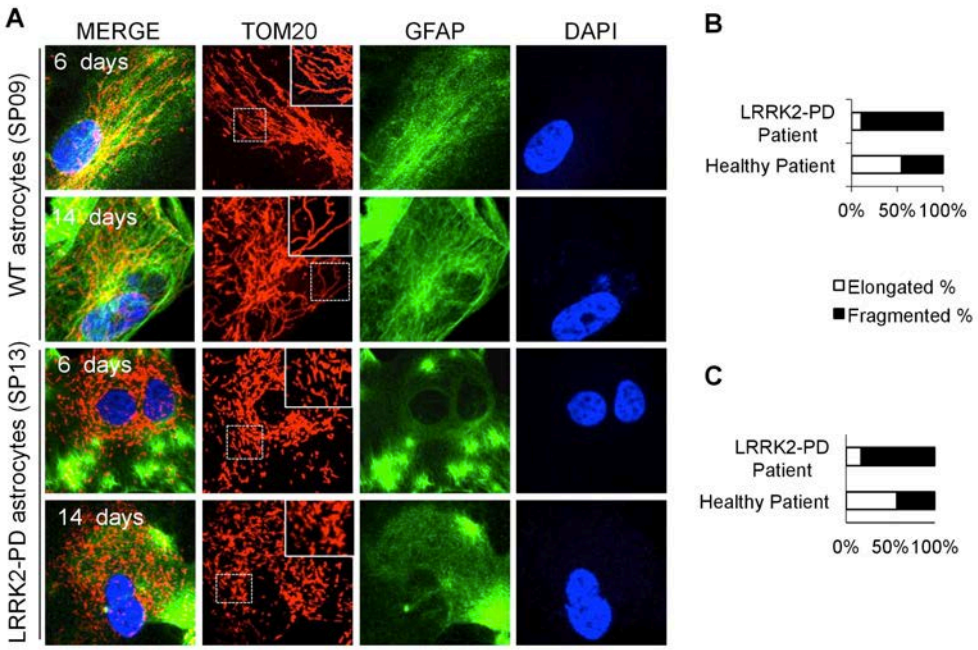

Figure 47. LRRK2-PD (SP13) Astrocytes Have Fragmented Mitochondria.

(**a**) Representative images of external mitochondrial marker TOM20, astrocyte marker GFAP, and nuclear marker DAPI in control and LRRK2 astrocytes at 6 and 14 days. Zoom provided to better visualize mitochondrial morphology. Scale bar 50µm. (**b**) Percentage of fragmented versus elongated mitochondria in LRRK2-PD and WT astrocytes at 6 days and (**c**) 14 days.

Mitochondrial external membrane marker translocase of outer membrane 20 (TOM20) was used to label the mitochondria of iPSC-derived adult astrocytes after 6 and 14 days (**Figs. 47a; 48a; 49a**). After 6 days in culture, a complex mitochondrial network was observed in the control astrocytes,

which was maintained after 14 days. In contrast, the LRRK2-PD and Sporadic-PD astrocytes displayed an unorganized mitochondrial network comprised mainly of fragmented mitochondria already after 6 days in culture.

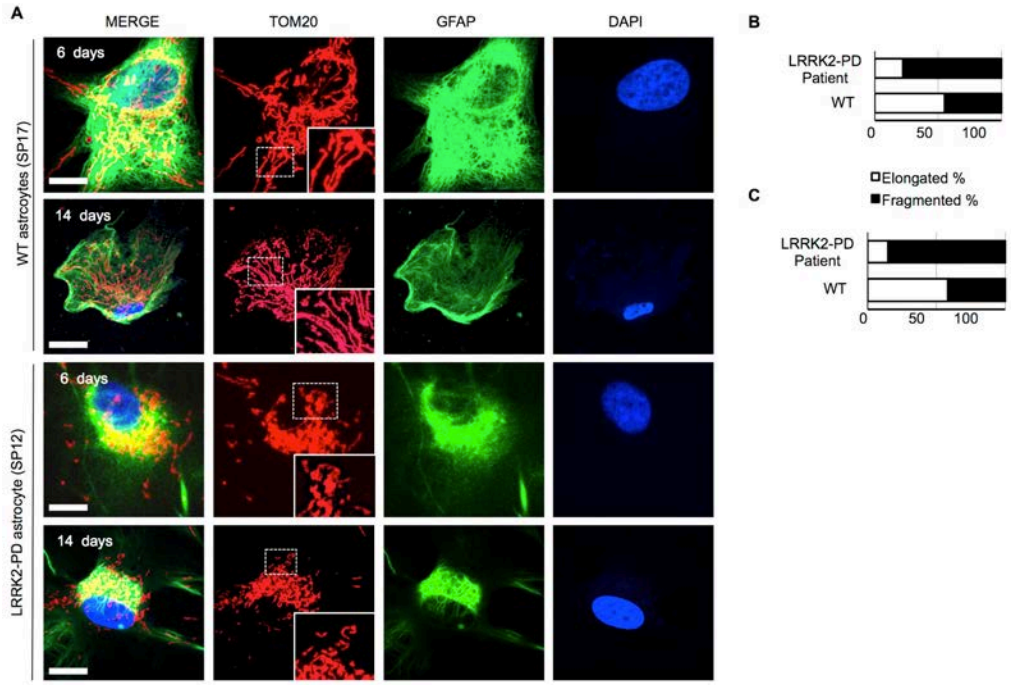

Figure 48. LRRK2-PD (SP12) Astrocytes Have Fragmented Mitochondria.

(**a**) Representative images of external mitochondrial marker TOM20, astrocyte marker GFAP, and nuclear marker DAPI in control and LRRK2 astrocytes at 6 and 14 days. Zoom provided to better visualize mitochondrial morphology. Scale bar 50µm. (**b**) Percentage of fragmented versus elongated mitochondria in LRRK2-PD and WT astrocytes at 6 days and (**c**) 14 days.

The fragmented mitochondria phenotype continued to be evident after 14 days of culture. After manual mitochondria counting, the control astrocytes

were revealed to have an equal number of fragmented versus elongated mitochondria whereas the LRRK2-PD astrocytes were comprised of 80-90% fragmented and 10-20% elongated mitochondria at both 6 and 14 days (**Fig. 47b,c; 48b,c**).

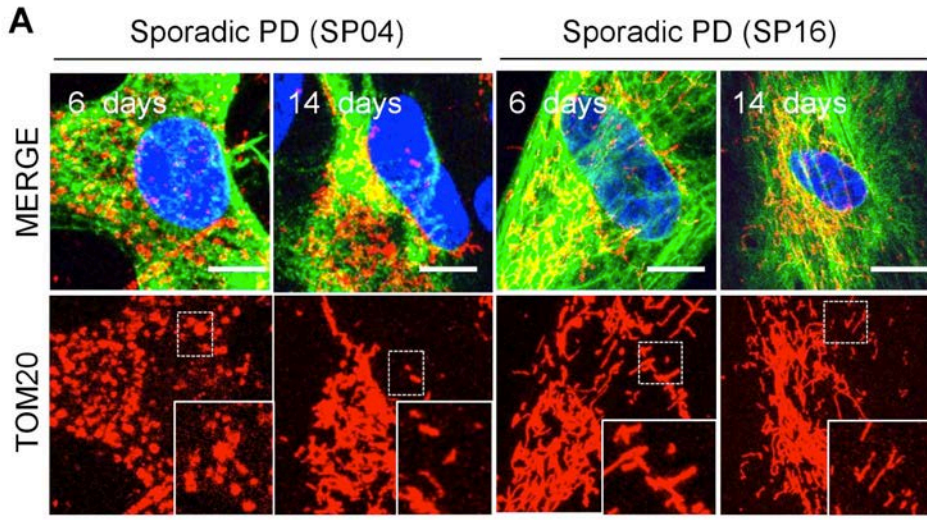

Figure 49. Sporadic-PD Astrocytes Have Fragmented Mitochondria.[*]

(**a**) Representative images of external mitochondrial marker TOM20, astrocyte marker GFAP, and nuclear marker DAPI in control and LRRK2 astrocytes at 6 and 14 days. Zoom provided to better visualize mitochondrial morphology. Scale bar 50μm.

To determine if the small size of these mitochondria was due to increased mitochondrial fission, we analyzed mitofusin protein levels within our cells. Cells were either not treated or treated with CCCP, a mitochondrial

[*]Done in collaboration with Isabel Fernandez Lopez of the Institute of Biomedicine at the University of Barcelona (IBUB).

uncoupler, as a positive control for 16 hours. Mitochondrial fission protein DRP1 phosphorylated form (pDRP1) was increased in LRRK2-PD astrocytes compared to controls (**Fig. 50a,c**). Levels of mitofusin protein responsible for mitochondrial fusion were the same between control and LRRK2-PD astrocytes and fibroblasts, those being MFN1/MFN2 (data not shown). LRRK2-PD astrocytes also displayed lowered levels of TOM20 compared to wild type (**Fig. 50b, d-e**).

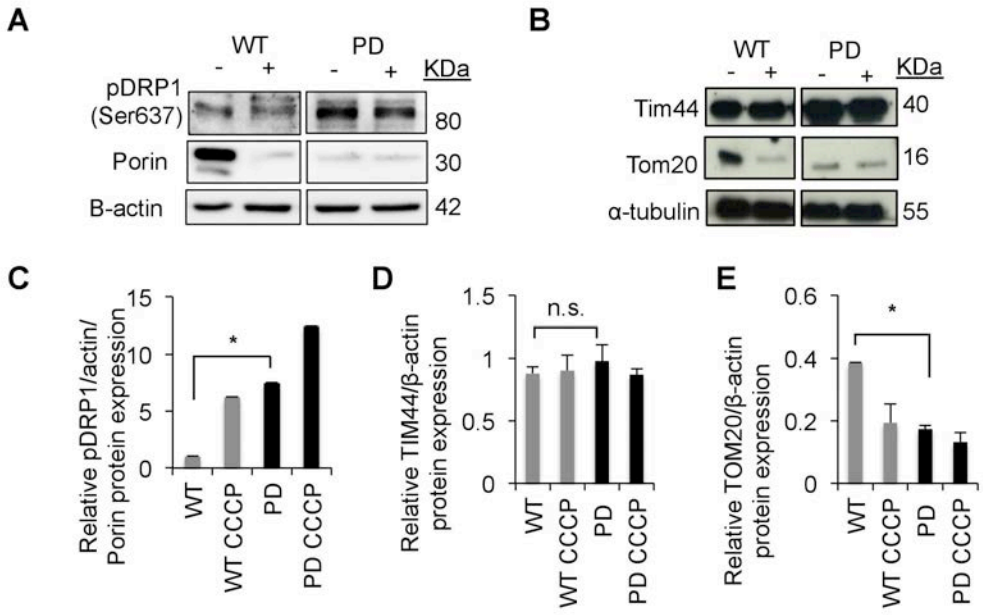

Figure 50. LRRK2-PD Astrocytes Have More Phosphorylated DRP1 Compared to Control Astrocytes.

(**a and c**) Western blot and corresponding graph revealing phosphorylated DRP1 and VDAC channel Porin protein levels in control and LRRK2-PD astrocytes in cells treated vs not treated with mitochondrial uncoupler drug CCCP, as a positive control (n = 2). (**b, d-e**) Western blot and representative graphs revealing TOM20 and TIM44 protein levels in control and LRRK2-PD astrocytes in cells treated versus not treated with CCCP (n = 2). All graphs plot mean ± s.e.m, unpaired two-tailed Student's t-test, *p<0.05, **p<0.01, ***p<0.001.

4.5.4 Chaperone Mediated Activator Drug Rescues Dysfunctional Autophagic Machinery and Alpha-Synuclein Accumulation

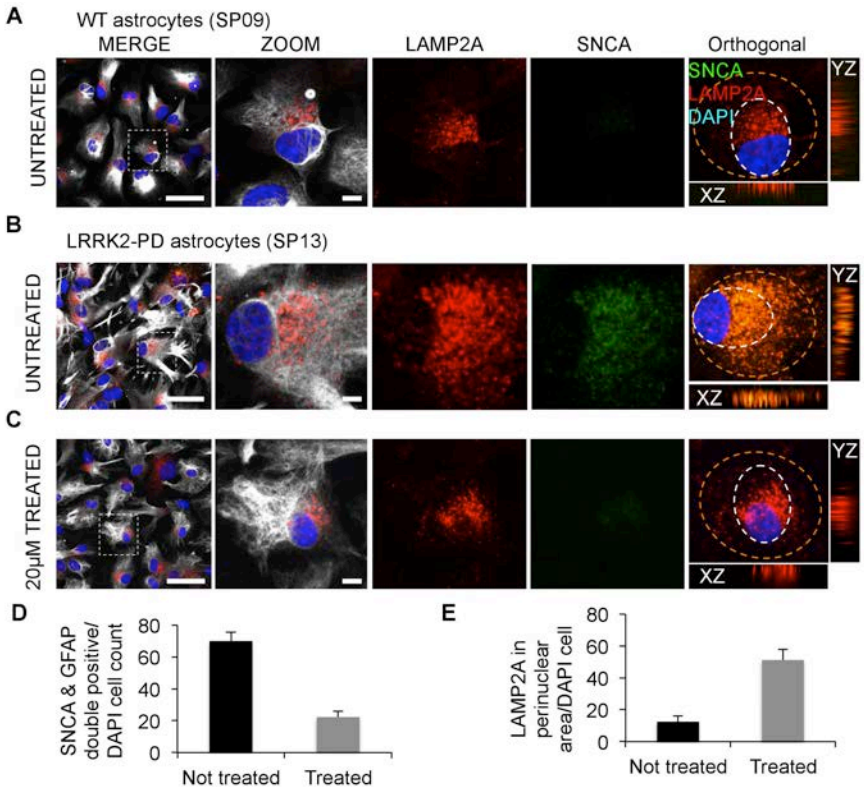

Figure 51. CMA Activator Drug Treatment Rescues SNCA Accumulation and Restores LAMP2A to Perinuclear Area.

(**a**) Representative images of 14-day WT astrocytes without treatment displaying LAMP2A in the perinuclear area and low levels of SNCA. (**b**) 14-day PD astrocytes without treatment displaying a mislocalization of LAMP2A out of the perinuclear area and accumulation of SNCA. Orthogonal views reveal positive co-localization of SNCA to LAMP2A. (**c**) 14-day PD astrocytes after 20μg of QX77.1 drug treatment for 5 days displaying LAMP2A localization restored to the perinuclear area and lower levels of SNCA. (**d**) Graph displaying percentage of cells/DAPI that are SNCA and GFAP double positive in LRRK2-PD astrocytes either not treated or treated (n = 2, total astrocytes counted = 299). (**e**) Graph displaying percentage of cells/DAPI with LAMP2A in perinuclear area in LRRK2-PD astrocytes either not treated or treated (n = 2, total astrocytes counted = 299). All graphs plot mean ± s.e.m, unpaired two-tailed Student's t-test, *p<0.05, **p<0.01, ***p<0.001. Scale bars 100μm and 20μm, respectively.

Intracellular accumulation of α-synuclein has been shown to contribute to cellular toxicity in PD and to further disrupt functioning of cellular proteostasis systems (Abeliovich & Gitler, 2016). We next investigated whether enhancing lysosomal clearance activity would ameliorate α-synuclein accumulation in LRRK2-PD astrocytes. LRRK2-PD astrocytes were treated with a novel CMA activator drug QX77 (derived from the original AR7 ref) with a concentration of 20μM for 5 days, and levels of α-synuclein were analyzed by immunofluorescence (**Fig. 51a-c**). LAMP-2A positive lysosomes, in LRRK2-PD astrocytes treated with the CMA activator, recovered the perinuclear distribution observed in control cells (**Fig. 51c,e),** suggesting re-activation of CMA in these cells. Consistent with higher CMA activity, QX77-treated cells had significantly lower α-synuclein content than untreated cells (**Fig. 51c,d**). These findings suggest that although multiple protein degradation pathways fail to efficiently degrade α-synuclein in LRRK2-PD cells, re-activation of one of these pathways, in our case CMA, is enough to restore normal α-synuclein proteostasis.

4.6 Western Blot Originals Un-Cropped

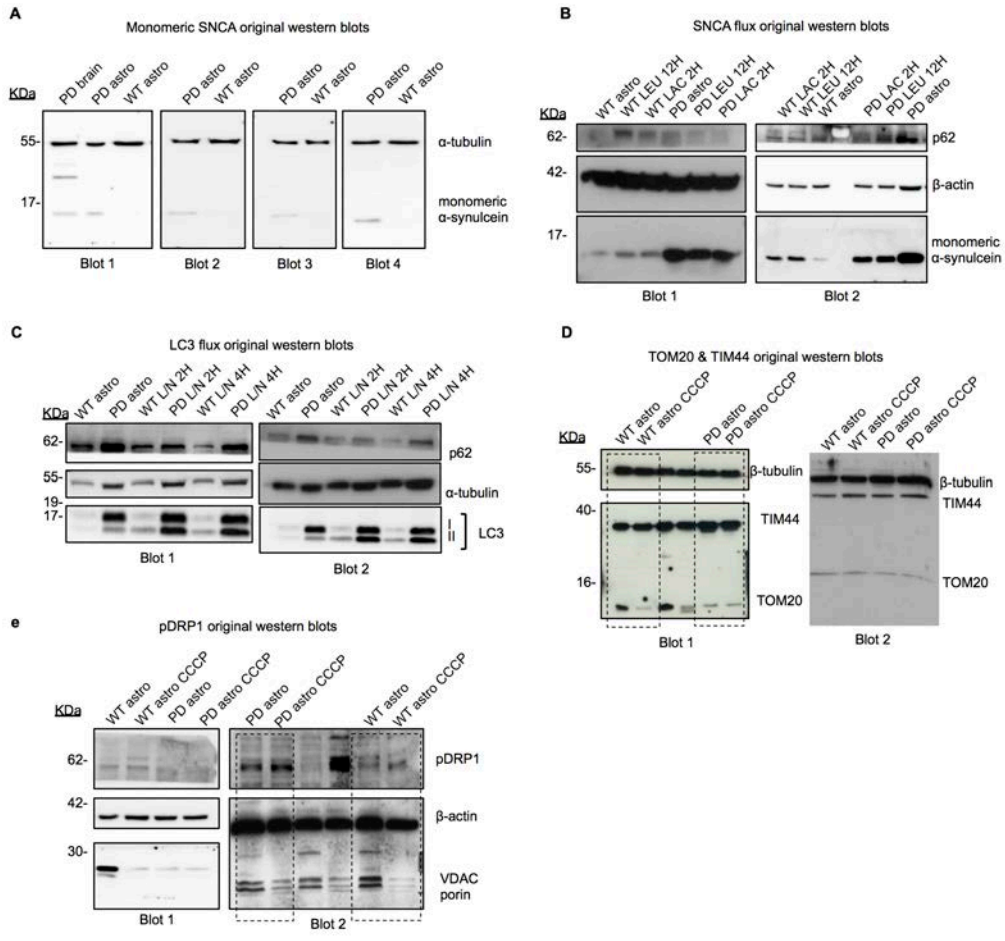

Figure 52. Original Western blots

5 DISCUSSION

5.1 Non-Cell Autonomy in Parkinson's Disease

Several previous studies have suggested a possible role for glia cells during PD pathogenesis, however the underlying contributions remain elusive. Post-mortem tissue of the SNpc of PD patients revealed α-synuclein accumulation in astrocytes (Wakabayashi et al., 2000). More recently, the scientific community has been delving into the investigation of inflammatory-mediated PD pathogenesis which has eluded to a glial contribution (Glass et al., 2010; Liddelow et al., 2017). However a direct link between astrocytes and neurodegeneration during PD is still unclear.

In this study, we have been able to unveil a crucial mechanism linking astrocyte pathogenesis to neurodegeneration. Once having co-cultured healthy WT vmDAn on both WT and LRRK2-PD astrocytes, an effect was clearly evident. When healthy WT neurons were co-cultured with LRRK2-PD astrocytes, they did not develop complex smooth arborizations as when co-cultured with WT astrocytes, but rather developed shorter and fewer neurites, as well as a select number (35-fold) adopting neurodegenerative characteristics, such as beaded-necklace neurites (**Figs. 19; 20**). These morphological effects indicate a neurotoxic effect of the PD astrocytes on the WT neurons, in line with recent findings (Hoenen et al., 2016; Liddelow et al., 2017).

PD pathogenesis is dopaminergic neuron specific. The exact cause for this specificity is still unknown, however, a recent study has show that vulnerability is mediated by synaptic excitability, calcium activity and specific viability of SNpc DA neurons which is mediated by the hyperpolarization-activated current (Carbone, Costa, Provensi, Mannaioni, & Masi, 2017). In this study we found, overall TH cell number diminished

when WT vmDA neurons were co-cultured on LRRK2-PD astrocytes compared to on WT astrocytes at both 2- and 4-week time-points (**Fig. 19**). When WT vmDA neurons were co-cultured with LRRK2-PD astrocytes, they displayed a 45% increase of TH/α-synuclein double positive cells, compared to when co-cultured on WT astrocytes (**Fig. 23**). This neurodegeneration was found to be TH specific as MAP2 numbers in both conditions did not change significantly.

The viability of both WT and LRRK2-PD astrocytes was similar, indicating that the degenerative effects on the neurons were not caused by astrocyte death (**Fig. 22**), but rather most likely were caused by other toxic molecules, which have not yet been detected. This evidence supports the fact that there are either neurotoxic factors secreted or a lack of secretion of neuroprotective factors by LRRK2-PD astrocytes that affect neuronal differentiation and survival, and more importantly which are targeting only the dopaminergic neuronal population (**Fig. 21**) (Liddelow et al., 2017).

5.2 The Spread of Astrocyte-Derived Alpha-Synuclein

Toxic oligomeric α-synuclein containing aggregates known as Lewy Bodies is a hallmark of PD (Spillantini, Crowther, Jakes, Hasegawa, & Goedert, 1998). In addition to WT vmDA neurons harboring neurodegenerative phenotypes when co-cultured with LRRK2-PD astrocytes (**Figs. 19; 20**), α-synuclein accumulation also was recapitulated in our *in vitro* model (**Figs. 23; 24**). There was an overall increase in α-synuclein levels in the entire co-culture with the LRRK2-PD astrocytes compared to those with WT astrocytes. Upon closer inspection, we identified that LRRK2-PD astrocytes themselves also contained high levels of α-synuclein compared to WT

astrocytes in the co-culture condition (**Fig. 24**). Post-mortem tissue of PD patients has revealed astrocytes with accumulated α-synuclein (Wakabayashi et al., 2000). In order to track the astrocytic-derived α-synuclein we used CRISPR-CASP9 editing technology to develop astrocyte lines that have α-synuclein tagged with a Flag (**Fig. 25**). After regenerating astrocytes with its endogenous α-synuclein tagged with a flag, we were able to demonstrate the direct transfer of α-synuclein from the PD α-synuclein Flag tagged astrocyte to the WT neuron during a 4-week co-culture (**Figs. 26; 27**) which was not present in the WT neuron when co-cultured on the WT astrocyte condition. This transfer of α-synuclein, which is known to be toxic to dopaminergic neurons during PD, most likely is a key factor inducing neurodegeneration in the WT neurons, thus confirming a main role for astrocytes during PD pathogenesis.

Recently, α-synuclein has been reported to play a role during inflammation-mediated PD pathogenesis (Brück et al., 2016). α-Synuclein secreted by neurons has been reported to directly activate microglia inducing an inflammatory response during PD (Q. S. Zhang et al., 2017). These α-synuclein-activated microglia thus release pro-inflammatory cytokines and in turn activate astrocytes. Astrocytes have also been reported to have the capability of activating microglia (Gu et al., 2010; Schmidt et al., 2011). Therefore, if astrocytes also accumulate and secrete α-synuclein, they could contribute to the activation of microglia and trigger a cascade of inflammatory-mediated pathways furthering PD pathogenesis.

5.3 Neuroprotective Role of Astrocytes

A link recently has been described between neuroprotection and neuroinflammatory response (Becerra-Calixto & Cardona-Gómez, 2017; Farina et al., 2007). The fact that WT astrocytes are able to rescue the morphological phenotype of neurodegeneration and clearance of neuronal α-synuclein when co-cultured with LRRK2-PD vmDA neurons validates a neuroprotective role (**Fig. 29; 30**), which the LRRK2-PD astrocytes are lacking (**Fig. 23**). An interesting observation was made when focusing on WT astrocytes in the co-culture LRRK2-PD neurons with WT astrocytes. The majority of WT astrocytes had an expected large and flat morphology with low GFAP signaling, however, a select few harbored a hypertrophic morphology with retracted processes (**Fig. 32**).

What is even more striking is the fact that these hypertrophic astrocytes accumulated high levels of α-synuclein, suggesting a neuroprotective effect via activation of the WT astrocyte. mRNA expression levels of TFEB, a gene suggested for neuroprotection and involved in autophagy, was present in WT astrocytes and lacking in LRRK2-PD astrocytes (**Fig. 33**). Several cytokines and chemokines, which have been described to be pathological, also can mediate neuroprotection (Belmadani, Tran, Ren, & Miller, 2006; Farina et al., 2007; Herx, Rivest, & Yong, 2000; Mason et al., 2000; Tran & Miller, 2003). There is a fine line between protection and harm, which can be shifted if a homeostatic balance is or is not maintained. Further analysis should be made to evaluate the exact inflammatory molecules being released, if any, by the WT astrocytes to validate this activation as reactivity.

5.4 Mutant LRRK2 and Autophagy

Correlation between mutant LRRK2 and several pathogenic mechanisms linked to PD progression have been reported, including alterations in autophagy, accumulation of α-synuclein, and mitochondrial dysfunction (Orenstein et al., 2013; Sanders et al., 2014; Tong et al., 2010). In this study, LRRK2-PD astrocytes were found to have a mislocalization of lysosomes from the perinuclear area and accumulation of α-synuclein (**Fig. 36-39**). A reporter line for CMA activity enabled us to monitor CMA activity and revealed a low functionality in LRRK2-PD astrocytes compared to WT (**Fig. 41**). Knockdown of the CMA receptor had no increase in α-synuclein levels in LRRK2-PD astrocytes compared to WT, revealing that this mechanism already was impaired (**Fig. 42**).

During PD pathogenesis, mutant LRRK2 was found to directly bind LAMP2A, the receptor responsible for chaperone-mediated autophagy (CMA) normally used by both LRRK2 and α-synuclein for degradation (Orenstein et al., 2013). The binding of mutant LRRK2 to LAMP2A blocks the proper functioning of the CMA translocation complex, resulting in defective CMA, leading to the accumulation of α-synuclein and cell death. When the CMA translocation complex is blocked, the cell responds by producing more reactive lysosomal receptors, in an attempt to compensate for the dysfunction. This lysosomal hyperactivity also was reported to affect macroautophagic functioning since when LRRK2 kinase activity was inhibited in human neuroglioma cells, macroautophagy was stimulated (Manzoni et al., 2013).

It is likely that the increase in intracellular levels of α-synuclein, due to its poor CMA degradation in LRRK2-PD astrocytes, may contribute to

precipitate the malfunctioning of other proteostasis mechanisms such as the proteasome and macroautophagy. In fact, we demonstrated that macroautophagy also was markedly impaired in these cells, by displaying higher basal levels of autophagosomes (LC3-II) and the autophagic cargo p62 and reduced autophagic flux (for LC3-II and p62) (**Fig 46**). The lower co-localization between the autophagosomal and lysosomal markers observed in LRRK2-PD astrocytes suggests that the reduced autophagic flux is, for the most part, due to a defect in autophagosome/lysosome fusion, similar to that previously described in PD neurons (Winslow et al., 2010).

The systems that contribute to cellular and organelle proteostasis act in a coordinate manner in the cell, and numerous examples support the idea that restoration of one of these systems has a positive effect on the functioning of the rest of the proteostasis network(Kaushik & Cuervo, 2015). Taking into consideration this coordinate functioning of the proteolytic systems, and the fact that CMA disruption seems to occur early during the development of PD pathology, we attempted to restore normal α-synuclein proteostasis by enhancing CMA activity. Our findings in cells treated with the chemical activators of CMA suggest that upregulation of CMA is still possible in these cells and that this intervention is sufficient to return levels of α-synuclein close to those in control cells (**Fig. 51**). Reduced levels of α-synuclein in these cells may be due not only to its enhanced degradation by CMA, but, in addition, considering the large contribution of the proteasome to the degradation of α-synuclein in control cells, it is possible that restoration of CMA activity and the subsequent reduction of α-synuclein levels also will release the inhibitory effect of α-synuclein on the proteasome and macroautophagy, further contributing to the restoration of intracellular protein and organelle homeostasis.

5.5 Mutant LRRK2 and Mitochondrial Dynamics

In alignment with the notion that protein degradation is impaired in LRRK2-PD astrocytes, and in light of the effects mutant LRRK2 have been reported to cause during PD, the mitochondria were investigated. LRRK2-PD astrocytes displayed more fragmented mitochondria compared to WT astrocytes (**Fig. 47; 48**). It is known that mutant LRRK2 phosphorylates, and thus induces the recruitment of DRP1 into the mitochondria, inducing mitochondrial fission(X. Wang et al., 2012). Indeed, the LRRK2-PD astrocytes not only had a reduced protein level of VDAC channel, namely Porin, but also had higher levels of phosphorylated DRP1 compared to WT astrocytes (**Fig. 50**). This increased level of fission can explain the mitochondrial fragmentation present in our LRRK2-PD astrocytes and perhaps increased mitophagy.

The exact mechanism of mitochondrial fragmentation during PD is unknown, however a recent study has elicited mutant LRRK2 binding a mitochondrial shuttling protein, Miro, thus blocking mitophagy (Hsieh et al., 2016). In addition, α-synuclein has been reported to bind to TOM20 and induce mitochondrial dysfunction during PD (Di Maio et al., 2016). The consequent α-synuclein accumulation found in LRRK2-PD astrocytes could further add to already observed mitochondrial dysfunction.

5.6 PD-Related Phenotypes in Sporadic-PD Astrocytes

The phenotypes found in the LRRK2-PD astrocytes had been previously reported in vmDA neurons and fibroblasts with the $LRRK2^{G2019S}$ mutation, and here are revealed for the first time in astrocytes. Sporadic cases are,

however, a different story, and reveal an intermediate phenotype, which will require a more in-depth investigation. Without a known genetic cause, Sporadic-PD cases are the most numerous cases of PD, and have been under intensive investigation in recent years, especially in terms of genetic variation (Loureiro & Silva, 2017). Several genome-wide association studies have revealed generic risk variants for Sporadic PD, which may aid to unveil several hidden pathogenic mechanisms (Satake et al., 2009; Sharma et al., 2012; Simón-Sánchez et al., 2009).

We approached these lines by observing whether or not they display phenotypes similar to those related to the LRRK2-PD mutation. Astrocytic α-synuclein-immunoreactive inclusions already have been described to develop in Sporadic-PD patients, however they were never further investigated (Braak et al., 2007). Sporadic-PD astrocytes displayed on average 20-40% increased α-synuclein accumulation (**Fig. 39**), which, when compared to LRRK2-PD (100%) and WT astrocytes (0%), reveals an intermediate phenotype. The same observation was made in terms of mitochondria fragmentation. Regarding macroautophagy, Sporadic-PD astrocytes displayed a large similarity to LRRK2-PD astrocytes revealing autophagosome accumulation and mislocalization of the lysosomes from the perinuclear area (**Fig. 45**). While LRRK2-PD astrocytes have a majority of fragmented mitochondria (80-90%), mitochondrial fragmentation dominance was not as evident in Sporadic-PD patients, yet still was present (**Fig. 49**). Previous studies have observed DRP-1 mediated mitochondrial fragmentation in Sporadic patients (Santos, Esteves, Silva, Januário, & Cardoso, 2015).

It is interesting that the phenotypes in the LRRK2-PD astrocytes have full penetrance and expressivity, whereas the Sporadic-PD astrocytes display a

partial effect. Depending on modifier genes, environmental factors, allelic variation, as well as complex genetic and environmental interactions, disease related phenotypes could show differences in penetrance and expressivity, therefore demonstrating the expression of intermediate phenotypes (Nadeau, 2001; Riazuddin et al., 2000; Weatherall, 2001).

6 CONCLUSIONS

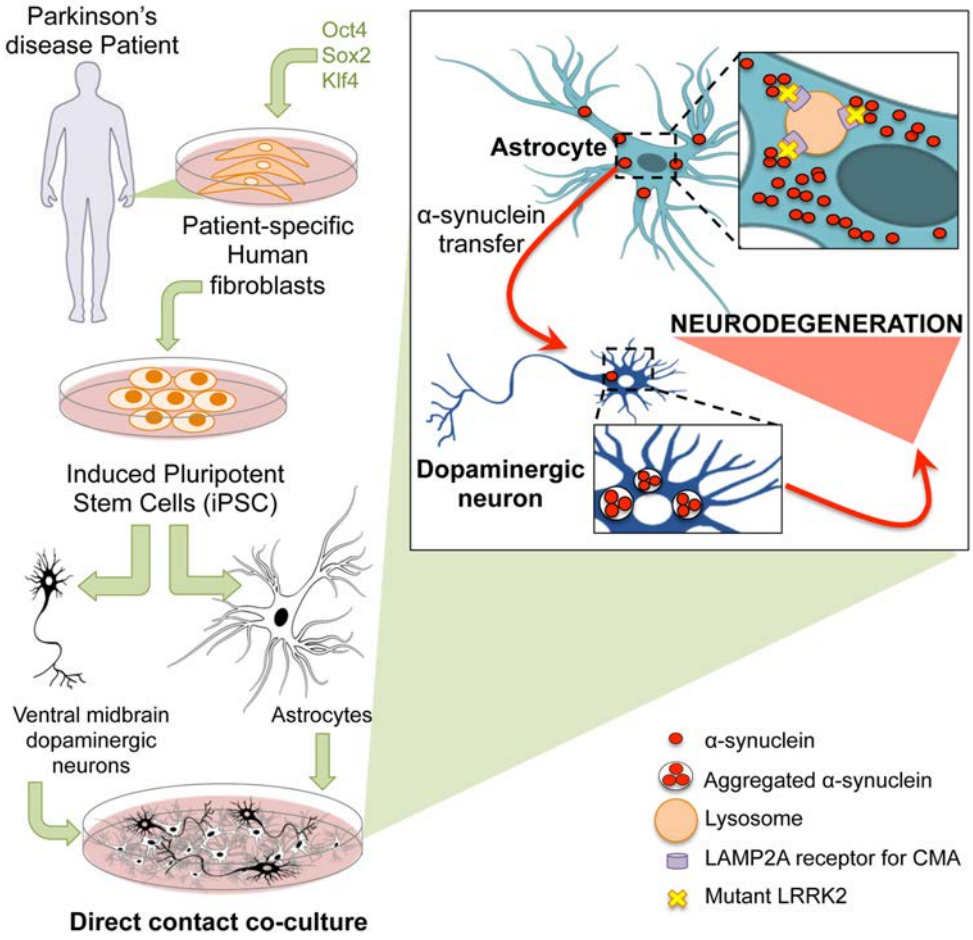

Figure 53. Astrocytes Contribute to Neurodegeneration During PD Pathogenesis

In conclusion, this study has revealed a crucial contribution of astrocytes during PD pathogenesis. Patient-specific astrocytes, two from LRRK2-PD, two from Sporadic-PD, and two from healthy WT individuals, were

successfully generated and fully characterized. In parallel, vmDA neurons from LRRK2-PD patients and WT patients also were generated in order to devise a co-culture system. Both direct contact and indirect contact (astrocyte conditioned medium) co-cultures were performed between all possible patient-specific cell combinations.

Not only were LRRK2-PD astrocytes found to induce neurodegeneration and to transfer astrocytic-derived α-synuclein to healthy WT neurons (both through direct and indirect contact), but WT astrocytes also were able to partially recover the observed neurodegenerative morphology and α-synuclein accumulation in LRRK2-PD neurons. WT astrocytes projected neuroprotection through the activation of inflammatory pathways, as those that accumulated the cleared α-synuclein had a hypertrophic morphology, retracted processes, and high expression of GFAP.

Upon a more in-depth investigation, LRRK2-PD astrocytes alone displayed dysfunctional CMA and consequent α-synuclein accumulation, as well as a lowered autophagosome flux and fragmented mitochondria, compared to WT astrocytes. Sporadic-PD astrocytes displayed a partial phenotype similar to LRRK2-PD astrocytes, which may be explained by several external factors affecting phenotypic penetrance and expressivity. A CMA activator drug, QX77.1, was able to rescue the accumulated α-synuclein and restore the lysosomes around the perinuclear area in LRRK2-PD astrocytes, suggesting a potential astrocyte-targeted therapeutic. These results open the door for non-cell autonomy during PD pathogenesis and can serve as a platform to further investigate potential therapies targeted directly at glia cells.

7 REFERENCES

Abbott, N. J., Rönnbäck, L., & Hansson, E. (2006). Astrocyte–endothelial interactions at the blood–brain barrier. *Nature Reviews Neuroscience*, *7*(1), 41–53.

Abeliovich, A., & Gitler, A. D. (2016). Defects in trafficking bridge Parkinson's disease pathology and genetics. *Nature*, *539*(7628), 207–216.

Ahmad, L., Zhang, S. Y., Casanova, J. L., & Sancho-Shimizu, V. (2016). Human TBK1: A Gatekeeper of Neuroinflammation. *Trends in Molecular Medicine*, *22*(6), 511–527.

Anderson, M. A., Burda, J. E., Ren, Y., Ao, Y., O'Shea, T. M., Kawaguchi, R., … Sofroniew, M. V. (2016). Astrocyte scar formation aids central nervous system axon regeneration. *Nature*, *0*(1), 1–20.

Beauquis, J., Pavía, P., Pomilio, C., Vinuesa, A., Podlutskaya, N., Galvan, V., & Saravia, F. (2013). Environmental enrichment prevents astroglial pathological changes in the hippocampus of APP transgenic mice, model of Alzheimer's disease. *Experimental Neurology*, *239*(1), 28–37.

Beauquis, J., Vinuesa, A., Pomilio, C., Pavía, P., Galván, V., & Saravia, F. (2014). Neuronal and glial alterations, increased anxiety, and cognitive impairment before hippocampal amyloid deposition in PDAPP mice, model of Alzheimer's disease. *Hippocampus*, *24*(3), 257–269.

Becerra-Calixto, A., & Cardona-Gómez, G. P. (2017). The Role of Astrocytes in Neuroprotection after Brain Stroke: Potential in Cell Therapy. *Frontiers in Molecular Neuroscience*, *10*(April), 1–12.

Belmadani, A., Tran, P. B., Ren, D., & Miller, R. J. (2006). Chemokines regulate the migration of neural progenitors to sites of neuroinflammation. *The Journal of Neuroscience : The Official Journal of the Society for Neuroscience*, *26*(12), 3182–91.

Ben Haim, L., Carrillo-de Sauvage, M.-A., Ceyzériat, K., & Escartin, C. (2015). Elusive roles for reactive astrocytes in neurodegenerative diseases. *Frontiers in Cellular Neuroscience*, *9*(August), 278.

Béraud, D., & Maguire-Zeiss, K. A. (2012). Misfolded α-synuclein and toll-like receptors: therapeutic targets for Parkinson's disease. *Parkinsonism & Related Disorders*, *18*, S17–S20.

Berger M., J. R. . A. (2004). The blood brain barrier in HIV infection. *Front Biosci*, *9*, 2680–2685.

Bir, A., Sen, O., Anand, S., Khemka, V. K., Banerjee, P., Cappai, R., … Chakrabarti, S. (2015). Alpha-synuclein-induced mitochondrial dysfunction in isolated preparation and intact cells: Implications in the pathogenesis of Parkinson's disease. *Journal of Neurochemistry*, *131*(6), 868–877.

Bonifati, V., Rizzu, P., van Baren, M. J., Schaap, O., Breedveld, G. J., Krieger, E., … Heutink, P. (2003). Mutations in the DJ-1 gene associated with autosomal recessive

early-onset parkinsonism. *Science (New York, N.Y.)*, *299*(5604), 256–259.

Booth, H. D. E., Hirst, W. D., & Wade-Martins, R. (2017). The Role of Astrocyte Dysfunction in Parkinson's Disease Pathogenesis. *Trends in Neurosciences*, *40*(6), 358–370.

Braak, H., & Del Tredici, K. (2008). Invited Article: Nervous system pathology in sporadic Parkinson disease. *Neurology*, *70*(20), 1916–1925.

Braak, H., Ghebremedhin, E., Rüb, U., Bratzke, H., & Del Tredici, K. (2004). Stages in the development of Parkinson's disease-related pathology. *Cell and Tissue Research*, *318*(1), 121–134.

Braak, H., Sastre, M., & Del Tredici, K. (2007). Development of α-synuclein immunoreactive astrocytes in the forebrain parallels stages of intraneuronal pathology in sporadic Parkinson's disease. *Acta Neuropathologica*, *114*(3), 231–241.

Braidy, N., Gai, W.-P., Xu, Y. H., Sachdev, P., Guillemin, G. J., Jiang, X.-M., … Chan, D. K. Y. (2013). Uptake and mitochondrial dysfunction of alpha-synuclein in human astrocytes, cortical neurons and fibroblasts. *Translational Neurodegeneration*, *2*(1), 20.

Broux, B., Gowing, E., & Prat, A. (2015). Glial regulation of the blood-brain barrier in health and disease. *Seminars in Immunopathology*, *37*(6), 577–590.

Brück, D., Wenning, G. K., Stefanova, N., & Fellner, L. (2016). Glia and alpha-synuclein in neurodegeneration: A complex interaction. *Neurobiology of Disease*, *85*, 262–274.

Cabezas, R., Avila, M. F., Torrente, D., El-bachá, R. S., Morales, L., Gonzalez, J., & Barreto, G. E. (2013). Astrocytes Role in Parkinson : A Double-Edged Sword. *"Neurodegenerative Diseases", Book, Chapter 20*.

Carbone, C., Costa, A., Provensi, G., Mannaioni, G., & Masi, A. (2017). The Hyperpolarization-Activated Current Determines Synaptic Excitability, Calcium Activity and Specific Viability of Substantia Nigra Dopaminergic Neurons. *Frontiers in Cellular Neuroscience*, *11*, 187.

Cerri, S., Siani, F., & Blandini, F. (2017). Investigational drugs in Phase I and Phase II for Levodopa-induced dyskinesias. *Expert Opinion on Investigational Drugs*, *26*(7), 777–791.

Chambers, S. M., Fasano, C. A., Papapetrou, E. P., Tomishima, M., Sadelain, M., & Studer, L. (2009). Highly efficient neural conversion of human ES and iPS cells by dual inhibition of SMAD signaling. *Nature Biotechnology*, *27*(3), 275–280.

Chandra, R., Hiniker, A., Kuo, Y.-M., Nussbaum, R. L., & Liddle, R. A. (2017). α - Synuclein in gut endocrine cells and its implications for Parkinson ' s disease. *JCI Insight*, *2*(12), e92295.

Chen, Y.-Z., Bennett, C. L., Huynh, H. M., Blair, I. P., Puls, I., Irobi, J., … Chance, P. F.

(2004). DNA/RNA helicase gene mutations in a form of juvenile amyotrophic lateral sclerosis (ALS4). *American Journal of Human Genetics*, *74*(6), 1128–35.

Cherra, S. J., Steer, E., Gusdon, A. M., Kiselyov, K., & Chu, C. T. (2013). Mutant LRRK2 elicits calcium imbalance and depletion of dendritic mitochondria in neurons. *American Journal of Pathology*, *182*(2), 474–484.

Christopherson, K. S., Ullian, E. M., Stokes, C. C. A., Mullowney, C. E., Hell, J. W., Agah, A., … Barres, B. a. (2005). Thrombospondins are astrocyte-secreted proteins that promote CNS synaptogenesis. *Cell*, *120*(3), 421–433.

Cloud Lee, Y.-T., & Danny Hsu, S.-T. (2016). Familial Mutations and Post-translational Modifications of UCH-L1 in Parkinson's Disease and Neurodegenerative Disorders. *Curr Protein Pept Sci*.

Collaborators, G. B. of D. S. 2013. (2015). Europe PMC Funders Group Global , regional , and national incidence , prevalence , and years lived with disability for 301 acute and chronic diseases and injuries in 188 countries , 1990 – 2013 : a systematic analysis for the Global Burden of Disease Stud. *Lancet*, *386*(9995), 743–800.

Colombrita, C., Onesto, E., Megiorni, F., Pizzuti, A., Baralle, F. E., Buratti, E., … Ratti, A. (2012). TDP-43 and FUS RNA-binding proteins bind distinct sets of cytoplasmic messenger RNAs and differently regulate their post-transcriptional fate in motoneuron-like cells. *The Journal of Biological Chemistry*, 1–24.

Covy, J. P., & Giasson, B. I. (2009). Identification of compounds that inhibit the kinase activity of leucine-rich repeat kinase 2. *Biochemical and Biophysical Research Communications*, *378*(3), 473–477.

Crotti, A., Benner, C., Kerman, B. E., Gosselin, D., Lagier-Tourenne, C., Zuccato, C., … Glass, C. K. (2014). Mutant Huntingtin promotes autonomous microglia activation via myeloid lineage-determining factors. *Nature Neuroscience*, *17*(4), 513–521.

Cuervo, A. M., Stefanis, L., Fredenburg, R., Lansbury, P. T., & Sulzer, D. (2004). Impaired degradation of mutant alpha-synuclein by chaperone-mediated autophagy. *Science (New York, N.Y.)*, *305*(5688), 1292–5.

Davies, D. C. (2002). Blood-brain barrier breakdown in septic encephalopathy and brain tumours. *Journal of Anatomy*, *200*(6), 639–646.

Dawson, T. M., Ko, H. S., & Dawson, V. L. (2010). Genetic Animal Models of Parkinson's Disease. *Neuron*, *66*(5), 646–661.

Di Maio, R., Barrett, P. J., Hoffman, E. K., Barrett, C. W., Zharikov, A., Borah, A., … Greenamyre, J. T. (2016). Alpha-Synuclein binds to TOM20 and inhibits mitochondrial protein import in Parkinsons disease. *Science Translational Medicine*, *8*(342), 342ra78-342ra78.

Dias, V., Junn, E., & Mouradian, M. M. (2013). The Role of Oxidative Stress in Parkinson's Disease. *Journal of Parkinson's Disease*, *3*(4), 461–491.

Dragicevic, E., Schiemann, J., & Liss, B. (2015). Dopamine midbrain neurons in health and Parkinson's disease: Emerging roles of voltage-gated calcium channels and ATP-sensitive potassium channels. *Neuroscience*, *284*, 798–814.

Dringen, R., Brandmann, M., Hohnholt, M. C., & Blumrich, E. M. (2015). Glutathione-Dependent Detoxification Processes in Astrocytes. *Neurochemical Research*, *40*(12), 2570–2582.

Dryanovski, D. I., Guzman, J. N., Xie, Z., Galteri, D. J., Volpicelli-Daley, L. a, Lee, V. M.-Y., … Surmeier, D. J. (2013). Calcium entry and α-synuclein inclusions elevate dendritic mitochondrial oxidant stress in dopaminergic neurons. *The Journal of Neuroscience : The Official Journal of the Society for Neuroscience*, *33*(24), 10154–64.

Du, J.-J., & Chen, S.-D. (2017). Current Nondopaminergic Therapeutic Options for Motor Symptoms of Parkinson's Disease. *Chinese Medical Journal*, *130*(15), 1856.

Ebrahimi-Fakhari, D., Wahlster, L., & McLean, P. J. (2012). Protein degradation pathways in Parkinson's disease: Curse or blessing. *Acta Neuropathologica*, *124*(2), 153–172.

Farina, C., Aloisi, F., & Meinl, E. (2007). Astrocytes are active players in cerebral innate immunity. *Trends in Immunology*, *28*(3), 138–145.

Ferraiuolo, L. (2014). The non-cell-autonomous component of ALS: new in vitro models and future challenges. *Biochemical Society Transactions*, *42*(5).

Fonzo, A. D., Dekker, M. C. J., Montagna, P., Baruzzi, A., Yonova, E. H., Guedes, L. C., … Bonifati, V. (2009). FBXO7 mutations cause autosomal recessive, early-onset parkinsonian- pyramidal syndrome. *Neurology*, *72*(3), 240–245.

Geloso, M. C., Corvino, V., Marchese, E., Serrano, A., Michetti, F., & D'Ambrosi, N. (2017). The Dual Role of Microglia in ALS: Mechanisms and Therapeutic Approaches. *Frontiers in Aging Neuroscience*, *9*, 242.

Gilks, W. P., Abou-Sleiman, P. M., Gandhi, S., Jain, S., Singleton, A., Lees, A. J., … Wood, N. W. (2005). A common LRRK2 mutation in idiopathic Parkinson's disease. *Lancet*, *365*(9457), 415–6.

Glass, C. K., Saijo, K., Winner, B., Marchetto, M. C., & Gage, F. H. (2010). Mechanisms Underlying Inflammation in Neurodegeneration. *Cell*, *140*(6), 918–934.

Gordon, G. R. J., Mulligan, S. J., & MacVicar, B. A. (2007). Astrocyte control of the cerebrovasculature. *GLIA*, *55*(12), 1214–1221.

Greenamyre, J. T., & Hastings, T. G. (2004). Biomedicine. Parkinson's-divergent causes, convergent mechanisms. *Science (New York, N.Y.)*, *304*(5674), 1120–1122.

Gu, X.-L., Long, C.-X., Sun, L., Xie, C., Lin, X., & Cai, H. (2010). Astrocytic expression of Parkinson's disease-related A53T alpha-synuclein causes neurodegeneration in mice.

Molecular Brain, *3*(1), 12.

Haidet-Phillips, A. M., Hester, M. E., Miranda, C. J., Meyer, K., Braun, L., Frakes, A., … Kaspar, B. K. (2011). Astrocytes from familial and sporadic ALS patients are toxic to motor neurons. *Nature Biotechnology*, *29*(9), 824–828.

Henkel, J. S., Beers, D. R., Zhao, W., & Appel, S. H. (2009). Microglia in ALS: the good, the bad, and the resting. *Journal of Neuroimmune Pharmacology : The Official Journal of the Society on NeuroImmune Pharmacology*, *4*(4), 389–98.

Herx, L. M., Rivest, S., & Yong, V. W. (2000). Central nervous system-initiated inflammation and neurotrophism in trauma: IL-1 beta is required for the production of ciliary neurotrophic factor. *Journal of Immunology (Baltimore, Md. : 1950)*, *165*(4), 2232–2239.

Hoenen, C., Gustin, A., Birck, C., Kirchmeyer, M., Beaume, N., Felten, P., … Heurtaux, T. (2016). Alpha-synuclein proteins promote pro-inflammatory cascades in microglia: Stronger effects of the a53t mutant. *PLoS ONE*, *11*(9), e0162717.

Hsieh, C. H., Shaltouki, A., Gonzalez, A. E., Bettencourt da Cruz, A., Burbulla, L. F., St. Lawrence, E., … Wang, X. (2016). Functional Impairment in Miro Degradation and Mitophagy Is a Shared Feature in Familial and Sporadic Parkinson's Disease. *Cell Stem Cell*, *19*(6), 709–724.

Huang, L., Deng, M., Zhang, S., Lu, S., Gui, X., & Fang, Y. (2017). β-asarone and levodopa coadministration increases striatal levels of dopamine and levodopa and improves behavioral competence in Parkinson's rat by enhancing dopa decarboxylase activity. *Biomedicine & Pharmacotherapy*, *94*, 666–678.

Hubbard, J. A., Szu, J. I., Yonan, J. M., & Binder, D. K. (2016). Regulation of astrocyte glutamate transporter-1 (GLT1) and aquaporin-4 (AQP4) expression in a model of epilepsy. *Experimental Neurology*, *283*, 85–96.

Huber, J. D., Witt, K. A., Hom, S., Egleton, R. D., Mark, K. S., & Davis, T. P. (2001). Inflammatory pain alters blood-brain barrier permeability and tight junctional protein expression. *American Journal of Physiology. Heart and Circulatory Physiology*, *280*(3), H1241–H1248.

Jang, A., Lee, H. J., Suk, J. E., Jung, J. W., Kim, K. P., & Lee, S. J. (2010). Non-classical exocytosis of alpha-synuclein is sensitive to folding states and promoted under stress conditions. *Journal of Neurochemistry*, *113*(5), 1263–1274.

Johnson, B. S., Snead, D., Lee, J. J., McCaffery, J. M., Shorter, J., & Gitler, A. D. (2009). TDP-43 is intrinsically aggregation-prone, and amyotrophic lateral sclerosis-linked mutations accelerate aggregation and increase toxicity. *The Journal of Biological Chemistry*, *284*(30), 20329–39.

Jones, V. C., Atkinson-Dell, R., Verkhratsky, A., & Mohamet, L. (2017). Aberrant iPSC-derived human astrocytes in Alzheimer's disease. *Cell Death & Disease*, *8*(3), e2696.

Kaushik, S., & Cuervo, A. M. (2015). Proteostasis and aging. *Nature Medicine*, *21*(12), 1406–1415.

Khakh, B. S., & Sofroniew, M. V. (2015). Diversity of astrocyte functions and phenotypes in neural circuits. *Nature Neuroscience*, *18*(7), 942–952.

Khasnavis, S., & Pahan, K. (2014). Cinnamon treatment upregulates neuroprotective proteins Parkin and DJ-1 and protects dopaminergic neurons in a mouse model of Parkinson's disease. *Journal of Neuroimmune Pharmacology*, *9*(4), 569–581.

Kiffin, R. (2004). Activation of Chaperone-mediated Autophagy during Oxidative Stress. *Molecular Biology of the Cell*, *15*(11), 4829–4840.

Kitada, T., Asakawa, S., Hattori, N., Matsumine, H., Yamamura, Y., Minoshima, S., … Shimizu, N. (1998). Mutations in the parkin gene cause autosomal recessive juvenile parkinsonism. *Nature*, *392*(6676), 605–608.

Koga, H., Martinez-Vicente, M., Macian, F., Verkhusha, V. V, & Cuervo, A. M. (2011). A photoconvertible fluorescent reporter to track chaperone-mediated autophagy. *Nature Communications*, *2*, 386.

Kortekaas, R., Leenders, K. L., Van Oostrom, J. C. H., Vaalburg, W., Bart, J., Willemsen, A. T. M., & Hendrikse, N. H. (2005). Blood-brain barrier dysfunction in Parkinsonian midbrain in vivo. *Annals of Neurology*, *57*(2), 176–179.

Kriks, S., Shim, J.-W., Piao, J., Ganat, Y. M., Wakeman, D. R., Xie, Z., … Studer, L. (2011). Dopamine neurons derived from human ES cells efficiently engraft in animal models of Parkinson's disease. *Nature*, *480*(7378), 547–51.

Kuo, Y. M., Li, Z., Jiao, Y., Gaborit, N., Pani, A. K., Orrison, B. M., … Nussbaum, R. L. (2010). Extensive enteric nervous system abnormalities in mice transgenic for artificial chromosomes containing Parkinson disease-associated α-synuclein gene mutations precede central nervous system changes. *Human Molecular Genetics*, *19*(9), 1633–1650.

Lee, A., & Pow, D. V. (2010). Astrocytes: Glutamate transport and alternate splicing of transporters. *The International Journal of Biochemistry & Cell Biology*, *42*(12), 1901–6.

Lee, G., & Bendayan, R. (2004). Functional expression and localization of P-glycoprotein in the central nervous system: Relevance to the pathogenesis and treatment of neurological disorders. *Pharmaceutical Research*, *21*(8), 1313–1330.

Lee, H. J., Suk, J. E., Patrick, C., Bae, E. J., Cho, J. H., Rho, S., … Lee, S. J. (2010). Direct transfer of α-synuclein from neuron to astroglia causes inflammatory responses in synucleinopathies. *Journal of Biological Chemistry*, *285*(12), 9262–9272.

Li, G., Yang, H., Zhu, D., Huang, H., Liu, G., & Lun, P. (2014). Targeted suppression of chaperone-mediated autophagy by miR-320a promotes alpha-synuclein aggregation.

International Journal of Molecular Sciences, *15*(9), 15845–15857.

Liddelow, S. A., & Barres, B. A. (2017). Reactive Astrocytes : Potential, Therapeutics. *Immunity*, *46*(6), 957–967.

Liddelow, S. A., Guttenplan, K. A., Clarke, L. E., Bennett, F. C., Bohlen, C. J., Schirmer, L., … Barres, B. A. (2017). Neurotoxic reactive astrocytes are induced by activated microglia. *Nature*, *541*(7638), 481–487.

Lill, C. M. (2016). Genetics of Parkinson's disease. *Molecular and Cellular Probes*, *30*(6), 386–396.

Liu, H.-N., Tjostheim, S., Dasilva, K., Taylor, D., Zhao, B., Rakhit, R., … Robertson, J. (2012). Targeting of Monomer/Misfolded SOD1 as a Therapeutic Strategy for Amyotrophic Lateral Sclerosis. *The Journal of Neuroscience : The Official Journal of the Society for Neuroscience*, *32*(26), 8791–9.

Lo, E. H., Dalkara, T., & Moskowitz, M. A. (2003). Mechanisms, challenges and opportunities in stroke. *Nature Reviews Neuroscience*, *4*(5), 399–415.

Loureiro, C., & Silva, R. H. (2017). Genetic Variants in SNCA and the Risk of Sporadic Parkinson ' s Disease and Clinical Outcomes : A Review. *Parkinson's Disease*, *2017*, 4318416.

Manzoni, C., Mamais, A., Dihanich, S., Abeti, R., Soutar, M. P. M., Plun-Favreau, H., … Lewis, P. A. (2013). Inhibition of LRRK2 kinase activity stimulates macroautophagy. *Biochimica et Biophysica Acta - Molecular Cell Research*, *1833*(12), 2900–2910.

Marroni, M., Marchi, N., Cucullo, L., Abbott, N. J., Signorelli, K., & Janigro, D. (2003). Vascular and parenchymal mechanisms in multiple drug resistance: a lesson from human epilepsy. *Current Drug Targets*, *4*(4), 297–304.

Martinez-Vicente, M., Talloczy, Z., Kaushik, S., Massey, A. C., Mazzulli, J., Mosharov, E. V., … Cuervo, A. M. (2008). Dopamine-modified alpha-synuclein blocks chaperone-mediated autophagy. *Journal of Clinical Investigation*, *118*(2), 777–778.

Mason, J. L., Jones, J. J., Taniike, M., Morell, P., Suzuki, K., & Matsushima, G. K. (2000). Mature oligodendrocyte apoptosis precedes IGF-1 production and oligodendrocyte progenitor accumulation and differentiation during demyelination/remyelination. *Journal of Neuroscience Research*, *61*(3), 251–262.

Massey, A. C., Follenzi, A., Kiffin, R., Zhang, C., & Cuervo, A. M. (2008). Early cellular changes after blockage of chaperone-mediated autophagy. *Autophagy*, *4*(4), 442–456.

Massey, A. C., Kaushik, S., Sovak, G., Kiffin, R., & Cuervo, A. M. (2006). Consequences of the selective blockage of chaperone-mediated autophagy. *Proceedings of the National Academy of Sciences*, *103*(15), 5805–5810.

Mbefo, M. K., Fares, M. B., Paleologou, K., Oueslati, A., Yin, G., Tenreiro, S., … Lashuel, H. a. (2015). Parkinson disease mutant E46K enhances α-synuclein phosphorylation

in mammalian cell lines, in yeast, and in vivo. *Journal of Biological Chemistry*, *290*(15), 9412–9427.

McCrate, M. E., & Kaspar, B. K. (2008). Physical activity and neuroprotection in amyotrophic lateral sclerosis. *Neuromolecular Medicine*, *10*(2), 108–17.

Melrose, H. L., Lincoln, S. J., Tyndall, G. M., & Farrer, M. J. (2006). Parkinson's disease: A rethink of rodent models. *Experimental Brain Research*, *173*(2), 196–204.

Molofsky, A. V, Kelley, K. W., Tsai, H.-H., Redmond, S. a, Chang, S. M., Madireddy, L., … Rowitch, D. H. (2014). Astrocyte-encoded positional cues maintain sensorimotor circuit integrity. *Nature*, *509*(7499), 189–194.

Nadeau, J. H. (2001). Modifier genes in mice and humans. *Nature Reviews Genetics*, *2*(3), 165–174.

Nash, K. R., Moran, P., Finneran, D. J., Hudson, C., Robinson, J., Morgan, D., & Bickford, P. C. (2014). Fractalkine Over Expression Suppresses α-Synuclein-mediated Neurodegeneration. *Molecular Therapy*, *23*(1), 17–23.

Nedergaard, M., Takano, T., & Hansen, A. J. (2002). Beyond the role of glutamate as a neurotransmitter. *Nature Reviews. Neuroscience*, *3*(9), 748–55.

Neupane, K., Solanki, A., Sosova, I., Belov, M., & Woodside, M. T. (2014). Diverse metastable structures formed by small oligomers of alpha-synuclein probed by force spectroscopy. *PLoS ONE*, *9*(1), e86495.

Nguyen, H. N., Byers, B., Cord, B., Shcheglovitov, A., Byrne, J., Gujar, P., … Pera, R. R. (2011). LRRK2 mutant iPSC-derived da neurons demonstrate increased susceptibility to oxidative stress. *Cell Stem Cell*, *8*(3), 267–280.

Nichols, W. C., Pankratz, N., Hernandez, D., Paisán-Ruíz, C., Jain, S., Halter, C. A., … Foroud, T. (2005). Genetic screening for a single common LRRK2 mutation in familial Parkinson's disease. *Lancet*, *365*(9457), 410–412.

O'Rourke, J. G., Bogdanik, L., Yanez, A., Lall, D., Wolf, A. J., Muhammad, A. K. M. G., … Baloh, R. H. (2016). C9orf72 is required for proper macrophage and microglial function in mice. *Science*, *351*(6279), 1324–1329.

Olabarria, M., Noristani, H. N., Verkhratsky, A., & Rodríguez, J. J. (2010). Concomitant astroglial atrophy and astrogliosis in a triple transgenic animal model of Alzheimer's disease. *GLIA*, *58*(7), 831–838.

Orenstein, S. J., Kuo, S.-H., Tasset, I., Arias, E., Koga, H., Fernandez-Carasa, I., … Cuervo, A. M. (2013). Interplay of LRRK2 with chaperone-mediated autophagy. *Nature Neuroscience*, *16*(4), 394–406.

Paisán-Ruíz, C., Jain, S., Evans, E. W., Gilks, W. P., Simón, J., Van Der Brug, M., … Singleton, A. B. (2004). Cloning of the gene containing mutations that cause

PARK8-linked Parkinson's disease. *Neuron*, *44*(4), 595–600.

Panatier, A., Vallée, J., Haber, M., Murai, K. K., Lacaille, J. C., & Robitaille, R. (2011). Astrocytes are endogenous regulators of basal transmission at central synapses. *Cell*, *146*(5), 785–798.

Park, C., Suh, Y., & Cuervo, A. M. (2015). Regulated degradation of Chk1 by chaperone-mediated autophagy in response to DNA damage. *Nature Communications*, *6*, 6823.

Perfeito, R., Lázaro, D. F., Outeiro, T. F., & Rego, A. C. (2014). Linking alpha-synuclein phosphorylation to reactive oxygen species formation and mitochondrial dysfunction in SH-SY5Y cells. *Molecular and Cellular Neuroscience*, *62*, 51–59.

Plaza-Zabala, A., Sierra-Torre, V., & Sierra, A. (2017). Autophagy and microglia: Novel partners in neurodegeneration and aging. *International Journal of Molecular Sciences*, *18*(3), 598.

Polymeropoulos, M. H., Lavedan, C., Leroy, E., Ide, S. E., Dehejia, A., Dutra, A., … Nussbaum, R. L. (1997). Mutation in the α -Synuclein Gene Identified in Families with Parkinson's Disease Mutation in the alpha-Synuclein Gene Identified in Families with Parkinson ' s Disease. *Science*, *276*(June), 2045–2047.

Ramirez, A., Heimbach, A., Gründemann, J., Stiller, B., Hampshire, D., Cid, L. P., … Kubisch, C. (2006). Hereditary parkinsonism with dementia is caused by mutations in ATP13A2, encoding a lysosomal type 5 P-type ATPase. *Nat Genet*, *38*(10), 1184–1191.

Rappold, P. M., & Tieu, K. (2011). NIH Public Access, *7*(4), 413–423.

Reinhardt, P., Schmid, B., Burbulla, L. F., Schöndorf, D. C., Wagner, L., Glatza, M., … Sterneckert, J. (2013). Genetic correction of a lrrk2 mutation in human iPSCs links parkinsonian neurodegeneration to ERK-dependent changes in gene expression. *Cell Stem Cell*, *12*(3), 354–367.

Reyes, J. F., Olsson, T. T., Lamberts, J. T., Devine, M. J., Kunath, T., & Brundin, P. (2015). A cell culture model for monitoring α-synuclein cell-to-cell transfer. *Neurobiology of Disease*, *77*, 266–275.

Riazuddin, S., Castelein, C. M., Ahmed, Z. M., Lalwani, a K., Mastroianni, M. a, Naz, S., … Wilcox, E. R. (2000). Dominant modifier DFNM1 suppresses recessive deafness DFNB26. *Nature Genetics*, *26*(4), 431–434.

Richard, J.-P., & Maragakis, N. J. (2014). Induced pluripotent stem cells from ALS patients for disease modeling. *Brain Research*, *1607*, 15–25.

Riederer, P., Sofic, E., Rausch, W. D., Schmidt, B., Reynolds, G. P., Jellinger, K., & Youdim, M. B. H. (1989). Transition Metals, Ferritin, Glutathione, and Ascorbic Acid in Parkinsonian Brains. *Journal of Neurochemistry*, *52*(2), 515–520.

Ritchie, C. M., & Thomas, P. J. (2012). Alpha-synuclein truncation and disease. *Health*,

4(11), 1167–1177.

Rothaug, M., Zunke, F., Mazzulli, J. R., Schweizer, M., Altmeppen, H., Lullmann-Rauch, R., … Blanz, J. (2014). LIMP-2 expression is critical for -glucocerebrosidase activity and -synuclein clearance. *Proceedings of the National Academy of Sciences*, *111*(43), 15573–15578.

Sadelli, K., Stamegna, J. C., Girard, S. D., Baril, N., Escoffier, G., Brus, M., … Roman, F. S. (2017). Global cerebral ischemia in rats leads to amnesia due to selective neuronal death followed by astroglial scar formation in the CA1 layer. *Neurobiology of Learning and Memory*, *141*, 168–178.

Saijo, K., Winner, B., Carson, C. T., Collier, J. G., Boyer, L., Rosenfeld, M. G., … Glass, C. K. (2009). A Nurr1/CoREST Pathway in Microglia and Astrocytes Protects Dopaminergic Neurons from Inflammation-Induced Death. *Cell*, *137*(1), 47–59.

Sánchez-Danés, A., Richaud-Patin, Y., Carballo-Carbajal, I., Jiménez-Delgado, S., Caig, C., Mora, S., … Raya, A. (2012). Disease-specific phenotypes in dopamine neurons from human iPS-based models of genetic and sporadic Parkinson's disease. *EMBO Molecular Medicine*, *4*(5), 380–395.

Sanders, L. H., Laganire, J., Cooper, O., Mak, S. K., Vu, B. J., Huang, Y. A., … Schle, B. (2014). LRRK2 mutations cause mitochondrial DNA damage in iPSC-derived neural cells from Parkinson's disease patients: Reversal by gene correction. *Neurobiology of Disease*.

Sanders, L. H., Paul, K. C., Howlett, E. H., Lawal, H., Boppana, S., Bronstein, J. M., … Greenamyre, J. T. (2017). Editor's Highlight: Base Excision Repair Variants and Pesticide Exposure Increase Parkinson's Disease Risk. *Toxicological Sciences*, *158*(1), 188–198.

Santos, D., Esteves, A. R., Silva, D. F., Januário, C., & Cardoso, S. M. (2015). The Impact of Mitochondrial Fusion and Fission Modulation in Sporadic Parkinson's Disease. *Molecular Neurobiology*, *52*(1), 573–586.

Satake, W., Nakabayashi, Y., Mizuta, I., Hirota, Y., Ito, C., Kubo, M., … Toda, T. (2009). Genome-wide association study identifies common variants at four loci as genetic risk factors for Parkinson's disease. *Nature Genetics*, *41*(12), 1303–7.

Schapira, A. H. (2006). Etiology of Parkinson's disease. *Neurology*, *66*(10 Suppl 4), S10-23.

Schmidt, S., Linnartz, B., Mendritzki, S., Sczepan, T., Lübbert, M., Stichel, C. C., & Lübbert, H. (2011). Genetic mouse models for Parkinson's disease display severe pathology in glial cell mitochondria. *Human Molecular Genetics*, *20*(6), 1197–1211.

Schneider, J. L., Villarroya, J., Diaz-Carretero, A., Patel, B., Urbanska, A. M., Thi, M. M., … Cuervo, A. M. (2015). Loss of hepatic chaperone-mediated autophagy accelerates proteostasis failure in aging. *Aging Cell*, *14*(2), 249–264.

Schwaninger, M., Sallmann, S., Petersen, N., Schneider, A., Prinz, S., Libermann, T. A., &

Spranger, M. (1999). Bradykinin induces interleukin-6 expression in astrocytes through activation of nuclear factor-B. *Journal of Neurochemistry*, *73*(4), 1461–1466.

Serio, A., Bilican, B., Barmada, S. J., Ando, D. M., Zhao, C., Siller, R., … Chandran, S. (2013). Astrocyte pathology and the absence of non-cell autonomy in an induced pluripotent stem cell model of TDP-43 proteinopathy. *Proceedings of the National Academy of Sciences of the United States of America*, *110*(12), 4697–702.

Sharma, M., Ioannidis, J. P. A., Aasly, J. O., Annesi, G., Brice, A., Van Broeckhoven, C., … Krger, R. (2012). Large-scale replication and heterogeneity in Parkinson disease genetic loci. *Neurology*, *79*(7), 659–667.

Shojaee, S., Sina, F., Banihosseini, S. S., Kazemi, M. H., Kalhor, R., Shahidi, G. A., … Elahi, E. (2008). Genome-wide Linkage Analysis of a Parkinsonian-Pyramidal Syndrome Pedigree by 500 K SNP Arrays. *American Journal of Human Genetics*, *82*(6), 1375–1384.

Simón-Sánchez, J., Schulte, C., Bras, J. M., Sharma, M., Gibbs, J. R., Berg, D., … Gasser, T. (2009). Genome-wide association study reveals genetic risk underlying Parkinson's disease. *Nature Genetics*, *41*(12), 1308–12.

Singleton, B., Farrer, M., Johnson, J., Singleton, A., Hague, S., Kachergus, J., … Gwinn-Hardy, K. (2003). alpha-Synuclein locus triplication causes Parkinson's disease. *Science (New York, N.Y.)*, *302*(5646), 841.

Solano, R. M., Casarejos, M. J., Menéndez-Cuervo, J., Rodriguez-Navarro, J. A., García De Yébenes, J., & Mena, M. A. (2008). Glial Dysfunction in Parkin Null Mice: Effects of Aging. *Neurobiology of Disease*, *28*(3), 598–611.

Song, H., Stevens, C. F., & Gage, F. H. (2002). Astroglia induce neurogenesis from adult neural stem cells. *Nature*, *417*(6884), 39–44.

Spencer, J. I., Bell, J. S., & DeLuca, G. C. (2017). Vascular pathology in multiple sclerosis: reframing pathogenesis around the blood-brain barrier. *Journal of Neurology, Neurosurgery & Psychiatry*, jnnp-2017-316011.

Spillantini, M. G., Crowther, R. A., Jakes, R., Hasegawa, M., & Goedert, M. (1998). alpha-Synuclein in filamentous inclusions of Lewy bodies from Parkinson's disease and dementia with lewy bodies. *Proc Natl Acad Sci U S A*, *95*(11), 6469–6473.

Su, Y. C., Guo, X., & Qi, X. (2015). Threonine 56 phosphorylation of Bcl-2 is required for LRRK2 G2019S-induced mitochondrial depolarization and autophagy. *Biochimica et Biophysica Acta - Molecular Basis of Disease*, *1852*(1), 12–21.

Subramanian, V., Crabtree, B., & Acharya, K. R. (2008). Human angiogenin is a neuroprotective factor and amyotrophic lateral sclerosis associated angiogenin variants affect neurite extension/pathfinding and survival of motor neurons. *Human Molecular Genetics*, *17*(1), 130–49.

Suzuki, A., Stern, S. A., Bozdagi, O., Huntley, G. W., Walker, R. H., Magistretti, P. J., &

Alberini, C. M. (2011). Astrocyte-neuron lactate transport is required for long-term memory formation. *Cell*, *144*(5), 810–823.

Tanaka, Y., Engelender, S., Igarashi, S., Rao, R. K., Wanner, T., Tanzi, R. E., … Ross, C. A. (2001). Inducible expression of mutant α-synuclein decreases proteasome activity and increases sensitivity to mitochondria-dependent apoptosis. *Human Molecular Genetics*, *10*(9), 919–926.

Tong, Y., Yamaguchi, H., Giaime, E., Boyle, S., Kopan, R., Kelleher, R. J., & Shen, J. (2010). Loss of leucine-rich repeat kinase 2 causes impairment of protein degradation pathways, accumulation of alpha-synuclein, and apoptotic cell death in aged mice. *Proceedings of the National Academy of Sciences of the United States of America*, *107*(21), 9879–84.

Tran, P. B., & Miller, R. J. (2003). Chemokine receptors: signposts to brain development and disease. *Nature Reviews. Neuroscience*, *4*(6), 444–455.

Tyzack, G. E., Sitnikov, S., Barson, D., Adams-Carr, K. L., Lau, N. K., Kwok, J. C., … Lakatos, A. (2014). Astrocyte response to motor neuron injury promotes structural synaptic plasticity via STAT3-regulated TSP-1 expression. *Nature Communications*, *5*, 4294.

Ullian, E. (2001). Control of Synapse Number by Glia. *Science*, *291*(5504), 657–661.

Ullian, E., Christopherson, K., & Barres, B. (2004). Role for glia in synaptogenesis. *GLIA*, *47*(3), 209–216.

Urrea, L., Segura-Feliu, M., Masuda-Suzukake, M., Hervera, A., Pedraz, L., Aznar, J. M. G., … Del Río, J. A. (2017). Involvement of Cellular Prion Protein in α-Synuclein Transport in Neurons. *Molecular Neurobiology*, 1–14.

Uwechue, N. M., Marx, M.-C., Chevy, Q., & Billups, B. (2012). Activation of glutamate transport evokes rapid glutamine release from perisynaptic astrocytes. *The Journal of Physiology*, *590*(10), 2317–2331.

Valente, E. M., Abou-Sleiman, P. M., Caputo, V., Muqit, M. M. K., Harvey, K., Gispert, S., … Wood, N. W. (2004). Hereditary early-onset Parkinson's disease caused by mutations in PINK1. *Science (New York, N.Y.)*, *304*(5674), 1158–60.

Vilarino-Guell, C., Wider, C., Ross, O. A., Dachsel, J. C., Kachergus, J. M., Lincoln, S. J., … Farrer, M. J. (2011). VPS35 mutations in parkinson disease. *American Journal of Human Genetics*, *89*(1), 162–167.

Wakabayashi, K., Hayashi, S., Yoshimoto, M., Kudo, H., & Takahashi, H. (2000). NACP/alpha-synuclein-positive filamentous inclusions in astrocytes and oligodendrocytes of Parkinson's disease brains. *Acta Neuropathologica*, *99*(1), 14–20.

Wang, L., Das, U., Scott, D. A., Tang, Y., McLean, P. J., & Roy, S. (2014). α-Synuclein multimers cluster synaptic vesicles and attenuate recycling. *Current Biology*, *24*(19),

2319–2326.

Wang, X., Yan, M. H., Fujioka, H., Liu, J., Wilson-delfosse, A., Chen, S. G., … Zhu, X. (2012). LRRK2 regulates mitochondrial dynamics and function through direct interaction with DLP1. *Human Molecular Genetics*, *21*(9), 1931–1944.

Weatherall, D. J. (2001). Phenotype-genotype relationships in monogenic disease: lessons from the thalassaemias. *Nature Reviews Genetics*, *2*(4), 245–255.

Webb, J. L., Ravikumar, B., Atkins, J., Skepper, J. N., & Rubinsztein, D. C. (2003). α-synuclein Is Degraded by Both Autophagy and the Proteasome. *Journal of Biological Chemistry*, *278*(27), 25009–25013.

Wilson, G. R., Sim, J. C. H., McLean, C., Giannandrea, M., Galea, C. A., Riseley, J. R., … Lockhart, P. J. (2014). Mutations in RAB39B cause X-linked intellectual disability and early-onset parkinson disease with α-synuclein pathology. *American Journal of Human Genetics*, *95*(6), 729–735.

Winslow, A. R., Chen, C. W., Corrochano, S., Acevedo-Arozena, A., Gordon, D. E., Peden, A. A., … Rubinsztein, D. C. (2010). α-Synuclein impairs macroautophagy: Implications for Parkinson's disease. *Journal of Cell Biology*, *190*(6), 1023–1037.

Winton, M. J., Igaz, L. M., Wong, M. M., Kwong, L. K., Trojanowski, J. Q., & Lee, V. M.-Y. (2008). Disturbance of nuclear and cytoplasmic TAR DNA-binding protein (TDP-43) induces disease-like redistribution, sequestration, and aggregate formation. *The Journal of Biological Chemistry*, *283*(19), 13302–9.

Ye, L., Yang, Y., Zhang, X., Cai, P., Li, R., Chen, D., … Zhang, H. (2015). The role of bFGF in the excessive activation of astrocytes is related to the inhibition of TLR4/NFκB signals. *International Journal of Molecular Sciences*, *17*(1).

Yi, J.-H., & Hazell, A. S. (2006). Excitotoxic mechanisms and the role of astrocytic glutamate transporters in traumatic brain injury. *Neurochemistry International*, *48*(5), 394–403.

Yuan, J., Liu, W., Zhu, H., Chen, Y., Zhang, X., Li, L., … Lin, J. (2017). Curcumin inhibits glial scar formation by suppressing astrocyte-induced inflammation and fibrosis in vitro and in vivo. *Brain Research*, *1655*, 90–103.

Zeltner, N., & Studer, L. (2015). Pluripotent stem cell-based disease modeling: Current hurdles and future promise. *Current Opinion in Cell Biology*, *37*, 102–110.

Zhang, Q. S., Heng, Y., Yuan, Y. H., & Chen, N. H. (2017). Pathological α-synuclein exacerbates the progression of Parkinson's disease through microglial activation. *Toxicology Letters*, *265*, 30–37.

Zhang, W. (2005). Aggregated -synuclein activates microglia: a process leading to disease progression in Parkinson's disease. *The FASEB Journal*, *19*(6), 533–542.

Zhu, Y. M., Gao, X., Ni, Y., Li, W., Kent, T. A., Qiao, S. G., … Zhang, H. L. (2017).

Sevoflurane postconditioning attenuates reactive astrogliosis and glial scar formation after ischemia–reperfusion brain injury. *Neuroscience*, *356*, 125–141.

Zimprich, A., Biskup, S., Leitner, P., Lichtner, P., Farrer, M., Lincoln, S., … Gasser, T. (2004). Mutations in LRRK2 cause autosomal-dominant parkinsonism with pleomorphic pathology. *Neuron*, *44*(4), 601–607.

Zis, P., Erro, R., Walton, C. C., Sauerbier, A., & Chaudhuri, K. R. (2015). The range and nature of non-motor symptoms in drug-naive Parkinson's disease patients: a state-of-the-art systematic review. *Npj Parkinson's Disease*, *1*(May), 8.

Zuo, L., & Motherwell, M. S. (2013). The impact of reactive oxygen species and genetic mitochondrial mutations in Parkinson's disease. *Gene*, *532*(1), 18–23.

8 APPENDICES

PUBLICATION TO WHICH I CONTRIBUTED DURING MY PH.D

1. Andreu Matamoros-Angles, Lucía Mayela Gayosso, Yvonne Richaud-Patin, **Angelique di Domenico**, *et al.* (2017) iPS Cell Cultures from a Gerstmann-Sträussler-Scheinker Patient with the Y218N PRNP Mutation Recapitulate tau Pathology. *Mol Neurobio.* DOI 10.1007/s12035-017-0506-6

Mol Neurobiol
DOI 10.1007/s12035-017-0506-6

iPS Cell Cultures from a Gerstmann-Sträussler-Scheinker Patient with the *Y218N PRNP* Mutation Recapitulate tau Pathology

Andreu Matamoros-Angles[1,2,3,4] · Lucía Mayela Gayosso[5,6,7] · Yvonne Richaud-Patin[8,9] · Angelique di Domenico[10,11] · Cristina Vergara[1,2,3,4,12] · Arnau Hervera[1,2,3,4] · Amaya Sousa[5] · Natalia Fernández-Borges[6,7,13] · Antonella Consiglio[10,11,14] · Rosalina Gavín[1,2,3,4] · Rakel López de Maturana[5] · Isidro Ferrer[3,4,11] · Adolfo López de Munain[15,16,17] · Ángel Raya[8,9,18] · Joaquín Castilla[6,7] · Rosario Sánchez-Pernaute[5,19] · José Antonio del Río[1,2,3,4]

Received: 7 December 2016 / Accepted: 21 March 2017

Abstract Gerstmann-Sträussler-Scheinker (GSS) syndrome is a fatal autosomal dominant neurodegenerative prionopathy clinically characterized by ataxia, spastic paraparesis, extrapyramidal signs and dementia. In some GSS familiar cases carrying point mutations in the *PRNP* gene, patients also showed comorbid tauopathy leading to mixed pathologies. In this study we developed an induced pluripotent stem (iPS) cell model derived from fibroblasts of a GSS patient harboring the

Andreu Matamoros-Angles, Lucía Mayela Gayosso, and Yvonne Richaud-Patin contribute equally to this study.

Electronic supplementary material The online version of this article (doi:10.1007/s12035-017-0506-6) contains supplementary material, which is available to authorized users.

✉ Ángel Raya
araya@cmrb.eu

✉ Joaquín Castilla
castilla@joaquincastilla.com

✉ Rosario Sánchez-Pernaute
rosario.sanchez.pernaute@juntadeandalucia.es

✉ José Antonio del Río
jadelrio@ibecbarcelona.eu; jadelrio@ub.edu

[1] Institute for Bioengineering of Catalonia (IBEC), Parc Científic de Barcelona, Baldiri Reixac 15-21, E-08028 Barcelona, Spain

[2] Department of Cell Biology, Physiology and Immunology, Universitat de Barcelona, Barcelona, Spain

[3] Centro de Investigación Biomédica en Red sobre Enfermedades Neurodegenerativas (CIBERNED), Barcelona, Spain

[4] Institute of Neuroscience, University of Barcelona, Barcelona, Spain

[5] Stem cells and neural repair laboratory, Fundación Inbiomed, San Sebastian, Gipuzkoa, Spain

[6] Proteomics unit (Prion lab), CIC bioGUNE, Parque tecnológico de Bizkaia, 48160 Derio, Bizkaia, Spain

[7] IKERBASQUE, Basque Foundation for Science, Bilbao, Bizkaia, Spain

[8] Centre de Medicina Regenerativa de Barcelona, c/ Dr. Aiguader 88, 08003 Barcelona, Spain

[9] Centro de Investigación Biomédica en Red en Bioingeniería, Biomateriales y Nanomedicina (CIBERBBN), Madrid, Spain

[10] Institut de Biomedicina de la Universitat de Barcelona, Barcelona, Spain

[11] Dept. Patologia i Terapèutica Experimental, Universitat de Barcelona, Barcelona, Spain

[12] Present address: Laboratory of Histology, Neuroanatomy and Neuropathology (CP 620), ULB Neuroscience Institute. Université Libre de Bruxelles, Faculty of Medicine, Brussels, Belgium

[13] Present address: CISA-INIA, Center for Animal Health Research, Madrid, Spain

[14] Department of Molecular and Translational Medicine, University of Brescia, Brescia, Italy

[15] Instituto Biodonostia-Hospital Universitario Donostia, San Sebastian, Gipuzkoa, Spain

[16] Neurosciences Department, University of the Basque Country UPV-EHU, Bilbao, Spain

[17] Centro de Investigación Biomédica en Red sobre Enfermedades Neurodegenerativas (CIBERNED), San Sebastian, Gipuzkoa, Spain

Published online: 02 May 2017

Y218N PRNP mutation, as well as an age-matched healthy control. This particular *PRNP* mutation is unique with very few described cases. One of the cases presented neurofibrillary degeneration with relevant Tau hyperphosphorylation. *Y218N* iPS-derived cultures showed relevant astrogliosis, increased phospho-Tau, altered microtubule-associated transport and cell death. However, they failed to generate proteinase K-resistant prion. In this study we set out to test, for the first time, whether iPS cell-derived neurons could be used to investigate the appearance of disease-related phenotypes (i.e, tauopathy) identified in the GSS patient.

Keywords Gerstmann-Sträussler-Scheinker · Induced pluripotent stem cells · Tau · Cellular prion protein

Introduction

Biomedical research on neurodegenerative diseases with low prevalence in humans relies on the possibility of analyzing brain samples only at very late stages of the disease. Thus, our view of the biochemical or molecular changes during the disease is partial. This drawback steadily increases with a faster neurodegenerative progression speed (e.g., in prionopathies [1] or rapid Alzheimer's disease [2]). This is also the case for most sporadic taupathies and in most cases of frontotemporal lobar degeneration (FTLD) displaying neurofibrillary degeneration [3, 4]. This limitation impedes the study of early onset changes in asymptomatic patients, making it impossible to investigate illness evolution, therefore hampering biochemical/molecular studies and drug discovery [5].

Gerstmann-Sträussler-Scheinker syndrome (GSS) is a rare autosomal dominant neurodegenerative prionopathy clinically characterized by a wide spectrum of manifestations including but not limited to ataxia, spastic paraparesis, extrapyramidal signs and dementia [6, 5]. Most GSS patients have the *P102L* mutation in the cellular prion protein (PrP^C) gene (*PRNP*) located in the short arm of chromosome 20 [5]. Cases of rapid progressive forms of GSS are rare [7] with an average duration after clinical diagnosis of 5–6 years (from 6 months to 13 years) [8, 5]. Histopathological examination of post-mortem GSS brains has revealed abnormal misfolded prion (PrP) aggregates in the form of unicentric and multicentric deposits in the cerebellum and cortical gray matter [5]. In addition, western blot analysis of aggregated PrP is distinguished by the presence of truncated protein fragments ranging between 6 and 10 KDa and a variable number of bands of higher molecular weight [9]. Parallel to this particular PrP deposition, pathological features characteristic of other neurodegenerative diseases such us parkinsonism or Alzheimer's disease have been observed in some GSS patients [5]. Indeed, an increase in hyperphosphorylated Tau is frequently observed in the pathological analysis of brains from GSS patients carrying *PRNP* mutations *P102L* [10], *P105L* [11], *A117V* [12], *V176G* [13], *F198S* [14, 15], *Q217R* [16, 15] and *Y218N* [17]. Although it has been shown that PrP^C with the *P102L* mutation display an increased binding to Tau [18], the role of these point mutations in the development of neurofibrillary degeneration is unknown. Nevertheless, in some *P102L* GSS cases with increased levels of p-Tau, the distribution of p-Tau tangles close to PrP deposits suggesting an active participation of PrP in the generation of p-Tau [10].

Due to the above-mentioned restrictions in this study we explored the usefulness of an induced pluripotent stem (iPS) cell model derived from somatic cells from a GSS patient. iPS cell technology is a tool for basic and translational research through generating in vitro models of disease-relevant cells reprogrammed directly from patients [19–21]. This approach has been shown to be particularly useful in the case of congenital or early-onset monogenic diseases [22] as well as other neurodegenerative diseases [23]. iPS cells have been generated from patients with Alzheimer's [24], Parkinson's [25, 26], Hungtinton's [27] diseases as well as FTLD [28], Amyotrophic Lateral Sclerosis (ALS) [29] and several others. However, there are no reports of iPS cell lines derived from patients with familial prionopathies.

In this study, we generated iPS cells from dermal fibroblasts of a family member of the *Y218N* GSS patient described by Alzualde and colleagues [17] and differentiated them into neurons using two previously published procedures [30, 31]. To date, very few individuals have been reported carrying this mutation [17, 32]. We were interested in this familiar since the *Y218N* patient displayed widespread neurofibrillary degeneration in the brain [17]. Results determined that although differentiated *Y218N* iPS cells were not able to spontaneously generate or propagate human prions, *Y218N*-derived cultures showed relevant astrogliosis and cell death. In addition, differentiated *Y218N*-derived neurons displayed high levels of p-Tau, thus recapitulating most of the neuropathological features reported in the patient [17].

Material and Methods

Case Patient The index case and the younger sister was examined at the Cognitive Disorders Unit at Donostia Hospital. The clinical report of the family and the *Y218N* patient can be seen in [17]. Dermal fibroblasts were obtained from the younger sister of the *Y218N* patient (54 years old in 2010) after having made complaints of poor concentration, apathy, emotional lability, and increasing difficulties in planning and

[18] Institució Catalana de Recerca i Estudis Avançats (ICREA), Barcelona, Spain

[19] Present address: Andalusian Initiative for Advanced Therapies, Junta de Andalusia, Seville, Spain

executing actions. She had previously been diagnosed with and treated for a depressive illness, and the neuropsychological examination revealed slight memory dysfunction in retrieval, language impairment followed by anomia with preserved verbal comprehension, and executive dysfunction. The Mini Mental State Examination (MMSE) score was 23/30. Magnetic resonance imaging showed slight frontotemporal atrophy and EEG analysis revealed intermittent frontotemporal delay. An additional EEG, 6 months later, showed slow background activity in the patient, with intermittent delta waves in the left hemisphere. 10 months after onset, she had language difficulties, with impairment in semantic knowledge, and MMSE score dropped to 13/30.

Generation of iPS Cells All experiments were performed under the guidelines and protocols of the Ethical Committee for Animal Experimentation (CEEA) of the University of Barcelona. All procedures adhered to internal and EU guidelines for research involving derivation of pluripotent cell lines. All subjects gave informed consent for the study using forms approved by the Ethical Committee on the Use of Human Subjects in Research at Hospital Donostia in San Sebastián, Spain. Generation of iPSC lines was approved by the Advisory Committee for Human Tissue and Cell Donation and Use, by the Commission on Guarantees concerning the Donation and Use of Human Tissues and Cells of the Carlos III Health Institute, Madrid, Spain (Ref: 589, 1/21/2015). All procedures were done in accordance with institutional guidelines and the cell lines have been (or will be) deposited at the Banco Nacional de Lineas Celulares (BNLC, ISCIII) following the Spanish legislation. Fibroblasts from a healthy individual and from the *Y218N* GSS patient were infected with retroviruses carrying human cDNA coding for *KLF4*, *SOX2*, and *OCT4*, with or without the addition of *c-MYC* as previously described [33]. Fibroblasts were maintained in DMEM (Sigma) supplemented with 10% FBS (Life Technologies) and 1% Pen/Strep solution (Life Technologies) before infection. After infection, fibroblasts were plated on irradiated human foreskin fibroblasts (HFF, ATCC) and maintained with hESC medium for 4–12 weeks until iPS cell colonies appeared. Several clones from each cell line were obtained and validated. *Y218N* patient (FH10) and parallel control (FHB1) iPS cell clones were analyzed in details (see below).

Characterization of iPS Cell Lines AP staining was performed using the Alkaline Phosphatase Blue Membrane Substrate Solution (Sigma). For immunocytochemistry, cells were grown on HFF feeder layers for 6–10 days and then fixed in 4% PFA for 10 min. After embryonic bodies (EB) formation, differentiation into the 3 germ layers was performed. For endoderm, EBs were plated on 6-well plates treated with Matrigel (BD Biosciences) for 1 h at room temperature, and maintained for 28 days with EB medium. The same procedure was used for mesoderm, but instead using EB medium with 0.5 mM of ascorbic acid. For ectoderm differentiation, EBs were maintained in suspension for 10 days with Neurobasal medium containing N2, B27 and FGF2 (N2B27 medium), prepared as previously described [26]. EBs were then plated on 6-well Matrigel-coated plates and maintained for 21 days with N2B27 medium without FGF supplementation. Differentiated cells were fixed in 4% PFA for 10 min. For nuclear DAPI staining (Invitrogen), 0.5 μg/ml was used. The slides were mounted with PVA:DABCO mounting medium. Images were acquired with an SP2 confocal system (Leica) and analyzed with ImageJ™ software. RT-qPCR analysis was performed as previously described [26]. All results were normalized to the average expression of Glyceraldehyde 3-phosphate dehydrogenase (*GAPDH*). Transcript-specific primers used are shown in Supplementary Table 1.

For karyotyping, iPS cells were grown on Matrigel and treated with colcemid (Life Technologies) at a final concentration of 20 ng/ml. Karyotyping analysis was carried out by Prenatal Genetics S.L. (Barcelona). For promoter methylation, testing reprogramming gene integration and sequencing to confirm that patient iPS cells were carrying mutations in *PRNP* gene, DNA was isolated using the QIAamp DNA Mini Kit (QIAGEN) following the manufacturer's instructions. Bisulfit conversion of the promoters was carried out using the Methylamp DNA modification kit (Epigentek). Five clones of each promoter for each cell line were analyzed by sequencing. The primers used for testing gene integration are shown in Supplementary Table 1.

iPS Cell Differentiation to Neural Cells In this study, two protocols were used to differentiate the iPS cells. In the first protocol, iPS cell colonies were mechanically passaged onto Matrigel-coated 6-well plates. 24 h later the mTeSR™ was replaced by DDM neural induction medium [34, 35] with the addition of the ALK inhibitor, SB431542 at 10 mM for 4 days (Tocris) and the BMP inhibitor, LDN-193189 at 100 nM (Miltenyi Biotech) for 12 days. Cells were propagated in this medium for 3 weeks. At about 24 days in vitro, cells were dissociated and plated onto wells coated with poly-L-lysine (33.3 mg/ml, BD) and laminin (3.3 mg/ml, BD), and the medium was changed to N2B27 medium. For immunofluorescence, neurons were dissociated with Accutase (Sigma) and replated on glass coverslips coated with poly-L-lysine and laminin. Characterization was done as previously described [36].

In the second procedure, spherical neural masses (SNMs) were obtained as previously described [37]. SNMs were fixed in 4% phosphate buffered paraformaldehyde (PFA) for 2 h and characterized by immunostaining. For nuclear DAPI staining (Invitrogen), 5 μg/ml was used. Mounting medium and imaging analysis were performed for in vitro differentiation testing. SNMs obtained from control and *Y218N* iPS cells, having

been maintained in suspension, were then plated on slide-flasks, 6-well plates, 35 mm ∅ plates or 10 mm ∅ plates all previously treated with Matrigel for 1 h at room temperature, and differentiated for 3, 6 or 9 weeks with N2B27 [26], without FGF supplementation to obtain neural cultures. The correct differentiation was assessed by immunostaining. Antibodies used are shown in Supplementary Table 2. For nuclear DAPI staining (Invitrogen), 0.5 μg/ml was used. The slides were mounted with Mowiol mounting medium.

RT-PCR Protocol Quantitative real time PCR was performed on total RNA extracted with mirVana's isolation kit (Ambion) from differentiating iPS cells. Purified RNAs were used to generate the corresponding cDNAs, which served as PCR templates for mRNA quantification. Quantitative RT-PCR assays were performed in duplicate on cDNA samples obtained from the retro-transcription reaction diluted 1:20 in 384-well optical plates (Kisker Biotech) using the ABI Prism 7900 HT Sequence Detection System (Applied Biosystems). The reactions were carried out using 20xTaqMan gene expression assays for genes and 2xTaqMan Universal PCR Master Mix (Applied Biosystems). The reactions were conducted using the following parameters: 50 °C for 2 min, 95 °C for 10 min, 40 cycles at 95 °C for 15 s and 60 °C for 1 min. The fold change was determined using the eq. $2^{-\Delta\Delta CT}$. Primers used in iPS cell differentiation experiments and Tau R3/R4 analysis can be seen in Supplementary Table 3.

Sample Collection and Proteinase K Treatment Samples of control and *Y218N* differentiating cultures were collected at several differentiation times and were homogenized in 10% lysis buffer (100 mM NaCl, 10 mM EDTA, 0.5% Nonidet P-40, 0.5% sodium deoxycholate, and 10 mM Tris, pH 7.5). Debris were removed with low-speed centrifugation at 3000×*g* for 10 min, and the supernatants were collected. To detect the presence of Proteinase K (PK)-resistant PrP in the supernatant, homogenates were digested with a final concentration of 10–50 μg/ml PK at 37 °C for 60 min prior to western blot analysis using 3F4 antibody against PrP^C. To evaluate the PK resistance of protein samples from the original *Y218N* patient [17], type I sporadic Creutzfeldt-Jakob disease (sCJD) and Type II sCJD brain homogenates were also processed in parallel. PK digestion was terminated by adding Laemmli buffer and heating the samples at 100 °C for 10 min.

Western Immunoblot Samples from different differentiation stages from iPS cells to neuronal cultures were processed for western blot, including human post-mortem samples and control cultured cells. The collected samples were homogenized in (10% wt/vol) of 50 mM Tris-HCl, pH 7.4/150 mM NaCl/0.5% Triton X-100/0.5% Nonidet P-40 and a mixture of proteinase inhibitors. After this, samples were centrifuged at 15,000 x g for 20 min at 4 °C. The resulting supernatant was normalized for protein content using BCA kit (Pierce). Cell extracts containing Laemmli buffer were boiled at 100 °C for 10 min, followed by 8–10% SDS electrophoresis, then electrotransferred to nitrocellulose membranes for 2 h at 4 °C. Membranes were then blocked with 5% not-fat milk in 0.1 M Tris-buffered saline (pH. 7.4) for 2 h and incubated overnight in 0.5% blocking solution containing primary antibodies. After incubation with peroxidase-tagged secondary antibodies (1:2000 diluted), membranes were revealed with ECL-plus chemiluminescence western blot kit (Amershan-Pharmacia Biotech). In our experiments, each nitrocellulose membrane was used to detect p-Tau (AT-8 and PHF1 antibodies), Actin, Tubulin as protein loading controls. A list of the antibodies used in these experiments can be seen in Supplementary Table 2.

Densitometry and Statistical Processing For quantification, developed films were scanned at 2400 × 2400 dpi (i800 MICROTEK high quality film scanner), and the densitometric analysis was performed using Quantity One Image Software Analysis (Biorad). Statistical analysis of the obtained data (RT-qPCR and Western blot) was performed using Bonferroni post hoc test (Multiple comparison test) using GraphPad Prism 6 (Mac OsX, Grahpad). Data are presented as mean ± standard error of the mean (S.E.M.). Differences between groups were considered statistically significant between **** $P < 0.001$, *** $P < 0.01$ and ** $P < 0.05$.

Immunohistochemistry Differentiating iPS cell cultures were fixed in 4% PFA at different days in culture and then permeabilized with 0.1% Triton X-100 (Sigma) in 0.1 M PBS. After fixation, and extensive rinsing with 0.1 M PBS, cultures were blocked with 10% FBS in 0.1 M PBS prior to incubation with primary antibodies (see Supplementary Table 2). After incubation with primary antibodies, cells were incubated with the pertinent Alexa Fluor-tagged secondary antibodies (Alexa-488 goat anti-mouse or Alexa-568 goat anti-rabbit) (Invitrogen-Life Technologies). Finally, cells were stained with 0.1 μM DAPI (Sigma) diluted in 0.1 M PBS, mounted on Mowiol, and viewed using an Olympus BX61 fluorescence microscope, Zeiss LSM or a Leica SP5 confocal microscopy.

Corrected Total Cell Fluorescence (CTCF) Measurement CTCF levels of p-Tau (red channel) and MAP2 (green channel) were measured in 150 (*Y218N*) and 165 (control) identified neurons after 21 days of differentiation using ImageJ™ software following published instructions http://sciencetechblog.com/2011/05/24/measuring-cell-fluorescence-using-imagej/. See also [38] for details. CTCF values were determined using the following formula. CTCF = Integrated Density – (Area of selected cell x Mean fluorescence of background readings). Statistical analysis of the obtained data was performed using Mann-Whitney U test

using GraphPad Prism 6 (Mac OsX, Grahpad). Differences between groups were considered statistically significant between **** $P < 0.001$.

Mitochondrial Movement Analysis in iPS Cell-Derived Neurons SNM-derived neurons were incubated after 21 days of differentiation with MitoTracker (Molecular Probes) and filmed using a Leica TCS SP2 confocal microscope (Leica) equipped with a 63× immersion oil objective. Time-lapse series of image stacks composed of 10 images (512 × 512 pixels) were taken every 3 s over 10 min. Movies were generated at 10 frames per second. Forty-two axons were registered and analyzed in each group recorded. In all cases, a mitochondrion was considered motile when it moved more than 0.5 μm during 1 min of recording. Distances and speeds of retrograde and anterograde transport were measured, and no tracking pluging was used. ImageJ™ software was used to quantify mitochondrial movement. For each mitochondrion movement, the minimum displacement and the average over time were plotted. Statistical analysis of the obtained data was performed using Mann-Whitney U test using GraphPad Prism 6 (Mac OsX, Grahpad). Differences between groups were considered statistically significant between *** $P < 0.01$ and ** $P < 0.05$.

Infectivity Assay Brain homogenates (10% in sterile PBS) were made fresh the day of the infection. One aliquot was kept frozen at −80 °C to repeat the exposure 72 h after the first infection, as described [39]. Representative samples were taken to confirm the presence of PK-resistant PrP in the homogenates, following digestion with 50 μg/ml for scrapie (263 K) and Creutzfeldt-Jakob disease (CJD) brains and 12.5 μg/ml for the *Y218N* brain [40]. Control and *Y218N* forebrain neuronal cultures were infected at early (30–40) and middle (60–80) differentiation times. Neurons were replated 5–6 days before the experiment. The culture supernatant was replaced by fresh media containing 10% brain homogenate (day 1) and this was repeated 72 h later (day 3). Two days later, fresh medium (without inocula) was added without removing the supernatant. At day 10 post-inocula (dpi) the entire medium was replaced and the cells were washed several times with sterile PBS before adding fresh Neurobasal containing B27 and N2 supplements. Medium was replaced every other day for the first 2 weeks and then twice a week until cells were collected or fixed for analysis, ~2 months later. All experiments were performed in a Biosafety level 3 security laboratory.

Results

Generation and Characterization of *Y218N* GSS Patient-Specific iPS Cells Fibroblasts were reprogrammed at early passages (5–7) through the retroviral delivery of *SOX2*, *KLF4*, *OCT4*, and c-*MYC* to generate up to 5 independent iPS cell lines for each individual (Fig. 1). We selected clones displaying embryonic stem cell-like morphology and positive AP staining (Fig. 1a). 5 clones representing each individual were chosen to be thoroughly characterized and shown to be fully reprogrammed, as judged by demethylation of *OCT4* and *NANOG* promoters (Fig. 1b), the silencing of the reprogramming transgenes (Fig. 1c), activation of endogenous pluripotency-associated factors (Fig. 1c), expression of pluripotency-associated transcription factors and surface markers (Fig. 1d), pluripotent differentiation ability in vitro and/or in vivo (Fig. 1f), and karyotype stability after more than 15 passages (Fig. 1e). Mutation analysis confirmed that iPS cells and their derivatives bore the mutation *Y218N* present in the patient fibroblasts (Fig. 1g).

Late Neuronal Maturation, Increased Reactive Astrogliosis and Absence of PrP Generation in *Y218N*-Derived iPS Cell Cultures Control and *Y218N*-derived iPS cells were differentiated into neural cells using two well-characterized procedures (see Methods). Neural induction was fast and efficient using both protocols (Fig. 2) and the cells sequentially expressed typical markers of neural progenitors, neuroblasts and mature neurons (Fig. 2b, f). In our first approach (Fig. 2a-d), taking into account morphology and marker expression, we established three differentiation stages: early (≈ 60 DIV), middle (≈ 60–120 DIV) and late (≈ 120–210 DIV) (Fig. 2a). Two weeks after neural induction, cultures were composed mainly of neural progenitors co-expressing SOX2 and NESTIN with a few differentiating neuroblasts (class III β-tubulin (TUJ1)-positive). By 4 weeks many neuroblasts and young neurons expressed PAX6 and the vast majority expressed Doublecortin (DCX) and Ubiquitin-protein ligase E3A (*UBE3A*) proteins (Fig. 2b). From the third month onwards, differentiating neurons expressed the mature post-mitotic neuronal marker NeuN (*RBFOX3*). In parallel and as also reported in vivo [41], PrP^{C} expression increased progressively over time during differentiation (Fig. 2c–d).

In the second protocol (Fig. 2e-h), control and *Y218N*-iPS cells were also differentiated to pure masses of neural precursors using a previously described protocol that involves the formation of EBs and the culture of neural precursor cells to form SNMs, whom can be expanded and differentiated into mature neurons after several weeks using neuronal induction medium (Fig. 2e). In these conditions, SNMs derived from control and *Y218N*-iPS cell lines homogeneously expressed neural progenitor markers such as PAX6, NESTIN, and SOX2, as well as the proliferation marker Ki67 (Fig. 2f). Furthermore, when iPS cell-derived SNMs were cultured in neuronal induction medium supplemented with N2 and B27, differentiation into mature neurons was evident within 3 to 5 weeks (Fig. 2f). After about 3 weeks in neuronal medium,

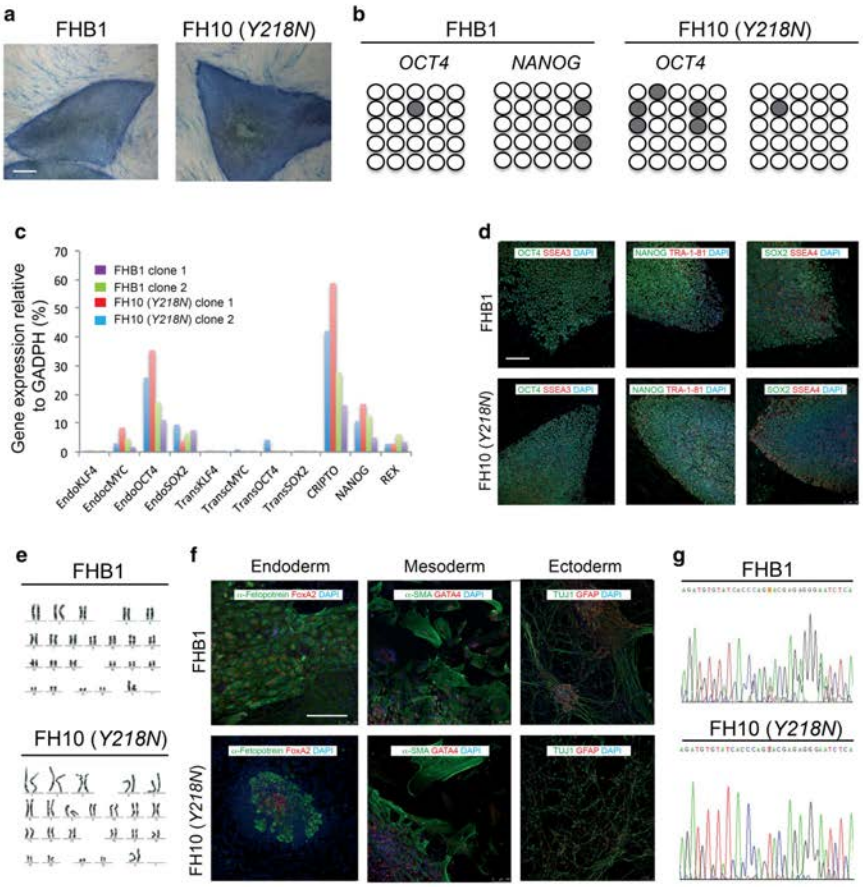

Fig. 1 Generation and characterization of iPS cells. (a) Control (cell line FHB1) and GSS-*Y218N*-iPS cell (cell line FH10) stained for AP activity. **(b)** Bisulphite genomic sequencing of the *OCT4* and *NANOG* promoters showing demethylation in FHB1 and FH10 (*Y218N*) cell lines. **(c)** RT-qPCR analyses of the expression levels of retroviral-derived reprogramming factors (transgenic) and endogenous expression levels (endogenous) of the indicated genes in FHB1 (two clones) and *Y218N*-iPS cells (cell line FH10, 2 clones). **(d)** Low fluorescence photomicrographs of representative colonies of FHB1 and FH10 (*Y218N*) stained positive for the pluripotency-associated markers OCT4, NANOG and SOX2 (green), SSEA3, TRA-1-81 and SSEA4 (red). **(e)** Normal karyotypes of FHB1 and FH10 (*Y218N*) at passage 20. **(f)** Immunofluorescence analyses of FHB1 and FH10 (*Y218N*) iPS cells differentiated in vitro show the potential to generate cell derivatives of all three primary germ cell layers including ectoderm (stained for TUJ1, green), endoderm (stained for α-fetoprotein, green, and FOXA2, red) and mesoderm (stained for smooth muscle actin, SMA, red). **(g)** Direct sequence of genomic DNA from Control (cell line FHB1) and GSS patient (FH10 (*Y218N*)) identifying the $PRNP^{Y218N}$ mutation. Scale bars in a, d and f = 50 μm

the cultures formed dense MAP2 and TUJ1-positive neuronal networks (Fig. 2f) in presence of astroglial cells (not shown). No mixed genotypes (GFAP + MAP2 or TUJ1 double labeled cells) were observed. As observed in the first approach, PrP^{C} was clearly present throughout neural differentiation (Fig. 2c,g, Supplementary Fig. 1). However, no detectable

PK-resistant PrP was observed in protein extracts treated with the enzyme in the *Y218N* and control-derived neurons generated with either protocol (Fig. 2d,h), in contrast to brain extracts from *Y218N* GSS or Type 1–2 CJD patients (Fig. 2h, Supplementary Fig. 2).

We next examined the transcriptional profile of neural cultures determined by RT-qPCR from early to late culture stages (Fig. 3a) and observed significant differences between control and *Y218N* cultures, particularly at the late stage (>120 days). While there were no differences in early progenitor markers such as *NES* and *SOX2*, which showed a similar time-dependent downregulation in both genotypes, a few neuronal transcripts were lower in the *Y218N* cultures early on, like *MAP2* and *CALB*. At the late stage (>120 days), there was a robust increase in *GFAP* mRNA and a concomitant decrease in mature neuronal markers including *MAPT* and *VGLUT1* mRNAs in *Y218N* cultures compared to controls. Next, these mRNA changes were checked by immunohistochemistry and cell counts (Fig. 3b, d). Cell counts revealed that the relative percentage of DCX and GFAP expressing cells was not significantly different between control and *Y218N* cultures (data not shown). Thus, the transcriptional increase in *GFAP* expression most likely due to a greater expression in reactive astroglial cells (Fig. 3c). Indeed, detailed analysis of immunoreacted cells revealed high content of GFAP forming thick fascicles in hypertrophic reactive astroglial cells at the late stage of *Y218N* cultures (Fig. 3c). Lastly, nuclear staining analysis in differentiating cultures revealed increased chromatin condensation and apoptosis in the *Y218N* at the late stage (Fig. 3d).

Increased tau Phosphorylation in *Y218N*-Derived Neurons in Vitro As indicated above, clinical and histopathological examination of the GSS patient carrying the *Y218N PRNP* mutation displayed relevant neurofibrillary degeneration with p-Tau deposits in several brain regions [17]. Therefore, we explored putative changes in Tau expression and phosphorylation in differentiating cultures (Fig. 4, Supplementary Figs. 3 and 4). As indicated above, *MAP2* and *MAPT* mRNA levels decreased in *Y218N*-derived cultures compared to controls suggesting delayed neuronal differentiation (Fig. 3). This was corroborated analyzing the appearance of the two Tau-splicing forms (4R and 3R) in differentiated cultures (Fig. 4a). RT-qPCR analysis demonstrated a delayed appearance of the 4R Tau form compared to 3R Tau in *Y218N*-derived cultures (Fig. 4a). This was corroborated by the biochemical analysis of the acetylated form of Tau at lysine 280 (K280-(ac)) Tau during the differentiation (Fig. 4b, Supplementary Fig. 4). This acetylated form is associated with Tau 4R [42, 43]. K280-(ac) Tau levels were constant in control-derived cultures from 15 to 45 DIV. However, *Y218N* cultures showed increased levels of K280-(ac) Tau between 15 to 41 DIV, following changes of Tau 4R (Fig. 4b, Supplementary Fig. 4). In parallel, biochemical detection of p-Tau during differentiation demonstrated the increase in p-Tau (detected by AT8 and PHF1 antibodies) in *Y218N*-derived neurons compared to control without relevant changes in PrP^C protein levels (Fig. 4b,c, Supplementary Fig. 3).

Next, we developed a CTCF analysis of p-Tau in identified MAP2-positive neurons (Fig. 4d,e). First we counted the total number of MAP2 and p-Tau-positive neurons in *Y218N*- and control-derived cultures. As suggested above with RT-qPCR, the total number of MAP2 and p-Tau double-positive cells was lower in *Y218N*-derived cultures (Fig. 4d,e). In addition, the relative percentage of double-labeled p-Tau/MAP2 neurons was also higher in *Y218N*-derived neurons. Changes in p-Tau level in differentiated neurons were also corroborated by the CTCF analysis of p-Tau in double-labeled p-Tau/MAP2-immunoreactive neurons (Control: 1566 ± 214.4; *Y218N*: 4357 ± 422.1; mean ± S.E.M. $P < 0.0001$, Mann-Whitney U test). Indeed, the ratio of p-Tau/MAP2 fluorescence was higher in *Y218N*-derived neurons compared to control-derived neurons (Control: 0.27 ± 0.02; *Y218N*: 0.680 ± 0.02; mean ± S.E.M. $P < 0.0001$, Mann-Whitney $U = 2628$) (Fig. 4e,f). Unfortunately, electron microscopy analyses failed to identify neurofibrillary tangle formation in *Y218N* differentiated neurons (not shown). Similar biochemical observations were also made using the direct cortical differentiation protocol (Supplementary Fig. 5). In conclusion, cultures derived from *Y218N* mutant iPS cells recapitulated in vitro several pathological features of the GSS patient, such as reactive astrocytosis, cell death and Tau hyperphosphorylation.

Impaired Mitochondria Movement in *Y218N*-Derived Neurons The effects of Tau hyperphosphorylation in several epitopes on mitochondria movement have been demonstrated in Alzheimer's disease [44, 28]. We checked the minimum and the mean velocity of identified mitochondria (Fig. 5). Results showed a decrease in both measurements in *Y218N* cultures compared with control (0.052 ± 0.014 (control, $n = 111$) vs 0.014 ± 0.006 (*Y218N*; $n = 105$); mean ± S.E.M., Min. velocity in μm/s; $P = 0.0004$; Mann-Whitney U value =4688. 0.310 ± 0.038 (control, $n = 111$) vs 0.1302 ± 0.014 (*Y218N*; $n = 105$); Mean ± S.E.M. Mean velocity in μm/s; $P = 0.0484$; Mann-Whitney U value =4921) (Fig. 5b).

Infectivity Assays In order to examine susceptibility to prion infection, *Y218N*- and control-differentiated cultures were exposed for 10 days to brain homogenates prepared from a sporadic CJD and from a GSS *Y218N* brain (Fig. 6a,b). Western blot analyses of the cultures showed the presence of PK-resistant PrP forms but only up to 2 weeks after removal of

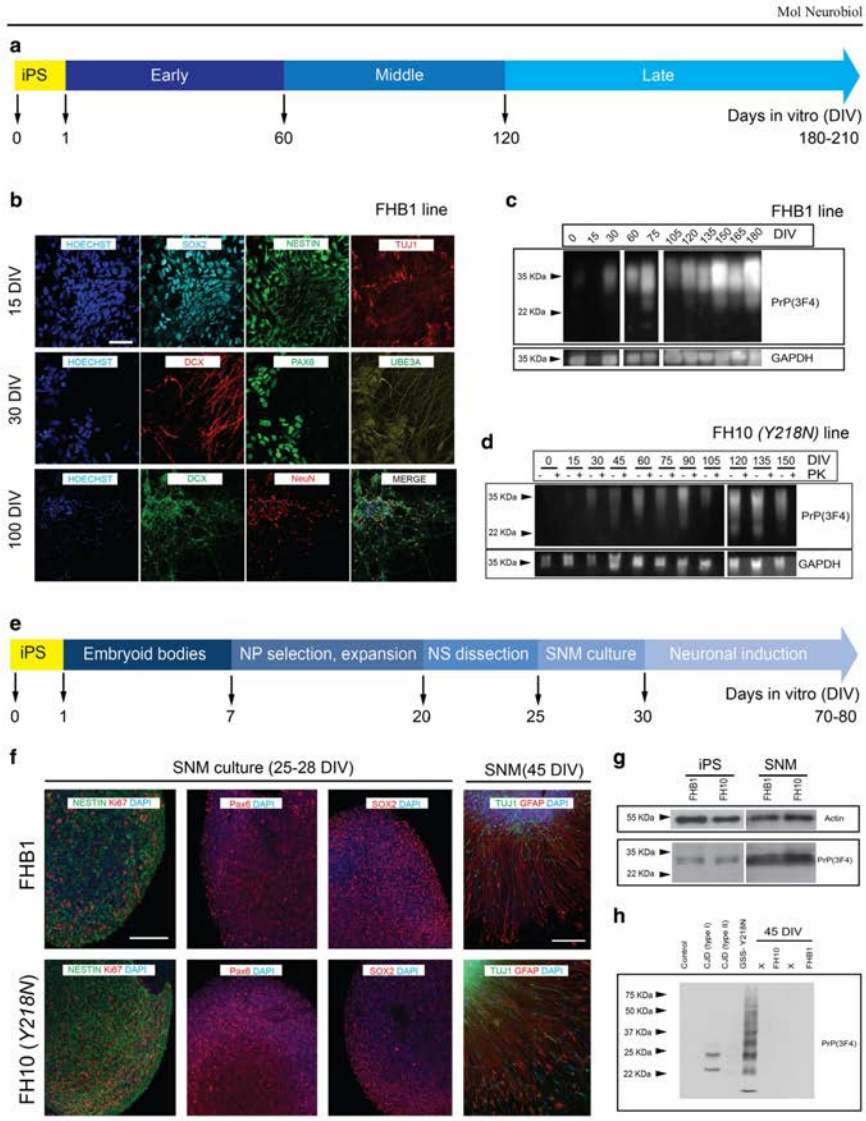

the inocula, indicating lack of prion infectivity (and propagation) in these conditions (Fig. 6c). A similar signal was observed in cultures infected with 263 K, a hamster scrapie prion strain which does not propagate to human cells (data not shown).

◀ **Fig. 2 Neural differentiation of FHB1 and FH10 (*Y218N*) iPS cells.** IPS cells from control (FHB1) and *Y218N* (FH10) GSS patient were differentiated using two procedures (**a** and **e**) (see Methods for details). **(b)** Low power photomicrographs of representative colonies of FHB1 and FH10 (*Y218N*) stained positive for SOX2, Nestin, DCX, TUJ1, PAX6, UBE3A antigens at different stages of maturation. **(c)** Western blot characterization of PrP^C expression in differentiating iPS cell cultures. **(d)** Example of the Western blot experiments illustrating the absence of PK-resistant PrP^C in FH10 (*Y218N*) cultures. **(e)** Low power photomicrographs of representative colonies of FHB1 and FH10 (*Y218N*) stained positive for Nestin, Ki67, SOX2, TUJ1, PAX6 and GFAP antigens. **(g)** Western blot characterization of PrP^C expression in iPS cells (passage 20) and SNMs (passage 3). **(h)** Western blots illustrating the absence of PK-resistant prion in FHB1 and FH10 (*Y218N*) in brain extracts from the GSS patient and two CJD (Type I and II) samples. Scale bars in b and f = 50 μm

Despite the absence of PK-resistant PrP in the cultures after two weeks, we observed some phenotypic changes that were more prominent in mutant neurons. In particular, we found a prominent redistribution of Tau signal with enhanced localization in the soma and proximal neurites in *Y218N* neurons exposed to either *GSS* or *CJD* inoculates was found (Fig. 6d,e).

Discussion

In the present study we have developed, for the first time, an iPS cell model of a familial human prionopathy. The donor GSS patient carrying the *Y218N PRNP* mutation showed relevant gliosis, cell death, massive deposits of PrP and neurofibrillary degeneration in different brain regions [17].

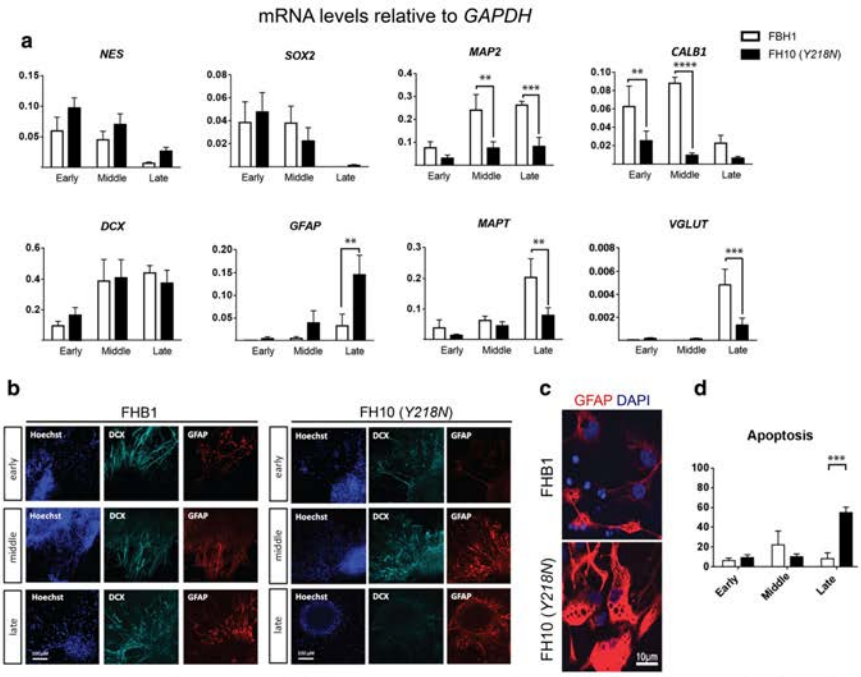

Fig. 3 Transcriptional profile of maturating iPS cell cultures. (a) Quantitative RT-PCR transcriptional profile of control and mutant cell cultures at the three maturation stages. Bars represent the mean ± S.E.M. of 2–4 time points for each stage from at least 2 independent differentiations. Data are presented as mean ± standard error of the mean (S.E.M.). Differences between groups were considered statistically significant **** $P < 0.001$, *** $P < 0.01$ and ** $P < 0.05$. Bonferroni post hoc test. **(b)** Representative immunofluorescence microphotographs of PrP^C, DCX and GFAP expression at the three differentiation stages. **(c)** Higher power image of GFAP positive cells at mid differentiation stage. **(d)**. Quantification of apoptotic nuclei (% over total Hoechst). *** $P < 0.01$, Bonferroni post hoc test. Scale bars in b = 100 μm and c = 10 μm

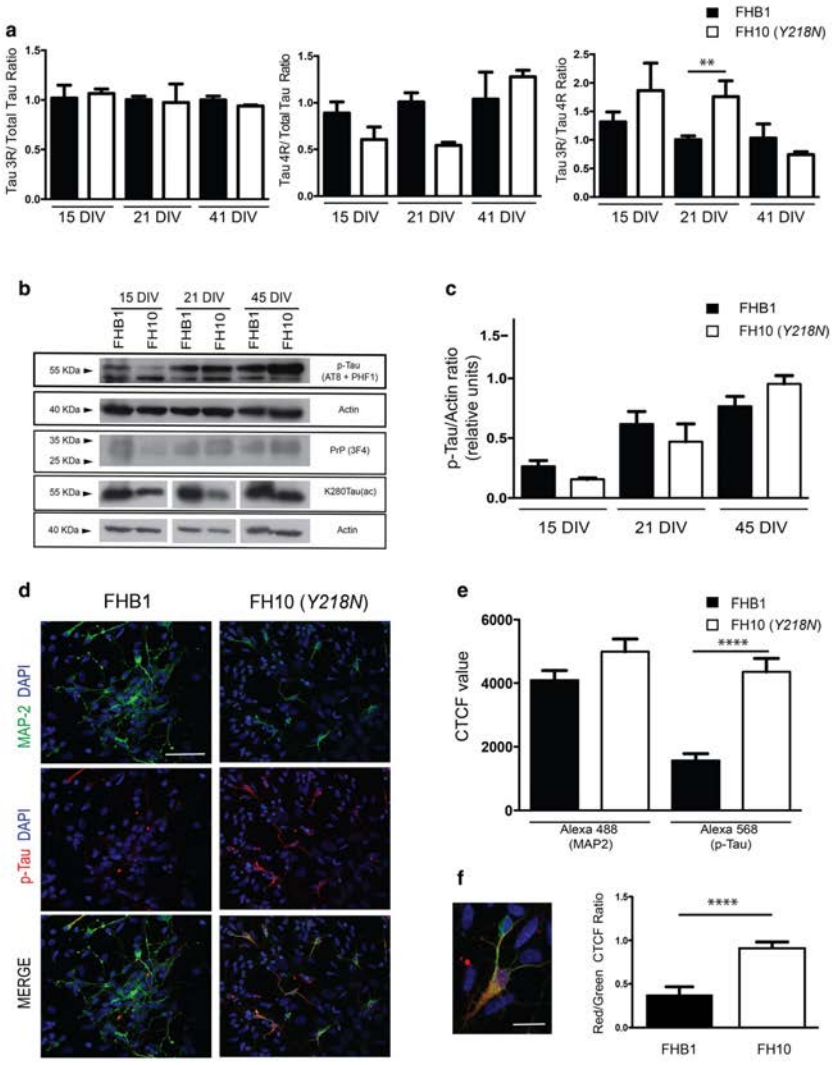
a
FHB1
FH10 (Y218N)
Tau 3R/ Total Tau Ratio
Tau 4R/ Total Tau Ratio
Tau 3R/ Tau 4R Ratio
**
15 DIV
21 DIV
41 DIV
b
15 DIV
21 DIV
45 DIV
FHB1
FH10
55 KDa
p-Tau (AT8 + PHF1)
40 KDa
Actin
35 KDa
25 KDa
PrP (3F4)
55 KDa
K280Tau(ac)
40 KDa
Actin
c
FHB1
FH10 (Y218N)
p-Tau/Actin ratio (relative units)
15 DIV
21 DIV
45 DIV
d
FHB1
FH10 (Y218N)
MAP-2 DAPI
p-Tau DAPI
MERGE
e
FHB1
FH10 (Y218N)
****
CTCF value
Alexa 488 (MAP2)
Alexa 568 (p-Tau)
f
****
Red/Green CTCF Ratio
FHB1
FH10

◀ **Fig. 4 Delayed *MAPT* maturation and increased p-Tau in *Y218N*-derived neurons. (a)** Histograms illustrating RT-qPCR results (mean ± S.E.M.) of Tau 3R/Total tau; Tau 4R/Total and Tau 3R/4R ratios in FHB1 and FH10 (Y218N) iPS cell cultures during differentiation at 15, 21 and 41 days in vitro. Asterisks in the right graph indicate $P < 0.05$, Bonferroni post hoc test; Mean Diff. -0.756; 95% confidence interval = −1.372 to - 0.1415). **(b)** Time course of p-Tau, PrP^C and K280Tau-(ac) expression in FHB1 and FH10 (*Y218N*) at 15, 21 and 45 DIV. Actin was used as control loading protein. **(c)** Graph of the densitometric values of p-Tau levels of (b). Plots show mean ± S.E.M. of three different experiments. Note the increase in p-Tau between *Y218N* and control cells. **(d)** High power photomicrographs illustrating MAP2 (green), p-Tau (red) in FHB1 and FH10 (*Y218N*) neural cultures. A high magnification of a labelled cell is showed in (**f**). **(e-f)** Quantification of CTCF values derived from experiments in (d). Plots show mean ± S.E.M. of four different experiments. Asterisks in (e) indicate statistical differences between groups and controls. **** $P < 0.001$; Mann-Whitney U test. Scale bars in d = 50 μm and f = 10 μm

Surprisingly, the presence of the *Y218N* mutation in other family member belies atypical parkinsonism phenotype instead of neurofibrillary degeneration [32]. Indeed, in parallel with the classical signs of GSS-associated degeneration, other clinical presentations, such as Alzheimer's-type, frontotemporal-like dementia, parkinsonism, and atypical psychiatric disorders, have all been reported (e.g., [45]). These different clinical manifestations have also been found in family members with the same *PRNP* mutation, attributed to the distinct abnormal isoforms of prion protein and polymorphisms at codon 129 [46, 47]. In fact, in this case the two GSS patients differ at the codon 129 polymorphism (129MV [32] and 129VV in [17]), which may contribute to clinical differences between cases.

We used two different well-characterized procedures to differentiate the iPS cells into neurons [34, 26]. The first was directed to obtaining forebrain cortical neurons [34] and the second one was directed to maintaining regulated developmental steps during neural development [26]. With both protocols we obtained similar results being able to determine that *Y218N*-derived cultures showed relevant GFAP reactivity, cell death, neuronal Tau redistribution, elevated p-Tau levels and changes in mitochondrial trafficking. Despite being unable to reproduce the spontaneous generation of PK-resistant forms or enabling prion propagation after inoculation in *Y218N*-iPS cell derived cultures, the differentiated neural cells recapitulated most of the pathological features observed in the GSS patient's brain. In this way, these *Y218N*-derived cultures could be used as an in vitro platform for neurodegenerative studies in familial prionopathies with the aim of characterizing the role of particular *PRNP* mutations in comorbid taupathies and cell death.

Unfortunately, *Y218N* cells did not generate PrP spontaneously and they were unable to propagate human prions (CJD and *Y218N* GSS prions) in vitro. This was disappointing but certainly not fully unexpected given that it has never been possible to propagate infectivity in primary neurons with human prions. Furthermore there are no studies of *Y218N* PrP propagation in vivo in contrast to other human mutations: i) *P102L* GSS human prion in *P101L* mice [48], ii) *A117V* GSS-derived human prion inoculum in *AV117 PRNP mice* [49] and iii) *P102L*, *A117V* or *F198S PRNP* mutations in bank voles [50].

Concerning the absence of endogenous prion generation in *Y218N*-derived neurons we might hypothesize, in a simplistic manner, that current in vitro times are not long enough for the endogenous generation of human PrP^{res}, considering the clinical onset and evolution of the GSS patient. However, we believe that the current scenario is not as simple, and that other, as yet unknown factors with key functions in protein misfolding and propagation may be absent from our cultures. In vitro prion propagation (of mostly mouse adapted strains) has been developed in neural and non-neural cell lines [51], primary neuronal cultures [52], cerebellar organotypic slices [53], and, with some controversy, in neurospheres (e.g., [54]). However, human prions have not been propagated in neuronal cultures to date. In fact, a single study of Ladogama et al. reported the transmission of human prions but using neuroblastoma cells [55]. In addition, the propagation of human strains was more successful when prions had been previously adapted to mice (e.g., M1000 [56]). Although endogenous expression levels could be relevant, we cannot rule out the participation of other non-neuronal cells (microglial cells) and inflammatory processes in protein misfolding and propagation [57] which did not fully develop in our iPS cell cultures, in contrast to other 3D organotypic approaches that could be assayed in future experiments [58].

In our study, the differentiation of *Y218N*-derived iPS cells was protracted. It is well known that appropriate temporal and transcriptional levels of *PRNP* are required for the correct differentiation of human embryonic stem cells [59] as well as other neural stem cells in vivo [60] and in vitro [61]. In fact, early attempts to ablate *PRNP* in mice using constitutive promoters and large *PRNP* mutations were not viable because *PRNP* expression starts around E7.5 in neural tissue [62]. Indeed, PrP^C is involved in several neural and non-neural developmental functions and its absence either delays or interferes with cell proliferation and maturation [63–65]. Although a clear explanation of the physiological impact of the *Y218N* mutation in these processes remains elusive, the mutation might induces aberrant folding of the protein [66], which may impair neuronal differentiation. In fact, in our experiments, mutant neurons showed decreased mRNA levels of *CALB*, *VGLUT1* and *MAP2* compared with control cells. In addition, *Y218N*-derived neurons showed very low numbers of Ca^{2+} transients analyzed by Fluo4-AM (data not shown).

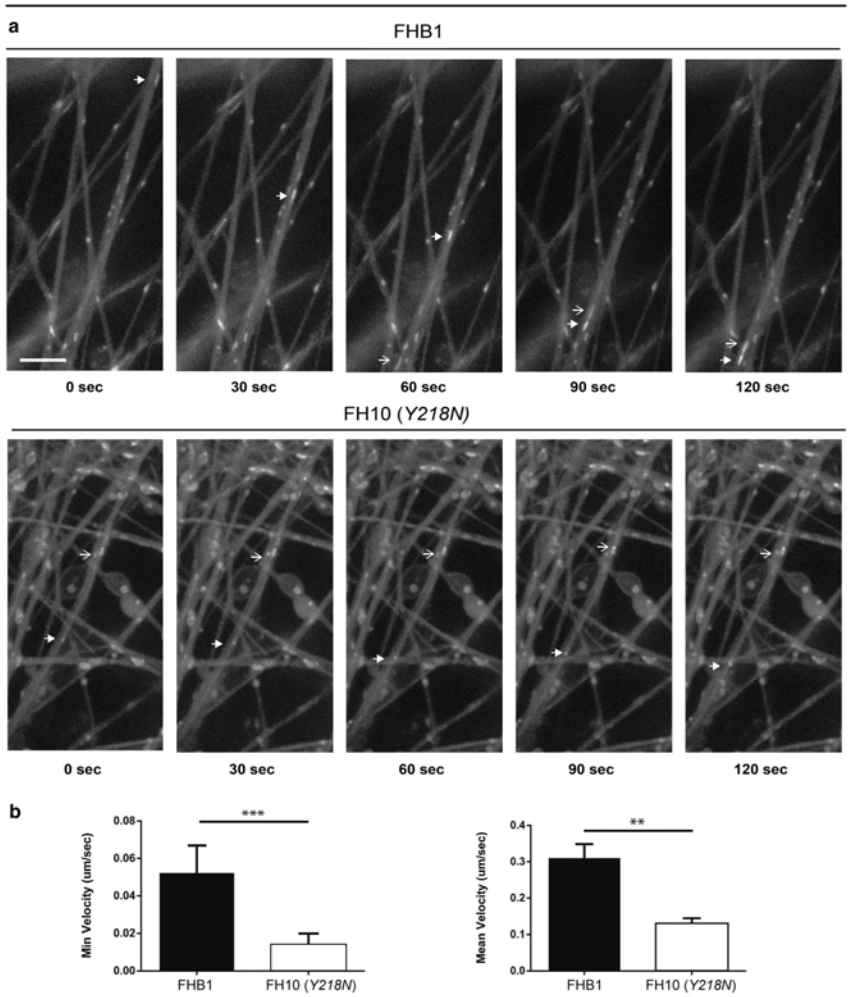

Fig. 5 FH10 *(Y218N)* cultures showed impaired mitochondria displacement. (a) Time-lapse fluorescence photomicrographs illustrating mitochondria movement in FHB1- (upper panels) and FH10 (*Y218N*)-(lower panels) derived neurons. The movement of two mitochondria (arrow and open arrow in (a) can be seen in the time lapse panels. **(b)** Plots illustrating the Minimum and Mean velocity values of tracked mitochondria in both types of cultures (see Methods for details). Notice the strong decreases in velocity in FH10 (*Y218N*)-derived cultures. Plots show mean ± S.E.M. of three different differentiation experiments. ***$P < 0.01$, ** $P < 0.05$. Mann Whitney *U* test. Scale bar: a = 2.5 μm

The deposition of hyperphosphorylated forms of Tau (p-Tau) has been described in familial and sporadic forms of prion diseases and in the brains of patients with variant CJD. Elevated levels of Tau (p-Tau and total Tau) have also been

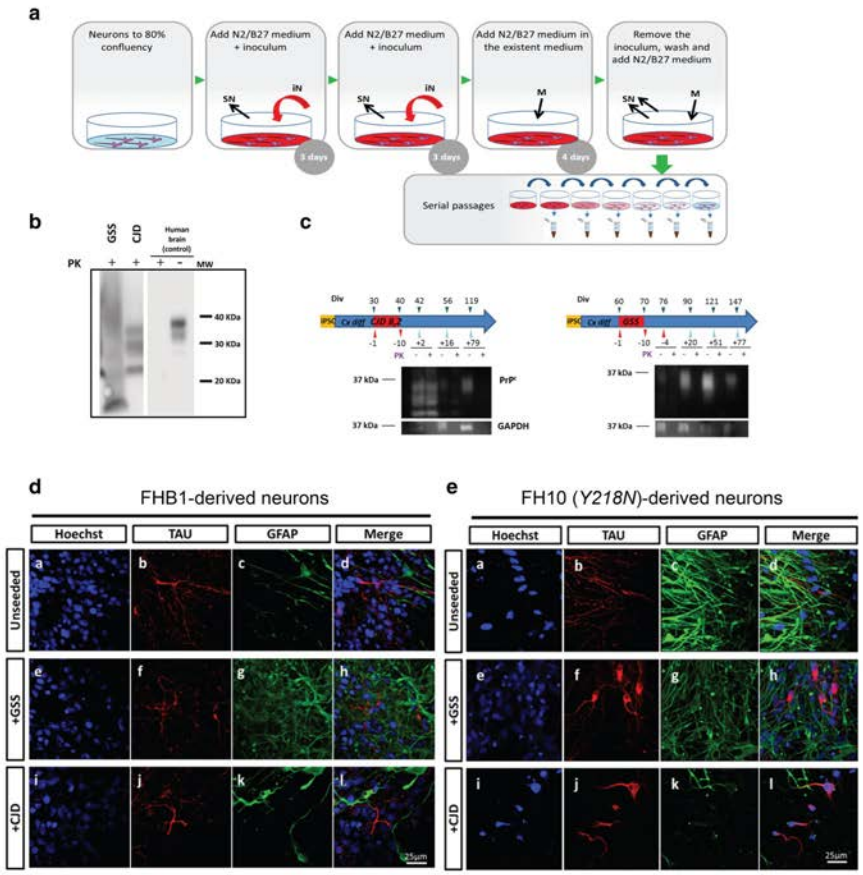

Fig. 6 Infectivity assay with brain inoculates. (**a**) Schematic representation of the inoculation protocol: infective brain homogenates were added at day 0 and day 3 and removed at day 10; cells were subsequently passaged several times to remove the inocula. (**b**) Inocula from the sources (10% of brain homogenates, see Methods for details) were processed to show PK-resistant PrP signal. *GSS*: human brain diagnosed of *Y218N*. *CJD*: human brain diagnosed of a sporadic CJD MM1. CJD samples were digested with 10–50 μg/ml of proteinase K (PK) and subjected to a standard biochemical analysis. GSS sample was treated as an atypical prion sample (see Methods). The samples were analyzed using the monoclonal antibody 3F4. MW: Molecular marker. (**c**) Representative examples of Western blot detection of PK-resistant PrP forms following inoculation with CJD and GSS brain samples. Note that PK-resistant PrP was only detected (when present) for the first 2 weeks after the infection. (**d**) Morphological analyses 2 months later revealed little effect of these inoculates in control neurons while mutant *Y218N* cultures (**e**) showed fewer neurons with marked cytoplasmic redistribution of Tau signal (**b**, **f**, **j**) and enhanced immunoreactivity for GFAP. Scale bars: 25 μm

reported in the cerebrospinal fluid (CSF) of patients with sporadic CJD [67]. In addition, rodents infected with BSE [68], 263 K [69] and human CJD [70] derived inocula also showed elevated levels of p-Tau. Indeed, neurons in encephalopathy-affected brain regions displaying PrP aggregates showed relevant Tau redistribution with increased perinuclear location. This perinuclear Tau reorganization was observed in *CJD*- and *GSS*-treated *Y218N*-derived neurons in this study. In this matter, it is

well known that aggregated prion peptides [71], as well as infectious prions [70], may modulate microtubule dynamics and stability, which may also in turn implicate Tau distribution. The increased presence and neuronal redistribution of Tau likely has a direct effect on the neuropathological process triggered by prion presence, because PrP^C binding to Tau is probably disrupted by the mutations (at least for P102L *PRNP* [18]). In fact, if we consider that *Y218N* might alter natural PrP^C functions associated with Tau, the cellular responses mediated by sCJD and GSS prions might be exacerbated in the presence of the *Y218N PRNP* mutation.

In conclusion, we report here the use of iPS cell-derived neurons to investigate the putative roles of the *Y218N PRNP* mutation in neural differentiation, Tau phosphorylation and cell death. This approach provides a powerful in vitro system for functional analysis of pathways regulating *PRNP* function in human cortical neurons, cellular mechanisms regulating tau phosphorylation in these models and for the identification and testing of candidate disease-modifying compounds.

Acknowledgements The authors thank Tom Yohannan for editorial advice and M. Segura-Feliu for technical assistance. We thank members of the Del Río, Sánchez-Pernaute, Castilla, Raya, Consiglio, López de Munain and Ferrer groups for stimulating discussions and ideas. We also thank to Lidia Bardia of the Advanced Confocal Microscopy service of the IRB-PCB for helping us with mitochondria tracking experiments. This research was supported by grants from the Spanish Ministry of Economy, Industry and Competitiveness (MINECO) (BFU2015-67777-R), the Spanish prion network (Prionet Spain, AGL2015-71764-REDT), the Generalitat de Catalunya (SGR2014-1218), CIBERNED (PI2014/02-4 (Rapid dementias) and PI2016/02 (MFDEND)), La Caixa Obra Social Foundation, La Marató de TV3 to J.A.D.R.. R.S.P was funded by the Joint Program in Neurodegenerative Diseases (DAMNDPATHS, AC14/00021). J.C. was funded by MINECO (AGL2015-65046-C2-1-R) and EiTB Maratoia (BioEF): BIO12/AL/004. A.R. was supported by MINECO (SAF2015-69706-R), Instituto de Salud Carlos III/FEDER (TerCel RD16/0011/0024, PIE14/00061), AGAUR (2014-SGR-1460), and Fundació La Marató de TV3 (201534-30) and CERCA Programme/Generalitat de Catalunya. I.F. was funded was supported by grants from CIBERNED (PI2014/02-4 Rapid dementias) and Fondo de Investigaciones Sanitarias (Instituto de Salud Carlos III), and co-funded by FEDER funds/European Regional Development Fund (ERDF) – a way to build Europe PIE14/00034 and PI14/00757. A.C. was also supported by BFU2013-49157-P and RETICTerCel grants from MINECO and the European Research Council (ERC) 2012-StG (311736- PD-HUMMODEL). A.L.M. was funded by grants from Fondo de Investigaciones Sanitarias (Instituto de Salud Carlos III (PI14/00436)), and the Joint Program in Neurodegenerative Diseases (DEMTEST). A.M-A. was supported by a fellowship from the Fundación Tatiana Pérez de Guzmán el Bueno. L.M.G. was supported by a CONACYT fellowship (CVU 357631, Mexico). The authors declare no conflicts of interest.

Author Contribution A.M-A.; L.M.G; Y.R-P. performed most of the experiments. Y.R-P.; A.D.D.; A.C.; A.R. generated the iPS cell lines and developed the second protocol of neuronal differentiation and their characterization with C.V.; R.G.; A.H.; I.F. and A.M-A.; A.S. L.M.G and R. S-P. developed the first protocol of iPS differentiation and their characterization with RL-M. L.M.G and N.F.B performed the infectivity assays and the analysis of results with J.C. and R. S-P. A.L.M.; A.R.; J.C.; R.S-P.; J.A.D.R. designed and supervised the experiments and wrote the manuscript. All authors reviewed the manuscript.

References

1. Ironside JW (1998) Prion diseases in man. J Pathol 186(3):227–234. doi:10.1002/(SICI)1096-9896(1998110)186:3<227::AID-PATH174>3.0.CO;2-3
2. Schmidt C, Haik S, Satoh K, Rabano A, Martinez-Martin P, Roeber S, Brandel JP, Calero-Lara M et al (2012) Rapidly progressive Alzheimer's disease: A multicenter update. J Alzheimers Dis 30(4):751–756. doi:10.3233/JAD-2012-120007
3. Hodges JR, Davies R, Xuereb J, Kril J, Halliday G (2003) Survival in frontotemporal dementia. Neurology 61(3):349–354
4. Roberson ED, Hesse JH, Rose KD, Slama H, Johnson JK, Yaffe K, Forman MS, Miller CA et al (2005) Frontotemporal dementia progresses to death faster than Alzheimer disease. Neurology 65(5):719–725. doi:10.1212/01.wnl.0000173837.82820.9f
5. Greenfield JG, Graham DI, Lantos PL (2002) Greenfield's neuropathology, 7th edn. Arnold, London, New York
6. Liberski PP, Ironside JW (2004) An outline of the neuropathology of transmissible spongiform encephalopathies (prion diseases). Folia Neuropathol 42(Suppl B):39–58
7. Iwasaki Y, Mori K, Ito M, Nokura K, Tatsumi S, Mimuro M, Kitamoto T, Yoshida M (2014) Gerstmann-Straeussler-Scheinker disease with P102L prion protein gene mutation presenting with rapidly progressive clinical course. Clin Neuropathol 33(5):344–353. doi:10.5414/NP300733
8. Collins S, McLean CA, Masters CL (2001) Gerstmann-Straussler-Scheinker syndrome,fatal familial insomnia, and kuru: A review of these less common human transmissible spongiform encephalopathies. J Clin Neurosci 8(5):387–397. doi:10.1054/jocn.2001.0919
9. Piccardo P, Seiler C, Dlouhy SR, Young K, Farlow MR, Prelli F, Frangione B, Bugiani O et al (1996) Proteinase-K-resistant prion protein isoforms in Gerstmann-Straussler-Scheinker disease (Indiana kindred). J Neuropathol Exp Neurol 55(11):1157–1163
10. Ishizawa K, Komori T, Shimazu T, Yamamoto T, Kitamoto T, Shimazu K, Hirose T (2002) Hyperphosphorylated tau deposition parallels prion protein burden in a case of Gerstmann-Straussler-Scheinker syndrome P102L mutation complicated with dementia. Acta Neuropathol 104(4):342–350. doi:10.1007/s00401-002-0547-3
11. Yamazaki M, Oyanagi K, Mori O, Kitamura S, Ohyama M, Terashi A, Kitamoto T, Katayama Y (1999) Variant Gerstmann-Straussler syndrome with the P105L prion gene mutation: An unusual case with nigral degeneration and widespread neurofibrillary tangles. Acta Neuropathol 98(5):506–511
12. Tranchant C, Sergeant N, Wattez A, Mohr M, Warter JM, Delacourte A (1997) Neurofibrillary tangles in Gerstmann-Straussler-Scheinker syndrome with the A117V prion gene mutation. J Neurol Neurosurg Psychiatry 63(2):240–246
13. Simpson M, Johanssen V, Boyd A, Klug G, Masters CL, Li QX, Pamphlett R, McLean C et al (2013) Unusual clinical and molecular-pathological profile of gerstmann-Straussler-Scheinker disease associated with a novel PRNP mutation (V176G). JAMA Neurol 70(9):1180–1185. doi:10.1001/jamaneurol.2013.165

14. Ghetti B, Tagliavini F, Giaccone G, Bugiani O, Frangione B, Farlow MR, Dlouhy SR (1994) Familial Gerstmann-Straussler-Scheinker disease with neurofibrillary tangles. Mol Neurobiol 8(1):41–48. doi:10.1007/BF02778006
15. Hsiao K, Dlouhy SR, Farlow MR, Cass C, Da Costa M, Conneally PM, Hodes ME, Ghetti B et al (1992) Mutant prion proteins in Gerstmann-Straussler-Scheinker disease with neurofibrillary tangles. Nat Genet 1(1):68–71. doi:10.1038/ng0492-68
16. Woulfe J, Kertesz A, Frohn I, Bauer S, George-Hyslop PS, Bergeron C (2005) Gerstmann-Straussler-Scheinker disease with the Q217R mutation mimicking frontotemporal dementia. Acta Neuropathol 110(3):317–319. doi:10.1007/s00401-005-1054-0
17. Alzualde A, Indakoetxea B, Ferrer I, Moreno F, Barandiaran M, Gorostidi A, Estanga A, Ruiz I et al (2010) A novel PRNP Y218N mutation in Gerstmann-Straussler-Scheinker disease with neurofibrillary degeneration. J Neuropathol Exp Neurol 69(8):789–800. doi:10.1097/NEN.0b013e3181e85737
18. Wang XF, Dong CF, Zhang J, Wan YZ, Li F, Huang YX, Han L, Shan B et al (2008) Human tau protein forms complex with PrP and some GSS- and fCJD-related PrP mutants possess stronger binding activities with tau in vitro. Mol Cell Biochem 310(1–2):49–55. doi:10.1007/s11010-007-9664-6
19. Takahashi K, Yamanaka S (2006) Induction of pluripotent stem cells from mouse embryonic and adult fibroblast cultures by defined factors. Cell 126(4):663–676. doi:10.1016/j.cell.2006.07.024
20. Takahashi K, Okita K, Nakagawa M, Yamanaka S (2007) Induction of pluripotent stem cells from fibroblast cultures. Nat Protoc 2(12):3081–3089. doi:10.1038/nprot.2007.418
21. Shi Y, Inoue H, Wu JC, Yamanaka S (2017) Induced pluripotent stem cell technology: A decade of progress. Nat Rev Drug Discov 16(2):115–130. doi:10.1038/nrd.2016.245
22. Rao M (2013) iPSC crowdsourcing: A model for obtaining large panels of stem cell lines for screening. Cell Stem Cell 13(4):389–391. doi:10.1016/j.stem.2013.09.005
23. Dolmetsch R, Geschwind DH (2011) The human brain in a dish: The promise of iPSC-derived neurons. Cell 145(6):831–834. doi:10.1016/j.cell.2011.05.034
24. Muratore CR, Rice HC, Srikanth P, Callahan DG, Shin T, Benjamin LN, Walsh DM, Selkoe DJ et al (2014) The familial Alzheimer's disease APPV717I mutation alters APP processing and tau expression in iPSC-derived neurons. Hum Mol Genet 23(13):3523–3536. doi:10.1093/hmg/ddu064
25. Schondorf DC, Aureli M, McAllister FE, Hindley CJ, Mayer F, Schmid B, Sardi SP, Valsecchi M et al (2014) iPSC-derived neurons from GBA1-associated Parkinson's disease patients show autophagic defects and impaired calcium homeostasis. Nat Commun 5:4028. doi:10.1038/ncomms5028
26. Sanchez-Danes A, Richaud-Patin Y, Carballo-Carbajal I, Jimenez-Delgado S, Caig C, Mora S, Di Guglielmo C, Ezquerra M et al (2012) Disease-specific phenotypes in dopamine neurons from human iPS-based models of genetic and sporadic Parkinson's disease. EMBO Mol Med 4(5):380–395. doi:10.1002/emmm.201200215
27. Jeon I, Lee N, Li JY, Park IH, Park KS, Moon J, Shim SH, Choi C et al (2012) Neuronal properties, in vivo effects, and pathology of a Huntington's disease patient-derived induced pluripotent stem cells. Stem Cells 30(9):2054–2062. doi:10.1002/stem.1135
28. Iovino M, Agathou S, Gonzalez-Rueda A, Del Castillo V-HM, Borroni B, Alberici A, Lynch T, O'Dowd S et al (2015) Early maturation and distinct tau pathology in induced pluripotent stem cell-derived neurons from patients with MAPT mutations. Brain 138(Pt 11):3345–3359. doi:10.1093/brain/awv222
29. Zhang K, Donnelly CJ, Haeusler AR, Grima JC, Machamer JB, Steinwald P, Daley EL, Miller SJ et al (2015) The C9orf72 repeat expansion disrupts nucleocytoplasmic transport. Nature 525(7567):56–61. doi:10.1038/nature14973
30. Zhang Y, Pak C, Han Y, Ahlenius H, Zhang Z, Chanda S, Marro S, Patzke C et al (2013) Rapid single-step induction of functional neurons from human pluripotent stem cells. Neuron 78(5):785–798. doi:10.1016/j.neuron.2013.05.029
31. Canals I, Soriano J, Orlandi JG, Torrent R, Richaud-Patin Y, Jimenez-Delgado S, Merlin S, Follenzi A et al (2015) Activity and high-order effective connectivity alterations in Sanfilippo C patient-specific neuronal networks. Stem Cell Reports 5(4):546–557. doi:10.1016/j.stemcr.2015.08.016
32. Ribosa-Nogue R, Pagonabarraga J, Gomez-Anson B, Granell-Moreno E, Sanchez-Valle R, Kulisevsky J (2015) Gerstmann-Straussler-Scheinker Disease Presenting with Atypical Parkinsonism, but Typical Magnetic Resonance Imaging Findings of Prion Disease. Movement Disorders:93–95.
33. Raya A, Rodriguez-Piza I, Guenechea G, Vassena R, Navarro S, Barrero MJ, Consiglio A, Castella M et al (2009) Disease-corrected haematopoietic progenitors from Fanconi anaemia induced pluripotent stem cells. Nature 460(7251):53–59. doi:10.1038/nature08129
34. Espuny-Camacho I, Michelsen KA, Gall D, Linaro D, Hasche A, Bonnefont J, Bali C, Orduz D et al (2013) Pyramidal neurons derived from human pluripotent stem cells integrate efficiently into mouse brain circuits in vivo. Neuron 77(3):440–456. doi:10.1016/j.neuron.2012.12.011
35. Gaspard N, Bouschet T, Herpoel A, Naeije G, van den Ameele J, Vanderhaeghen P (2009) Generation of cortical neurons from mouse embryonic stem cells. Nat Protoc 4(10):1454–1463. doi:10.1038/nprot.2009.157
36. Aguila JC, Blak A, van Arensbergen J, Sousa A, Vazquez N, Aduriz A, Gayosso M, Lopez Mato MP et al (2014) Selection based on FOXA2 expression is not sufficient to enrich for dopamine neurons from human pluripotent stem cells. Stem Cells Transl Med 3(9):1032–1042. doi:10.5966/sctm.2014-0011
37. Cho MS, Hwang DY, Kim DW (2008) Efficient derivation of functional dopaminergic neurons from human embryonic stem cells on a large scale. Nat Protoc 3(12):1888–1894. doi:10.1038/nprot.2008.188
38. McCloy RA, Rogers S, Caldon CE, Lorca T, Castro A, Burgess A (2014) Partial inhibition of Cdk1 in G 2 phase overrides the SAC and decouples mitotic events. Cell Cycle 13(9):1400–1412. doi:10.4161/cc.28401
39. Oelschlegel AM, Geissen M, Lenk M, Riebe R, Angermann M, Schatzl H, Groschup MH (2015) A bovine cell line that can be infected by natural sheep scrapie prions. PLoS One 10(1):e0117154. doi:10.1371/journal.pone.0117154
40. Pirisinu L, Nonno R, Esposito E, Benestad SL, Gambetti P, Agrimi U, Zou WQ (2013) Small ruminant nor98 prions share biochemical features with human gerstmann-straussler-scheinker disease and variably protease-sensitive prionopathy. PLoS One 8(6):e66405. doi:10.1371/journal.pone.0066405
41. Bendheim PE, Brown HR, Rudelli RD, Scala LJ, Goller NL, Wen GY, Kascsak RJ, Cashman NR et al (1992) Nearly ubiquitous tissue distribution of the scrapie agent precursor protein. Neurology 42(1):149–156
42. Grinberg LT, Wang X, Wang C, Sohn PD, Theofilas P, Sidhu M, Arevalo JB, Heinsen H et al (2013) Argyrophilic grain disease differs from other tauopathies by lacking tau acetylation. Acta Neuropathol 125(4):581–593. doi:10.1007/s00401-013-1080-2
43. Cohen TJ, Guo JL, Hurtado DE, Kwong LK, Mills IP, Trojanowski JQ, Lee VM (2011) The acetylation of tau inhibits its function and promotes pathological tau aggregation. Nat Commun 2:252. doi:10.1038/ncomms1255
44. Shahpasand K, Uemura I, Saito T, Asano T, Hata K, Shibata K, Toyoshima Y, Hasegawa M et al (2012) Regulation of mitochondrial transport and inter-microtubule spacing by tau phosphorylation at the sites hyperphosphorylated in Alzheimer's disease. J

Neurosci 32(7):2430–2441. doi:10.1523/JNEUROSCI.5927-11.2012

45. Webb TE, Poulter M, Beck J, Uphill J, Adamson G, Campbell T, Linehan J, Powell C et al (2008) Phenotypic heterogeneity and genetic modification of P102L inherited prion disease in an international series. Brain 131(Pt 10):2632–2646. doi:10.1093/brain/awn202
46. Furukawa H, Doh-ura K, Kikuchi H, Tateishi J, Iwaki T (1998) A comparative study of abnormal prion protein isoforms between Gerstmann-Straussler-Scheinker syndrome and Creutzfeldt-Jakob disease. J Neurol Sci 158(1):71–75
47. Parchi P, Chen SG, Brown P, Zou W, Capellari S, Budka H, Hainfellner J, Reyes PF et al (1998) Different patterns of truncated prion protein fragments correlate with distinct phenotypes in P102L Gerstmann-Straussler-Scheinker disease. Proc Natl Acad Sci U S A 95(14):8322–8327
48. Asante EA, Grimshaw A, Smidak M, Jakubcova T, Tomlinson A, Jeelani A, Hamdan S, Powell C et al (2015) Transmission properties of human PrP 102L prions challenge the relevance of mouse models of GSS. PLoS Pathog 11(7):e1004953. doi:10.1371/journal.ppat.1004953
49. Asante EA, Linehan JM, Smidak M, Tomlinson A, Grimshaw A, Jeelani A, Jakubcova T, Hamdan S et al (2013) Inherited prion disease A117V is not simply a proteinopathy but produces prions transmissible to transgenic mice expressing homologous prion protein. PLoS Pathog 9(9):e1003643. doi:10.1371/journal.ppat.1003643
50. Pirisinu L, Di Bari MA, D'Agostino C, Marcon S, Riccardi G, Poleggi A, Cohen ML, Appleby BS et al (2016) Gerstmann-Straussler-Scheinker disease subtypes efficiently transmit in bank voles as genuine prion diseases. Scientific reports 6:20443. doi:10.1038/srep20443
51. Klohn PC, Stoltze L, Flechsig E, Enari M, Weissmann C (2003) A quantitative, highly sensitive cell-based infectivity assay for mouse scrapie prions. Proc Natl Acad Sci U S A 100(20):11666–11671. doi:10.1073/pnas.1834432100
52. Cronier S, Laude H, Peyrin JM (2004) Prions can infect primary cultured neurons and astrocytes and promote neuronal cell death. Proc Natl Acad Sci U S A 101(33):12271–12276. doi:10.1073/pnas.0402725101
53. Falsig J, Aguzzi A (2008) The prion organotypic slice culture assay–POSCA. Nat Protoc 3(4):555–562. doi:10.1038/nprot.2008.13
54. Giri RK, Young R, Pitstick R, DeArmond SJ, Prusiner SB, Carlson GA (2006) Prion infection of mouse neurospheres. Proc Natl Acad Sci U S A 103(10):3875–3880. doi:10.1073/pnas.0510902103
55. Ladogana A, Liu Q, Xi YG, Pocchiari M (1995) Proteinase-resistant protein in human neuroblastoma cells infected with brain material from Creutzfeldt-Jakob patient. Lancet 345(8949):594–595
56. Lewis V, Hill AF, Haigh CL, Klug GM, Masters CL, Lawson VA, Collins SJ (2009) Increased proportions of C1 truncated prion protein protect against cellular M1000 prion infection. J Neuropathol Exp Neurol 68(10):1125–1135. doi:10.1097/NEN.0b013e3181b96981
57. Heikenwalder M, Zeller N, Seeger H, Prinz M, Klohn PC, Schwarz P, Ruddle NH, Weissmann C et al (2005) Chronic lymphocytic inflammation specifies the organ tropism of prions. Science 307(5712):1107–1110. doi:10.1126/science.1106460
58. Falsig J, Julius C, Margalith I, Schwarz P, Heppner FL, Aguzzi A (2008) A versatile prion replication assay in organotypic brain slices. Nat Neurosci 11(1):109–117. doi:10.1038/nn2028
59. Lee YJ, Baskakov IV (2014) The cellular form of the prion protein guides the differentiation of human embryonic stem cells into neuron-, oligodendrocyte-, and astrocyte-committed lineages. Prion 8(3):266–275. doi:10.4161/pri.32079
60. Steele AD, Emsley JG, Ozdinler PH, Lindquist S, Macklis JD (2006) Prion protein (PrPc) positively regulates neural precursor proliferation during developmental and adult mammalian neurogenesis. Proc Natl Acad Sci U S A 103(9):3416–3421. doi:10.1073/pnas.0511290103
61. Santos TG, Silva IR, Costa-Silva B, Lepique AP, Martins VR, Lopes MH (2011) Enhanced neural progenitor/stem cells self-renewal via the interaction of stress-inducible protein 1 with the prion protein. Stem Cells 29(7):1126–1136. doi:10.1002/stem.664
62. Tremblay P, Bouzamondo-Bernstein E, Heinrich C, Prusiner SB, DeArmond SJ (2007) Developmental expression of PrP in the post-implantation embryo. Brain Res 1139:60–67. doi:10.1016/j.brainres.2006.12.055
63. Del Rio JA, Gavin R (2016) Functions of the cellular prion protein, the end of Moore's law, and Ockham's razor theory. Prion 10(1):25–40. doi:10.1080/19336896.2015.1126038
64. Linden R, Martins VR, Prado MA, Cammarota M, Izquierdo I, Brentani RR (2008) Physiology of the prion protein. Physiol Rev 88(2):673–728. doi:10.1152/physrev.00007.2007
65. Llorens F, Carulla P, Villa A, Torres JM, Fortes P, Ferrer I, del Rio JA (2013) PrP(C) regulates epidermal growth factor receptor function and cell shape dynamics in Neuro2a cells. J Neurochem 127(1):124–138. doi:10.1111/jnc.12283
66. Cheng CJ, Daggett V (2014) Different misfolding mechanisms converge on common conformational changes: Human prion protein pathogenic mutants Y218N and E196K. Prion 8(1):125–135
67. Otto M, Wiltfang J, Tumani H, Zerr I, Lantsch M, Kornhuber J, Weber T, Kretzschmar HA et al (1997) Elevated levels of tau-protein in cerebrospinal fluid of patients with Creutzfeldt-Jakob disease. Neurosci Lett 225(3):210–212
68. Bautista MJ, Gutierrez J, Salguero FJ, Fernandez de Marco MM, Romero-Trevejo JL, Gomez-Villamandos JC (2006) BSE infection in bovine PrP transgenic mice leads to hyperphosphorylation of tau-protein. Vet Microbiol 115(4):293–301. doi:10.1016/j.vetmic.2006.02.017
69. Wang GR, Shi S, Gao C, Zhang BY, Tian C, Dong CF, Zhou RM, Li XL et al (2010) Changes of tau profiles in brains of the hamsters infected with scrapie strains 263 K or 139 a possibly associated with the alteration of phosphate kinases. BMC Infect Dis 10:86. doi:10.1186/1471-2334-10-86
70. Lawson VA, Klemm HM, Welton JM, Masters CL, Crouch P, Cappai R, Ciccotosto GD (2011) Gene knockout of tau expression does not contribute to the pathogenesis of prion disease. J Neuropathol Exp Neurol 70(11):1036–1045. doi:10.1097/NEN.0b013e318235b471
71. Brown DR (2000) Altered toxicity of the prion protein peptide PrP106-126 carrying the ala(117)–>Val mutation. Biochem J 346(Pt 3):785–791

PUBLICATIONS RELATED TO MY PH.D PROJECT

1. **Angelique di Domenico**, Giulia Carola, Carles Calatayud, Juan Pablo Muñoz, Yvonne Richaud-Patin, Armida Faella, Jordi Soriano, Isidro Ferrer, Eduardo Tolosa, Antonio Zorzano, Ana Maria Cuervo, Angel Raya, Antonella Consiglio (2017) Patient-specific iPSC-derived astrocytes contribute to non-cell autonomous neurodegeneration during Parkinson's disease. *Cell Reports* (Submitted September 2017).

Cell Reports

Patient-specific iPSC-derived astrocytes contribute to non-cell autonomous neurodegeneration in Parkinson's disease

--Manuscript Draft--

Manuscript Number:	CELL-REPORTS-D-17-02953
Full Title:	Patient-specific iPSC-derived astrocytes contribute to non-cell autonomous neurodegeneration in Parkinson's disease
Article Type:	Research Article
Keywords:	iPSC, Parkinson's disease, non-cell autonomous, astrocytes, alpha-synuclein
Corresponding Author:	Antonella Consiglio Institute of Biomedicine of the University of Barcelona Barcelona, SPAIN
First Author:	Angelique di Domenico
Order of Authors:	Angelique di Domenico
	Giulia Carola
	Carles Calatayud
	Juan Pablo Muñoz
	Yvonne Richaud-Patin
	Armida Faella
	Jordi Soriano
	Isidro Ferrer
	Eduardo Tolosa
	Antonio Zorzano
	Ana Maria Cuervo
	Angel Raya
	Antonella Consiglio
Abstract:	Parkinson's disease (PD) is associated with the degeneration of ventral midbrain dopaminergic (vmDA) neurons and the accumulation of toxic alpha-synuclein. Numerous observational studies have suggested a non-cell autonomous contribution, in particular of astrocytes, during PD pathogenesis; however, such studies remain to be experimentally tested. Here, we generated astrocytes from iPSC-derived familial mutant LRRK2G2019S PD patients (LRRK2-PD), as well as healthy age matched individuals (WT). Upon co-culture, WT vmDA neurons co-cultured on top of PD astrocytes displayed morphological signs of neurodegeneration and abnormal, astrocyte-derived, α-synuclein accumulation. Conversely, the appearances of disease-related neurodegenerative phenotypes were partially prevented in LRRK2-PD vmDA neurons when co-cultured with WT astrocytes. PD astrocytes displayed phenotypes reminiscent of those observed in PD-iPSC-derived vmDA neurons including alterations in autophagy and a progressive accumulation of α-synuclein. Our findings unveil a crucial non-cell autonomous contribution of astrocytes during PD pathogenesis, and open the path to exploring novel therapeutic strategies.
Suggested Reviewers:	Kevin Eggan Harvard University eggan@mcb.harvard.edu
	Alysson Muotri University of California muotri@ucsb.edu
	Jeffrey Kordower

PATIENT-SPECIFIC IPSC-DERIVED ASTROCYTES CONTRIBUTE TO NON-CELL AUTONOMOUS NEURODEGENERATION IN PARKINSON'S DISEASE.

Angelique di Domenico[1,2], Giulia Carola[1,2], Carles Calatayud [1,2,3], Juan Pablo Muñoz[4], Yvonne Richaud-Patin[3], Armida Faella[1,2], Jordi Soriano[5], Isidro Ferrer[2,6], Eduardo Tolosa[6,7], Antonio Zorzano[4], Ana Maria Cuervo[8], Angel Raya[3,9,10*,] Antonella Consiglio[1,2,11†‡]

[1] Institute of Biomedicine of the University of Barcelona (IBUB), Carrer Baldiri Reixac 15-21, Barcelona 08028, Spain,
[2] Department of Pathology and Experimental Therapeutics, University of Barcelona, C/ Feixa Llarga s/n 08907 L'Hospitalet de Llobregat, Barcelona, Spain
[3] Center for Regenerative Medicine of Barcelona (CMRB), Carrer del Dr. Aiguader, 88, 08003 Barcelona, Spain.
[4] Institute for Research in Biomedicine (IRB), Carrer Baldiri Reixac 10, Barcelona 08028, Spain.
[5] Departament d'Estructura i Constituents de la Matèria, Universitat de Barcelona, 08028 Barcelona, Spain.
[6] Centre for Networked Biomedical Research on Neurodegenerative Diseases (CIBERNED) C/ Nicolás Cabrera 1, Campus de Cantoblanco, 28049 Madrid, Spain.
[7] Department of Neurology, Hospital Clínic de Barcelona, Institut d'Investigacions Biomèdiques August Pi i Sunyer (IDIBAPS), University of Barcelona (UB), 08036 Barcelona, Spain.
[8] Albert Einstein College of Medicine, 300 Morris Park Ave, Bronx, NY 10461, United States.
[9] Centre for Networked Biomedical Research on Bioengineering, Biomaterials and Nanomedicine (CIBER-BBN), 28029 Madrid, Spain.
[10] Institució Catalana de Recerca i Estudis Avançats (ICREA), 08010 Barcelona, Spain
[11] Department of Molecular and Translational Medicine, University of Brescia, Piazza del Mercato, 15, 25121 Brescia BS, Italy.

[*] Corresponding author to araya@cmrb.eu (A.R.)
[†] Corresponding author to consiglio@ub.edu (A.C.)
[‡] Lead contact

Summary

Parkinson's disease (PD) is associated with the degeneration of ventral midbrain dopaminergic (vmDA) neurons and the accumulation of toxic alpha-synuclein. Numerous observational studies have suggested a non-cell autonomous contribution, in particular of astrocytes, during PD pathogenesis; however, such studies remain to be experimentally tested. Here, we generated astrocytes from iPSC-derived familial mutant $LRRK2^{G2019S}$ PD patients (LRRK2-PD), as well as healthy age matched individuals (WT). Upon co-culture, WT vmDA neurons co-cultured on top of PD astrocytes displayed morphological signs of neurodegeneration and abnormal, astrocyte-derived, α-synuclein accumulation. Conversely, the appearances of disease-related neurodegenerative phenotypes were partially prevented in LRRK2-PD vmDA neurons when co-cultured with WT astrocytes. PD astrocytes displayed phenotypes reminiscent of those observed in PD-iPSC-derived vmDA neurons including alterations in autophagy and a progressive accumulation of α-synuclein. Our findings unveil a crucial non-cell autonomous contribution of astrocytes during PD pathogenesis, and open the path to exploring novel therapeutic strategies.

Keywords: iPSC, Parkinson's disease, non-cell autonomous, astrocytes, alpha-synuclein

Introduction

Parkinson´s disease (PD) is the most prevalent movement disorder and second most chronic neurodegenerative disease after Alzheimer´s disease affecting seven to 10 million people worldwide (Collaborators, 2015). The main motor symptoms observed in patients with PD include resting tremor, bradykinesia, postural instability, and severe muscle rigidity. PD is characterized by a significant loss of ventral midbrain dopaminergic neurons (vmDAn) in the substantia nigra pars compacta and consequent reduction of dopamine. The presence of intracellular protein aggregates of the toxic insoluble oligomeric form of α-synuclein (encoded by the *SNCA* gene), forming part of large structures, known as Lewy Bodies (Greenamyre & Hastings, 2004), in the surviving vmDAn as well as in both astrocytic and oligodendroglial cells, is a hallmark of PD. The number of inclusions in glial cells usually correlates with the severity of nigral neuronal loss, thus indicating that abnormal accumulation of α-synuclein in glial cells is a pathological feature of PD related to its progression (Wakabayashi et al., 2000). In addition, microglial activation and an increase in astroglia and lymphocyte infiltration also occur in PD (Glass et al., 2010).

Despite significant advances in the identification of genes and proteins involved in PD, there are still appreciable gaps in our understanding of the mechanisms underlying the chronic neurodegenerative process in this disease (Melrose et al., 2006; Dawson et al., 2010). Most PD cases are sporadic (85%), but familial mutations are accountable for 15% of patients (Lill, 2016). Mutations in the gene encoding leucine-riche repeat kinase 2 (*LRRK2*), causing an autosomal dominant form of PD, account for 5% of familial cases and 2% of sporadic cases (Gilks et al., 2005; Nichols et al., 2005). LRRK2 is a highly complex protein with both GTPase and kinase functions with multiple enzymatic domains. It has been reported to be involved in mitochondrial function, vesicle trafficking together with endocytosis, retromer complex modulation and autophagy (Cherra et al., 2013; Orenstein et al., 2013; Su et al., 2015). With its main roles still elusive, mutations affecting the protein kinase domain of LRRK2 (such as the most prevalent LRRK2^{G2019S} mutation) have been reported to significantly increase kinase activity (Covy & Giasson, 2009).

Correlation between mutant LRRK2 and several pathogenic mechanisms linked to PD progression have been reported, including alterations in autophagy and accumulation of α-synuclein. During PD pathogenesis, mutant LRRK2 was found to directly bind LAMP-2A, the receptor responsible for chaperone-mediated autophagy (CMA) normally used by both LRRK2 and α-synuclein for degradation (Orenstein et al., 2013). This binding blocks the proper functioning of the CMA translocation complex, resulting in defective CMA leading to the accumulation of α-synuclein and cell death. When the CMA translocation complex is blocked, the cell responds in producing more reactive lysosomal receptors, trying to compensate for the dysfunction. This lysosomal hyperactivity was also reported to affect macroautophagic functioning. When LRRK2 kinase activity was inhibited in human neuroglioma cells, macroautophagy was stimulated (Manzoni et al., 2013).

Induced pluripotent stem cells (iPSC), when generated from patients of genetic conditions, can be exploited to create genuinely human experimental models of human diseases(Zeltner & Studer, 2015). In the case of PD, previous studies by our groups and others have generated iPSC from patients of PD associated to *LRRK2* mutations, and described the appearance of disease-specific phenotypes in iPSC-derived neurons, including impaired

axonal outgrowth and deficient autophagic vacuoles clearance (Nguyen et al., 2011; Reinhardt et al., 2013; Sánchez-Danés et al., 2012). Moreover, DAn from LRRK2-mutant patient-specific iPSC displayed alterations in CMA that were, at least in part, responsible for the abnormal accumulation of α-synuclein observed in these cells, which predated any morphological signs of neurodegeneration (Orenstein et al., 2013).

Studies investigating PD pathogenesis have been mostly focused on the mechanisms underlying vmDAn degeneration and death. However, there is evidence of astrocytes up-taking and accumulating α-synuclein during PD through post-mortem analysis(Braak et al., 2007; Wakabayashi et al., 2000). Altered α-synuclein released by axon terminals in the surrounding synapses is taken up by astrocytes, supporting the hypothesis of the spread of α-synuclein through neuron-astrocyte interactions (Braak et al., 2007; H. J. Lee et al., 2010). Overexpression of mutant *SNCA* in primary astrocytes altered their normal functioning and impaired proper blood-brain barrier control, glutamate homeostasis, and eventually resulted in a significant loss of vmDAn (Gu et al., 2010). In a different study also overexpressing mutant α-synuclein in PD mice, astrocytes were found to have altered mitochondria and a reduced secretion of factors fundamental to neuronal survival (Schmidt et al., 2011). Furthermore, uptake of neuronal-derived or recombinant α-synuclein by both primary and human astrocytes were observed to result in impaired mitochondrial function (Braidy et al., 2013; H. J. Lee et al., 2010). These findings suggest that α-synuclein accumulation in astrocytes may be of great importance to the initiation of PD (reviewed in (Brück et al., 2016)). Nevertheless, the main roles of astrocytes during the progression and development of PD pathogenesis still remain elusive.

In the present studies, we generated patient-specific iPSC-derived astrocytes and vmDAn from PD patients with *LRRK2*^{G2019S} mutation, as well as from healthy individuals. We consistently generated a population of human vmDAn in vitro that expressed postmitotic dopaminergic markers and fired action potentials. Subsequently, we co-cultured healthy iPSC-derived vmDAn with iPSC-derived astrocytes expressing the mutated form of LRRK2 associated to PD. In our co-cultures, we detected a specific decrease in the number of vmDAn in the presence of LRRK2-mutated astrocytes, which correlated well with the abnormal accumulation of α-synuclein. Conversely, WT astrocytes were able to partially rescue disease-related phenotypes in LRRK2-PD neurons when co-cultured together, suggesting LRRK2-PD astrocytes are lacking neuroprotective functions found in the WT astrocytes. A more in-depth investigation revealed PD-related phenotypes, such as impaired autophagic components, as well as a progressive accumulation of α-synuclein in LRRK2-PD astrocytes, compared to healthy controls. Moreover, by treating the cells with an activator of CMA, we were able to prevent the α-synuclein accumulation. Together, this data represents a first direct indication that astrocytes play a role during PD pathogenesis and may have broad implications for future intervention in early stages of PD.

Results

Generation and characterization of iPSC-derived patient specific astrocytes

Using a previously published protocol (Serio et al., 2013), astrocyte-like cells were successfully differentiated from iPSC lines representing four independent individuals: two from PD patients carrying the *LRRK2*^{G2019S} mutation (SP12-iPSC and SP13-iPSC) and two healthy age-matched controls (Ctr-SP17 and Ctrl-SP09). All iPSC-derived astrocytes were fully characterized through immunocytochemistry (ICC) using the appropriate markers (**Fig.**

1A). Cells positively stained for astrocyte progenitor markers CD44 when at the progenitor level. Once reaching complete astrocyte identity and maturity, the cells were further characterized by positively staining for astrocyte maturity marker S100 calcium-binding protein β (S100β), as well as excitatory amino acid transporter 2 (EAAT2 also known as GLT1). Additional markers including general neuronal marker TUJ1, neuronal maturity marker MAP2, and oligodendrocyte marker NG2 were negatively stained. The vast majority (85-90%) of the cells expressed astrocytic marker glial fibrillary acidic protein (GFAP), indicating a highly pure population of iPSC-derived astrocytes (**Fig. 1C; Fig. S1**).

Quantitative RT- PCR was performed in parallel revealing mRNA expression of astrocyte endfeet marker aquaporin4 in both control and LRRK2-PD astrocytes (**Fig. 1B; Fig. S1**). These results were consistent for all PD and non-PD astrocytes. After the full characterization of LRRK2-PD and non-PD human astrocytes, differences between the control and PD astrocytes were investigated. We determined the functional maturation of the hiPSC-derived astrocytes using FLUO-4AM calcium indicator (**Fig. 1D, E; Fig. S1**). Ca2+ recordings from PD and non-PD astrocytes showed a heterogeneous pattern of calcium fluctuations under basal conditions, revealing functionality. Finally, control and LRRK2-PD astrocytes produced similar levels of ATP (**Fig. 1F; Fig. S1**), further supporting the successful generation of functionally equivalent astrocyte-like cells from both groups.

Generation of vmDA neurons and set up of neuron-astrocyte co-culture system

A newly devised co-culture system was created (**Fig. 2A**) to evaluate glial contribution during PD. Neurons were generated using a combination of two previously published protocols and fully characterized(Chambers et al., 2009; Kriks et al., 2011). After 80 days under differentiation conditions, the cells expressed neuronal markers such as MAP2, and vmDAn lineage markers tyrosine hydroxylase (TH), FOXA2, and G protein- activated K+ channel (GIRK2) (**Fig. S2**). Neuronal cultures typically comprised approximately of 30% TH positive neurons, and within that population, 30% were TH/FOXA2, and 60% were TH/GIRK double positive cells (**Fig. S2**). These neurons were determined functional through successful generation of Ca^{2+} fluctuation waves (**Fig. S2**). The co-culture system was efficacious and astrocytes were able to allow for the proper maturation of TH neurons and glutamate exchange through GLT1 expression (**Fig. 2B**), as well as promote neuronal synapse formation (**Fig. 2C**) and an overall healthy neuronal network comprised of MAP2 positive cells (**Fig. 2D**).

WT iPSC-derived vmDA neurons show morphological signs of neurodegeneration when co-cultured with LRRK2-PD astrocytes

We then examined the effects of astrocytes expressing mutated LRRK2 on the survival of WT iPSC-derived vmDA neurons upon co-culture (**Fig. 3A**). After 2 weeks of culture with PD astrocytes, WT vmDA neurons started to show some signs of aberrant morphology (**Fig. S3**). We detected a decrease of 50% of TH positive cells (**Fig. S3**) compared to ones cultured with WT astrocytes **Fig. S3**). After four weeks in co-culture, WT vmDAn on the top of WT astrocytes developed many arborizations comprised of several long smooth neurites forming complex networks (**Fig. 3B**). In contrast, WT neurons placed on LRRK2-PD astrocytes for 4-weeks rarely formed more than 2 neurites, some displaying overt signs of neurodegeneration (short/few arborizations and beaded-necklace neurites) (**Fig. 3C**), and

were overall lower in number (TH/DAPI) compared to when on healthy astrocytes (**Fig. 3H**). Upon performing Sholl analysis, when WT neurons were co-cultured on the top of WT astrocytes neurons averaged around 10 neurite intersections per neuron with a neurite length reaching 280 microns (**Fig. 3D; Fig. S3**). In contrast, when WT neurons were cultured with LRRK2-PD astrocytes, neurons barely reached two neurite intersections per neurons with a maximum neurite length of 100 microns (**Fig. 3D; Fig. S3**).

WT vmDAn when co-cultured on LRRK2-PD astrocytes were comprised of 35-fold more TH neurons with neurodegenerative phenotypes compared to when on WT astrocytes (**Fig. 3E**). Interestingly, this neurodegeneration was TH specific as MAP2/DAPI positive cell numbers were maintained at similar levels in both conditions. (**Fig. 3I; Fig. S3**). Viability tests of both WT and LRRK2-PD astrocytes at 2 and 4-weeks were performed revealing highly similar values, indicating that neurodegenerative signs displayed by WT vmDAn were not caused by the PD astrocytes dying (**Fig. 3M; Fig. S3**).

WT vmDA neurons accumulate α-synuclein when co-cultured with LRRK2-PD astrocytes

α-Synuclein was barely detectable in the cytoplasm of WT vmDAn when co-cultured with WT astrocytes (**Fig. 3F**). Apart from displaying morphological neurodegenerative phenotypes and a lack of complex neuronal networks, WT vmDAn were also found to accumulate α-synuclein when co-cultured with LRRK2-PD astrocytes after 4 weeks (**Fig. 3G**). Notably, while WT astrocytes had no or low levels of α-synuclein (**Fig. 3K**), PD astrocytes displayed high levels of α-synuclein when co-cultured with WT neurons (**Fig. 3L**). WT vmDAn positive for α-synuclein accumulation were 47% more when co-cultured on LRRK2-PD astrocytes compared to when on WT astrocytes (**Fig. 4J**). Around 100% of LRRK2-PD astrocytes expressed high levels of α-synuclein compared to co-cultures with WT astrocytes (**Fig. 4N**). In order to directly visualize whether or not α-synuclein was spread from the PD astrocyte to the WT neuron, α-synuclein-flag tagged astrocyte lines were newly generated and fully characterized (**Fig. 3O; Fig. S3**). Indeed, the tagged α-synuclein in the PD astrocytes was directly transferred to the WT neurons and accumulated (**Fig. 3P, Q**), which was not present when WT vmDAn were co-cultured with WT astrocytes. The presence of α-synuclein in WT iPSC-derived vmDAn cell body and major processes were confirmed by z-section of confocal imagining. In addition to co-culturing cells with direct glia-neuron contact, we also tested the effect of supplying WT neurons with medium conditioned by WT or PD astrocytes (**Fig. 3P**). α-synuclein was also accumulated in WT neurons cultured with PD astrocyte-conditioned medium (**Fig. S3**). The effect of astrocyte-conditioned medium on TH/DAPI number revealed a degenerative morphology and α-synuclein accumulation in 100% of TH neurons when cultured with PD astrocyte medium compared to WT astrocyte medium conditions (**Fig. S3**).

LRRK2-PD neurons restore arborized morphology when co-cultured with WT astrocytes

In order to test whether the neurodegeneration could be rescued or prevented by healthy astrocytes, we co-cultured vmDA neurons derived from patients carrying the G2019S mutation on the LRRK2 gene with both WT and LRRK2-PD astrocytes (**Fig. 4A**). LRRK2-PD neurons alone (data not shown) show signs of neurodegeneration as early as 50 days of differentiation and accumulate α-synuclein in the soma when cultured with medium without factors. These LRRK2-PD neurons alone barely reach the 80 day time-point when cultured without factors, however, in order to visualize a phenotype, the factors had to be removed. After a 4-week co-culture, LRRK2-PD neurons showed a recovered neurite number and

complex neurite arborization when co-cultured on WT astrocytes (**Fig. 4C**) as opposed to when cultured with LRRK2-PD astrocytes (**Fig. 4B**). Sholl analysis revealed the average LRRK2-PD neuron whilst on WT astrocyte harboring maximum five neurite intersections per neuron with a neurite length reaching 180 microns (**Fig. 4D**). Whereas LRRK2-PD neurons when co-cultured with LRRK2-PD astrocytes never reach more than two neurite intersections per neuron with a maximum neurite length of 100 microns (**Fig. 4D**). When comparing the rescued LRRK2-PD neuron neurite intersection number created by co-culturing with WT astrocytes, (average of five neurite intersections per neuron) with the condition of WT neuron on WT astrocyte (average of ten neurite intersections per neuron), there is still a large difference, however, the difference between LRRK2-PD neuron on WT astrocyte (average of five neurite intersections per neuron) compared to LRRK2-PD astrocyte (average of two neurite intersections per neuron) is statistically significant.

PD neurons have less accumulated alpha-synuclein when co-cultured with WT astrocytes

Levels of α-synuclein were also diminished in LRRK2-PD neurons when co-cultured with WT astrocytes compared to when co-cultured with LRRK2-PD astrocytes after 4 weeks (**Fig. 4E**). LRRK2-PD neurons on the top of WT astrocytes reach 25% TH/DAPI after two weeks in culture compared to when on LRRK2-PD astrocytes at 12% (**Fig. 4F**). After 4 weeks in culture LRRK2-PD neurons on the top of WT astrocytes increase to 45% TH/DAPI compared to when on LRRK2-PD astrocytes there is a decrease to 6% (**Fig. 4H**). Overall MAP2 positive cells (normalized to DAPI) are similar in number when LRRK2-PD neurons are co-cultured with WT and LRRK2-PD astrocytes, revealing the fluctuation in cell number is TH specific (**Fig. 4G**). Most WT astrocytes when co-cultured with LRRK2-PD neurons adopted a flat morphology with low levels of alpha-synuclein, however, a select few harbored a hypertrophic morphology with retracted processes which accumulated alpha-synuclein (**Fig. 4I**).

Dysfunctional chaperone mediated autophagy and progressive α-synuclein accumulation in LRRK2-PD astrocytes

Since LRRK2-PD astrocytes displayed higher levels of α-synuclein compared to controls, we next investigated possible differences in α-synuclein turnover in these cells. α-synuclein has previously shown to undergo degradation both by the ubiquitin/proteasome system and by autophagy (Cuervo et al., 2004; Webb et al., 2003), thereforeα-synuclein flux in the presence of lysosomal and proteasome inhibitors (Leupeptin 100μM and Lactacystin 5μM, respectively) was evaluated in control and LRRK2-PD astrocytes at 14 days (**Fig. 5F**). Treatment with the inhibitors revealed a 20% increase of α-synuclein after a 12-hour Leupeptin treatment ($p<0.05$), and 65% after 2-hour Lactacystin treatment ($p<0.01$) in WT cells, whereas α-synuclein levels remained unchanged upon addition of both inhibitors in the LRRK2-PD astrocytes (**Fig. 5G**). These findings suggest major alterations in α-synuclein proteostasis due to poor degradation by both proteasome and lysosomal systems p62 protein levels increased in controls after inhibitor treatment whereas in the LRRK2-PD it decreased (**Fig. S4**).

Degradation of α-synuclein in lysosomes occurs in large extent through chaperone-mediated autohagy (CMA)(Cuervo et al., 2004; Martinez-Vicente et al., 2008). To investigate possible changes in CMA in LRRK2-PD astrocytes, we first stained at 6 and 14 days for both α-

synuclein and LAMP2A, the receptor for CMA (**Fig. 5A**). The control astrocytes showed LAMP-2A in the perinuclear area (perinuclear lysosomal positioning occurs during CMA activation(Kiffin, 2004)) and low basal levels of α-synuclein at both 6 and 14 days. In contrast, LRRK2-PD astrocytes displayed LAMP-2A positive vesicles all around the cell body as early as 6 days, which continued to be present after 14 days. Moreover, higher α-synuclein levels were confirmed in LRRK2-PD iPSC-derived astrocytes after 14 days of culture, compared to control (**Fig. 5A; Fig. S4**). Interestingly, this accumulation was not present after 6 days of culture, suggesting progressive α-synuclein accumulation over the 14-day time-point. Co-localization analyses of α-synuclein with the LAMP-2A receptor revealed a positive co-localization that was higher in LRRK2-PD iPSC-derived astrocytes (**Fig. 5B; Fig. S4**). CMA substrates are usually rapidly internalized and degraded inside lysosomes, but we have previously described a similar persistent association of α-synuclein with LAMP-2A positive lysosomes in PD models due to blockage in α-synuclein translocation inside lysosomes(Orenstein et al., 2013). These findings suggest thus a similar CMA blockage in the LRRK2-PD astrocytes at the receptor level. Also supportive of reduced α-synuclein degradation, western blot analysis confirmed a higher monomeric protein level of α-synuclein in the LRRK2-PD mutant compared to controls ($p<0.01$, **Fig. 5C, D**). By using an antibody that detects specifically oligomeric α-synuclein, we were able to detect other pathogenic forms of α-synuclein in the LRRK2-PD astrocytes (**Fig. S6**), which were similar to those of PD post mortem brain.

CMA activity was monitored using a photoactivatable CMA reporter KFREQ-Dendra (Koga et al., 2011) in both control and LRRK2-PD astrocytes for 52 hours after photoactivation (**Fig. 5E**). KFREQ-Dendra is present in the cytosol (diffuse fluorescent pattern) but as it is delivered to lysosomes via CMA it changes to a fluorescent punctate pattern. The WT astrocytes displayed this puncta indicative of functional CMA, whereas the signal in the LRRK2-PD astrocytes remained diffused in the cytosol suggestive of an inactive CMA.

To investigate the contribution of the defect in CMA to the progressive accumulation of α-synuclein in the LRRK2-PD astrocytes, we next performed a knockdown of LAMP-2A using lentiviral-mediated shRNA targeting and silencing the LAMP-2A gene (shLAMP-2A) and in parallel an shRNA targeting the Luciferase gene (shLuc) as a control (**Fig. 5H**). The shLuc control astrocytes displayed an expected low level of α-synuclein, whereas after shLAMP-2A transduction, there was a highly significant 2.5-fold increase comparable to the levels observed in LRRK2-PD astrocytes ($p<0.001$) in α-synuclein puncta (**Fig. 5I, J**). Knockdown of LAMP-2A did not changed α-synuclein puncta levels in the LRRK2-PD astrocytes further suggesting defective CMA for α-synuclein in these cells.

Impaired macroautophagy in LRRK2-PD astrocytes

Cells often respond to blockage in CMA by upregulating other autophagic pathways such as macroautophagy(A. C. Massey et al., 2006; Schneider et al., 2015), however, altered macroautophagy has also been reported in the context of PD (Sánchez-Danés et al., 2012; Winslow et al., 2010). To investigate the status of macroautophagy, lysosomal marker LAMP1, autophagosome marker LC3, astrocyte marker GFAP and nuclear DAPI were used during ICC on WT and LRRK2-PD astrocytes at both 6- and 14 days (**Fig. 6A; Fig. S5**). In the controls, there was lysosomal LAMP1 staining in the perinuclear area and very few visible autophagasomes both at 6 and 14 days. In the LRRK2-PD astrocytes, as for LAMP-2A, LAMP1 positive vesicles loss the preferable perinuclear distribution and were found throughout the entire cell. In addition, there was a marked increase in autophagosome

number (LC3 positive vesicles) starting as early as 6 days that continued increasing throughout the 14-day time-point. Most of the accumulated autophagosomes in the LRRK2-PD astrocytes did not co-localize with the LAMP1 lysosomes (**Fig. 6B; Fig. S5**), suggesting that persistence of autophagosomes in these cells was due to their poor clearance by lysosomes.

In agreement with the fluorescence studies, basal LC3 II levels were found to be higher in LRRK2-PD astrocytes compared to controls (mean ± s.e.m, *t* test, * $p<0.05$) through WB analysis (**Fig. 6C**). LC3 flux (measured as the increase in LC3-II levels upon blockage of lysosomal proteolysis with Leupeptin (100μM) and NH4Cl (20mM)), was significantly reduced in the LRRK2-PD astrocytes compared to controls ($p<0.001$, **Fig. 6D, E**). Lastly, basal p62 levels were higher in the LRRK2-PD astrocytes compared to controls ($p<0.05$, **Fig. 6F, G**) and degradation of this macroautophagy receptor was also severely impaired in these cells (**Fig. S5**). Overall these findings suggest that severe alterations in both autophagic pathways, CMA and macroautophagy, contribute to the altered α-synuclein proteostasis observed in LRRK2-PD astrocytes.

Restoration of α-synuclein proteostasis in LRRK2-PD astrocytes

Intracellular accumulation of α-synuclein has been shown to contribute to cellular toxicity in PD and to further disrupt functioning of cellular proteostasis systems (reviewed in (Abeliovich & Gitler, 2016)). We next investigated whether α-synuclein accumulation in LRRK2-PD astrocytes could be ameliorated by enhancing lysosomal activity. LRRK2-PD astrocytes were treated with a novel CMA activator drug QX77 (derived from the original AR7 ref) with a concentration of 20μM for 5 days and levels of α-synuclein were analysed by immunofluorescence (**Fig. 7**). LAMP2A positive lysosomes, in LRRK2-PD astrocytes treated with the CMA activator ($p<0.001$, **Fig. 7C, E**) recovered the perinuclear distribution observed in control cells (**Fig. 7A**) compared to when not treated (**Fig. 7B),** suggesting re-activation of CMA in these cells. Consistent with higher CMA activity, QX77-treated cells had significantly lower α-synuclein content than untreated cells ($p<0.001$, **Fig. 7C, D**). These findings suggest that although multiple protein degradation pathways fail to efficiently degrade α-synuclein in LRRK2-PD cells, re-activation of one of these pathways, in our case CMA, is enough to restore normal α-synuclein proteostasis.

Discussion

The purpose of this study was to evaluate the possible pathological contributions of astrocytes during PD using patient-specific iPSC-derived cells recapitulating PD-related disease phenotypes. LRRK2-PD astrocytes from two patients carrying the GS2019S mutation on the LRRK2 gene, as well as two healthy control lines were successfully generated using a previously published protocol and fully characterized. In addition, vmDA neurons from WT patients were also generated to co-culture with the astrocytes.

Once having co-cultured healthy WT vmDAn on both WT and LRRK2-PD astrocytes, a clear affect was evident. When healthy WT neurons were co-cultured with PD astrocytes, they did not develop complex smooth arborizations as when on WT astrocytes, but rather shorter and fewer neurites, as well as a select number adopting neurodegenerative characteristics, such as beaded-necklace neurites, as well as short and few neurites (**Fig. 3**), which indicates a neurotoxic affect of the PD astrocytes on the WT neurons. In addition, overall TH cell number diminished when WT vmDA neurons were co-cultured on LRRK2-

PD astrocytes compared to on WT astrocytes at both 2- (**Fig. S3**) and 4-week time-points (**Fig. 3H**). When WT vmDA neurons were co-cultured with LRRK2-PD astrocytes they displayed a 35-fold increase of TH with a degenerative morphology and 45% increase of TH/α-synuclein double positive cells, compared to when cultured on WT astrocytes (**Fig. 3E**). The viability of both WT and LRRK2-PD astrocytes were similar, meaning that the degenerative effects on the neurons were not caused by a dying astrocyte (**Fig. 3M; Fig. S3**), however, most likely due to other toxic molecules, which have not yet been detected. This evidence supports the fact that there are factors that come from the LRRK2-PD astrocytes that affect neuronal differentiation and survival, and more importantly are targeting only the dopaminergic neuronal population (**Fig. 3I, Fig. S3**).

In addition to WT vmDA neurons harboring neurodegenerative phenotypes when co-cultured with LRRK2-PD astrocytes (**Fig. 3C**), α-synuclein accumulation was also evident (**Fig. 3G**). There was an overall increase in α-synuclein levels in the entire co-culture with the LRRK2-PD astrocytes compared to ones with WT astrocytes. After taking a closer look, we identified that LRRK2-PD astrocytes themselves also contained high levels of α-synuclein compared to WT astrocytes in the co-culture condition (**Fig. 3L**). After having developed astrocyte lines that have α-synuclein tagged with a flag (**Fig. 3O, Fig. S3**), we were able to demonstrate the direct transfer of α-synuclein from the PD α-synuclein Flag tagged astrocyte to the WT neuron during a 4-week co-culture (**Fig. 3P, Q**), which was not present in the WT neuron on WT astrocyte condition. This transfer of α-synuclein, which is known to be toxic to dopaminergic neurons during PD, is most likely a key factor inducing neurodegeneration in the WT neurons, thus confirming a main role for astrocytes during PD pathogenesis.

The fact that WT astrocytes are able to rescue the morphological phenotype of neurodegeneration and clearance of neuronal alpha-synuclein when co-cultured with LRRK2-PD vmDA neurons validates a neuroprotective role (**Fig. 4C**), which the LRRK2-PD astrocytes are lacking (**Fig. 4B**). An interesting observation was made when focusing on WT astrocytes in the co-culture LRRK2-PD neurons with WT astrocytes. The majority of WT astrocytes had an expected large and flat morphology with low GFAP signalling, however, a select few harboured a hypertrophic morphology with retracted processes (**Fig. 4I**). What is even more striking is the fact that these hypertrophic astrocytes accumulate high levels of alpha-synulcein, suggesting a neuroprotective affect via activation of the WT astrocyte. Further analysis should be made to evaluate the exact inflammatory molecules being released, if any, by the WT astrocytes to validate this activation as reactivity.

Considering our PD astrocytes come from patients who harbor the G2019S mutation on the LRRK2 gene, we investigated whether or not disease specific phenotypes related to the mutation, were present. The α-synuclein accumulation in our co-culture system lead us to believe there would be a disruption in the way α-synuclein is usually degraded in the PD astrocyte. Degradation of α-synuclein has been shown to occur by both proteasome and autophagic pathways, and conversely, high levels of α-synuclein have demonstrated to be toxic for both systems(Tanaka et al., 2001; Webb et al., 2003; Winslow et al., 2010). Here we found that degradation of α-synuclein both by proteasome and lysosomes was severely inhibited in LRRK2-PD astrocytes (**Fig. 5G**). We have previously described in neurons derived from Parkinson's disease patients that one of the early events in the dysfunction of the proteostasis systems in these cells is the disruption of CMA by mutant LRRK2 binding to the receptor for CMA, LAMP-2A, thus causing the accumulation of α-synuclein (Sánchez-Danés et al., 2012). Our studies demonstrate that CMA is also altered in LRRK2-

PD astrocytes as lysosomes lose their perinuclear location (typically associated to higher CMA activity) and they display lower levels of the artificial CMA substrate in lysosomes. As in the case of PD neurons, CMA disruption seems to be due to reduced lysosomal internalization of α-synuclein, that remains instead associated with the lysosomal surface (higher α-synuclein association with LAMP-2A positive vesicles) (**Fig. 5B**). The lack of an additive effect of LAMP-2A knock-down in α-synuclein levels in LRRK2-PD astrocytes confirmed that α-synuclein degradation by CMA in these cells was almost completely abolished.

It is likely that the increase in intracellular levels of α-synuclein due to its poor CMA degradation in LRRK2-PD astrocytes, may contribute to precipitate malfunctioning of other proteostasis mechanisms such as the proteasome and macroautophagy. In fact, we demonstrated that macroautophagy was also markedly impaired in these cells, by displaying higher basal levels of autophagosomes (LC3-II) and the autophagic cargo p62 (**Fig. 6A-C, Fig. S5**) and reduced autophagic flux (for LC3-II and p62) (**Fig 6D, E; Fig. S5**). The lower co-localization between the autophagosomal and lysosomal markers observed in LRRK2-PD astrocytes suggest that the reduced autophagic flux is, for the most part, due to a defect in autophagosome/lysosome fusion, similar to the one previously described in PD neurons (Winslow et al., 2010).

The systems that contribute to cellular and organelle proteostasis act in a coordinate manner in the cell, and numerous examples support that restoration of one of these systems has a positive effect in the functioning of the rest of the proteostasis network (Kaushik & Cuervo, 2015). Taking into consideration this coordinate functioning of the proteolytic systems and the fact that CMA disruption seems to occur early during the development of PD pathology, we attempted to restore normal α-synuclein proteostasis by enhancing CMA activity. Our findings in cells treated with the chemical activators of CMA suggest that upregulation of CMA is still possible in these cells and that this intervention is sufficient to return levels of α-synuclein close to those in control cells (**Fig. 7**). Reduced levels of α-synuclein in these cells may be due not only to its enhanced degradation by CMA, but in addition, considering the large contribution of the proteasome in the degradation of α-synuclein in control cells, it is possible that restoration of CMA activity and the subsequent reduction of α-synuclein levels, will also release the inhibitory effect of α-synuclein on the proteasome and macroautophagy, further contributing to restore intracellular protein and organelle homeostasis.

From this study we can confirm that astrocytes play a crucial role during Parkinson's disease. PD-specific phenotypes specifically related to dysfunctions in the pathways of protein degradation have been observed in LRRK2-PD astrocytes and not in WT astrocytes. Dysfunctional CMA, progressive α-synuclein accumulation and glia to neuron transfer found in our LRRK2-PD astrocytes are all aspects that can compromise neuronal survival during PD pathogenesis. It would be useful to test which other factors are being secreted or omitted by the LRRK2-PD astrocytes in future studies to evaluate exactly what is triggering this degeneration. iPSC technology allows for the proper recapitulation of patient-specific disease related phenotypes, which will aid in the discovery of new therapies.

Statistical Analysis. Statistical analyses of the obtained data was performed using two-tailed unequal variance Student *t*-tests (* $p<0.05$, ** $p<0.01$, *** $p<0.001$) and the mean and standard error of the mean were plotted using Microsoft Excel (Mac OsX).

Author Contributions. Conceptualization, A.C. and A.R.: Methodology, I.F. J.P.M., A.Z., A.M.C., and J.S.; Formal Analysis, A.D.; Investigation Y.R.P, A.D., G.C., C.C., and A.F.; Validation, A.C. and A.R.; Writing – Original draft, A.D.; Writing – Review & Editing, A.C. and A.R.; Visualization, A.D.; Resources, A.Z., A.M.C., J.S., A.C. and A.R.; Funding Acquisition, A.C.; Supervision, A.C.

Acknowledgments. The authors are indebted to the patients with PD who have participated in this study. The authors thank Chrysanthi Blithikioti for helping with some co-culture experiments and immunocytochemistry, Neus Bayó-Puxan for her advice on western blotting, Irene Fernandez for help with the high content microscopy analysis through FIJI, Jose Miquel Andres Vaquero (CMRB) for performing the Flow cytometry viability tests of the astrocytes and David Maynar for excellent artwork. We are grateful to the Advanced Fluorescence Microscopy Unit of the Institute of Biomedicine of the University of Barcelona (especially to Elena Rebollo Arredondo). Research from the authors' laboratories is supported by the European Research Council-ERC (2012-StG-311736-PD-HUMMODEL), the Spanish Ministry of Economy and Competitiveness-MINECO (SAF2015-69706-R and BFU2013-49157-P), Instituto de Salud Carlos III-ISCIII/FEDER (Red de Terapia Celular - TerCel RD16/0011/0024), AGAUR (2014-SGR-1460), and CERCA Programme / Generalitat de Catalunya. A.D. is supported by the PD-HUMMODEL European Research Council (ERC)-Ideas PhD fellowship. C.C. and G.C. are partially supported by pre-doctoral fellowships from the Spanish Ministry of Education-MEC (FPU12/03332) and Economy and Competitiveness-MINECO (BES-2014-069603), respectively. The authors declare that they have no competing interests.

References

Abbott, N. J., Rönnbäck, L., & Hansson, E. (2006). Astrocyte–endothelial interactions at the blood–brain barrier. *Nature Reviews Neuroscience*, *7*(1), 41–53.

Abeliovich, A., & Gitler, A. D. (2016). Defects in trafficking bridge Parkinson's disease pathology and genetics. *Nature*, *539*(7628), 207–216.

Ahmad, L., Zhang, S. Y., Casanova, J. L., & Sancho-Shimizu, V. (2016). Human TBK1: A Gatekeeper of Neuroinflammation. *Trends in Molecular Medicine*, *22*(6), 511–527.

Anderson, M. A., Burda, J. E., Ren, Y., Ao, Y., O'Shea, T. M., Kawaguchi, R., … Sofroniew, M. V. (2016). Astrocyte scar formation aids central nervous system axon regeneration. *Nature*, *0*(1), 1–20.

Beauquis, J., Pavía, P., Pomilio, C., Vinuesa, A., Podlutskaya, N., Galvan, V., & Saravia, F. (2013). Environmental enrichment prevents astroglial pathological changes in the hippocampus of APP transgenic mice, model of Alzheimer's disease. *Experimental Neurology*, *239*(1), 28–37.

Beauquis, J., Vinuesa, A., Pomilio, C., Pavía, P., Galván, V., & Saravia, F. (2014). Neuronal and glial alterations, increased anxiety, and cognitive impairment before hippocampal

amyloid deposition in PDAPP mice, model of Alzheimer's disease. *Hippocampus*, *24*(3), 257–269.

Becerra-Calixto, A., & Cardona-Gómez, G. P. (2017). The Role of Astrocytes in Neuroprotection after Brain Stroke: Potential in Cell Therapy. *Frontiers in Molecular Neuroscience*, *10*(April), 1–12.

Belmadani, A., Tran, P. B., Ren, D., & Miller, R. J. (2006). Chemokines regulate the migration of neural progenitors to sites of neuroinflammation. *The Journal of Neuroscience : The Official Journal of the Society for Neuroscience*, *26*(12), 3182–91.

Ben Haim, L., Carrillo-de Sauvage, M.-A., Ceyzériat, K., & Escartin, C. (2015). Elusive roles for reactive astrocytes in neurodegenerative diseases. *Frontiers in Cellular Neuroscience*, *9*(August), 278.

Béraud, D., & Maguire-Zeiss, K. A. (2012). Misfolded α-synuclein and toll-like receptors: therapeutic targets for Parkinson's disease. *Parkinsonism & Related Disorders*, *18*, S17–S20.

Berger M., J. R. . A. (2004). The blood brain barrier in HIV infection. *Front Biosci*, *9*, 2680–2685.

Bir, A., Sen, O., Anand, S., Khemka, V. K., Banerjee, P., Cappai, R., … Chakrabarti, S. (2015). Alpha-synuclein-induced mitochondrial dysfunction in isolated preparation and intact cells: Implications in the pathogenesis of Parkinson's disease. *Journal of Neurochemistry*, *131*(6), 868–877.

Bonifati, V., Rizzu, P., van Baren, M. J., Schaap, O., Breedveld, G. J., Krieger, E., … Heutink, P. (2003). Mutations in the DJ-1 gene associated with autosomal recessive early-onset parkinsonism. *Science (New York, N.Y.)*, *299*(5604), 256–259.

Booth, H. D. E., Hirst, W. D., & Wade-Martins, R. (2017). The Role of Astrocyte Dysfunction in Parkinson's Disease Pathogenesis. *Trends in Neurosciences*, *40*(6), 358–370.

Braak, H., & Del Tredici, K. (2008). Invited Article: Nervous system pathology in sporadic Parkinson disease. *Neurology*, *70*(20), 1916–1925.

Braak, H., Ghebremedhin, E., Rüb, U., Bratzke, H., & Del Tredici, K. (2004). Stages in the development of Parkinson's disease-related pathology. *Cell and Tissue Research*, *318*(1), 121–134.

Braak, H., Sastre, M., & Del Tredici, K. (2007). Development of α-synuclein immunoreactive astrocytes in the forebrain parallels stages of intraneuronal pathology in sporadic Parkinson's disease. *Acta Neuropathologica*, *114*(3), 231–241.

Braidy, N., Gai, W.-P., Xu, Y. H., Sachdev, P., Guillemin, G. J., Jiang, X.-M., … Chan, D. K. Y. (2013). Uptake and mitochondrial dysfunction of alpha-synuclein in human astrocytes, cortical neurons and fibroblasts. *Translational Neurodegeneration*, *2*(1),

20.

Broux, B., Gowing, E., & Prat, A. (2015). Glial regulation of the blood-brain barrier in health and disease. *Seminars in Immunopathology*, *37*(6), 577–590.

Brück, D., Wenning, G. K., Stefanova, N., & Fellner, L. (2016). Glia and alpha-synuclein in neurodegeneration: A complex interaction. *Neurobiology of Disease*, *85*, 262–274.

Cabezas, R., Avila, M. F., Torrente, D., El-bachá, R. S., Morales, L., Gonzalez, J., & Barreto, G. E. (2013). Astrocytes Role in Parkinson : A Double-Edged Sword. *"Neurodegenerative Diseases", Book, Chapter 20*.

Carbone, C., Costa, A., Provensi, G., Mannaioni, G., & Masi, A. (2017). The Hyperpolarization-Activated Current Determines Synaptic Excitability, Calcium Activity and Specific Viability of Substantia Nigra Dopaminergic Neurons. *Frontiers in Cellular Neuroscience*, *11*, 187.

Cerri, S., Siani, F., & Blandini, F. (2017). Investigational drugs in Phase I and Phase II for Levodopa-induced dyskinesias. *Expert Opinion on Investigational Drugs*, *26*(7), 777–791.

Chambers, S. M., Fasano, C. A., Papapetrou, E. P., Tomishima, M., Sadelain, M., & Studer, L. (2009). Highly efficient neural conversion of human ES and iPS cells by dual inhibition of SMAD signaling. *Nature Biotechnology*, *27*(3), 275–280.

Chandra, R., Hiniker, A., Kuo, Y.-M., Nussbaum, R. L., & Liddle, R. A. (2017). α - Synuclein in gut endocrine cells and its implications for Parkinson ' s disease. *JCI Insight*, *2*(12), e92295.

Chen, Y.-Z., Bennett, C. L., Huynh, H. M., Blair, I. P., Puls, I., Irobi, J., … Chance, P. F. (2004). DNA/RNA helicase gene mutations in a form of juvenile amyotrophic lateral sclerosis (ALS4). *American Journal of Human Genetics*, *74*(6), 1128–35.

Cherra, S. J., Steer, E., Gusdon, A. M., Kiselyov, K., & Chu, C. T. (2013). Mutant LRRK2 elicits calcium imbalance and depletion of dendritic mitochondria in neurons. *American Journal of Pathology*, *182*(2), 474–484.

Christopherson, K. S., Ullian, E. M., Stokes, C. C. A., Mullowney, C. E., Hell, J. W., Agah, A., … Barres, B. a. (2005). Thrombospondins are astrocyte-secreted proteins that promote CNS synaptogenesis. *Cell*, *120*(3), 421–433.

Cloud Lee, Y.-T., & Danny Hsu, S.-T. (2016). Familial Mutations and Post-translational Modifications of UCH-L1 in Parkinson's Disease and Neurodegenerative Disorders. *Curr Protein Pept Sci*.

Collaborators, G. B. of D. S. 2013. (2015). Europe PMC Funders Group Global , regional , and national incidence , prevalence , and years lived with disability for 301 acute and chronic diseases and injuries in 188 countries , 1990 – 2013 : a systematic analysis for the Global Burden of Disease Stud. *Lancet*, *386*(9995), 743–800.

Colombrita, C., Onesto, E., Megiorni, F., Pizzuti, A., Baralle, F. E., Buratti, E., … Ratti, A. (2012). TDP-43 and FUS RNA-binding proteins bind distinct sets of cytoplasmic messenger RNAs and differently regulate their post-transcriptional fate in motoneuron-like cells. *The Journal of Biological Chemistry*, 1–24.

Covy, J. P., & Giasson, B. I. (2009). Identification of compounds that inhibit the kinase activity of leucine-rich repeat kinase 2. *Biochemical and Biophysical Research Communications*, *378*(3), 473–477.

Crotti, A., Benner, C., Kerman, B. E., Gosselin, D., Lagier-Tourenne, C., Zuccato, C., … Glass, C. K. (2014). Mutant Huntingtin promotes autonomous microglia activation via myeloid lineage-determining factors. *Nature Neuroscience*, *17*(4), 513–521.

Cuervo, A. M., Stefanis, L., Fredenburg, R., Lansbury, P. T., & Sulzer, D. (2004). Impaired degradation of mutant alpha-synuclein by chaperone-mediated autophagy. *Science (New York, N.Y.)*, *305*(5688), 1292–5.

Davies, D. C. (2002). Blood-brain barrier breakdown in septic encephalopathy and brain tumours. *Journal of Anatomy*, *200*(6), 639–646.

Dawson, T. M., Ko, H. S., & Dawson, V. L. (2010). Genetic Animal Models of Parkinson's Disease. *Neuron*, *66*(5), 646–661.

Di Maio, R., Barrett, P. J., Hoffman, E. K., Barrett, C. W., Zharikov, A., Borah, A., … Greenamyre, J. T. (2016). Alpha-Synuclein binds to TOM20 and inhibits mitochondrial protein import in Parkinsons disease. *Science Translational Medicine*, *8*(342), 342ra78-342ra78.

Dias, V., Junn, E., & Mouradian, M. M. (2013). The Role of Oxidative Stress in Parkinson's Disease. *Journal of Parkinson's Disease*, *3*(4), 461–491.

Dragicevic, E., Schiemann, J., & Liss, B. (2015). Dopamine midbrain neurons in health and Parkinson's disease: Emerging roles of voltage-gated calcium channels and ATP-sensitive potassium channels. *Neuroscience*, *284*, 798–814.

Dringen, R., Brandmann, M., Hohnholt, M. C., & Blumrich, E. M. (2015). Glutathione-Dependent Detoxification Processes in Astrocytes. *Neurochemical Research*, *40*(12), 2570–2582.

Dryanovski, D. I., Guzman, J. N., Xie, Z., Galteri, D. J., Volpicelli-Daley, L. a, Lee, V. M.-Y., … Surmeier, D. J. (2013). Calcium entry and α-synuclein inclusions elevate dendritic mitochondrial oxidant stress in dopaminergic neurons. *The Journal of Neuroscience : The Official Journal of the Society for Neuroscience*, *33*(24), 10154–64.

Du, J.-J., & Chen, S.-D. (2017). Current Nondopaminergic Therapeutic Options for Motor Symptoms of Parkinson's Disease. *Chinese Medical Journal*, *130*(15), 1856.

Ebrahimi-Fakhari, D., Wahlster, L., & McLean, P. J. (2012). Protein degradation pathways in Parkinson's disease: Curse or blessing. *Acta Neuropathologica*, *124*(2), 153–172.

Farina, C., Aloisi, F., & Meinl, E. (2007). Astrocytes are active players in cerebral innate immunity. *Trends in Immunology*, *28*(3), 138–145.

Ferraiuolo, L. (2014). The non-cell-autonomous component of ALS: new in vitro models and future challenges. *Biochemical Society Transactions*, *42*(5).

Fonzo, A. D., Dekker, M. C. J., Montagna, P., Baruzzi, A., Yonova, E. H., Guedes, L. C., … Bonifati, V. (2009). FBXO7 mutations cause autosomal recessive, early-onset parkinsonian- pyramidal syndrome. *Neurology*, *72*(3), 240–245.

Geloso, M. C., Corvino, V., Marchese, E., Serrano, A., Michetti, F., & D'Ambrosi, N. (2017). The Dual Role of Microglia in ALS: Mechanisms and Therapeutic Approaches. *Frontiers in Aging Neuroscience*, *9*, 242.

Gilks, W. P., Abou-Sleiman, P. M., Gandhi, S., Jain, S., Singleton, A., Lees, A. J., … Wood, N. W. (2005). A common LRRK2 mutation in idiopathic Parkinson's disease. *Lancet*, *365*(9457), 415–6.

Glass, C. K., Saijo, K., Winner, B., Marchetto, M. C., & Gage, F. H. (2010). Mechanisms Underlying Inflammation in Neurodegeneration. *Cell*, *140*(6), 918–934.

Gordon, G. R. J., Mulligan, S. J., & MacVicar, B. A. (2007). Astrocyte control of the cerebrovasculature. *GLIA*, *55*(12), 1214–1221.

Greenamyre, J. T., & Hastings, T. G. (2004). Biomedicine. Parkinson's-divergent causes, convergent mechanisms. *Science (New York, N.Y.)*, *304*(5674), 1120–1122.

Gu, X.-L., Long, C.-X., Sun, L., Xie, C., Lin, X., & Cai, H. (2010). Astrocytic expression of Parkinson's disease-related A53T alpha-synuclein causes neurodegeneration in mice. *Molecular Brain*, *3*(1), 12.

Haidet-Phillips, A. M., Hester, M. E., Miranda, C. J., Meyer, K., Braun, L., Frakes, A., … Kaspar, B. K. (2011). Astrocytes from familial and sporadic ALS patients are toxic to motor neurons. *Nature Biotechnology*, *29*(9), 824–828.

Henkel, J. S., Beers, D. R., Zhao, W., & Appel, S. H. (2009). Microglia in ALS: the good, the bad, and the resting. *Journal of Neuroimmune Pharmacology : The Official Journal of the Society on NeuroImmune Pharmacology*, *4*(4), 389–98.

Herx, L. M., Rivest, S., & Yong, V. W. (2000). Central nervous system-initiated inflammation and neurotrophism in trauma: IL-1 beta is required for the production of ciliary neurotrophic factor. *Journal of Immunology (Baltimore, Md. : 1950)*, *165*(4), 2232–2239.

Hoenen, C., Gustin, A., Birck, C., Kirchmeyer, M., Beaume, N., Felten, P., … Heurtaux, T. (2016). Alpha-synuclein proteins promote pro-inflammatory cascades in microglia: Stronger effects of the a53t mutant. *PLoS ONE*, *11*(9), e0162717.

Hsieh, C. H., Shaltouki, A., Gonzalez, A. E., Bettencourt da Cruz, A., Burbulla, L. F., St. Lawrence, E., … Wang, X. (2016). Functional Impairment in Miro Degradation and

Mitophagy Is a Shared Feature in Familial and Sporadic Parkinson's Disease. *Cell Stem Cell*, *19*(6), 709–724.

Huang, L., Deng, M., Zhang, S., Lu, S., Gui, X., & Fang, Y. (2017). β-asarone and levodopa coadministration increases striatal levels of dopamine and levodopa and improves behavioral competence in Parkinson's rat by enhancing dopa decarboxylase activity. *Biomedicine & Pharmacotherapy*, *94*, 666–678.

Hubbard, J. A., Szu, J. I., Yonan, J. M., & Binder, D. K. (2016). Regulation of astrocyte glutamate transporter-1 (GLT1) and aquaporin-4 (AQP4) expression in a model of epilepsy. *Experimental Neurology*, *283*, 85–96.

Huber, J. D., Witt, K. A., Hom, S., Egleton, R. D., Mark, K. S., & Davis, T. P. (2001). Inflammatory pain alters blood-brain barrier permeability and tight junctional protein expression. *American Journal of Physiology. Heart and Circulatory Physiology*, *280*(3), H1241–H1248.

Jang, A., Lee, H. J., Suk, J. E., Jung, J. W., Kim, K. P., & Lee, S. J. (2010). Non-classical exocytosis of alpha-synuclein is sensitive to folding states and promoted under stress conditions. *Journal of Neurochemistry*, *113*(5), 1263–1274.

Johnson, B. S., Snead, D., Lee, J. J., McCaffery, J. M., Shorter, J., & Gitler, A. D. (2009). TDP-43 is intrinsically aggregation-prone, and amyotrophic lateral sclerosis-linked mutations accelerate aggregation and increase toxicity. *The Journal of Biological Chemistry*, *284*(30), 20329–39.

Jones, V. C., Atkinson-Dell, R., Verkhratsky, A., & Mohamet, L. (2017). Aberrant iPSC-derived human astrocytes in Alzheimer's disease. *Cell Death & Disease*, *8*(3), e2696.

Kaushik, S., & Cuervo, A. M. (2015). Proteostasis and aging. *Nature Medicine*, *21*(12), 1406–1415.

Khakh, B. S., & Sofroniew, M. V. (2015). Diversity of astrocyte functions and phenotypes in neural circuits. *Nature Neuroscience*, *18*(7), 942–952.

Khasnavis, S., & Pahan, K. (2014). Cinnamon treatment upregulates neuroprotective proteins Parkin and DJ-1 and protects dopaminergic neurons in a mouse model of Parkinson's disease. *Journal of Neuroimmune Pharmacology*, *9*(4), 569–581.

Kiffin, R. (2004). Activation of Chaperone-mediated Autophagy during Oxidative Stress. *Molecular Biology of the Cell*, *15*(11), 4829–4840.

Kitada, T., Asakawa, S., Hattori, N., Matsumine, H., Yamamura, Y., Minoshima, S., … Shimizu, N. (1998). Mutations in the parkin gene cause autosomal recessive juvenile parkinsonism. *Nature*, *392*(6676), 605–608.

Koga, H., Martinez-Vicente, M., Macian, F., Verkhusha, V. V, & Cuervo, A. M. (2011). A photoconvertible fluorescent reporter to track chaperone-mediated autophagy. *Nature Communications*, *2*, 386.

Kortekaas, R., Leenders, K. L., Van Oostrom, J. C. H., Vaalburg, W., Bart, J., Willemsen, A. T. M., & Hendrikse, N. H. (2005). Blood-brain barrier dysfunction in Parkinsonian midbrain in vivo. *Annals of Neurology*, *57*(2), 176–179.

Kriks, S., Shim, J.-W., Piao, J., Ganat, Y. M., Wakeman, D. R., Xie, Z., … Studer, L. (2011). Dopamine neurons derived from human ES cells efficiently engraft in animal models of Parkinson's disease. *Nature*, *480*(7378), 547–51.

Kuo, Y. M., Li, Z., Jiao, Y., Gaborit, N., Pani, A. K., Orrison, B. M., … Nussbaum, R. L. (2010). Extensive enteric nervous system abnormalities in mice transgenic for artificial chromosomes containing Parkinson disease-associated α-synuclein gene mutations precede central nervous system changes. *Human Molecular Genetics*, *19*(9), 1633–1650.

Lee, A., & Pow, D. V. (2010). Astrocytes: Glutamate transport and alternate splicing of transporters. *The International Journal of Biochemistry & Cell Biology*, *42*(12), 1901–6.

Lee, G., & Bendayan, R. (2004). Functional expression and localization of P-glycoprotein in the central nervous system: Relevance to the pathogenesis and treatment of neurological disorders. *Pharmaceutical Research*, *21*(8), 1313–1330.

Lee, H. J., Suk, J. E., Patrick, C., Bae, E. J., Cho, J. H., Rho, S., … Lee, S. J. (2010). Direct transfer of α-synuclein from neuron to astroglia causes inflammatory responses in synucleinopathies. *Journal of Biological Chemistry*, *285*(12), 9262–9272.

Li, G., Yang, H., Zhu, D., Huang, H., Liu, G., & Lun, P. (2014). Targeted suppression of chaperone-mediated autophagy by miR-320a promotes alpha-synuclein aggregation. *International Journal of Molecular Sciences*, *15*(9), 15845–15857.

Liddelow, S. A., & Barres, B. A. (2017). Reactive Astrocytes : Potential, Therapeutics. *Immunity*, *46*(6), 957–967.

Liddelow, S. A., Guttenplan, K. A., Clarke, L. E., Bennett, F. C., Bohlen, C. J., Schirmer, L., … Barres, B. A. (2017). Neurotoxic reactive astrocytes are induced by activated microglia. *Nature*, *541*(7638), 481–487.

Lill, C. M. (2016). Genetics of Parkinson's disease. *Molecular and Cellular Probes*, *30*(6), 386–396.

Liu, H.-N., Tjostheim, S., Dasilva, K., Taylor, D., Zhao, B., Rakhit, R., … Robertson, J. (2012). Targeting of Monomer/Misfolded SOD1 as a Therapeutic Strategy for Amyotrophic Lateral Sclerosis. *The Journal of Neuroscience : The Official Journal of the Society for Neuroscience*, *32*(26), 8791–9.

Lo, E. H., Dalkara, T., & Moskowitz, M. A. (2003). Mechanisms, challenges and opportunities in stroke. *Nature Reviews Neuroscience*, *4*(5), 399–415.

Loureiro, C., & Silva, R. H. (2017). Genetic Variants in SNCA and the Risk of Sporadic Parkinson ' s Disease and Clinical Outcomes : A Review. *Parkinson's Disease*, *2017*,

4318416.

Manzoni, C., Mamais, A., Dihanich, S., Abeti, R., Soutar, M. P. M., Plun-Favreau, H., … Lewis, P. A. (2013). Inhibition of LRRK2 kinase activity stimulates macroautophagy. *Biochimica et Biophysica Acta - Molecular Cell Research*, *1833*(12), 2900–2910.

Marroni, M., Marchi, N., Cucullo, L., Abbott, N. J., Signorelli, K., & Janigro, D. (2003). Vascular and parenchymal mechanisms in multiple drug resistance: a lesson from human epilepsy. *Current Drug Targets*, *4*(4), 297–304.

Martinez-Vicente, M., Talloczy, Z., Kaushik, S., Massey, A. C., Mazzulli, J., Mosharov, E. V., … Cuervo, A. M. (2008). Dopamine-modified alpha-synuclein blocks chaperone-mediated autophagy. *Journal of Clinical Investigation*, *118*(2), 777–778.

Mason, J. L., Jones, J. J., Taniike, M., Morell, P., Suzuki, K., & Matsushima, G. K. (2000). Mature oligodendrocyte apoptosis precedes IGF-1 production and oligodendrocyte progenitor accumulation and differentiation during demyelination/remyelination. *Journal of Neuroscience Research*, *61*(3), 251–262.

Massey, A. C., Follenzi, A., Kiffin, R., Zhang, C., & Cuervo, A. M. (2008). Early cellular changes after blockage of chaperone-mediated autophagy. *Autophagy*, *4*(4), 442–456.

Massey, A. C., Kaushik, S., Sovak, G., Kiffin, R., & Cuervo, A. M. (2006). Consequences of the selective blockage of chaperone-mediated autophagy. *Proceedings of the National Academy of Sciences*, *103*(15), 5805–5810.

Mbefo, M. K., Fares, M. B., Paleologou, K., Oueslati, A., Yin, G., Tenreiro, S., … Lashuel, H. a. (2015). Parkinson disease mutant E46K enhances α-synuclein phosphorylation in mammalian cell lines, in yeast, and in vivo. *Journal of Biological Chemistry*, *290*(15), 9412–9427.

McCrate, M. E., & Kaspar, B. K. (2008). Physical activity and neuroprotection in amyotrophic lateral sclerosis. *Neuromolecular Medicine*, *10*(2), 108–17.

Melrose, H. L., Lincoln, S. J., Tyndall, G. M., & Farrer, M. J. (2006). Parkinson's disease: A rethink of rodent models. *Experimental Brain Research*, *173*(2), 196–204.

Molofsky, A. V, Kelley, K. W., Tsai, H.-H., Redmond, S. a, Chang, S. M., Madireddy, L., … Rowitch, D. H. (2014). Astrocyte-encoded positional cues maintain sensorimotor circuit integrity. *Nature*, *509*(7499), 189–194.

Nadeau, J. H. (2001). Modifier genes in mice and humans. *Nature Reviews Genetics*, *2*(3), 165–174.

Nash, K. R., Moran, P., Finneran, D. J., Hudson, C., Robinson, J., Morgan, D., & Bickford, P. C. (2014). Fractalkine Over Expression Suppresses α-Synuclein-mediated Neurodegeneration. *Molecular Therapy*, *23*(1), 17–23.

Nedergaard, M., Takano, T., & Hansen, A. J. (2002). Beyond the role of glutamate as a neurotransmitter. *Nature Reviews. Neuroscience*, *3*(9), 748–55.

Neupane, K., Solanki, A., Sosova, I., Belov, M., & Woodside, M. T. (2014). Diverse metastable structures formed by small oligomers of alpha-synuclein probed by force spectroscopy. *PLoS ONE*, *9*(1), e86495.

Nguyen, H. N., Byers, B., Cord, B., Shcheglovitov, A., Byrne, J., Gujar, P., … Pera, R. R. (2011). LRRK2 mutant iPSC-derived da neurons demonstrate increased susceptibility to oxidative stress. *Cell Stem Cell*, *8*(3), 267–280.

Nichols, W. C., Pankratz, N., Hernandez, D., Paisán-Ruíz, C., Jain, S., Halter, C. A., … Foroud, T. (2005). Genetic screening for a single common LRRK2 mutation in familial Parkinson's disease. *Lancet*, *365*(9457), 410–412.

O'Rourke, J. G., Bogdanik, L., Yanez, A., Lall, D., Wolf, A. J., Muhammad, A. K. M. G., … Baloh, R. H. (2016). C9orf72 is required for proper macrophage and microglial function in mice. *Science*, *351*(6279), 1324–1329.

Olabarria, M., Noristani, H. N., Verkhratsky, A., & Rodríguez, J. J. (2010). Concomitant astroglial atrophy and astrogliosis in a triple transgenic animal model of Alzheimer's disease. *GLIA*, *58*(7), 831–838.

Orenstein, S. J., Kuo, S.-H., Tasset, I., Arias, E., Koga, H., Fernandez-Carasa, I., … Cuervo, A. M. (2013). Interplay of LRRK2 with chaperone-mediated autophagy. *Nature Neuroscience*, *16*(4), 394–406.

Paisán-Ruíz, C., Jain, S., Evans, E. W., Gilks, W. P., Simón, J., Van Der Brug, M., … Singleton, A. B. (2004). Cloning of the gene containing mutations that cause PARK8-linked Parkinson's disease. *Neuron*, *44*(4), 595–600.

Panatier, A., Vallée, J., Haber, M., Murai, K. K., Lacaille, J. C., & Robitaille, R. (2011). Astrocytes are endogenous regulators of basal transmission at central synapses. *Cell*, *146*(5), 785–798.

Park, C., Suh, Y., & Cuervo, A. M. (2015). Regulated degradation of Chk1 by chaperone-mediated autophagy in response to DNA damage. *Nature Communications*, *6*, 6823.

Perfeito, R., Lázaro, D. F., Outeiro, T. F., & Rego, A. C. (2014). Linking alpha-synuclein phosphorylation to reactive oxygen species formation and mitochondrial dysfunction in SH-SY5Y cells. *Molecular and Cellular Neuroscience*, *62*, 51–59.

Plaza-Zabala, A., Sierra-Torre, V., & Sierra, A. (2017). Autophagy and microglia: Novel partners in neurodegeneration and aging. *International Journal of Molecular Sciences*, *18*(3), 598.

Polymeropoulos, M. H., Lavedan, C., Leroy, E., Ide, S. E., Dehejia, A., Dutra, A., … Nussbaum, R. L. (1997). Mutation in the α -Synuclein Gene Identified in Families with Parkinson's Disease Mutation in the alpha-Synuclein Gene Identified in Families with Parkinson ' s Disease. *Science*, *276*(June), 2045–2047.

Ramirez, A., Heimbach, A., Gründemann, J., Stiller, B., Hampshire, D., Cid, L. P., … Kubisch, C. (2006). Hereditary parkinsonism with dementia is caused by mutations

in ATP13A2, encoding a lysosomal type 5 P-type ATPase. *Nat Genet*, *38*(10), 1184–1191.

Rappold, P. M., & Tieu, K. (2011). NIH Public Access, *7*(4), 413–423.

Reinhardt, P., Schmid, B., Burbulla, L. F., Schöndorf, D. C., Wagner, L., Glatza, M., … Sterneckert, J. (2013). Genetic correction of a lrrk2 mutation in human iPSCs links parkinsonian neurodegeneration to ERK-dependent changes in gene expression. *Cell Stem Cell*, *12*(3), 354–367.

Reyes, J. F., Olsson, T. T., Lamberts, J. T., Devine, M. J., Kunath, T., & Brundin, P. (2015). A cell culture model for monitoring α-synuclein cell-to-cell transfer. *Neurobiology of Disease*, *77*, 266–275.

Riazuddin, S., Castelein, C. M., Ahmed, Z. M., Lalwani, a K., Mastroianni, M. a, Naz, S., … Wilcox, E. R. (2000). Dominant modifier DFNM1 suppresses recessive deafness DFNB26. *Nature Genetics*, *26*(4), 431–434.

Richard, J.-P., & Maragakis, N. J. (2014). Induced pluripotent stem cells from ALS patients for disease modeling. *Brain Research*, *1607*, 15–25.

Riederer, P., Sofic, E., Rausch, W. D., Schmidt, B., Reynolds, G. P., Jellinger, K., & Youdim, M. B. H. (1989). Transition Metals, Ferritin, Glutathione, and Ascorbic Acid in Parkinsonian Brains. *Journal of Neurochemistry*, *52*(2), 515–520.

Ritchie, C. M., & Thomas, P. J. (2012). Alpha-synuclein truncation and disease. *Health*, *4*(11), 1167–1177.

Rothaug, M., Zunke, F., Mazzulli, J. R., Schweizer, M., Altmeppen, H., Lullmann-Rauch, R., … Blanz, J. (2014). LIMP-2 expression is critical for -glucocerebrosidase activity and -synuclein clearance. *Proceedings of the National Academy of Sciences*, *111*(43), 15573–15578.

Sadelli, K., Stamegna, J. C., Girard, S. D., Baril, N., Escoffier, G., Brus, M., … Roman, F. S. (2017). Global cerebral ischemia in rats leads to amnesia due to selective neuronal death followed by astroglial scar formation in the CA1 layer. *Neurobiology of Learning and Memory*, *141*, 168–178.

Saijo, K., Winner, B., Carson, C. T., Collier, J. G., Boyer, L., Rosenfeld, M. G., … Glass, C. K. (2009). A Nurr1/CoREST Pathway in Microglia and Astrocytes Protects Dopaminergic Neurons from Inflammation-Induced Death. *Cell*, *137*(1), 47–59.

Sánchez-Danés, A., Richaud-Patin, Y., Carballo-Carbajal, I., Jiménez-Delgado, S., Caig, C., Mora, S., … Raya, A. (2012). Disease-specific phenotypes in dopamine neurons from human iPS-based models of genetic and sporadic Parkinson's disease. *EMBO Molecular Medicine*, *4*(5), 380–395.

Sanders, L. H., Laganire, J., Cooper, O., Mak, S. K., Vu, B. J., Huang, Y. A., … Schle, B. (2014). LRRK2 mutations cause mitochondrial DNA damage in iPSC-derived neural cells from Parkinson's disease patients: Reversal by gene correction. *Neurobiology of*

Disease.

Sanders, L. H., Paul, K. C., Howlett, E. H., Lawal, H., Boppana, S., Bronstein, J. M., … Greenamyre, J. T. (2017). Editor's Highlight: Base Excision Repair Variants and Pesticide Exposure Increase Parkinson's Disease Risk. *Toxicological Sciences*, *158*(1), 188–198.

Santos, D., Esteves, A. R., Silva, D. F., Januário, C., & Cardoso, S. M. (2015). The Impact of Mitochondrial Fusion and Fission Modulation in Sporadic Parkinson's Disease. *Molecular Neurobiology*, *52*(1), 573–586.

Satake, W., Nakabayashi, Y., Mizuta, I., Hirota, Y., Ito, C., Kubo, M., … Toda, T. (2009). Genome-wide association study identifies common variants at four loci as genetic risk factors for Parkinson's disease. *Nature Genetics*, *41*(12), 1303–7.

Schapira, A. H. (2006). Etiology of Parkinson's disease. *Neurology*, *66*(10 Suppl 4), S10-23.

Schmidt, S., Linnartz, B., Mendritzki, S., Sczepan, T., Lübbert, M., Stichel, C. C., & Lübbert, H. (2011). Genetic mouse models for Parkinson's disease display severe pathology in glial cell mitochondria. *Human Molecular Genetics*, *20*(6), 1197–1211.

Schneider, J. L., Villarroya, J., Diaz-Carretero, A., Patel, B., Urbanska, A. M., Thi, M. M., … Cuervo, A. M. (2015). Loss of hepatic chaperone-mediated autophagy accelerates proteostasis failure in aging. *Aging Cell*, *14*(2), 249–264.

Schwaninger, M., Sallmann, S., Petersen, N., Schneider, A., Prinz, S., Libermann, T. A., & Spranger, M. (1999). Bradykinin induces interleukin-6 expression in astrocytes through activation of nuclear factor-B. *Journal of Neurochemistry*, *73*(4), 1461–1466.

Serio, A., Bilican, B., Barmada, S. J., Ando, D. M., Zhao, C., Siller, R., … Chandran, S. (2013). Astrocyte pathology and the absence of non-cell autonomy in an induced pluripotent stem cell model of TDP-43 proteinopathy. *Proceedings of the National Academy of Sciences of the United States of America*, *110*(12), 4697–702.

Sharma, M., Ioannidis, J. P. A., Aasly, J. O., Annesi, G., Brice, A., Van Broeckhoven, C., … Krger, R. (2012). Large-scale replication and heterogeneity in Parkinson disease genetic loci. *Neurology*, *79*(7), 659–667.

Shojaee, S., Sina, F., Banihosseini, S. S., Kazemi, M. H., Kalhor, R., Shahidi, G. A., … Elahi, E. (2008). Genome-wide Linkage Analysis of a Parkinsonian-Pyramidal Syndrome Pedigree by 500 K SNP Arrays. *American Journal of Human Genetics*, *82*(6), 1375–1384.

Simón-Sánchez, J., Schulte, C., Bras, J. M., Sharma, M., Gibbs, J. R., Berg, D., … Gasser, T. (2009). Genome-wide association study reveals genetic risk underlying Parkinson's disease. *Nature Genetics*, *41*(12), 1308–12.

Singleton, B., Farrer, M., Johnson, J., Singleton, A., Hague, S., Kachergus, J., … Gwinn-Hardy, K. (2003). alpha-Synuclein locus triplication causes Parkinson's disease.

Science (New York, N.Y.), *302*(5646), 841.

Solano, R. M., Casarejos, M. J., Menéndez-Cuervo, J., Rodriguez-Navarro, J. A., García De Yébenes, J., & Mena, M. A. (2008). Glial Dysfunction in Parkin Null Mice: Effects of Aging. *Neurobiology of Disease*, *28*(3), 598–611.

Song, H., Stevens, C. F., & Gage, F. H. (2002). Astroglia induce neurogenesis from adult neural stem cells. *Nature*, *417*(6884), 39–44.

Spencer, J. I., Bell, J. S., & DeLuca, G. C. (2017). Vascular pathology in multiple sclerosis: reframing pathogenesis around the blood-brain barrier. *Journal of Neurology, Neurosurgery & Psychiatry*, jnnp-2017-316011.

Spillantini, M. G., Crowther, R. A., Jakes, R., Hasegawa, M., & Goedert, M. (1998). alpha-Synuclein in filamentous inclusions of Lewy bodies from Parkinson's disease and dementia with lewy bodies. *Proc Natl Acad Sci U S A*, *95*(11), 6469–6473.

Su, Y. C., Guo, X., & Qi, X. (2015). Threonine 56 phosphorylation of Bcl-2 is required for LRRK2 G2019S-induced mitochondrial depolarization and autophagy. *Biochimica et Biophysica Acta - Molecular Basis of Disease*, *1852*(1), 12–21.

Subramanian, V., Crabtree, B., & Acharya, K. R. (2008). Human angiogenin is a neuroprotective factor and amyotrophic lateral sclerosis associated angiogenin variants affect neurite extension/pathfinding and survival of motor neurons. *Human Molecular Genetics*, *17*(1), 130–49.

Suzuki, A., Stern, S. A., Bozdagi, O., Huntley, G. W., Walker, R. H., Magistretti, P. J., & Alberini, C. M. (2011). Astrocyte-neuron lactate transport is required for long-term memory formation. *Cell*, *144*(5), 810–823.

Tanaka, Y., Engelender, S., Igarashi, S., Rao, R. K., Wanner, T., Tanzi, R. E., … Ross, C. A. (2001). Inducible expression of mutant α-synuclein decreases proteasome activity and increases sensitivity to mitochondria-dependent apoptosis. *Human Molecular Genetics*, *10*(9), 919–926.

Tong, Y., Yamaguchi, H., Giaime, E., Boyle, S., Kopan, R., Kelleher, R. J., & Shen, J. (2010). Loss of leucine-rich repeat kinase 2 causes impairment of protein degradation pathways, accumulation of alpha-synuclein, and apoptotic cell death in aged mice. *Proceedings of the National Academy of Sciences of the United States of America*, *107*(21), 9879–84.

Tran, P. B., & Miller, R. J. (2003). Chemokine receptors: signposts to brain development and disease. *Nature Reviews. Neuroscience*, *4*(6), 444–455.

Tyzack, G. E., Sitnikov, S., Barson, D., Adams-Carr, K. L., Lau, N. K., Kwok, J. C., … Lakatos, A. (2014). Astrocyte response to motor neuron injury promotes structural synaptic plasticity via STAT3-regulated TSP-1 expression. *Nature Communications*, *5*, 4294.

Ullian, E. (2001). Control of Synapse Number by Glia. *Science*, *291*(5504), 657–661.

Ullian, E., Christopherson, K., & Barres, B. (2004). Role for glia in synaptogenesis. *GLIA*, *47*(3), 209–216.

Urrea, L., Segura-Feliu, M., Masuda-Suzukake, M., Hervera, A., Pedraz, L., Aznar, J. M. G., … Del Río, J. A. (2017). Involvement of Cellular Prion Protein in α-Synuclein Transport in Neurons. *Molecular Neurobiology*, 1–14.

Uwechue, N. M., Marx, M.-C., Chevy, Q., & Billups, B. (2012). Activation of glutamate transport evokes rapid glutamine release from perisynaptic astrocytes. *The Journal of Physiology*, *590*(10), 2317–2331.

Valente, E. M., Abou-Sleiman, P. M., Caputo, V., Muqit, M. M. K., Harvey, K., Gispert, S., … Wood, N. W. (2004). Hereditary early-onset Parkinson's disease caused by mutations in PINK1. *Science (New York, N.Y.)*, *304*(5674), 1158–60.

Vilarino-Guell, C., Wider, C., Ross, O. A., Dachsel, J. C., Kachergus, J. M., Lincoln, S. J., … Farrer, M. J. (2011). VPS35 mutations in parkinson disease. *American Journal of Human Genetics*, *89*(1), 162–167.

Wakabayashi, K., Hayashi, S., Yoshimoto, M., Kudo, H., & Takahashi, H. (2000). NACP/alpha-synuclein-positive filamentous inclusions in astrocytes and oligodendrocytes of Parkinson's disease brains. *Acta Neuropathologica*, *99*(1), 14–20.

Wang, L., Das, U., Scott, D. A., Tang, Y., McLean, P. J., & Roy, S. (2014). α-Synuclein multimers cluster synaptic vesicles and attenuate recycling. *Current Biology*, *24*(19), 2319–2326.

Wang, X., Yan, M. H., Fujioka, H., Liu, J., Wilson-delfosse, A., Chen, S. G., … Zhu, X. (2012). LRRK2 regulates mitochondrial dynamics and function through direct interaction with DLP1. *Human Molecular Genetics*, *21*(9), 1931–1944.

Weatherall, D. J. (2001). Phenotype-genotype relationships in monogenic disease: lessons from the thalassaemias. *Nature Reviews Genetics*, *2*(4), 245–255.

Webb, J. L., Ravikumar, B., Atkins, J., Skepper, J. N., & Rubinsztein, D. C. (2003). α-synuclein Is Degraded by Both Autophagy and the Proteasome. *Journal of Biological Chemistry*, *278*(27), 25009–25013.

Wilson, G. R., Sim, J. C. H., McLean, C., Giannandrea, M., Galea, C. A., Riseley, J. R., … Lockhart, P. J. (2014). Mutations in RAB39B cause X-linked intellectual disability and early-onset parkinson disease with α-synuclein pathology. *American Journal of Human Genetics*, *95*(6), 729–735.

Winslow, A. R., Chen, C. W., Corrochano, S., Acevedo-Arozena, A., Gordon, D. E., Peden, A. A., … Rubinsztein, D. C. (2010). α-Synuclein impairs macroautophagy: Implications for Parkinson's disease. *Journal of Cell Biology*, *190*(6), 1023–1037.

Winton, M. J., Igaz, L. M., Wong, M. M., Kwong, L. K., Trojanowski, J. Q., & Lee, V. M.-Y. (2008). Disturbance of nuclear and cytoplasmic TAR DNA-binding protein (TDP-

43) induces disease-like redistribution, sequestration, and aggregate formation. *The Journal of Biological Chemistry*, *283*(19), 13302–9.

Ye, L., Yang, Y., Zhang, X., Cai, P., Li, R., Chen, D., … Zhang, H. (2015). The role of bFGF in the excessive activation of astrocytes is related to the inhibition of TLR4/NFκB signals. *International Journal of Molecular Sciences*, *17*(1).

Yi, J.-H., & Hazell, A. S. (2006). Excitotoxic mechanisms and the role of astrocytic glutamate transporters in traumatic brain injury. *Neurochemistry International*, *48*(5), 394–403.

Yuan, J., Liu, W., Zhu, H., Chen, Y., Zhang, X., Li, L., … Lin, J. (2017). Curcumin inhibits glial scar formation by suppressing astrocyte-induced inflammation and fibrosis in vitro and in vivo. *Brain Research*, *1655*, 90–103.

Zeltner, N., & Studer, L. (2015). Pluripotent stem cell-based disease modeling: Current hurdles and future promise. *Current Opinion in Cell Biology*, *37*, 102–110.

Zhang, Q. S., Heng, Y., Yuan, Y. H., & Chen, N. H. (2017). Pathological α-synuclein exacerbates the progression of Parkinson's disease through microglial activation. *Toxicology Letters*, *265*, 30–37.

Zhang, W. (2005). Aggregated -synuclein activates microglia: a process leading to disease progression in Parkinson's disease. *The FASEB Journal*, *19*(6), 533–542.

Zhu, Y. M., Gao, X., Ni, Y., Li, W., Kent, T. A., Qiao, S. G., … Zhang, H. L. (2017). Sevoflurane postconditioning attenuates reactive astrogliosis and glial scar formation after ischemia–reperfusion brain injury. *Neuroscience*, *356*, 125–141.

Zimprich, A., Biskup, S., Leitner, P., Lichtner, P., Farrer, M., Lincoln, S., … Gasser, T. (2004). Mutations in LRRK2 cause autosomal-dominant parkinsonism with pleomorphic pathology. *Neuron*, *44*(4), 601–607.

Zis, P., Erro, R., Walton, C. C., Sauerbier, A., & Chaudhuri, K. R. (2015). The range and nature of non-motor symptoms in drug-naive Parkinson's disease patients: a state-of-the-art systematic review. *Npj Parkinson's Disease*, *1*(May), 8.

Zuo, L., & Motherwell, M. S. (2013). The impact of reactive oxygen species and genetic mitochondrial mutations in Parkinson's disease. *Gene*, *532*(1), 18–23.

Figure Legends

Figure 1. iPSC-derived patient specific astrocyte generation and characterization (**A**) Representative images of two control lines and two LRRK2-PD lines staining positive for astrocytic markers CD44 (precursor), GFAP (general astrocytes), and S100β (mature astrocytes), GLT1 (excitatory amino acid transporter 2) and negative or low expression for TUJ1 (immature neuron), no MAP2 (mature neuron) nor NG2 (oligodendrocytes) expression (n = 3). Scale bar 100μm. (**B**) qRT-PCR revealing mRNA expression levels of

astrocitic end-feet marker Aquaporin 4 in both WT and LRRK2-PD lines and not present in fibroblasts. (**C**) Astrocyte cultures are approximately composed of 90% astrocytes, 8% neurons and 2% other (n = 3). (**D, E**) Graph representing single functional astrocyte calcium waves of WT (SP09) line and LRRK2-PD (SP13) astrocytes (n = 2). (**F**) Graph plotting functional ATP production luminescence (counts) in both WT (SP09) and LRRK2-PD (SP13) astrocytes (n = 3), differences are non-significant (mean ± s.e.m, unpaired two-tailed Student's t-test, n.s.).

Figure 2. vmDA neuron generation and co-culture set up (**A**) Diagram of co-culture system. (**B**) Representative images of 4-week co-culture staining positive for WT vmDA neurons (TH), WT astrocytes (GFAP) and nuclear DAPI. Scale bar 20 µm. (**C**) Representative images of pre-synaptic marker, Synapsin I of a WT vmDA neuron (TH) on the top of WT astrocytes at 4 weeks. Scale bar 20 µm. (**D**) Representative images of WT vmDA neuron (TH) and mature neurons (MAP2) on the top of WT astrocytes (GFAP) during a 4-week co-culture. Scale bar 20µm.

Figure 3. WT neurons show signs of neurodegeneration and accumulate alpha-synuclein when co-cultured with PD astrocytes. (**A**) Scheme representing co-culture system of WT neurons on the top of both WT and PD astrocytes for 4-weeks. Representative images of WT neurons, TH, on WT astrocytes (**B**) and LRRK2-PD astrocytes (**C**) for 4-week co-cultures. (**D**) Graph representing Scholl analysis of number of neurite intersections per neuron on average for WT neurons when co-cultured on WT astrocytes or PD astrocytes for 4 weeks (n = 3, total neurons counted = 40). (**E**) Graph plotting fold increase of TH with degenerative morphology during a 4-week co-culture on either WT or LRRK2-PD astrocytes normalized to total TH. Representative images of WT vmDAn (TH) and alpha-synuclein (SNCA) when co-cultured with both WT (**F**) and LRRK2-PD (**G**) astrocytes after 4 weeks in culture, scale bar 0.2µm. (**H**) Graph representing TH/DAPI WT neuron count when co-cultured with WT or LRRK2-PD astrocytes at 4 weeks (fold change normalized to WT condition, n = 3, total neurons counted = 1160). (**I**) MAP2/DAPI count in co-cultures on WT and LRRK2-PD astrocytes (n = 2, total neurons counted = 3583). (**J**) Graph plotting SNCA positive TH in both co-culture conditions. Representative images of GFAP either for WT astrocytes (**K**) or LRRK2-PD astrocytes (**L**) and alpha-synuclein (SNCA) when co-cultured with WT vmDAn after 4 weeks in culture, scale bar 20µm. (**M**) Contour plot of WT and PD astrocyte viability at 4 weeks. (K) Scheme representing generation of SNCA-flag astrocyte lines. (**L**) PD astrocyte expressing co-localized SNCA and Flag staining. (**N**) Graph plotting SNCA positive GFAP in both co-culture conditions. (**N**) Co-localization analysis of SNCA and Flag in a 4-week co-culture of WT vmDAn (TH) on the top of LRRK2-PD SNCA Flag astrocytes, scale bar 20µm. (**O**) Scheme depicting generation of SNCA-flag astrocyte lines with an immunocytochemical staining of LRRK2-PD SNCA-flag 14-day astrocyte staining for SNCA and FLAG. (**P**) Co-localization analysis of SNCA and Flag in a 4-week co-culture of WT vmDAn (TH) on the top of LRRK2-PD SNCA Flag astrocytes, scale bar 20µm. (**Q**) Flag staining inside WT TH neuron during a 4-weeks co-culture when on the top of SNCA Flag PD astrocytes. All graphs plot mean ± s.e.m, unpaired two-tailed Student's t-test, *p<0.05, **p<0.01, ***p<0.001.

Figure 4. PD neurons restore arborized morphology and accumulate less alpha-synuclein when co-cultured with WT astrocytes. (A) Scheme representing co-culture system of PD neurons on the top of both WT and PD astrocytes for 4-weeks. (B and C) Scholl analysis image of neurite traces of PD neurons in both co-culture conditions. (D) Graph representing Scholl analysis of number of neurite intersections in PD neurons when co-cultured on WT

astrocytes or PD astrocytes for 4 weeks (*n* = 3, total neurons counted = 40). (E) Immunofluorescence representations of alpha-synuclein (SNCA) levels during a 4-week co-culture with PD neurons (TH) on the top of WT astrocytes (GFAP) (F) and PD neurons on the top of PD astrocytes. (G) Graph plotting MAP2 (normalized to DAPI) positive neurons in co-cultures with both WT and PD astrocytes (*n* = 2, total neurons counted = 4219). (H) Graph plotting TH/DAPI in co-cultures with PD neurons on the top of WT and PD astrocytes at 2 and 4 weeks (*n* = 2, total neurons counted = 6301). (I) Immunofluorescence representing PD neurons (TH) on the top of WT astrocytes (GFAP) with a focus on alpha-synulcein (SNCA). All graphs plot mean ± s.e.m, unpaired two-tailed Student's t-test, *p<0.05, **p<0.01, ***p<0.001).

Figure 5. Altered CMA and SNCA accumulation in LRRK2-PD astrocytes (**A**) Representative images of the receptor for CMA (LAMP2A), astrocyte marker GFAP, SNCA and nuclear marker DAPI in control and LRRK2-PD astrocytes at 6 and 14 days, scale bar 10µm. Smaller white circles represent perinuclear area, whereas larger green circle represents non-perinuclear area. Scale bar 20µm. (**B**) Positive co-localization between LAMP2A and SNCA in LRRK2-PD astrocytes. (**C**) Western blot of SNCA protein levels in control and LRRK2-PD astrocytes after 14 days, actin as a loading control, quantification in graph (n = 3) (**D**). (**E**) KFERQ-DENDRA (CMA reporter) in control and LRRK2-PD astrocytes 52 hours after photo-activation with UV light. (**F**) Western blot of SNCA flux protein levels after the addition of inhibitors of autophagy and proteasomal degradation. (**G**) Effects of inhibitors of SNCA accumulation (n = 2). (**H**) Knock-down shLAMP2A and shLuciferase (as a control) in control and LRRK2-PD astrocytes after 14 days. (**I**) SNCA puncta area percentage per cell in WT and LRRK2-PD astrocytes with shLuciferase or shLAMP2A (n = 2). (**J**) SNCA puncta increase ratio in control and LRRK2-PD astrocytes with shLuciferase or CMA knock down shLAMP2A (n = 2). All graphs plot mean ± s.e.m, unpaired two-tailed Student's t-test, *p<0.05, **p<0.01, ***p<0.001.

Figure 6. Dysfunctional macroautophagy in LRRK2-PD astrocytes (**A**) Representative images of lysosomal protein marker LAMP1 and autophagosome marker LC3 in control and LRRK2-PD astrocytes at 6 and 14 days. Smaller white circles represent perinuclear area, whereas larger green circle represents non-perinuclear area. Scale bar 50µm. (**B**) Orthogonal view representing a lack of co-localization between LAMP1 and LC3 in LRRK2-PD astrocytes. (**C**) Western blot of LC3 II protein levels with corresponding quantification (*n* = 2). (**D**) LC3-flux ratio (2hr treatment/no treatment) representing the speed of fusion (*n* = 2). (**E**) Western blot of p62 protein levels with quantification (mean ± s.e.m) in graph (*n* = 2) (**F**). All graphs plot mean ± s.e.m, unpaired two-tailed Student's t-test, *p<0.05, **p<0.01, ***p<0.001.

Figure 7. CMA activator drug rug treatment QX77.1 rescues SNCA accumulation and restores LAMP2A to perinuclear area (**A**) Representative images of 14 day WT astrocytes without treatment displaying LAMP2A in the perinuclear area and low levels of SNCA. (**B**) PD astrocytes (14 days) without treatment display a mis-localization of LAMP2A out of the perinuclear area and accumulation of SNCA. Orthogonal views reveal positive co-localization of SNCA to LAMP2A. (**C**) 14 day PD astrocytes after 20µg of QX77.1 drug treatment for 5 days displaying LAMP2A localization restored back around the perinuclear area and lower levels of SNCA. (**D**) Graph displaying percentage of cells/DAPI that are SNCA and GFAP double positive in LRRK2-PD astrocytes either not

treated or treated (n = 2, total astrocytes counted = 299). (**E**) Graph displaying percentage of cells/DAPI with LAMP2A in perinuclear area in LRRK2-PD astrocytes either not treated or treated (n = 2, total astrocytes counted = 299). All graphs plot mean ± s.e.m, unpaired two-tailed Student's t-test, *p<0.05, **p<0.01, ***p<0.001. Scale bars 100µm and 20µm, respectively.

Materials and Methods

iPSC-derived astrocyte generation. As previously described(Sánchez-Danés et al., 2012), fibroblasts were collected from two patients harboring the GS2019S mutation on the LRRK2 gene and two healthy age-matched controls and generated into spherical neural masses (SNMs). SNMs were pushed towards an astrocytic lineage following a previously published protocol(Serio et al., 2013). First, the SNMs were grown in suspension for 28 days with medium supplemented with LIF and EGF, and then for a further 21 days with medium containing FG2 and EGF. Finally, SNMs were left with accutase (LabClinics) for 15 minutes at 37ºC and mechanically desegregated and plated on matrigel-coated plates (let set for 1 hour at RT) as a monolayer. The monolayer of neural progenitors was cultured for 14 more days in CNTF (Prospec Cyt-272) medium (Neurobasal, Glutamax, PenStrep, NEAA, CNTF), a stage in which considered astrocyte progenitors and therefore characterized. These astrocyte progenitors were successfully frozen in Astrocyte Freezing Medium (90% CNTF medium and 10% DMSO) and stored in liquid nitrogen to be kept for future use. When needed for an experiment, vials were thawed in medium containing FBS and resuspended in CNTF medium and plated on matrigel-coated plates. Cells were passaged four times before considered mature and then further characterized. Plastic cover slides were coated with matrigel in 24-well plates to conduct experiments.

iPSC-derived vmDAn generation and co-culture system. Using a combination of two previously published protocols, vmDA neurons were obtained after 35 days after which were co-cultured with LRRK2-PD and healthy astrocytes. The vmDAn were fully characterized and displayed functional viability with calcium imaging techniques (data not shown). After 35 days of differentiation 20% of overall cells stained positive for TH, a number which increased with time reaching 45% after 50 days, a point in which the protocol named the neurons mature. The co-culture system was aimed to house immature/young neurons and continue the differentiation process on the top of the astrocytes, therefore day 35 neurons were used. Astrocytes were plated one week before the neurons to ensure the development of mature astrocytes and sufficient co-culturing time before the cells could feel the effects of being in culture for too long. vmDAn from a LRRK2-PD line were generated and $5x10^4$ cells/well were plated on the top of one week old astrocytes ($2x10^4$ cells/well), which were plated on the top of matrigel coated glass coverslides in 24-well plates for two and four weeks. The medium used contained Neurobasal, NEAA, PenStrep, and Glutamax. Cells were fixed with 4% PFA for 15 mins and washed three times with PBS for 15 minutes before performing ICC. After confocal images were acquired, TH positive cells and DAPI were counted for a series of 600 cells per condition using FIJI is Just ImageJ™ cell counter plugin.

Immunocytochemistry. After medium removal, samples were fixed using 4% PFA for 15 minutes and then washed three times for 15 minutes with PBS. Samples were blocked with TBS++ with low triton (TBS1x, NDS 3%, Triton 0.01%) for two hours and 48-hour incubation with primary antibodies at 4ºC. Primary antibodies used include CD44, GFAP anti-Guinea pig (Synaptic Systems, 173 004), GFAP anti-Rabbit (Dako, Z0334), S100β anti-

Rabbit, (Dako, 311), Vimentin anti-Mouse IgM (Iowa, 3CB2), TUJ1 anti-Mouse (Covance, MMS-435P), MAP2 anti-Rabbit (Sant Cruz, sc-20172), NG2 anti-Rabbit (Millipore, AB5320), GLT1 anti-Guinea pig (Millipore, AB1783), Synaptophysin anti-Mouse (Millipore, MAB332), PSD-95, TOM20 anti-Mouse (BD, 612278), TOM20 anti-Rabbit (Sant Cruz, sc-11415), LC3B (Cell Signaling, 2775), LAMP-2A anti-Rabbit (Abcam, 18528), α-synuclein anti-Mouse (BD, 610787), Oligomeric α-synuclein anti-Mouse (Agisera AS13 2718), TH anti-Sheep (Pel-Freez, P60101-0), TH anti-Rabbit (Santa Cruz, sc-14007), LAMP1 (Iowa, H4A3). After 48-hour incubation with the primary antibody, samples were then washed with TBS 1x for 15 minutes three times, before being blocked again for one hour at room temperature. Samples were incubated with their rightful secondary antibody (all at a dilution of 1:200) for two hours at room temperature. Secondary antibodies used include the following: Alexa Fluor 488 anti-Mouse IgG (Jackson 715-545-150), Cy3 anti-rabbit IgG (Jackson 711-165-152), DyLight 649 anti-Guinea pig IgG (Jackson 706-495-148), Alexa Fluor 647 anti-Sheep (Jackson 713-605-147), Cy™2 AffiniPure Donkey Anti-Rabbit IgG (H+L) (Jackson 711-225-152), Cy™3 AffiniPure Donkey Anti-Mouse IgG (H+L) (Jackson 715-165-151). Samples were then further washed with TBS 1x for 15 minutes three times and then incubated with nuclear staining DAPI (Invitrogen, dilution 1:5000) for 10 minutes. After having washed the samples twice with TBS 1x for 10 minutes, samples were mounted with PVA:DABCO and stored at 4ºC until imaged. Samples were imaged using an SP5 confocal microscope (Leica) and analyzed with FIJI is Just ImageJ™.

Quantitative Real Time PCR. The isolation of total mRNA was performed by guanidinium thiocynate–phenol–chloro- form extraction (TRIzol, Invitrogen) and treated with DNase I. One microgram was used to synthesize cDNA with the SuperScript III Reverse Transcriptase Synthesis Kit (Invitrogen). Quantitative RT-PCR analyzes were done in triplicate on 50ng with Platinum Syber Green qPCR Super Mix (Invitrogen) in an ABI Prism 7000 thermocycler (Applied Biosystems). All results were normalized to GAPDH. The primers used were Aquaporin 4 (Forward AG AT CA GC AT CG CC AA GT CT; Reverse AA CC AG GA GA CC AT GA CC AG), p62 (Forward CC CT GA GG AA CA GA TG GA; Reverse GA CT GG AG TT CA CC TG TA GA), GapDH (Forward GC AC CG TC AA GG CT GA GA AC; Reverse AG GG AT CT CG CT CC TG GAA).

Protein extraction. Live cells were washed twice with PBS and incubated for six minutes at 37ºC with accutase (Sigma). Cells were lifted and collected in washing medium containing FBS and centrifuged at 800rpm for five minutes. After centrifugation, cells were resuspended in cold PBS and placed in 1.5mL eppendorfs and centrifuged for five minutes at 4ºC at 600x*g*. After discarding the supernatant, pellets were immediately stored at -80ºC for future use. Alternatively, the protein extraction could immediately take place after pellet collection at 4ºC. Pellets were homogenized in 50 mM Tris-HCl, pH 7.4/150 mM NaCl/0.5% Triton X-100/0.5% Nonidet P-40 and a mixture of proteinase inhibitors (Sigma, Roche tablet). Samples were then centrifuged at 15,000x*g* for 20 minutes at 4ºC. The resulting supernatant was normalized for protein using BCA kit (Pierce).

Protein extraction for oligomeric α-synuclein: Mila lysis buffer (0.5M Tris at pH 7.4 containing 0.5 methylenediaminetetraacetic acid at pH 8.0, 5M NaCl, 0.5% Na doxicholic, 0.5% Nonidet P-40, 1mM phenylmethylsulfonyl fluoride, bi-distilled water, protease and phosphatase inhibitor cocktails) (Roche Molecular Systems, Pleasanton, CA, USA), and then centrifuged for 15 min at 13,000rpm at 4°C (Ultracentrifuge Beckman with 70Ti rotor, CA, USA).

Western blot. Cell extracts were then boiled at 100ºC for 5 minutes, followed by 7-15% electrophoresis, then electrotransferred 100v to PVDF membranes for 1.5 hours at 4ºC. After treating the membranes with Ponceau S solution (Sigma) to be able to cut separately the protein of interest and the loading control protein for separated antibody incubations, the membranes were then blocked with 5% not-fat milk in 0.1M Tris-buffered saline (pH. 7.4) for 1 hour and incubated overnight in TBS 1x/BSA 3%/TWEEN 0.1% containing primary antibodies. After incubation with peroxidase-tagged secondary antibodies (dilution 1:10,000), membranes were revealed with ECL-plus chemiluminescence western blot kit (Amershan-Pharmacia Biotech). This study used the following antibodies: pDRP1 anti-rabbit (Cell Signalling 3455), Porin VDAC1 anti-mouse (abcam, ab14734), α-synuclein anti-mouse (BD 610787), Synaptophysin anti-rabbit (abcam), PSD-95 anti-mouse (Milipore AB5475), TH anti-rabbit (Sigma T8700), FOXA2 anti-mouse (Santa Cruzz sc-101060), GFAP anti-guinea pig (Synaptic Systems 173 004), CD44 anti-mouse (abcam ab6124), S100β anti-rabbit (Dako 311), TUJ1 anti-mouse (Biolegend 801202), NG2 anti-rabbit (Milipore AB5320), MAP2 anti-chicken IgY (abcam ab5392), LAMP-2A anti-rabbit (abcam 18528), LC3B anti-rabbit (Cell Signaling 2775), p62 anti-rabbit (Enzo Life Science BML-PW9860) and as protein loading controls Actin (Millipore), Tubulin (Millipore).

Densitometry. After having been developed at several different times (1 second, 30 seconds, 1 minute, 3 minutes, 5 minutes, 10 minutes, and 20 minutes to burn) films were scanned at 2,400 x 2,400 dpi (i800 MICROTEK high quality film scanner), and the densitometric analysis was performed using FIJI is Just ImageJ™. Other membranes were imaged using the ChemiTouch machine under the 'Optimal exposure' setting.

Calcium Imaging. Live cells were incubated with Fluro4-AM flurofore for 30 minutes slowly shaking at room temperature. Cells were then imaged for 20-minute recordings using the Hokawo program and when finished data was converted from video to images. The data was then put through the NeuroImage program where Calcium Activity Map and individual Calcium Graphs were generated. Data is further analyzed in a Matlab code made by Jordi Soriano.

Cell Viability Assay Calcein Green AM (Thermofisher ref. C3100MP) (1μM final concentration) was added to the cells in 0,5ml suspension medium (not exceeding more than 1M cells) containing PBS. In addition, 2μL of Propidium iodide (Sigma ref. P4170) (1mg/mL) was also added to the cells and incubated 5 min in the same conditions as above. Flow cytometry analysis was performed with excitation at 488 nm and emission collected at ~520 nm (FITC channel) for Calcein Green AM, and at ~ 585nm (Phycoerythrin channel) for the PI. Cells were run on a Gallios flow cytometer analyser and file analysis was done using Kaluza Software, both from Beckman Coulter Inc (Brea, CA).

CMA Reporter KFERQ-DENDRA. CMA activity was measured using a photoactivatable CMA fluorescent reporter with a CMA targeting motif added to the PS-dendra protein (KFERQ-PS-dendra) developed and updated by (Koga et al., 2011; Park et al., 2015). Cells transduced with the lentivirus carrying the reporter were photoactivated with a UV light for 3 minutes and then imaged after 52 hours to monitor CMA activity.

CMA knockdown (shLAMP-2A). After 14 days in culture, cells were transduced with a lentivirus containing shLAMP-2A(Ashish C Massey et al., 2008). Half of the medium was added the following day, and the virus was left to take affect for 72 hours. Cells were then fixed with 4% PFA for 15 mins and stained with anti-GFAP and anti-α-synuclein in ICC,

protocol previously described in ICC section. α-synuclein puncta were counted using a macro developed in FIJI is for ImageJ measuring α-synuclein area within the cell. 100 cells per condition were measured. The shLAMP-2A plasmid was kindly supplied by AMC.

LC3 Flux Assay. After 14 days of culture, cells were either not treated with a drug (control), treated with Leupeptin (100 µg, Sigma L2884) and NH4Cl (20 µg, Sigma A9434) for 2 hours. The assay was terminated by washing the cells twice in PBS. The pellets were collected as previously described under 'protein extraction' section. Western blots were performed using 13% gels, and as previously described in WB section. Ratio of 2-hour drug treatment versus no drug was performed per line to determine speed of fusion.

α-synuclein Flux Assay. After 14 days of culture, cells were either not treated with a drug (control), treated with Lactacystin (5mM, Enzo BML-PI104) for 2 hours, or Leupeptin (100 µg, Sigma L2884) for 12 hours. The assay was terminated by washing the cells twice in cold PBS. The pellets were collected as previously described under 'protein extraction' section. WB was performed using 12.5% gels, and as previously described in WB section.

CRISPR guideRNA (gRNA) and Donor Plasmid Design. CRISPR/Cas9 gRNAs against the last exon-3'UTR junction of the human *SNCA* gene were designed so that the spacer sequence overlapped the STOP codon. Complementary oligos encoding for the desired spacer sequences were annealed into the BbsI site of the gRNA scaffold of the Cas9-T2A-EGFP/gRNA co-expression plasmid px458 (Addgene #48138). For increased expression of the Cas9 protein in hPSC, Cbh promoter was replaced by a full-length version of the CAGGS promoter. The cleavage efficiency of two gRNAs was tested by T7EI assay. Both gRNAs displayed a similar cutting efficiency but gRNA2-OL was selected for the editing process.

Donor plasmid for knocking-in a FLAG tag fused C-terminal to the α-synuclein open reading frame (ORF) was engineered using the following elements. Two homology arms (HAs) spanning approximately 800 bp from both sides of the STOP codon. The sequence encoding for the FLAG tag was placed right after the last codon of the SNCA ORF and before the STOP codon. A selection cassette (pRex1-NeoR) surrounded by loxP sites was cloned between the STOP codon and the 3'HA. The sequence of the cloning primers and gRNA oligonucleotides can be found in Supp. Table 1.

CRISPR-mediated SNCA locus edition in hiPSC. The day before transfection, 800.000 hiPSC were seeded in a 10cm plate coated with matrigel. The following day, hiPSC were co-transfected with a mix of 6 µg of Cas9-T2A-EGFP/gRNA, 9 µg of the donor plasmid, 45 µL of FuGENE HD (Promega) transfection reagent and KO-DMEM up to 750 µL. The transfection mixture was incubated for 15 minutes at room temperature and subsequently added dropwise to the cells. Geneticin (G-418; 50 µg/mL) selection was initiated 72h post-transfection and was maintained until the emerging colonies were transferred to another plate. Between 10 and 14 days after the initiation of the selection, colonies were large enough as to be screened.

Half of the colony was sampled in order to check site-specific integration by means of PCR. Primers to check the targeted integration of the FLAG tag and the selection cassette are listed below. Those colonies that were positive for the targeted recombination were

transferred to a different well in order to be transfected with a CRE-recombinase expressing plasmid. After CRE transfection, cells were singularized and seeded at a low density on top of irradiated human fibroblast feeder layer in the presence of ROCK inhibitor (Miltenyi). Once, the colonies attained a certain size, they were isolated and screened for selection cassette-excision. Those clones whose both SNCA alleles were tagged with the FLAG epitope were expanded and characterized in terms of pluripotency and genome stability.

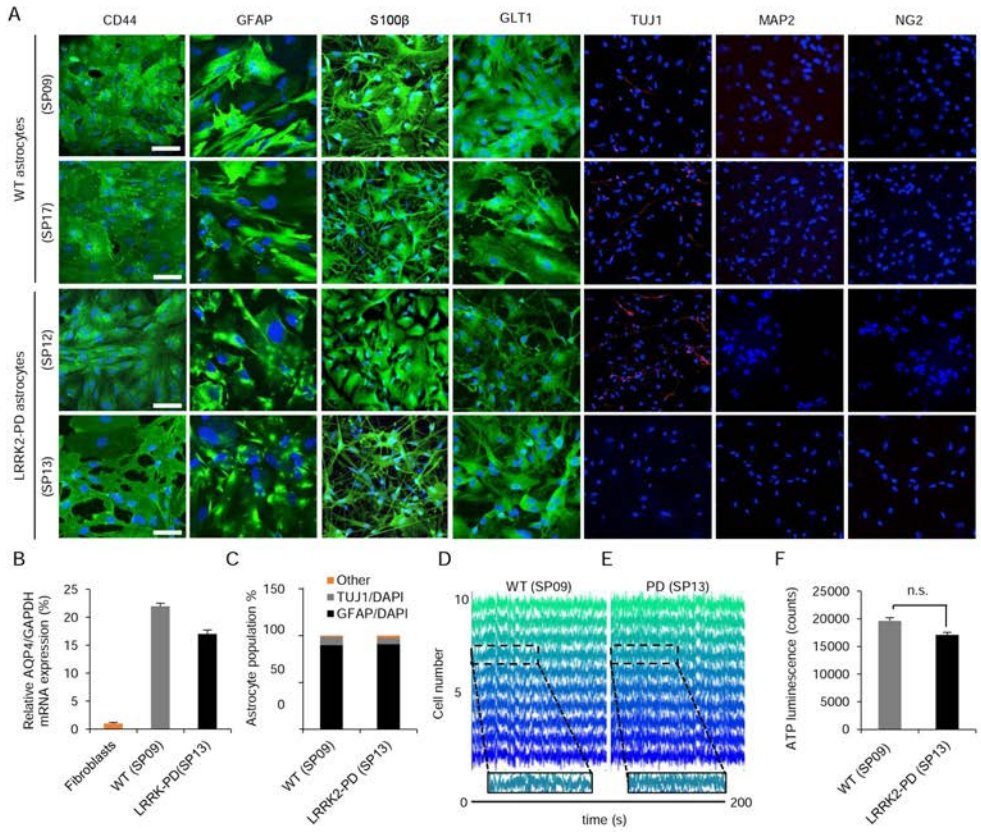
A
CD44
GFAP
S100β
GLT1
TUJ1
MAP2
NG2
WT astrocytes
(SP09)
(SP17)
LRRK2-PD astrocytes
(SP12)
(SP13)
B
Relative AQP4/GAPDH mRNA expression (%)
Fibroblasts
WT (SP09)
LRRK-PD(SP13)
C
Astrocyte population %
Other
TUJ1/DAPI
GFAP/DAPI
WT (SP09)
LRRK2-PD (SP13)
D
WT (SP09)
Cell number
time (s)
E
PD (SP13)
F
ATP luminescence (counts)
n.s.
WT (SP09)
LRRK2-PD (SP13)

Figure 1

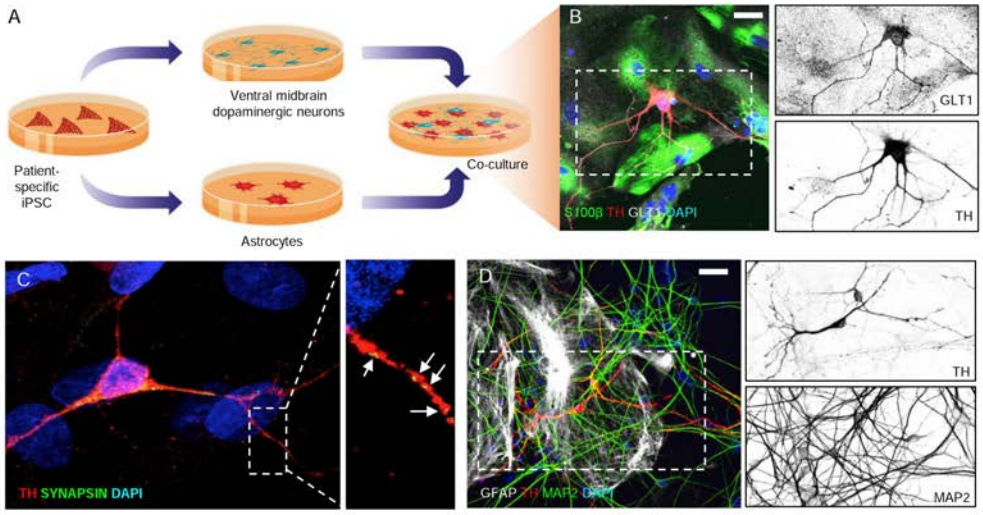
A
Ventral midbrain dopaminergic neurons
Patient-specific iPSC
Astrocytes
Co-culture
B
S100β TH GLT1 DAPI
GLT1
TH
C
TH SYNAPSIN DAPI
D
GFAP TH MAP2 DAPI
TH
MAP2

Figure 2

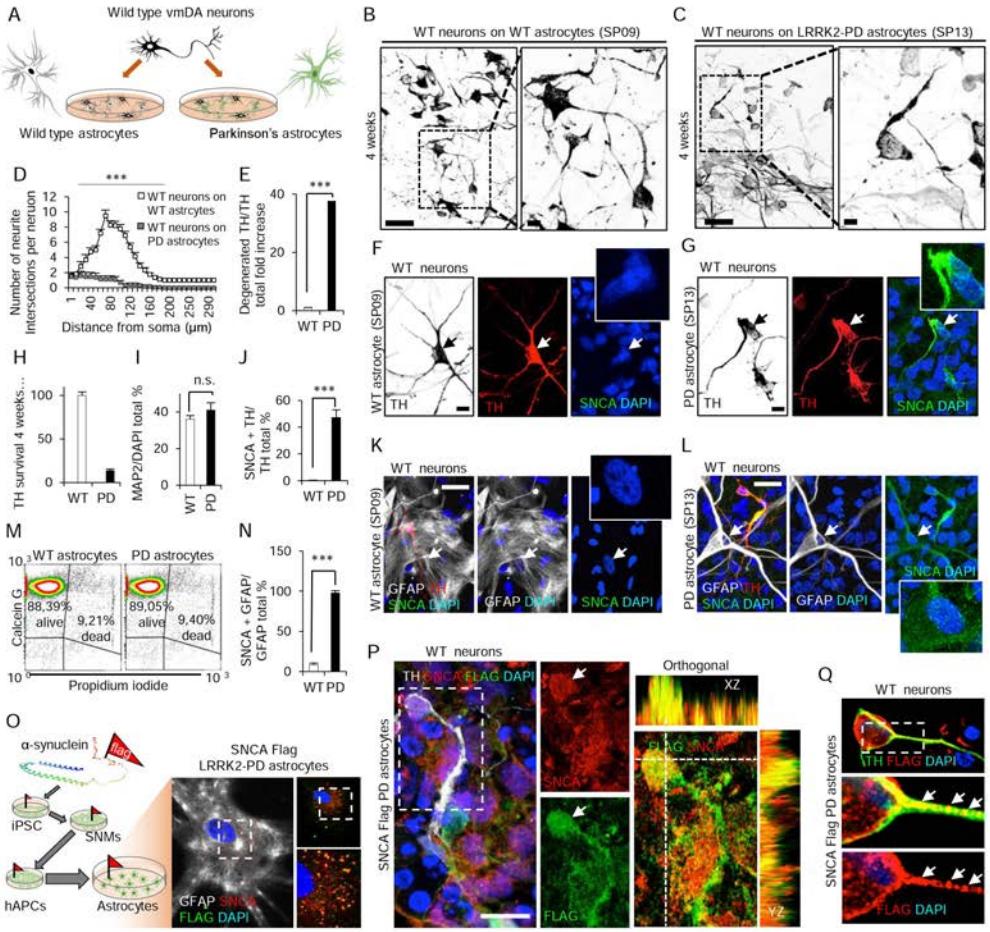
A
Wild type vmDA neurons
Wild type astrocytes
Parkinson's astrocytes
B
WT neurons on WT astrocytes (SP09)
4 weeks
C
WT neurons on LRRK2-PD astrocytes (SP13)
4 weeks
D
***
WT neurons on WT astrcytes
WT neurons on PD astrocytes
Number of neurite Intersections per neruon
Distance from soma (µm)
E
***
Degenerated TH/TH total fold increase
WT PD
F
WT neurons
WT astrocyte (SP09)
TH
SNCA DAPI
G
WT neurons
PD astrocyte (SP13)
TH
SNCA DAPI
H
TH survival 4 weeks...
WT PD
I
n.s.
MAP2/DAPI total %
WT PD
J
***
SNCA + TH/ TH total %
WT PD
K
WT neurons
WT astrocyte (SP09)
GFAP TH SNCA DAPI
GFAP DAPI
SNCA DAPI
L
WT neurons
PD astrocyte (SP13)
GFAP TH SNCA DAPI
GFAP DAPI
SNCA DAPI
M
WT astrocytes
PD astrocytes
Calcein G
88,39% alive
9,21% dead
89,05% alive
9,40% dead
Propidium iodide
N
***
SNCA + GFAP/ GFAP total %
WT PD
O
α-synuclein
flag
iPSC
SNMs
hAPCs
Astrocytes
SNCA Flag LRRK2-PD astrocytes
GFAP SNCA FLAG DAPI
P
WT neurons
TH SNCA FLAG DAPI
SNCA Flag PD astrocytes
SNCA
FLAG
Orthogonal
XZ
FLAG SNCA
YZ
Q
WT neurons
TH FLAG DAPI
SNCA Flag PD astrocytes
FLAG DAPI

Figure 3

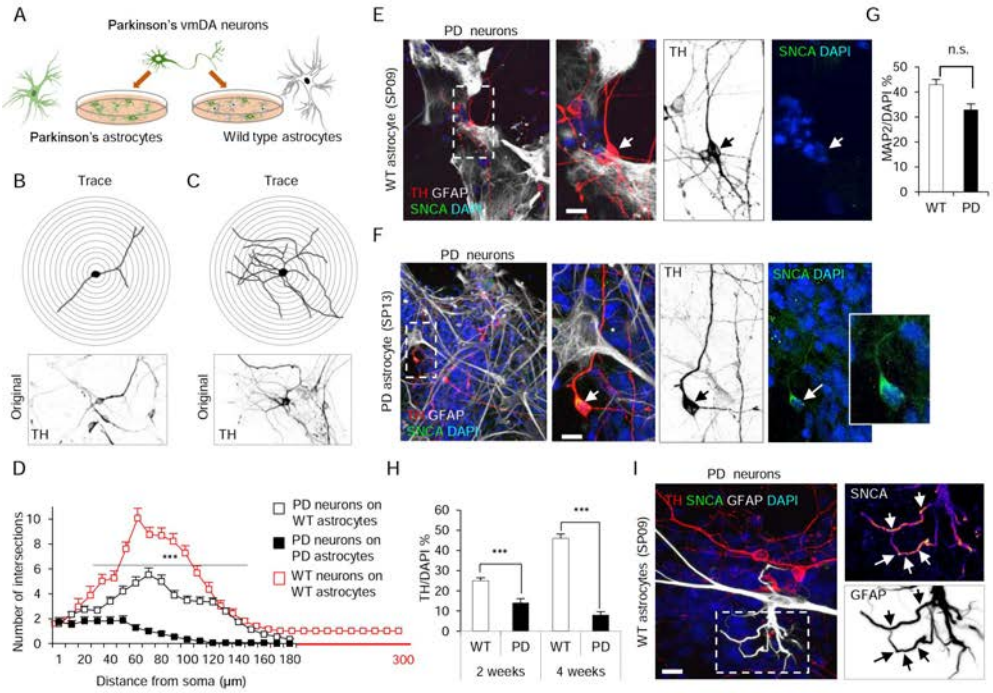
A
Parkinson's vmDA neurons
Parkinson's astrocytes
Wild type astrocytes
B
Trace
Original
TH
C
Trace
Original
TH
D
Number of intersections
Distance from soma (µm)
PD neurons on WT astrocytes
PD neurons on PD astrocytes
WT neurons on WT astrocytes
***
E
PD neurons
WT astrocyte (SP09)
TH GFAP
SNCA DAPI
TH
SNCA DAPI
F
PD neurons
PD astrocyte (SP13)
GFAP
SNCA DAPI
TH
SNCA DAPI
G
n.s.
MAP2/DAPI %
WT
PD
H
TH/DAPI %
***
***
WT
PD
WT
PD
2 weeks
4 weeks
I
PD neurons
WT astrocytes (SP09)
TH SNCA GFAP DAPI
SNCA
GFAP

Figure 4

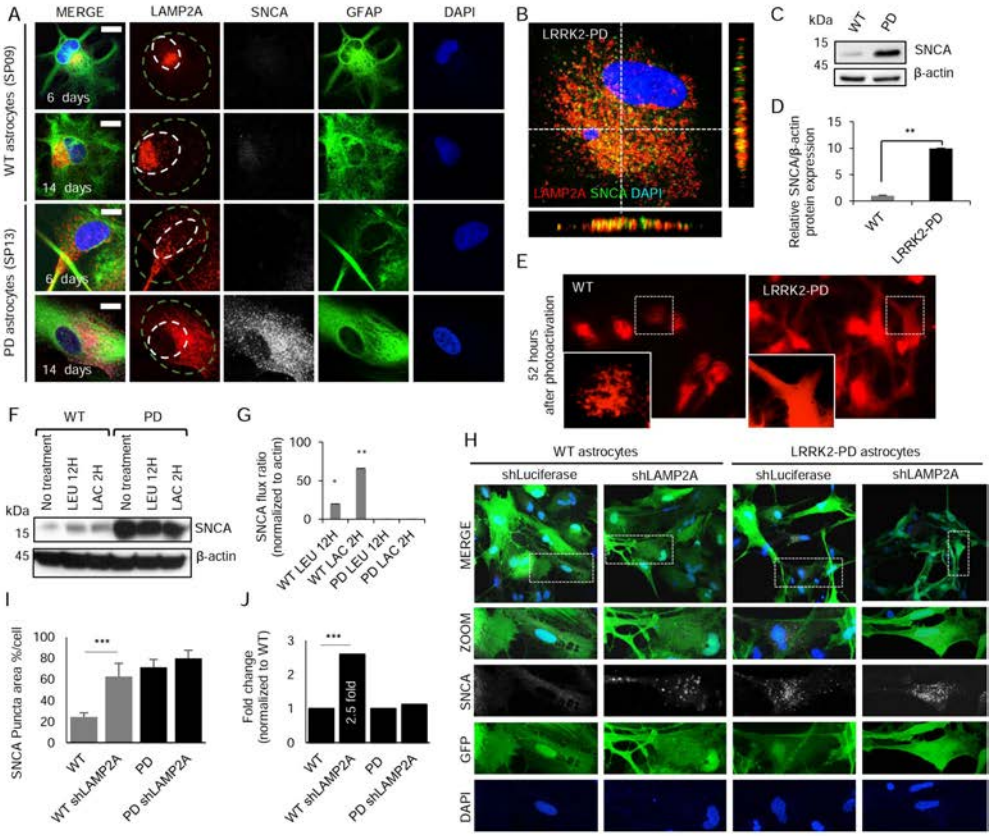
A
MERGE
LAMP2A
SNCA
GFAP
DAPI
WT astrocytes (SP09)
PD astrocytes (SP13)
6 days
14 days
6 days
14 days
B
LRRK2-PD
LAMP2A SNCA DAPI
C
kDa
WT
PD
15
45
SNCA
β-actin
D
Relative SNCA/β-actin protein expression
WT
LRRK2-PD
E
WT
LRRK2-PD
52 hours after photoactivation
F
WT
PD
No treatment
LEU 12H
LAC 2H
kDa
15
45
SNCA
β-actin
G
SNCA flux ratio (normalized to actin)
WT LEU 12H
WT LAC 2H
PD LEU 12H
PD LAC 2H
H
WT astrocytes
LRRK2-PD astrocytes
shLuciferase
shLAMP2A
MERGE
ZOOM
SNCA
GFP
DAPI
I
SNCA Puncta area %/cell
WT
WT shLAMP2A
PD
PD shLAMP2A
J
Fold change (normalized to WT)
2.5 fold
WT
WT shLAMP2A
PD
PD shLAMP2A

Figure 5

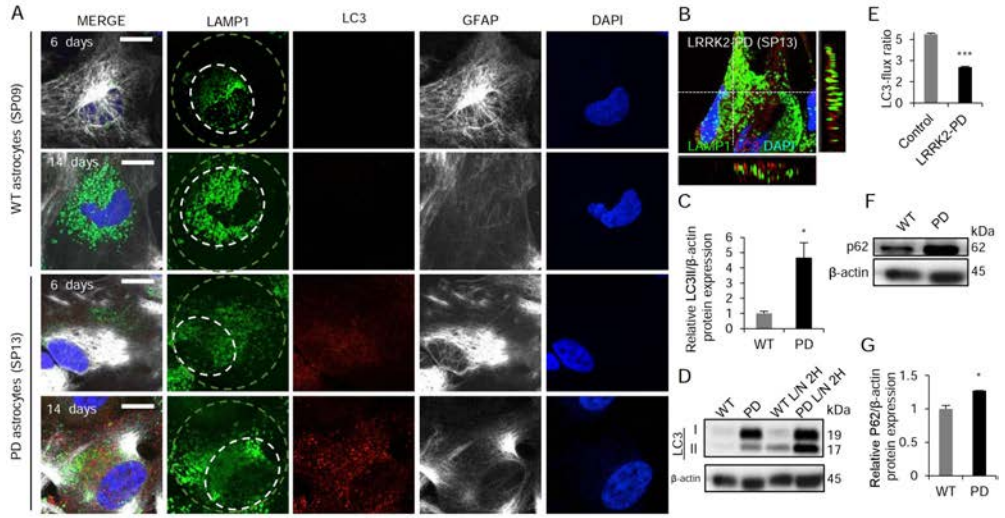
A
MERGE
LAMP1
LC3
GFAP
DAPI
WT astrocytes (SP09)
PD astrocytes (SP13)
6 days
14 days
6 days
14 days
B
LRRK2-PD (SP13)
LAMP1
DAPI
C
Relative LC3II/β-actin protein expression
WT
PD
D
WT
PD
WT LiN 2H
PD LiN 2H
kDa
LC3
I
II
19
17
β-actin
45
E
LC3-flux ratio
***
Control
LRRK2-PD
F
WT
PD
kDa
p62
62
β-actin
45
G
Relative P62/β-actin protein expression
*
WT
PD

Figure 6

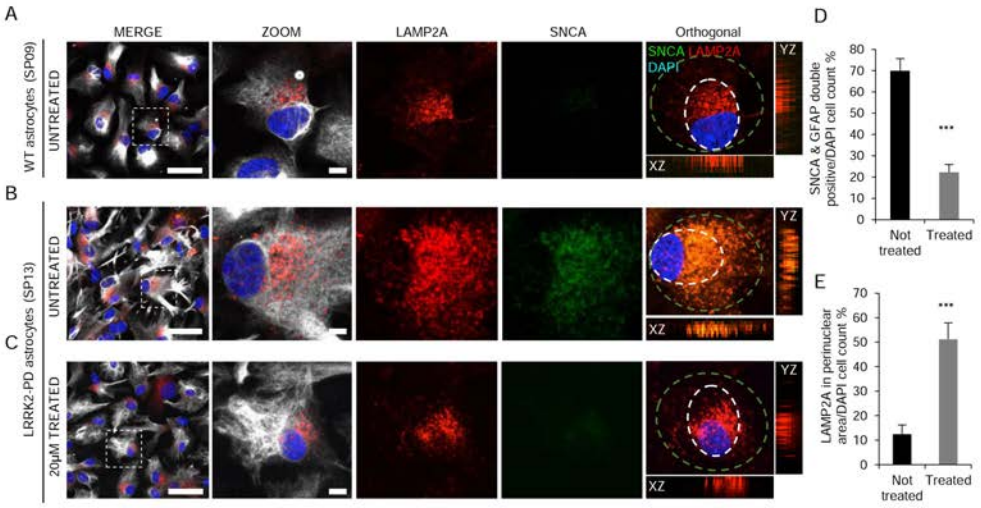
A
MERGE
ZOOM
LAMP2A
SNCA
Orthogonal
WT astrocytes (SP09)
UNTREATED
SNCA LAMP2A
DAPI
YZ
XZ
B
C
LRRK2-PD astrocytes (SP13)
UNTREATED
20μM TREATED
D
SNCA & GFAP double positive/DAPI cell count %
Not treated
Treated
E
LAMP2A in perinuclear area/DAPI cell count %
Not treated
Treated

Figure 7

Supplementary Information for

iPSC-derived astrocytes contribute to non-cell autonomous neurodegeneration during Parkinson's disease

Angelique di Domenico[1,2], Giulia Carola[1,2], Carles Calatayud Aristoy[1,2,3], Juan Pablo Muñoz[4], Yvonne Richaud-Patin[3], Armida Faella[1,2], Jordi Soriano[5], Isidro Ferrer[2,6], Eduardo Tolosa[6,7], Antonio Zorzano[4], Ana Maria Cuervo[8], Angel Raya[3,9,10*], Antonella Consiglio[1,2,11†¥]

* Corresponding author to araya@cmrb.com (A.R.)
† Corresponding author to consiglio@ub.edu (A.C.)
¥ Lead contact

This PDF file includes:

Purpose	Oligo name	Sequence
Annealed oligo cloning of gRNAs	SNCA_gRNA1_OL-F	AAAGATATTTCTTAGGCTTC
	SNCA_gRNA1_OL-R	GAAGCCTAAGAAATATCTTT
	SNCA_gRNA2_OL-F	TGGGAGCAAAGATATTTCTT
	SNCA_gRNA2_OL-R	AAGAAATATCTTTGCTCCCA
Primers for generating the donor plasmid	SNCA_5-F_XhoI	AACTCGAGACTCAAGCTTAGGAACAAGGA
	SNCA_5Flag-R_SalI	AAGTCGACTTACTTGTCGTCATCGTCTTTGT AGTCGGCTTCAGGTTCGTAGTCTT
	Rex1_F-loxP-SalI	AAGTCGACATAACTTCGTATAGCATACATTA TACGAAGTTATGACCGATTCCTCCCGATAAG
	Neo_R-loxP-BamHI	AAGGATCCATAACTTCGTATAGCATACATTA TACGAAGTTATTAAGATACATTGATGAGTTT GGA
	SNCA_3-F_BamHI	AAGGATCCGAAATATCTTTGCTCCCAGT
	SNCA_3-R_NotI	AAGCGGCCGCTTAAGGAACCAGTGCATAC
Primers for screening PCR	SNCA_5Out_R	
	Check_Rex1Neo_5HA_R	CTTATCGGGAGGAATCGGTC
	Check_Rex1Neo_3HA_F	CCCGTCTGTTGTGTGACTC
	SNCA_3Out_R	ACGTAAAGCAAACATTGACAGG

Table S1

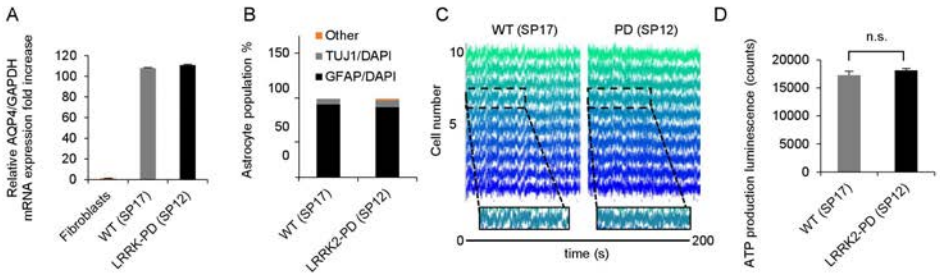

Figure S1 iPSC-derived astrocyte characterization (**a**) qRT-PCR revealing relative mRNA expression levels of astrocitic endfeet marker Aquaporin 4 in both control (SP17) and LRRK2-PD (SP12) lines and not present in fibroblasts. Fold change normalized to fibroblast levels (n = 2). (**b**) Astrocyte cultures are approximately composed of 90% astrocytes, 8% neurons and 2% other. (**c**) Graph representing single functional astrocyte calcium waves of WT (SP17) line and LRRK2-PD (SP12) astrocytes (n = 3). (**d**) Graph plotting functional ATP production luminescence (counts) in both WT (SP17) and LRRK2-PD (SP12) astrocytes, differences are non-significant (n = 3). All graphs plot mean ± s.e.m, unpaired two-tailed Student's t-test, *p<0.05, **p<0.01, ***p<0.001.

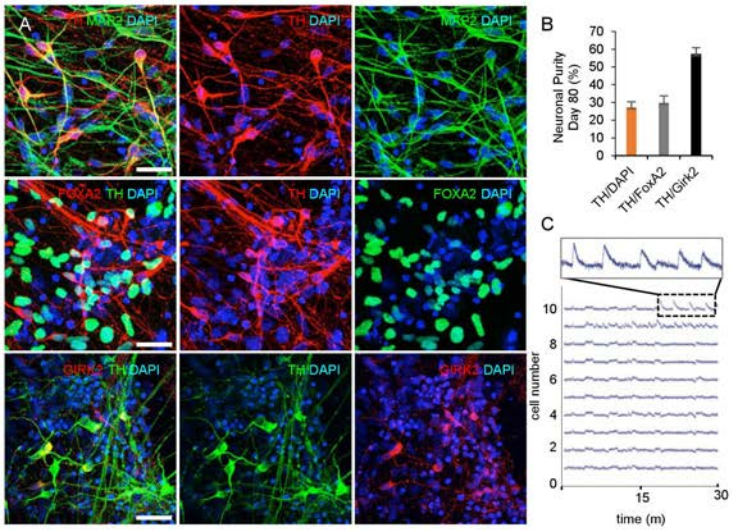

Figure S2 vmDA neuron generation and co-culture set up. (**a**) Representative immunofluorescence images of vmDAn after neuronal differentiation (80 days). iPSC-derived neural cultures express markers specific for neurons (MAP2), mature DA neurons (TH), and midbrain-type DA neurons (FoxA2 and Girk2), scale bar 20µm. (**b**) Percentage of vmDAn staining positive for Tyrosine hydroxylase (TH)/DAPI, double positive for TH & FOXA2 (transcriptional activator for vmDAn differentiation) and TH & GIRK (G-protein in vmDAn). (**c**) Graph representing day 35 vmDA neurons calcium wave flux recording over 30 minutes with calcium marker Fluo8-AM (n = 3).

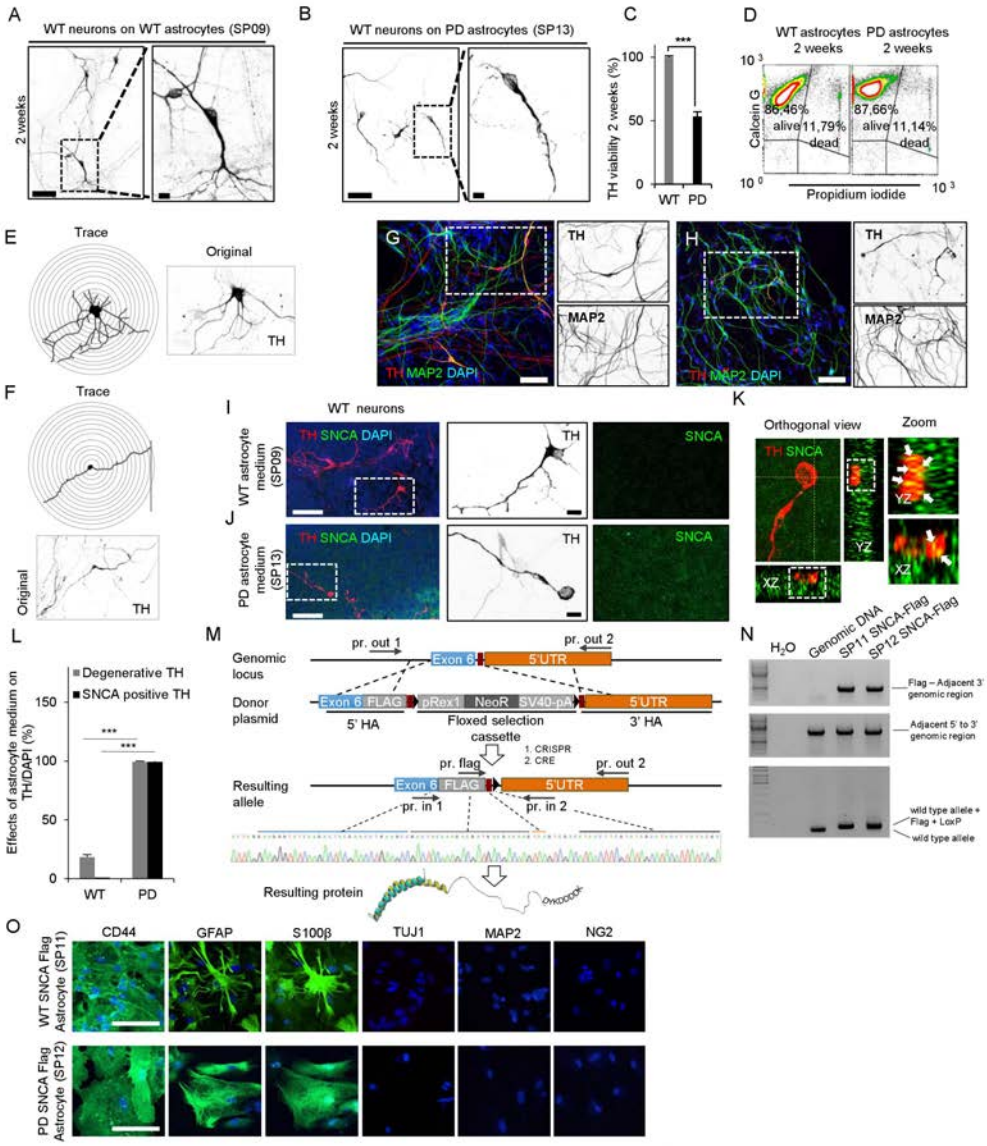

Figure S4 WT vmDAn show signs of neurodegeneration and accumulate alpha-synuclein when co-cultured with LRRK2-PD astrocytes (**A**) Representative images staining WT vmDAn (TH) on the top of WT astrocytes during a 2-week co-culture, scale bar 20μm and 0.2μm zoom. (**B**) WT vmDAn (TH) on the top of LRRK2-PD astrocytes during a 2-week co-culture, scale bar 20μm and 0.2μm zoom. (**C**) Graph representing TH/DAPI WT neuron count when co-cultured with WT or LRRK2-PD astrocytes at 2 weeks, (n = 3, total neurons counted = 1245). (**D**) Contour plot of astrocyte viability at 2 weeks. (**E**) Scholl analysis image of neurite traces of WT neurons when co-cultured on WT astrocytes and PD astrocytes (**F**). (**G**) WT vmDAn (TH) and mature neuron marker (MAP2) on the top of WT astrocytes (GFAP) during a 4 week co-culture, scale bar 20μm. (**H**) WT vmDAn (TH) and mature neuron marker (MAP2) on the top of LRRK2-PD astrocytes (GFAP) during a 4 week co-culture, scale bar 20μm. (**I**) Representative images of WT vmDAn (TH) and alpha-synuclein (SNCA) when co-cultured with medium from both WT and (**J**) LRRK2-PD astrocytes after 4 weeks in culture, scale bar 50μm, zoom 0.2μm. (**K**) Orthogonal view confirming co-localization of SNCA with TH in WT neurons cultured with LRRK2-PD astrocyte medium. (**L**) Graph representing the effects of astrocyte medium on WT neurons in terms of neurons positive for SNCA inclusions as well as harboring a degenerated morphology (fewer than 2 neurites or beaded like neurites). (**M**) Scheme of flag gene editing using CRISP/CASP9 (**N**) Gel of flag tagged SNCA insertion (**O**) Characterization of WT and LRRK2-PD astrocyte SNCA flag lines, CD44, GFAP, S100β, TUJ1, MAP2, NG2. All graphs plot mean ± s.e.m, unpaired two-tailed Student's t-test, *p<0.05, **p<0.01, ***p<0.001.

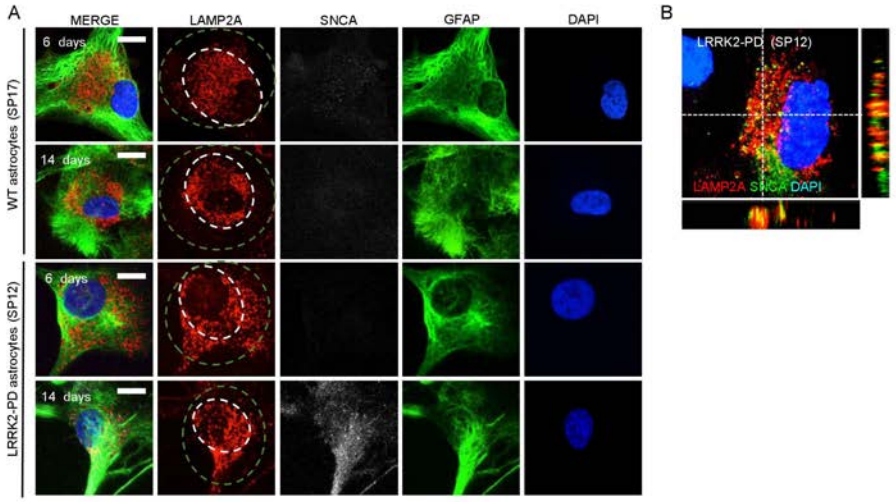

Figure S5 Altered CMA and SNCA accumulation in LRRK2-PD astrocytes (**a**) Representative images of the receptor for CMA (LAMP2A), astrocyte marker GFAP, SNCA and nuclear marker DAPI in second WT and second LRRK2-PD astrocyte lines at 6 and 14 days, scale bar 10μm. Smaller white circles represent perinuclear area, whereas larger green circle represents non-perinuclear area. (**b**) Positive co-localization between LAMP2A and SNCA in second LRRK2-PD astrocyte line.

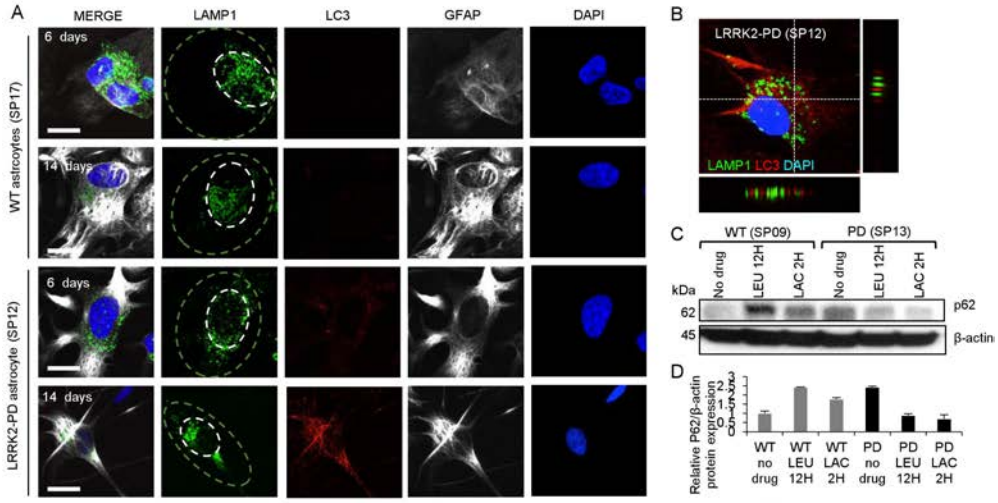

Figure S6 Dysfunctional macroautophagy in LRRK2-PD astrocytes. (**a**) Representative images of lysosomal protein marker LAMP1 and autophagosome marker LC3 in second WT and LRRK2-PD astrocyte lines at 6 and 14 days, scale bar 10μm. Smaller white circles represent perinuclear area, whereas larger green circle represents non-perinuclear area. (**b**) Lack of co-localization between LAMP1 and LC3 in second LRRK2-PD astrocyte line. (**c**) Western blot of P62 after treatment with inhibitors of autophagy and the proteosomal system, mean ± s.e.m plotted in graph (**d**).

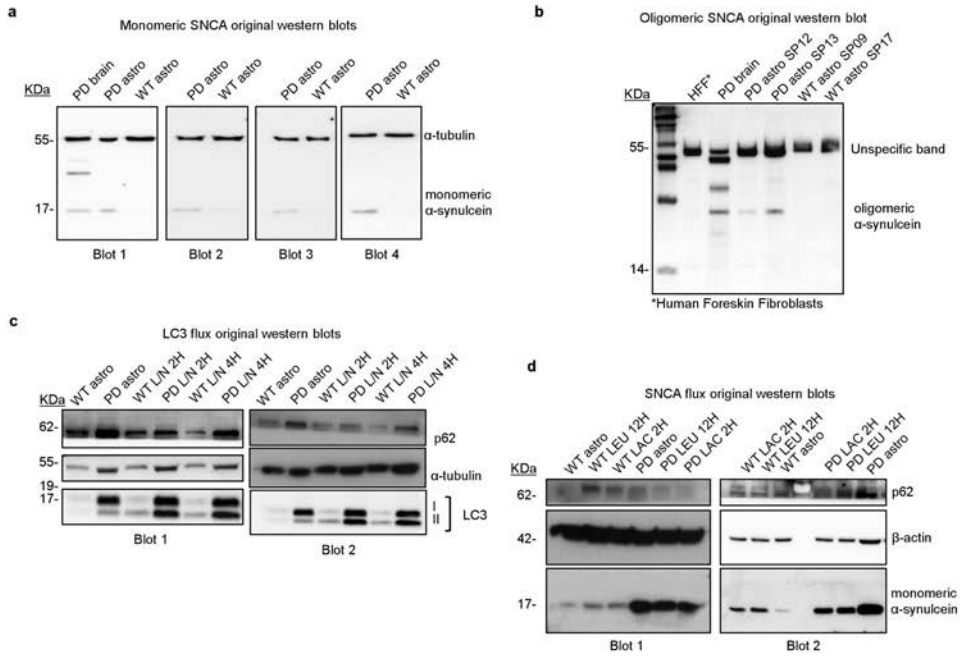

Figure S7 Original western blots (a) Monomeric alpha-synuclein western blots (b) oligomeric alpha-synuclein western blot (c) LC3 flux western blots (d) Alpha-synuclein flux western blots.

Thank you!